Stochastic Geometry Analysis of LTE-A Cellular Networks

Peng Guan

NNT : 2015SACLS252

THESE DE DOCTORAT
DE
L'UNIVERSITE PARIS-SACLAY
PREPAREE A
L'UNIVERSITE PARIS-SUD

ECOLE DOCTORALE N° 580
Sciences et technologies de l'information et de la communication

Spécialité de doctorat : Réseaux, Information et Communications

Par

M. Peng GUAN

Stochastic Geometry Analysis of LTE-A Cellular Networks

Thèse présentée et soutenue à Gif sur Yvette, le 16 Décembre 2015:

Composition du Jury :

M. DUHAMEL, Pierre	Directeur de recherche (L2S, CNRS, France)	Président
M. DECREUSEFOND, Laurent	Professor (Telecom ParisTech, France)	Rapporteur
M. GHRAYEB, Ali	Professor (Texas A&M University at Qatar, Qatar)	Rapporteur
M. BACCELLI, François	Directeur de recherche (INRIA, France)	Examinateur
	Professor (University of Texas at Austin, USA)	Examinateur
M. SCHOBER, Robert	Professor (University Erlangen-Nürnberg, Germany)	Examinatrice
M. BUSSON, Anthony	Professor (Université Lyon 1, France)	Directeur de thèse
M. DI RENZO, Marco	Chargé de recherché (L2S, CNRS, France)	Co-directeur de thèse

Titre : Analyse de Réseaux Cellulaires LTE-A : Une Approche Fondée sur la Géométrie Stochastique

Mots clés : Géométrie stochastique, réseaux cellulaires, LTE-A, processus de Poisson, Évaluation de performances

Résumé : L'objectif principal de cette thèse est l'analyse des performances des réseaux LTE-A (Long Term Evolution- Advanced) au travers de la géométrie stochastique. L'analyse mathématique des réseaux cellulaires est un problème difficile, pour lesquels ils existent déjà un certain nombre de résultats mais qui demande encore des efforts et des contributions sur le long terme. L'utilisation de la géométrie aléatoire et des processus ponctuels de Poisson (PPP) s'est avérée être une approche permettant une modélisation pertinente des réseaux cellulaires et d'une complexité faible (tractable). Dans cette thèse, nous nous intéressons tout particulièrement à des modèles s'appuyant sur ces processus de Poisson : PPP-based abstraction. Nous développons un cadre mathématique qui permet le calcul de quantités reflétant les performances des réseaux LTE-A, tels que la probabilité d'erreur, la probabilité et le taux de couverture, pour plusieurs scénarios couvrant entre autres le sens montant et descendant. Nous considérons également des transmissions multi-antennes, des déploiements hétérogènes, et des systèmes de commande de puissance de la liaison montante. L'ensemble de ces propositions a été validé par un grand nombre de simulations. Le cadre mathématique développé dans cette thèse se veut général, et doit pouvoir s'appliquer à un nombre d'autres scénarios importants. L'intérêt de l'approche proposée est de permettre une évaluation des performances au travers de l'évaluation des formules, et permettent en conséquences d'éviter des simulations qui peuvent prendre énormément de temps en terme de développement ou d'exécution.

Title : Stochastic Geometry Analysis of LTE-A Cellular Networks

Keywords : Stochastic Geometry, Cellular Networks, LTE-A, Poisson Point Process, Performance Analysis

Abstract : The main focus of this thesis is on performance analysis and system optimization of Long Term Evolution - Advanced (LTE-A) cellular networks by using stochastic geometry. Mathematical analysis of cellular networks is a long-lasting difficult problem. Modeling the network elements as points in a Poisson Point Process (PPP) has been proven to be a tractable yet accurate approach to the performance analysis in cellular networks, by leveraging the powerful mathematical tools such as stochastic geometry. In particular, relying on the PPP-based abstraction model, this thesis develops the mathematical frameworks to the computations of important performance measures such as error probability, coverage probability and average rate in several application scenarios in both uplink and downlink of LTE-A cellular networks, for example, multi-antenna transmissions, heterogeneous deployments, uplink power control schemes, etc. The mathematical frameworks developed in this thesis are general enough and the accuracy has been validated against extensive Monte Carlo simulations. Insights on performance trends and system optimization can be done by directly evaluating the formulas to avoid the time-consuming numerical simulations.

To my family. . .

Acknowledgements

This work has been performed in 2013-2015, at the Laboratory of signals and systems (L2S) – a research unit of the Centre national de la recherche scientifique (CNRS), CentraleSupélec and Paris-Sud University.

I would like to thank the European Commission for generously supporting my research under the auspices of the FP7-PEOPLE MITN-CROSSFIRE (unCooRdinated netwOrk StrategieS for enhanced interFerence, mobIlity, radio Resource, and Energy saving management in LTE-Advanced networks) project (grant 317126).

I would like to thank my supervisors Prof. Anthony Busson and Dr. Marco Di Renzo for their guidance throughout the whole thesis work.

I would like to thank my colleague Wei Lu for the useful discussions throughout the whole thesis work.

Last but not least, I am indebted to all my friends and family for their love and encouragement.

Gif sur Yvette, 15 October 2015 Peng Guan

Abstract

The main focus of this thesis is on performance analysis and system optimization of Long Term Evolution - Advanced (LTE-A) cellular networks by using stochastic geometry. Mathematical analysis of cellular networks is a long-lasting difficult problem. Modeling the network elements as points in a Poisson Point Process (PPP) has been proven to be a tractable yet accurate approach to the performance analysis in cellular networks, by leveraging the powerful mathematical tools such as stochastic geometry. In particular, relying on the PPP-based abstraction model, this thesis develops the mathematical frameworks to the computations of important performance measures such as error probability, coverage probability and average rate in several application scenarios in both uplink and downlink of LTE-A cellular networks, for example, multi-antenna transmissions, heterogeneous deployments, uplink power control schemes, *etc*. The mathematical frameworks developed in this thesis are general enough and the accuracy has been validated against extensive Monte Carlo simulations. Insights on performance trends and system optimization can be done by directly evaluating the formulas to avoid the time-consuming numerical simulations.

Key words: Stochastic Geometry, Cellular Networks, LTE-A, Poisson Point Process, Performance Analysis, Error Probability, Coverage, Rate

Résumé

L'objectif principal de cette thèse est l'analyse des performances des réseaux LTE-A (Long Term Evolution- Advanced) au travers de la géométrie stochastique. L'analyse mathématique des réseaux cellulaires est un problème difficile, pour lesquels ils existent déjà un certain nombre de résultats mais qui demande encore des efforts et des contributions sur le long terme. L'utilisation de la géométrie aléatoire et des processus ponctuels de Poisson (PPP) s'est avérée être une approche permettant une modélisation pertinente des réseaux cellulaires et d'une complexité faible (tractable). Dans cette thèse, nous nous intéressons tout particulièrement à des modèles s'appuyant sur ces processus de Poisson : PPP-based abstraction. Nous développons un cadre mathématique qui permet le calcul de quantités reflétant les performances des réseaux LTE-A, tels que la probabilité d'erreur, la probabilité et le taux de couverture, pour plusieurs scénarios couvrant entre autres le sens montant et descendant. Nous considérons également des transmissions multi-antennes, des déploiements hétérogènes, et des systèmes de commande de puissance de la liaison montante. L'ensemble de ces propositions a été validé par un grand nombre de simulations. Le cadre mathématique développé dans cette thèse se veut général, et doit pouvoir s'appliquer à un nombre d'autres scénarios importants. L'intérêt de l'approche proposée est de permettre une évaluation des performances au travers de l'évaluation des formules, et permettent en conséquences d'éviter des simulations qui peuvent prendre énormément de temps en terme de développement ou d'exécution.

Mots clefs : Géométrie stochastique, réseaux cellulaires, LTE-A, processus de Poisson, Évaluation de performances, probabilité d'erreur, probabilité de couverture, taux de couverture.

Contents

Acknowledgements i

Abstract (English/Français) iii

Acronyms xi

Notation xv

List of figures xvii

List of tables xix

1 Introduction 1

1.1 Background . . . 3

1.1.1 LTE-A Cellular Networks . . . 3

1.1.2 Challenges in the Mathematical Analysis of Cellular Networks . . . 3

1.2 Stochastic Geometry: A Powerful Tool to the Mathematical Analysis of Cellular Networks . . . 4

1.2.1 State of the Art . . . 5

1.2.2 Methodologies . . . 8

1.3 Thesis Overview and Major Contributions . . . 10

1.4 Publications . . . 12

2 A Mathematical Framework to the Computation of the Error Probability of Downlink MIMO Cellular Networks by Using Stochastic Geometry 17

2.1 Related Work and Contributions . . . 20

2.2 System Model . . . 21

2.3 Downlink SISO Cellular Networks . . . 24

2.3.1 Characteristic Function of the Other-Cell Interference . . . 25

2.3.2 Average Pairwise Error Probability: Exact Analysis . . . 28

2.3.3 Average Pairwise Error Probability: Asymptotic Analysis . . . 30

2.3.4 Average Pairwise Error Probability: Piecewise Single-Integral Bounds . . . 30

2.3.5 Nearest Neighbor Approximation of the Average Symbol Error Probability 31

2.3.6 On the Computation of Hypergeometric Functions: The Need for Approximations . . . 31

2.4 Downlink MIMO Cellular Networks . . . 33
2.4.1 Characteristic Function of the Other-Cell Interference at the Output of the Demodulator . . . 33
2.4.2 Average Pairwise Frame Error Probability: Exact Analysis . . . 35
2.4.3 Nearest Neighbor Approximation of the Average Frame Error Probability 36
2.5 Insights from the Mathematical Framework: Main Performance Trends . . . 38
2.6 Numerical and Simulation Results . . . 41
2.7 Conclusion . . . 50
2.8 Appendices . . . 51
2.8.1 Proof of Theorem 2.1 . . . 51
2.8.2 Proof of Lemma 2.1 . . . 52
2.8.3 Proof of Theorem 2.2 . . . 53
2.8.4 Proof of Proposition 2.5 . . . 54
2.8.5 Proof of Theorem 2.3 . . . 54
2.8.6 Proof of Theorem 2.4 . . . 55
2.8.7 Proof of Proposition 2.6 . . . 55

3 Stochastic Geometry Modeling and Analysis of Downlink MIMO Cellular Networks Using the Gil-Pelaez Inversion Theorem 57
3.1 Introduction . . . 60
3.2 System Model . . . 61
3.2.1 PPP-Based Cellular Networks Modeling . . . 61
3.2.2 Problem Formulation . . . 61
3.3 MIMO Transmission Schemes in Downlink Cellular Networks . . . 62
3.3.1 Spatial Multiplexing and Per-Stream ZF Receiver . . . 62
3.3.2 Orthogonal Space-Time Block Coding . . . 63
3.3.3 Fixed Rate SVD Multiplexing . . . 64
3.3.4 MIMO MRC . . . 65
3.3.5 Selection Diversity and Combining . . . 66
3.4 Gil-Pelaez Based Mathematical Frameworks to the Computations of Coverage and Rate . . . 67
3.4.1 Coverage Probability . . . 67
3.4.2 Average Rate . . . 68
3.5 Case Study: Coverage and Rate in Downlink Cellular Networks with Gamma Distributed Per-Link Power Gains . . . 68
3.5.1 Coverage Probability . . . 69
3.5.2 Average Rate . . . 70
3.6 Case Study: Service Success Probability in Partially Loaded Downlink Cellular Networks . . . 71
3.6.1 Modified System Model and Problem Formulation . . . 71
3.6.2 Load Modeling . . . 72
3.6.3 Service Success Probability . . . 74

3.7 Numerical and Simulation Results . . . 75
3.8 Conclusion . . . 78
3.9 Appendices . . . 80
3.9.1 Proof of Theorem 3.1 . . . 80
3.9.2 Proof of Proposition 3.6 . . . 80

4 Stochastic Geometry Modeling, System-Level Analysis and Optimization of Uplink Heterogeneous Cellular Networks with Multi-Antenna Base Stations 81
4.1 Introduction . . . 84
4.1.1 Challenges in Stochastic Geometry Modeling of the Uplink . . . 84
4.1.2 Related Work . . . 84
4.1.3 Contributions . . . 85
4.2 System Model . . . 86
4.2.1 PPP-Based Cellular Networks Modeling . . . 87
4.2.2 Channel Modeling . . . 87
4.2.3 Cell Association Modeling . . . 88
4.2.4 Power Control Modeling . . . 89
4.2.5 Signal Model and Demodulator . . . 90
4.2.6 Problem Statement . . . 92
4.2.7 Preliminaries . . . 93
4.3 System-Level Analysis of Maximum Ratio Combining . . . 95
4.3.1 Coverage Probability . . . 96
4.3.2 Average Rate . . . 99
4.3.3 Massive MIMO Regime . . . 100
4.4 System-Level Analysis of Optimum Combining . . . 102
4.4.1 Coverage Probability . . . 103
4.4.2 Average Rate . . . 107
4.4.3 Massive MIMO Regime . . . 107
4.5 System-Level Optimization . . . 109
4.6 Numerical and Simulation Results . . . 110
4.7 Conclusion . . . 117
4.8 Appendices . . . 119
4.8.1 Proof of Proposition 4.1 . . . 119
4.8.2 Proof of Proposition 4.3 . . . 120

5 Conclusion and Future Work 125
5.1 Conclusion . . . 126
5.2 Future Work . . . 126
5.2.1 Millimeter Wave Cellular Networks . . . 127
5.2.2 Interference-Aware Uplink Power Control Schemes . . . 129
5.2.3 Non-PPP Abstraction Models . . . 130

A Basic Properties of the Poisson Point Process 133

B Simulation Results: Interference–Aware Power Control in Uplink Cellular Networks 137

Reference 143

Acronyms

AFEP	Average Frame Error Probability
APEP	Average Pairwise Error Probability
ASEP	Average Symbol Error Probability
AWGN	Additive White Gaussian Noise
BS	Base Station
BPP	Binomial Point Process
CCDF	Complementary Cumulative Distribution Function
CDF	Cumulative Distribution Function
CDMA	Code Division Multiple Access
CF	Characteristic Function
CSI	Channel State Information
E-UTRAN	Evolved Universal Terrestrial Access Network
GHQ	Gauss-Hermite Quadrature
GPP	Ginibre Point Process
HCPP	Hard Core Point Process
LTE	Long Term Evolution
LTE-A	Long Term Evolution Advanced
LOS	Line of Sight
MC	Monte Carlo
MGF	Moment Generating Function
MMSE	Minimum Mean Square Error

mmWave	Milimeter Wave
ML	Maximum Likelihood
MIMO	Multiple Input Multiple Output
MRC	Maximal Ratio Combining
MRT	Maximum Ratio Transmission
MT	Mobile Terminal
NN	Nearest Neighbor
NLOS	Non Line of Sight
OC	Optimum Combing
OSTBC	Orthogonal Space-Time Block Coding
PCP	Poisson Cluster Process
PDF	Probability Distribution Function
PGFL	Probability Generating Functional
PHCP	Poisson hard-core process
PEP	Pairwise Error Probability
PMF	Probability Mass Function
PP	Point Process
PPP	Poisson Point Process
PSK	Phase-Shift Keying
PSD	Power Spectral Density
QAM	Quadrature Amplitude Modulation
RV	Random Variable
SD	Selection Diversity
SDMA	Space Division Multiple Access
SNR	Signal-to-Noise Ratio
SINR	Signal-to-Interference-plus-Noise Ratio
SIR	Signal-to-Interference Ratio

SISO	Single Input Single Output
SMX	Spatial Multiplexing
SP	Strauss process Strauss process
SVD	Singular Value Decomposition
SUBF	Single User Beamforming
UMTS	Universal Mobile Telecommunications System
ZF	Zero Forcing
3GPP	The 3rd Generation Partnership Project

Notation

The following notation is used throughout this thesis.

e	the Euler's number
γ_{EM}	the Euler-Mascheroni constant
j	the imaginary unit $j = \sqrt{-1}$
$(\cdot)_k$	the Pochhammer symbol
z	a complex number; a scaler
$\lvert z \rvert$	the modulus of z
$\arg\{z\}$	the phase of z
$\mathbb{C}$	the field of complex numbers
$\mathbb{S}$	a set
$\mathrm{card}\{\mathbb{S}\}$	the cardinality of the set $\mathbb{S}$
$\mathbf{x}$	a vector
$\mathbf{x}^{(l)}$	the lth entry of $\mathbf{x}$
$\lVert \mathbf{x} \rVert$	the norm of $\mathbf{x}$
$\mathbf{X}$	a matrix
$\mathbf{X}^{(l,m)}$	the (l,m)th entry of $\mathbf{X}$
$\lVert \mathbf{X} \rVert$	the Frobenius norm of $\mathbf{X}$
$vec(\mathbf{X})$	the vectorization of $\mathbf{X}$
$\mathbf{I}_N$	a $N \times N$ identity matrix
$\mathbf{0}_N$	a $N \times N$ all-zero matrix
$(\cdot)^T$	the transpose operator
$(\cdot)^H$	the Hermitian operator
$[\cdot]_t$	the (t,t)-th element in a square matrix
$(\cdot)!$	the factorial operator
$\mathbb{1}(\cdot)$	the indicator function
$\min\{\cdot,\cdot\}$	the minimum function
$\max\{\cdot,\cdot\}$	the maximum function
$\binom{n}{k}$	the binomial coefficient
$f^{(n)}(t)$	the nth derivative of $f(t)$
$\mathrm{Re}\{\cdot\}$	the real part operator
$\mathrm{Im}\{\cdot\}$	the imaginary part operators
$\mathbb{E}\{\cdot\}$	the expectation operator

$\Pr\{\cdot\}$	the probability measure function
$\exp\{\cdot\}$	the exponential function

The following definitions are used for random variables (RVs) X and Y.

$f_X(\cdot)$	the Probability Density Function (PDF) of X
$F_X(\cdot)$	the Cumulative Distribution Function (CDF) of X $F_X(\xi) = \Pr\{X \leq \xi\}$
$\bar{F}_X(\cdot)$	the Complementary CDF (CCDF) of X $\bar{F}_X(\xi) = 1 - F_X(\xi)$
$\mathscr{M}_X(\cdot)$	the Moment Generating Function (MGF) of X:
	if X is real, $\mathscr{M}_X(s) = \mathbb{E}_X\{\exp(-sX)\}$
$\psi_X(\cdot)$	the Characteristic Function (CF) of X:
	if X is real, $\psi_X(\omega) = \mathbb{E}_X\{\exp(j\omega X)\}$;
	if X is complex, $X = \mathrm{Re}\{X\} + j\mathrm{Im}\{X\} = X^{(\mathrm{re})} + jX^{(\mathrm{im})}$, let $\boldsymbol{\omega} = (\omega_1, \omega_2)$
	$\psi_X(\boldsymbol{\omega}) = \mathbb{E}_X\{\exp\{j\boldsymbol{\omega}X\}\} = \mathbb{E}\{\exp\{j(\omega_1 X^{(\mathrm{re})} + \omega_2 X^{(\mathrm{im})})\}\}$
$X \overset{d}{=} Y$	the RVs X and Y are equal in distribution

The following distributions of the RV X are used throughout this thesis.

$\mathscr{N}(\mu, \sigma^2)$	a real Gaussian distribution with mean μ and variance σ^2
$\mathscr{CN}(\mu, \sigma^2)$	a complex Gaussian distribution with mean μ and variance σ^2
$\mathscr{U}(a, b)$	a uniform distribution in (a, b)
$\mathrm{Gamma}(m, \Omega)$	a Gamma distribution with PDF as $f_X(\xi) = \frac{m^m \xi^{m-1}}{\Omega^m \Gamma(m)} \exp\left(-\frac{m}{\Omega}\xi\right)$ [60, Eq. (2.21)]
$\mathrm{LogN}(\mu, \sigma^2)$	a Log-Normal distribution with PDF of $10\log_{10}(X)$ as $f_{10\log_{10}(X)}(\xi) = \frac{10\log_{10}(e)}{\sqrt{2\pi\sigma^2}\xi} \exp\left(-\frac{(10\log_{10}(\xi)-\mu)^2}{2\sigma^2}\right)$ [60, Sec. 2.2.3.1]
$\mathrm{Gamma/LogN}(m, \eta, \sigma^2)$	a Gamma distribution by conditioning upon its mean power, which follows a Log-Normal distribution [60, Sec. 2.2.3.1]

The following special functions are used throughout this thesis.

$\Gamma(\cdot)$	the Gamma function [56, Eq. 6.1.1]
$\Gamma(\cdot, \cdot)$	the upper-incomplete Gamma function
$\mathrm{erf}(\cdot)$	the error function [56, Eq. 7.1.1]
$U(\cdot, \cdot, \cdot)$	the Tricomi confluent hypergeometric function [57]
${}_pF_q(a_1, \ldots, a_p; b_1, \ldots, b_q; \cdot)$	the generalized hypergeometric function [57, Ch. IV]
$G_{\tilde{p},\tilde{q}}^{\tilde{m},\tilde{n}}\left((\cdot) \middle\vert \begin{matrix}(\mathbf{a}_{\tilde{p}})\\(\mathbf{b}_{\tilde{q}})\end{matrix}\right)$	the Meijer G-function [58, Sec. 2.24]

List of Figures

2.1 Illustration of a PPP-based cellular network deployment. 22
2.2 Illustration of the accuracy of the GHQ closed-form approximation in (2.10). . . 27
2.3 Accuracy of the approximations in (2.19) (top) and (2.20) (bottom). 33
2.4 ASEP/AFEP of a $N_t \times N_r$ system against the reference SNR $E/\mathcal{N}_0$: comparison between PPP- and grid-based abstraction models. 43
2.5 ASEP of a $N_t \times N_r = 1 \times 1$ system against the reference SNR $E/\mathcal{N}_0$. 44
2.6 ASEP of a $N_t \times N_r = 1 \times 1$ system against the reference SNR $E/\mathcal{N}_0$. 45
2.7 ASEP/AFEP of a $N_t \times N_r = N_t \times 2$ system against the reference SNR $E/\mathcal{N}_0$. . . . 46
2.8 ASEP of a $N_t \times N_r = 1 \times 1$ system against the reference SNR $E/\mathcal{N}_0$. 46
2.9 ASEP of a $N_t \times N_r = 1 \times 1$ system against the reference SNR $E/\mathcal{N}_0$. 47
2.10 AFEP of a $N_t \times N_r = 2 \times 2$ system against the reference SNR $E/\mathcal{N}_0$. 47
2.11 ASEP/AFEP of a $N_t \times N_r$ system against the reference SNR $E/\mathcal{N}_0$. 48
2.12 ASEP/AFEP of a $N_t \times N_r$ system against the reference SNR $E/\mathcal{N}_0$. 48
2.13 AFEP of a $N_t \times N_r$ system providing Rate = 4 bpcu against the reference SNR $E/\mathcal{N}_0$. 49
2.14 AFEP of a $N_t \times N_r = N_t \times 2$ system providing Rate = 4 bpcu against the reference SNR $E/\mathcal{N}_0$. 49

3.1 $\mathrm{P}_{\mathrm{cov}}^{[\infty]}(\cdot)$ as a function of T and $\mathscr{K} = (\Omega_0/\Omega_I)(1/m_0)$. 76
3.2 $\mathscr{R}^{[\infty]}$ as a function of $\mathscr{K} = (\Omega_0/\Omega_I)(1/m_0)$ and α. 76
3.3 $\mathrm{P}_{\mathrm{service}}^{[\infty]}(\cdot)$ and $\tilde{\mathrm{P}}_{\mathrm{cov}}^{[\infty]}(\cdot)$ of different MIMO transmission schemes. 77
3.4 The impact of N_{RB} and $\lambda^{(\mathrm{MT})}/\lambda$ on $\mathrm{P}_{\mathrm{service}}^{[\infty]}(\cdot)$. 78

4.1 Void probability of an area A of radius R_{A} centered at the origin ($\mathsf{A} = \pi\mathsf{R}_{\mathsf{A}}^2$). . . . 111
4.2 Validation of the proposed mathematical frameworks against those in [50] (a) and [48] (b). 112
4.3 Percentile and average rate of OC and MRC as a function of ε. 113
4.4 Percentile and average rate of OC and MRC as a function of ε. 114
4.5 Average transmit power of the typical MT as a function of ε. 114
4.6 5th percentile rate of OC and MRC as a function of the number of receive antennas (N_1). 115
4.7 90th percentile rate of OC and MRC as a function of the number of receive antennas (N_1). 116

4.8 Percentile and average rate of a two-tier cellular network corresponding to the optimal pair $\left(\hat{\mathscr{T}}_{\text{opt}}, \varepsilon_{\text{opt}}\right)$. 117

B.1 MT transmit power $\mathscr{P}_{\text{MT}}$ (mean and standard deviation) against (a) ε, (b) $P_{\max}$ and (c) $P_0^{(I)}$, respectively. 139
B.2 Coverage Probability against the reliability threshold. 139
B.3 (a) Average rate, (b) 5^{th} percentile rate and (c) 90^{th} percentile rate against N_R. . 140
B.4 (a) Average rate, (b) 5^{th} percentile rate and (c) 90^{th} percentile rate against ε . . 141
B.5 (a) Average rate, (b) 5^{th} percentile rate and (c) 90^{th} percentile rate against $P_{\max}$ 141
B.6 (a) Average rate, (b) 5^{th} percentile rate and (c) 90^{th} percentile rate against $P_0^{(I)}$. 142

List of Tables

1.1 3GPP LTE-A Requirements. 3
1.2 Prior works on the mathematical modeling of cellular networks based on the PPP-based abstraction model. 9

3.1 MIMO Transmission Schemes in Downlink Cellular Networks. 62

4.1 Optimal pair $\left(\hat{\mathcal{T}}_{\text{opt}}, \varepsilon_{\text{opt}}\right)$ corresponding to the case studies of Fig. 4.8. 117

B.1 Simulation Parameters: Interference–Aware Power Control in Uplink Cellular Networks 138

1 Introduction

This chapter begins with *Section 1.1* which introduces the LTE-A cellular networks and challenges in the mathematical analysis of such networks. *Section 1.2* provides a comprehensive literature review on the research work on the stochastic geometry analysis of wireless communications systems with Poisson Point Process (PPP) based abstraction models. *Section 1.3* highlights the major contributions in this thesis work and the organization of the thesis. *Section 1.4* provides lists of publications produced during my Ph.D. candidature.

1.1 Background 3

1.1.1 LTE-A Cellular Networks 3

1.1.2 Challenges in the Mathematical Analysis of Cellular Networks 3

1.2 Stochastic Geometry: A Powerful Tool to the Mathematical Analysis of Cellular Networks 4

1.2.1 State of the Art 5

1.2.2 Methodologies 8

1.3 Thesis Overview and Major Contributions 10

1.4 Publications 12

1.1 Background

1.1.1 LTE-A Cellular Networks

Long Term Evolution - Advanced (LTE-A) is one of current major mobile communication standards. It was standardized by the 3rd Generation Partnership Project (3GPP) in March 2011 as 3GPP Release 10 [1]. It is intended to satisfy the ever growing demands on data rates and to improve the capacity and coverage. The main requirements for LTE-A cellular networks are identified in [1], some of which are summarized in the *Table 1.1*.

Table 1.1: 3GPP LTE-A Requirements (Spectrum Efficiency is for base station (BS) with 4 antennas and mobile terminal (MT) with 2 antennas).

Peak Data Rate (Downlink)	1 Gbps
Peak Data Rate (Uplink)	500 Mbps
Spectrum Allocation	Up to 100 MHz
Latency (User Plane)	10 ms
Latency (Control Plane)	50 ms
Spectrum Efficiency (Peak, Downlink)	30 bps/Hz
Spectrum Efficiency (Peak, Uplink)	15 bps/Hz
Spectrum Efficiency (Average, Downlink)	2.6 bps/Hz
Spectrum Efficiency (Average, Uplink)	2.0 bps/Hz
Spectrum Efficiency (Cell-Edge, Downlink)	0.09 bps/Hz
Spectrum Efficiency (Cell-Edge, Uplink)	0.07 bps/Hz

To achieve these technical requirements, LTE-A pushes the cells closer together and brings networks closer to the user by adding many low-power nodes, for example, micro-, pico-, femto- BSs in the coverage area of macro BSs to improve the coverage and rate performance. Thus, topologically, heterogeneous deployment is emerging where smaller cells are located heterogeneously in the networks. Heterogeneous deployment is one of the most important new features supported by LTE-A. The other enhancement features include carrier aggregation, relaying and advanced Multiple Input Multiple Output (MIMO) transmission [1, 2].

The heterogeneous deployment in LTE-A cellular networks leads to a more flexible and irregular network topology and co-channel interference from other cells becomes one of the dominant factors of the network performance. To deal with the irregular topology and to better understand the network interference, mathematical modeling and analysis is a necessary task and it is the direct motivation of the research work reported in this thesis.

1.1.2 Challenges in the Mathematical Analysis of Cellular Networks

The mathematical modeling of cellular networks is usually performed through abstraction models, which rely upon simplified spatial models for the locations of the BSs. Common

approaches include the Wyner model, the single-cell interfering model and the hexagonal grid model [3, 4, 5]. However, these abstraction models are either inaccurate for many operating conditions or they require extensive numerical computations [6, 7]. As a result, the analysis and design of cellular networks is often conducted by resorting to network simulations for selected scenarios, which represent specific arrangements of BSs. More specifically,

- in [3], the capacity of multi-cell systems is evaluated by presuming a one dimension arrangement of BSs and a unit gain from each BS to the tagged MT and an equal gain that is less than one to the two MTs in the two neighboring cells. However, the Wyner model and related mean-value approaches are particularly inaccurate, unless there is a very large amount of interference averaging over space, such as in the uplink of heavily-loaded CDMA systems [8].

- In [4], a two-cell multi-antennas system is studied and the interference is assumed from a single interfering cell. However, the single-cell interfering model obviously neglects most sources of interference in the network and is over-simplified.

- In [5], the concept of the cellular network arrangement and certain mathematical properties of hexagonal cellular geometry are introduced. Although widely accepted, the hexagonal grid model has important limitations as well: i) the resulting Signal-to-Interference-plus-Noise-Ratio (SINR) by using the hexagonal grid model is still a random variable (RV), thus, commonly complicated and time-consuming Monte Carlo simulations are needed and they rarely provide insights in network designs and optimization; ii) the grid-based abstraction model is increasingly inaccurate for heterogeneous deployments of network elements in today's LTE-A cellular networks, where the cell size of a BS varies considerably, for example, in macro, micro, pico and femto cells.

1.2 Stochastic Geometry: A Powerful Tool to the Mathematical Analysis of Cellular Networks

To circumvent the accuracy problems and tractability problems, a new abstraction model to the mathematical analysis of cellular networks is emerging, which is referred to as Poisson Point Process (PPP)-based abstraction [6, 7, 10, 11, 12]. With the aid of this abstraction model, in single-tier cellular networks, the locations of the BSs are modeled as points of a homogeneous PPP. Meanwhile, the multi-tier heterogeneous cellular networks can be modeled as the superposition of many tiers of BSs having different transmit powers, densities, path-loss exponents, fading parameters and distributions, and flexible bias factors for various tier association schemes. And the positions of the BSs in each tier are modeled as points of an independent PPP.

Recent results have confirmed that the PPP-based abstraction model is capable of accurately reproducing the main structural characteristics of operational cellular networks [13, 14, 15]:

- in [13], the authors compare the PPP-based and the hexagonal grid-based abstraction models with real base station deployments in urban areas worldwide provided by the open source project OpenCellID and show that the PPP-based abstraction model gives upper bounds of the coverage probabilities for urban areas and is more accurate than the hexagonal grid model.

- In [14], the authors introduce the concept of "deployment gain", which allows one to carry out the analysis based on the mathematically tractable PPP-based abstraction model, subject to a correction factor (*i.e.*, the deployment gain) that can be estimated and taken into account for a better and more accurate system design and optimization.

- In [15], the authors investigate the accuracy of PPP-based abstraction model, by explicitly taking realistic base station locations, building footprints, spatial blockages and antenna radiation patterns into account. It confirms that the abstraction model based on stochastic geometry is capable of accurately modeling the communication performance of cellular networks in dense urban environments.

The usefulness of the PPP-based abstraction model originates from its analytical tractability and from the possibility of leveraging mathematical tools from applied probability, such as stochastic geometry, for mathematical performance analysis [16, 17, 18]. Some basic definitions, properties and theorems of the PPP are introduced in *Appendix A*.

1.2.1 State of the Art

The PPP-based abstraction model is now routinely used to the analysis and design of wireless networks in general and cellular networks in particular. [19] provides a comprehensive literature survey till year 2013. Notable examples include [6, 7], [20]–[53].

Wireless Networks in the Presence of a Poisson Field of interferers Interferes in wireless networks, including ad hoc networks, cognitive radio networks, and underlay device-to-device wireless networks, *etc.*, can be modeled as a Poisson field of interferers, where the distance from the transmitter to the receiver is fixed and the interferers can be closer to the receiver than the intended transmitter. Error probability, outage probability and ergodic capacity in such wireless networks in the presence of a Poisson field of interferers have been studied in the literature [20]–[28]. For example,

- in [20], a mathematical framework based on characterizing the aggregate interference as an symmetric alpha-stable ($S\alpha S$) random variable has been introduced.

- In [22], the ergodic capacity of a multi-cell multi-antenna cooperative cellular network with co-channel interference is studied. The approach relies upon an interference model based on the $S\alpha S$ distribution.

- In [24], a comprehensive framework is introduced for computing the error probability of a multi-antenna receiver in the presence of different models of network interference.
- In [25], by considering a similar interference model as in [24], the outage probability is studied.
- In [26], the effect of spatial interference correlation on the performance of maximum ratio combining is investigated.

Downlink Cellular Networks In cellular networks, where the BS-to-MT cell association policy is considered, the PPP-based abstraction has also been successfully applied for the modeling of other-cell interference, characterization of SINR and performance analysis of coverage and rate, for example, in single-tier downlink cellular networks [6, 29], multi-antenna cellular networks [30, 31], heterogeneous cellular networks [7, 32, 33, 35, 36, 42], and millimeter-wave cellular networks [44, 45, 46]. More specifically,

- in [6], the coverage probability and the average rate of cellular networks for transmission over Rayleigh fading channels are computed in closed-form.
- In [7], the authors introduce a framework for computing the average rate of heterogeneous cellular networks with biased cell association and for transmission over general fading channels.
- In [32], the framework of [6] is extended to heterogeneous cellular networks, which are modeled as the superposition of many PPPs.
- In [33], the authors study heterogeneous cellular networks based on the PPP-based abstraction model by assuming a cell association criterion based on the maximum SINR. The analysis in [33] assumes that the SINR threshold is greater than 0 dB. This assumption is removed in [34], where arbitrary SINR thresholds are considered.
- In [35], the framework in [34] is generalized for a biased cell association criterion.
- In [36], the framework in [32] is generalized by studying heterogeneous cellular networks that employ a biased cell association criterion.
- In [30], MIMO cellular networks are studied with the aid of tools from stochastic geometry and stochastic ordering. Various downlink MIMO transmission schemes are studied and compared, including Space Division Multiple Access (SDMA), Single User Beamforming (SUBF) and the baseline Single-Input-Single-Output (SISO) transmission.
- In [41], the authors incorporate the load characteristics of the BSs into the mathematical framework, by using a conditionally thinning approach.

Uplink Cellular Networks A few researchers have developed mathematically tractable yet accurate analytical frameworks for the uplink of heterogeneous cellular networks. The following contributions are worth being mentioned:

- In [47], the authors study single-tier cellular networks with fractional power control.
- In [48], the authors study cellular networks with truncated channel inversion power control.
- In [49], the authors study two-tier cellular networks with power control and a biased cell association. The point process of the interfering MTs is modeled using a thinning approach based on curve fitting.
- In [50], the authors study multi-tier cellular networks with fractional power control and a weighted cell association. Similar to [49], a thinning-based approach for modeling the point process of the interfering MTs is used. The proposed method, however, does not require any fitting based on simulations. Also, the optimality of using a decoupled downlink/uplink association is mathematically assessed.
- In [51], the authors study, from a utility optimization standpoint, multi-tier cellular networks with fractional power control and a weighted cell association. To this end, a utility function based on the proportionally fair criterion is introduced and optimized.
- In [52], the authors study two-tier cellular networks to characterize the association probabilities of downlink and uplink transmissions.
- In [53], the authors generalize [52]. They study the rate of the typical MT and validate their findings against a real-world system-level simulator.

Non-PPP Abstraction Models The PPP-based abstraction model has some fundamental limitations because it assumes the mutual independence among all points in the point process, which allows two points to be arbitrarily close to each other. It is then not suitable for networks with repulsion, where the locations of points are spatially correlated. Some more realistic abstraction models than the PPP have been considered in the following notable papers:

- In [14], the authors use the Poisson hard-core process (PHCP), the Strauss process (SP), and the perturbed triangular lattice to model the locations of BSs in real cellular networks and introduce the “deployment gain” to measure how close a point set is to the PPP and to further compare the performance of different models analytically.
- In [19], as a survey, the authors introduce other popular PPs other than PPP used in modeling wireless communications systems, including the Binomial Point Process (BPP), the Hard Core Point Process (HCPP) and the Poisson Cluster Process (PCP).

- In [106], the authors introduce the Ginibre point process (GPP) to model the wireless networks with repulsion and compute the mean and variance of the interference by the Palm measure approach and the reduced second moment approach.

However, the non-PPP abstraction models are usually not mathematically tractable as PPP-based abstraction model. Thus, the latter is the main focus of this thesis and a brief summary of prior work on the stochastic geometry analysis of cellular networks based on the PPP-based abstraction model is available in Table 1.2.

1.2.2 Methodologies

Different techniques to the mathematical modeling and performance evaluation of cellular networks based on stochastic geometry have been reported [19]. To the best of the authors knowledge, eight techniques are commonly used to the computation of important performance metrics, which include coverage probability, average rate and error probability. They offer a different trade-off in terms of modeling accuracy, mathematical tractability, numerical complexity, *etc.* [19, Sec. III-F]. These techniques can be classified as based on:

- the Rayleigh fading assumption [19, Sec. III-A], [6];
- the dominant or nearest interferers approximation [19, Sec. III-B];
- approximations of the distribution of the other-cell interference [19, Sec. III-C];
- the Plancherel-Parseval theorem that is applicable to arbitrary fading for the desired link [19, Sec. III-D], [6];
- numerically inverting the Moment Generating Function (MGF) of the other-cell interference [19, Sec. III];
- MGF-based equivalent representations of the performance metrics of interest [7];
- equivalent in distribution representations of the other-cell interference [29]
- the direct computation of spatial averages without using the MGF [38].

Table 1.2: Prior works on the mathematical modeling of cellular networks based on the PPP-based abstraction model (ZF = Zero-Forcing; SMX = Spatial Multiplexing).

Reference	Single-Tier/Multi-Tier	Downlink/Uplink	SISO/MIMO	Cell Association	Performance Metric
[6]	Single-Tier	Downlink	SISO	Shortest Distance	Coverage and Rate
[7]	Multi-Tier	Downlink	SISO	Shortest Distance	Rate
[30]	Multi-Tier	Downlink	MIMO(SDMA,SUBF)	max Received Power	Coverage and Rate
[32]	Multi-Tier	Downlink	SISO	Shortest Distance	Camping Probability
[33]	Multi-Tier	Downlink	SISO	max-SINR (> 0 dB)	Coverage and Rate
[34]	Multi-Tier	Downlink	SISO	max-SINR	Coverage
[35]	Multi-Tier	Downlink	SISO	max-SINR with Bias	Coverage
[36]	Multi-Tier	Downlink	SISO	Shortest Distance with Bias	Coverage and Rate
[41]	Multi-Tier	Downlink	SISO	max-SINR with Load	Coverage
[37]	Multi-Tier	Downlink	MIMO(ZF)	Fixed Distance	Coverage and Rate
[47]	Single-Tier	Uplink	SISO	Shortest Distance	Coverage
[48]	Multi-Tier	Uplink	SISO	Shortest Distance	Outage
[49, 50]	Multi-Tier	Uplink	SISO	Weighted Association	Coverage and Rate
[51]	Multi-Tier	Uplink	SISO	Weighted Association	Coverage and Rate
[52, 53]	Multi-Tier	Both	SISO	Weighted Association	Coverage and Rate

1.3 Thesis Overview and Major Contributions

The major contributions of this thesis are three-fold: i) this thesis studies the error performance mathematically in downlink MIMO cellular networks for the first time; ii) this thesis develops a general mathematical approach to the computation of coverage and rate in cellular networks; iii) this thesis proposes a novel and accurate modeling approach of uplink cellular networks, which is general and proven to be very useful in the uplink cellular system analysis and optimization.

Chapter 2 is on a mathematical framework to the computation of the error probability of downlink MIMO cellular networks by using stochastic geometry. Major contributions include:

- *Theorems 2.1* and *2.3*: The characteristic functions (CF) of other-cell interference in downlink SISO and MIMO cellular networks, respectively;
- *Theorem 2.2*: The exact mathematical formulation of the Average Pairwise Error Probability (APEP) in downlink SISO cellular networks, which is applicable to arbitrary distributions of the fading envelope;
- *Theorem 2.4*: The exact mathematical formulation of the Average Pairwise Frame Error Probability ($\text{APEP}^{(\text{F})}$) in downlink MIMO cellular networks, which is applicable to arbitrary fading distributions on the useful link and to Rayleigh fading on the interfering links;
- *Corollaries 2.1* and *2.3* provide the simplified CF of other-cell interference for a constant-envelope modulation in downlink SISO and MIMO cellular networks, respectively;
- *Corollary 2.2* provides asymptotic analysis of APEP in the noise- and interference-limited regime of downlink SISO cellular networks;
- *Corollaries 2.4* and *2.5* provide approximate closed-form expressions of $\text{APEP}^{(\text{F})}$ in the noise- and interference-limited regime;
- *Propositions 2.1* and *2.2* provide CFs of other-cell interference with Gamma distributed and Gamma/Log-Normal distributed per-link power gains , respectively;
- *Propositions 2.3* and *2.4* provide APEPs with Gamma distributed and Gamma/Log-Normal distributed per-link power gains, respectively;
- *Proposition 2.5* provides APEP bounds based on *Theorem 2.4* and *Corollary 2.2*.

Chapter 3 is on stochastic geometry modeling and analysis in downlink MIMO cellular networks by using the Gil-Pelaez inversion theorem. Major contributions include:

- *Theorem 3.1*: The exact mathematical framework to compute coverage probability for a downlink cellular network with arbitrary per-link power gains;

- *Theorem 3.2*: The exact mathematical framework to compute average rate for a dowlink cellular network with arbitrary per-link power gains;
- *Theorem 3.3*: The exact mathematical framework to compute service success probability for a partially loaded cellular network with arbitrary per-link power gains;
- *Corollaries 3.1*, *3.2* and *3.3* provide asymptotic frameworks for the mathematical computation of coverage, average rate and service success probability in the interference-limited regime, respectively;
- *Propositions 3.1 – 3.5* confirm the applicability of proposed mathematical frameworks for downlink cellular networks with different MIMO transmission schemes.
- *Propositions 3.6* and *3.7* provide approximated close-form formulas for the mathematical computation of coverage and average rate in the interference-limited regime with Gamma distributed per-link power gains, respectively.
- *Propositions 3.9* and *3.11* provide BS inactive probability and MT selection probability on a randomly selected resource blocks in partially loaded cellular networks where N_{RB} resource blocks are available at each BS, respectively.

Chapter 4 is on stochastic geometry modeling, system-level analysis and optimization of uplink heterogeneous cellular networks with multi-antenna base stations. Maximum Ratio Combining (MRC) and Optimum Combining (OC) at the BSs are studied and compared. A generalized cell association criterion and fractional power control mechanism are considered. Major contributions include:

- *Proposition 4.1*: The exact mathematical framework to compute coverage probability for a heterogeneous uplink cellular networks with MRC receiver;
- *Proposition 4.2*: The exact mathematical framework to compute average rate for a heterogeneous uplink cellular networks with MRC receiver;
- *Proposition 4.3*: The exact mathematical framework to compute average rate for a heterogeneous uplink cellular networks with OC receiver;
- *Corollaries 4.3 – 4.7* provide simplified frameworks for relevant system setups based on Proposition 4.1;
- *Corollaries 4.8* and *4.9* provide asymptotic frameworks to compute coverage probability and average rate for massive MRC receiver;
- *Corollaries 4.10 – 4.18* provide simplified frameworks for relevant system setups based on *Proposition 4.3*;
- *Corollary 4.19* provides asymptotic frameworks to compute the coverage probability for massive OC receiver.

Chapter 5 concludes this thesis and proposes possible future work.

1.4 Publications

Journal Papers The following is a list of publications in refereed journals produced during my Ph.D. candidature. These journal papers [108, 109, 110] are used as the basis for this thesis .

(*J*1) M. Di Renzo and P. Guan, "A mathematical framework to the computation of the error probability of downlink MIMO cellular networks by using stochastic geometry", *IEEE Transactions on Communications*, vol. 62, no. 8, pp. 2860–2879, Aug. 2014. [108]
Abstract: In this paper, mathematical frameworks for system-level analysis and optimization of uplink heterogeneous cellular networks with multiple BSs antennas are introduced. MRC and OC at the BSs are studied and compared. A generalized cell association criterion and fractional power control mechanism are considered. The locations of each tier of BSs are modeled as points of homogeneous and independent Poisson point processes. With the aid of stochastic geometry, coverage and rate are formulated in integral but mathematically and computationally tractable expressions. Based on them, performance trends for small- and large-scale multi-antenna BSs are discussed. Coverage and rate are shown to highly depend on several parameters, including the path-loss exponent, the fractional power control compensation factor and the maximum transmit power of the mobile terminals. The gain of OC compared to MRC is shown to increase if a more aggressive power control is used and if the number of BSs antennas increases but is finite. For the same number of BSs antennas, OC is shown to reach the noise-limited asymptote faster than MRC. Based on the proposed frameworks, a heuristic algorithm for system-level optimization is proposed and its effectiveness is demonstrated with the aid of Monte Carlo simulations.

(*J*2) M. Di Renzo and P. Guan, "Stochastic geometry modeling of coverage and rate of cellular networks using the Gil-Pelaez inversion theorem", *IEEE Communications Letters*, vol. 18, no. 9, pp. 1575–1578, Sep. 2014. [109]
Abstract: In this Letter, we introduce new mathematical frameworks to the computation of coverage probability and average rate of cellular networks by relying on a stochastic geometry abstraction modeling approach. With the aid of the Gil-Pelaez inversion formula, we prove that coverage and rate can be compactly formulated as a two-fold integral for arbitrary per-link power gains. In the interference-limited regime, single-integral expressions are obtained. As a case study, Gamma distributed per-link power gains are investigated further and approximated closed-form expressions for coverage and rate in the interference-limited regime are obtained, which shed light on the impact of channel parameters and physical-layer transmission schemes.

(*J*3) P. Guan and M. Di Renzo, "Stochastic Geometry Modeling, System-Level Analysis and Optimization of Uplink Heterogeneous Cellular Networks with Multi-Antenna Base

Stations", *IEEE Transactions on Communications*, submitted, 2015. [110]
Abstract: In this paper, a mathematical framework to the computation of the error probability of downlink cellular networks is introduced. It is based on the PPP-based abstraction for modeling the spatial locations of the BSs and it exploits results from stochastic geometry for characterizing the distribution of the other-cell interference. The framework is applicable to spatial multiplexing MIMO systems with an arbitrary number of antennas at the transmitter (N_t) and at the receiver (N_r). If $N_t = N_r = 1$, the mathematical approach can be used for arbitrary fading distributions on both useful and interfering links. If either $N_t > 1$ or $N_r > 1$, it can be applied to arbitrary fading distributions on the useful link and to Rayleigh fading on the interfering links. It is shown that the proposed approach leads to easy-to-compute integral expressions, which reduce to closed-form formulas in some asymptotic regimes. Furthermore, the framework is shown to provide insights for system design and optimization. The accuracy of the mathematical analysis is substantiated through extensive Monte Carlo simulations for various cellular network setups.

Conference Papers The following is a list of publications in refereed conference proceedings produced during my Ph.D. candidature. The conference papers [111, 112, 113, 116] contain material overlapping with the journal publications. The conference papers [114, 115] contain material not presented in this thesis.

($C1$) P. Guan and M. Di Renzo, "Stochastic geometry analysis of the average error probability of downlink cellular networks", *2014 IEEE International Conference on Computing, Networking and Communications (ICNC)*, pp. 1–7, Feb. 2014. [111]
Abstract: In this paper, we introduce a mathematical framework for computing the average error probability of downlink cellular networks in the presence of other–cell interference, Rayleigh fading, and thermal noise. A stochastic geometry based abstraction model for the locations of the BSs is used, hence the BSs are modeled as points of a homogeneous spatial PPP. The MT is assumed to be served by the BS that is closest to it. The technical contribution of this paper is twofold: 1) we provide an exact closed–form expression of the Characteristic Function (CF) of the aggregate other–cell interference at the MT, which takes into account the shortest distance based cell association mechanism; and 2) by relying on the Gil-Pelaez inversion theorem, we provide an exact closed–form expression of the Average Pairwise Error Probability, which accounts for Rayleigh fading and for the spatial distribution of the BSs. From the APEP, the Average Symbol Error Probability is obtained by using the Nearest Neighbor (NN) approximation, which is shown to provide accurate estimates. Finally, the mathematical framework is substantiated through extensive Monte Carlo simulations and insights on the achievable performance are discussed.

($C2$) P. Guan and M. Di Renzo, "Stochastic Geometry Analysis of the Energy Efficiency of Downlink MIMO Cellular Networks", *2015 IEEE Vehicular Technology Conference Spring*

(VTC-Spring), vol., no., pp.1,5, 11-14 May 2015. [112]
Abstract: In this paper, an approximation to the mathematical evaluation of the spectral and energy efficiency of multi-antenna downlink cellular networks is introduced. The locations of the BSs are modeled as points of a PPP and stochastic geometry is used for system-level performance assessment. The approximation is applicable to spatial multiplexing MIMO systems having an arbitrary number of antennas at the transmitter (N_t) and at the receiver (N_r). A Rayleigh fading channel model is assumed. The accuracy of the proposed approximation is substantiated with the aid of Monte Carlo simulations.

($C3$) P. Guan; M. Di Renzo; C. Verikoukis and T. Q. Duong, "Error Probability of Downlink MIMO Cellular Networks by Using Stochastic Geometry", *2015 European Conference on Networks and Communications (EuCNC)*, to appear, July 2015. [113]
Abstract: In this paper, a mathematical framework to the computation of the error probability of downlink cellular networks is introduced. It is based on the PPP-based abstraction for modeling the spatial locations of the BSs and it exploits results from stochastic geometry for characterizing the distribution of the other-cell interference. The framework is applicable to spatial multiplexing MIMO systems with an arbitrary number of antennas at the transmitter (N_t) and at the receiver (N_r). It is shown that the proposed mathematical approach leads to easy-to-compute integral expressions, which reduce to closed-form formulas in some asymptotic regimes. The accuracy of the mathematical analysis is substantiated through extensive Monte Carlo simulations for various setups.

($C4$) P. Guan and M. Di Renzo, "Stochastic Geometry Modeling and Performance Evaluation of Downlink MIMO Cellular Networks", *2015 IEEE Vehicular Technology Conference Fall (VTC-Fall)*, to appear, Sept. 2015. [114]
Abstract: In this paper, a mathematical framework for evaluating the error probability of downlink MIMO cellular networks is introduced. It is based on the PPP-based abstraction for modeling the spatial locations of the BSs and it exploits results from stochastic geometry to characterize the distribution of the other-cell interference. The framework is applicable to spatial multiplexing MIMO systems with an arbitrary number of antennas at the transmitter (N_t) and at the receiver (N_r). It is shown that the proposed framework leads to easy-to-compute integral expressions, which provide insights for network design and optimization. The accuracy of the mathematical analysis is substantiated through extensive Monte Carlo simulations for various MIMO cellular network setups.

($C5$) P. Guan and M. Di Renzo, " Stochastic Geometry Analysis of Uplink Cellular Networks with Multi-Antenna Base Stations and Interference-Aware Fractional Power Control", *2015 IEEE International Conference on Computing, Management and Telecommunications (ComManTel)*, to appear, Dec. 2015. [115]
Abstract: In this paper, uplink cellular networks with multiantenna BSs and interference-aware power control are studied. The locations of the multi-antenna BSs are modeled as

points of a PPP, and MRC and Optimum Combining OC receivers are compared. Extensive system-level simulations are carried out and the impact of interference-unaware and interference-aware fractional power control is analyzed. Several numerical results and performance trends are illustrated in terms of coverage probability, rate and power consumption. It is shown that competing performance trends emerge for the achievable performance of cell-edge and cell-center MTs.

(*C*6) P. Guan and M. Di Renzo, "Stochastic Geometry Analysis and Optimization of Uplink Cellular Networks with Fractional Power Control and Optimum Combining", *2016 IEEE International Conference on Communications (ICC)*, submitted, 2015. [116]
Abstract: In this paper, mathematical frameworks for system-level analysis and optimization of uplink cellular networks with optimum combining receivers at multi-antenna BSs are introduced. Fractional power control is taken into account as well. The locations of the BSs are modeled as points of a homogeneous Poisson point process. With the aid of stochastic geometry, coverage and rate are formulated in integral but mathematically tractable expressions. Based on them, performance trends for small- and large-scale multi-antenna BSs are discussed. Coverage and rate are shown to be highly dependent on several parameters, including the path-loss exponent, the fractional power control compensation factor and the maximum transmit power of the mobile terminals. Based on the proposed frameworks, a heuristic algorithm for system-level optimization is proposed and its effectiveness is demonstrated with the aid of Monte Carlo simulations.

Best Paper Award The following is a list of awards during my Ph.D. candidature.

1. 2015 IEEE ComManTel Best Paper Award
   P. Guan and M. Di Renzo, " Stochastic Geometry Analysis of Uplink Cellular Networks with Multi-Antenna Base Stations and Interference-Aware Fractional Power Control", *2015 IEEE International Conference on Computing, Management and Telecommunications (ComManTel)*, to appear, Dec. 2015. [115]

2 A Mathematical Framework to the Computation of the Error Probability of Downlink MIMO Cellular Networks by Using Stochastic Geometry

Chapter 2. A Mathematical Framework to the Computation of the Error Probability of Downlink MIMO Cellular Networks by Using Stochastic Geometry

In this chapter, a mathematical framework to the computation of the error probability of downlink cellular networks is introduced. It is based on the PPP-based abstraction for modeling the spatial locations of the BSs and it exploits results from stochastic geometry for characterizing the distribution of the other-cell interference. The framework is applicable to spatial multiplexing MIMO systems with an arbitrary number of antennas at the transmitter (N_t) and at the receiver (N_r). If $N_t = N_r = 1$, the mathematical approach can be used for arbitrary fading distributions on both useful and interfering links. If either $N_t > 1$ or $N_r > 1$, it can be applied to arbitrary fading distributions on the useful link and to Rayleigh fading on the interfering links. It is shown that the proposed approach leads to easy-to-compute integral expressions, which reduce to closed-form formulas in some asymptotic regimes. Furthermore, the framework is shown to provide insights for system design and optimization. The accuracy of the mathematical analysis is substantiated through extensive Monte Carlo simulations for various cellular network setups.

The present chapter is organized as follows. In *Section 2.1*, the related work is reviewed and the major new contributions are summarized. In *Section 2.2*, the system model is introduced. In *Section 2.3*, a general mathematical framework to the computation of the error probability of downlink SISO cellular networks is proposed, which is applicable to arbitrary fading distributions. In *Section 2.4*, the mathematical analysis is extended to downlink spatial multiplexing MIMO cellular networks by assuming a Rayleigh fading channel model for the interfering BSs. In *Section 2.5*, the performance trends of downlink SISO and MIMO cellular networks are studied, as a function of system and channel parameters. In *Section 2.6*, numerical examples substantiating the mathematical findings are shown. Finally, *Section 2.7* concludes the present chapter.

2.1 Related Work and Contributions 20

2.2 System Model 21

2.3 Downlink SISO Cellular Networks 24

2.3.1 Characteristic Function of the Other-Cell Interference 25

2.3.2 Average Pairwise Error Probability: Exact Analysis 28

2.3.3 Average Pairwise Error Probability: Asymptotic Analysis 30

2.3.4 Average Pairwise Error Probability: Piecewise Single-Integral Bounds . . 30

2.3.5 Nearest Neighbor Approximation of the Average Symbol Error Probability 31

2.3.6 On the Computation of Hypergeometric Functions: The Need for Approximations 31

2.4 Downlink MIMO Cellular Networks 33

2.4.1 Characteristic Function of the Other-Cell Interference at the Output of the Demodulator . . . 33
2.4.2 Average Pairwise Frame Error Probability: Exact Analysis . . . 35
2.4.3 Nearest Neighbor Approximation of the Average Frame Error Probability 36
2.5 Insights from the Mathematical Framework: Main Performance Trends . . . 38
2.6 Numerical and Simulation Results . . . 41
2.7 Conclusion . . . 50
2.8 Appendices . . . 51
2.8.1 Proof of Theorem 2.1 . . . 51
2.8.2 Proof of Lemma 2.1 . . . 52
2.8.3 Proof of Theorem 2.2 . . . 53
2.8.4 Proof of Proposition 2.5 . . . 54
2.8.5 Proof of Theorem 2.3 . . . 54
2.8.6 Proof of Theorem 2.4 . . . 55
2.8.7 Proof of Proposition 2.6 . . . 55

2.1 Related Work and Contributions

As introduced in *Section 1.2.1*, notable examples on the stochastic geometry modeling and analysis of downlink cellular networks include [6, 7] and [31] – [46]. These papers mentioned above are focused on the computation of the coverage/outage probability and of the average rate of a typical MT. To the best of the authors knowledge, on the other hand, there are no mathematical frameworks to the analysis of the average error probability of PPP-based cellular networks. In addition, with the exception of a few papers, *e.g.*, [30], the mathematical analysis is limited to single-antenna BSs and to single-antenna MTs. Compared to [30], in particular, the present chapter has three main differences: i) the performance metrics are different. In the present chapter, we focus our attention on the error probability, while the authors of [30] study coverage probability and area spectral efficiency; ii) the downlink MIMO transmission schemes are different. In the present chapter, we focus our attention on open-loop spatial multiplexing, while the authors of [30] study closed-loop SDMA and SUBF. As discussed in [30], several downlink MIMO transmission schemes exist in the literature, each one having its own advantages and disadvantages. Open-loop spatial multiplexing MIMO is a practical case study that it is usually considered for its mathematical tractability and practical applications; and iii) the method of analysis is different. In [30], the authors exploit stochastic ordering for performance analysis and comparison. On the other hand, other tools are used in the present chapter, as detailed in what follows. The only exception to this *status quo* is [29], which was submitted during my Ph.D. candidature. It considers, however, only single-antenna BSs and single-antenna MTs.

Indeed, error probability, outage probability and ergodic capacity in the presence of a Poisson field of interferers have been studied in the literature [20]–[28]. These frameworks, however, are not applicable to cellular networks, since the BS-to-MT cell association is neglected. The interferers are, in fact, assumed to be arbitrarily close to the typical MT, even closer than the serving BS. Thus, they are applicable to, *e.g.*, ad hoc, cognitive and underlay device-to-device wireless networks, where the distance from the transmitter to the receiver is fixed and the interferers can be closer to the receiver than the intended transmitter.

Motivated by these considerations, in the present chapter we introduce a mathematical framework for computing the error probability of spatial multiplexing MIMO cellular networks, by explicitly taking into account the cell association criterion based on the shortest BS-to-MT distance. The framework is applicable to cellular networks where the locations of the BSs are modeled according to a homogeneous PPP, the downlink channels experience independent and identically distributed fading and an arbitrary number of antennas is available at the BSs (N_t) and at the MT (N_r). If $N_t = N_r = 1$, the mathematical approach is applicable to arbitrary fading distributions on both useful and interfering links. If either $N_t > 1$ or $N_r > 1$, it can be applied to arbitrary fading distributions on the useful link and to Rayleigh fading on the interfering links. The technical contribution of the present chapter is threefold: 1) we provide an exact closed-form expression of the Characteristic Function (CF) of the aggregate other-cell interference at the MT; 2) by using the Gil-Pelaez inversion theorem [54], we provide

an exact closed-form expression of the average pairwise frame error probability, which is averaged with respect to the fading distribution and to all BSs deployments. From the average pairwise error probability, the average frame error probability is obtained by using the Nearest Neighbor (NN) approximation [55, p. 138]; and 3) simplified but asymptotically accurate mathematical frameworks are proposed, which are shown to provide insight on the achievable error performance as a function of important system parameters. The proposed frameworks are useful for better understanding and for simplifying the analysis of cellular networks, since they do not require explicit generation and simulation of BSs locations using Monte Carlo simulations.

2.2 System Model

We consider a bi-dimensional downlink cellular network deployment, where a probe/typical multi-antenna MT is located at the origin and the multi-antenna BSs are modeled as points of a homogeneous PPP (Φ) of density λ. A diagrammatic representation of a PPP-based cellular network deployment is illustrated in Fig. 2.1. The number of antennas at each BS and at the MT is denoted by N_t and N_r, respectively. Based on the properties of homogeneous PPPs, there is no loss of generality in assuming the MT to be located at the origin [16]. The distance from the ith BS to the MT is denoted by r_i for $i \in \Phi$. The MT is assumed to be tagged to the nearest BS, *i.e.*, a shortest distance cell association criterion is assumed. The serving BS is denoted by BS_0, and its distance from the MT is denoted by r_0. Owing to the random nature of the PPP-based abstraction model, r_0 is a RV with PDF equal to $f_{r_0}(\xi) = 2\pi\lambda\xi \exp\left(-\pi\lambda\xi^2\right)$ [6]. According to the Slivnyak-Mecke's theorem [16, Vol. 1, Th. 1.4.5], the set of interfering BSs $i \in \Phi \setminus \{\mathrm{BS}_0\}$ is still a homogeneous PPP outside the ball centered at the origin and of radius r_0, and it is denoted by $\Phi^{(\setminus 0)}$. By definition of shortest distance cell association, $r_i > r_0$ for $i \in \Phi^{(\setminus 0)}$. A full frequency reuse scheme is assumed, *i.e.*, all interfering BSs transmit in the same frequency band as BS_0. Upon completion of the cell association, it is assumed that the interfering BSs transmit packets, in each channel use, with equal probability $0 \leq p \leq 1$. These probabilities represent independent activity factors of the interfering BSs. This model finds application to the analysis of, *e.g.*, slotted-ALOHA cellular networks [59] and it is particularly suited in the context of a PPP-based abstraction modeling of cellular networks, since, due to the independent thinning property of the PPPs [16, Proposition 1.3.5], the set of interfering BSs $\Phi^{(\setminus 0)}$ is still a PPP of density $p\lambda$.

Remark 2.1 *As seen in Fig. 2.1, two BSs could be arbitrarily close to each other if using the PPP-based abstraction to model the locations of BSs. It is indeed the fundamental limitation of PPP-based abstraction model and it is especially not suitable for networks with repulsion, where the locations of points are spatially correlated. However, it have been confirmed in the literature that the PPP-based abstraction model is capable of accurately reproducing the main structural characteristics of operational cellular networks [13, 14, 15]. In addition, in the later Section 2.6 of this chapter, we compare Monte Carlo simulations obtained by modeling the BS locations via*

grid-based and PPP-based abstraction models and we observe a reasonable agreement between the two abstraction models by direct inspection of Fig. 2.4.

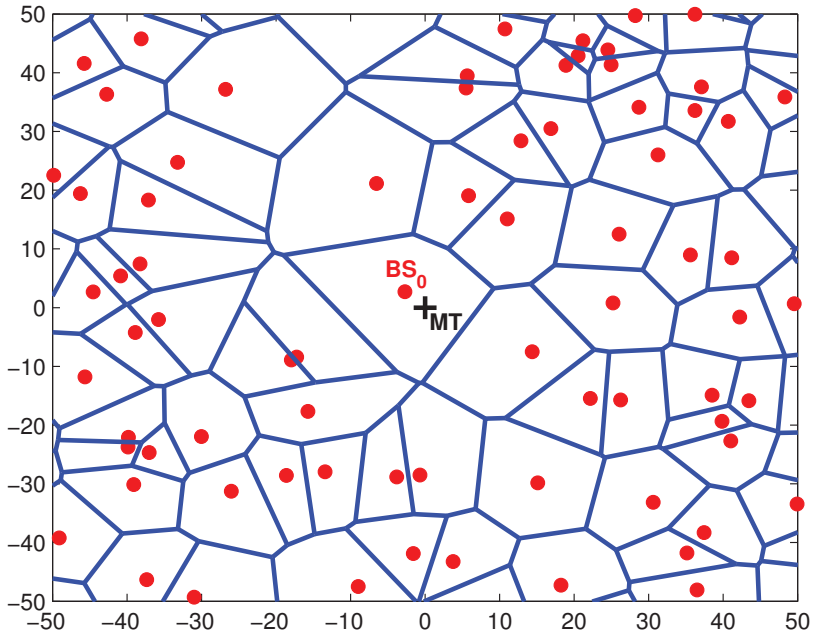

Figure 2.1: Illustration of a PPP-based cellular network deployment. A normalized bi-dimensional area of 100×100 is shown, where the MT is located at the origin and the serving BS is denoted by BS_0. The red dots denote the BSs. The density of BSs is $\lambda = 8 \times 10^{-3}$. The blue lines denote the coverage regions, which form a Voronoi tessellation and are computed based on the shortest distance cell association criterion.

In the depicted downlink MIMO cellular network model, the signal received at the MT_0 can be formulated as follows:

$$\mathbf{y_0} = \underbrace{\sqrt{E/N_t}\, r_0^{-b} \mathbf{H}_0 \mathbf{s}_0}_{\mathbf{x_0}} + \underbrace{\sqrt{E/N_t} \sum_{i \in \Phi^{(\setminus 0)}} r_i^{-b} \mathbf{H}_i \mathbf{s}_i}_{\mathbf{i}_{\mathrm{agg}}(r_0)} + \mathbf{n_0} \tag{2.1}$$

where $\mathbf{y_0} \in \mathbb{C}^{N_r \times 1}$, $\mathbf{x_0} \in \mathbb{C}^{N_r \times 1}$ is the useful signal transmitted by BS_0, $\mathbf{i}_{\mathrm{agg}}(r_0) \in \mathbb{C}^{N_r \times 1}$ is the aggregate other-cell interference and $\mathbf{n_0} \in \mathbb{C}^{N_r \times 1}$ is the Additive White Gaussian Noise (AWGN). It is worth mentioning that the aggregate other-cell interference depends on r_0, since all the interfering BSs must lie outside a disk of radius r_0 that is centered at the origin of the bi-dimensional plane. This originates from the shortest distance cell association. More specifically: i) E is the BSs transmit-energy per transmission, which is equally split among the N_t available antennas; ii) $\mathbf{s}_0 \in \mathbb{M}^{N_t \times 1} \subseteq \mathbb{C}^{N_t \times 1}$ is the vector of information symbols emitted by BS_0, where $\mathbf{s}_0^{(t)} = \left|\mathbf{s}_0^{(t)}\right| \exp\left\{j \arg\left\{\mathbf{s}_0^{(t)}\right\}\right\} \in \mathbb{M} \subseteq \mathbb{C}$ and $\mathbb{E}\left\{\left|\mathbf{s}_0^{(t)}\right|^2\right\} = 1$ for $t = 1, 2, \ldots, N_t$. $\mathbb{M}$ is the set of modulated symbols and $\mathsf{M} = \mathrm{card}\{\mathbb{M}\}$. The M symbols of $\mathbb{M}$ are denoted by $\mu_\chi \in \mathbb{C}$ for $\chi = 1, 2, \ldots, \mathsf{M}$. For example, they can be the M symbols of either a Phase Shift Keying

(PSK) or a Quadrature Amplitude Modulation (QAM) constellation diagram; iii) $\mathbf{H}_0 \in \mathbb{C}^{N_r \times N_t}$ is the channel matrix of the BS_0-to-MT_0 link, where $\mathbf{H}_0^{(r,t)} = \left|\mathbf{H}_0^{(r,t)}\right| \exp\left\{j \arg\left\{\mathbf{H}_0^{(r,t)}\right\}\right\} \in \mathbb{C}$ and $\arg\left\{\mathbf{H}_0^{(r,t)}\right\} \sim \mathscr{U}(0, 2\pi)$ for $t = 1, 2, \ldots, N_t$ and $r = 1, 2, \ldots, N_r$. The distribution of $\left|\mathbf{H}_0^{(r,t)}\right|$ is provided in Section 2.3 and Section 2.4; iv) $b > 1$ denotes the amplitude path-loss exponent, which is the same for useful and interfering links; and v) $\mathbf{n_0} \in \mathbb{C}^{N_r \times 1}$, where $\mathbf{n_0^{(r)}} \sim \mathscr{CN}(\mathbf{0}, \mathscr{N}_\mathbf{0})$ are independent and identically distributed (i.i.d.) RVs for $r = 1, 2, \ldots, N_r$. A similar notation is adopted for all the interfering channels of $\mathbf{i}_{\text{agg}}(\cdot)$. As for the other-cell interference model, (2.1) implicitly assumes the so-called isotropic scenario [24, Sec. II-B], where the N_r antennas at the MT are omnidirectional and are subject to the interference generated by all the interferers $i \in \Phi^{(\backslash 0)}$. Also, the antennas at the transmitter and receiver are assumed to be co-located, which implies that the transmission distances r_0 and r_i for $i \in \Phi^{(\backslash 0)}$ are independent of the antennas' inter-distances. The downlink channels are i.i.d. with mean square value $\mathbb{E}\left\{\left|\mathbf{H}_0^{(r,t)}\right|^2\right\} = \mathbb{E}\left\{\left|\mathbf{H}_i^{(r,t)}\right|^2\right\} = \Omega$ for $t = 1, 2, \ldots, N_t$, $r = 1, 2, \ldots, N_r$ and $i \in \Phi^{(\backslash 0)}$.

At the MT, an interference-unaware Maximum-Likelihood (ML)-optimum demodulator is considered. It is assumed to have perfect Channel State Information (CSI) of the BS_0-to-MT link (*i.e.*, $\mathbf{H}_0$ is known), while it is assumed to ignore other-cell interference. Although this assumption inherently limits the achievable performance, it provides a reasonable trade-off between performance and complexity. As such, it is widely used in the literature [6], [7], [34]–[30]. The generalization of the analysis to interference-aware demodulators is postponed to future research.

In mathematical terms, the interference-unaware ML-optimum demodulator can be formulated as [60, Ch. 7]:

$$\hat{\mathbf{s}}_0 = \underset{\tilde{\mathbf{s}}_0 \in \mathbb{M}^{N_t \times 1}}{\arg\min} \left\{ \Lambda(\tilde{\mathbf{s}}_0) = \left\| \mathbf{y_0} - \sqrt{E/N_t}\, r_0^{-b} \mathbf{H}_0 \tilde{\mathbf{s}}_0 \right\|^2 \right\} \tag{2.2}$$

By inserting (2.1) in (2.2) and with the aid of some algebra, the decision metric $\Lambda(\cdot)$ can be formulated as follows:

$$\begin{aligned} \Lambda(\tilde{\mathbf{s}}_0) &\propto r_0^{-2b} \frac{E}{N_t} \sum_{r=1}^{N_r} \left| \sum_{t=1}^{N_t} \mathbf{H}_0^{(r,t)} \Delta_0^{(t)} \right|^2 + 2 r_0^{-b} \sqrt{\frac{E}{N_t}} \mathrm{Re}\left\{ \sum_{r=1}^{N_r} \mathbf{v}^{(r)}(r_0) \sum_{t=1}^{N_t} \left(\mathbf{H}_0^{(r,t)} \Delta_0^{(t)} \right)^H \right\} \\ &= r_0^{-2b} \left(E/N_t\right) \mathrm{U} + 2 r_0^{-b} \sqrt{E/N_t}\, \mathrm{Re}\{\mathrm{I}(r_0)\} + 2 r_0^{-b} \sqrt{E/N_t}\, \mathrm{Re}\{\mathrm{N}\} \end{aligned} \tag{2.3}$$

where $\mathbf{\Delta}_0 = \mathbf{s}_0 - \tilde{\mathbf{s}}_0 \in \mathbb{C}^{N_t \times 1}$, $\mathbf{v}(r_0) = \mathbf{i}_{\text{agg}}(r_0) + \mathbf{n_0} \in \mathbb{C}^{N_r \times 1}$ and:

$$\begin{aligned} \mathrm{U} &= \sum_{r=1}^{N_r} \left| \sum_{t=1}^{N_t} \mathbf{H}_0^{(r,t)} \Delta_0^{(t)} \right|^2 \\ \mathrm{I}(r_0) &= \sum_{r=1}^{N_r} \mathbf{i}_{\text{agg}}^{(r)}(r_0) \sum_{t=1}^{N_t} \left(\mathbf{H}_0^{(r,t)} \Delta_0^{(t)} \right)^H \\ \mathrm{N} &= \sum_{r=1}^{N_r} \mathbf{n_0^{(r)}} \sum_{\mathbf{t=1}}^{\mathbf{N_t}} \left(\mathbf{H_0^{(r,t)}} \Delta_{\mathbf{0}}^{(\mathbf{t})} \right)^{\mathbf{H}} \end{aligned} \tag{2.4}$$

In the next sections, the achievable error probability performance of the demodulator in (2.2) is studied.

2.3 Downlink SISO Cellular Networks

Let us consider a SISO cellular network, *i.e.*, $N_t = N_r = 1$. The decision metric in (2.3) reduces to:

$$\Lambda(\tilde{s}_0) \propto r_0^{-2b} E |\Delta_0|^2 |h_0|^2 + 2 r_0^{-b} \sqrt{E} \mathrm{Re}\left\{ v(r_0)\, h_0^H \Delta_0^H \right\} \tag{2.5}$$

where, for simplicity, the following notation is introduced: i) $\mathbf{H}_0^{(1,1)} = h_0$; ii) $\mathbf{H}_i^{(1,1)} = h_i$; iii) $\Delta_0 = \mathbf{s}_0^{(1)} - \tilde{\mathbf{s}}_0^{(1)} = s_0 - \tilde{s}_0$; iv) $\mathbf{s}_i^{(1)} = s_i$; v) $\mathbf{n_0^{(1)}} = \mathbf{n}$; vi) $\mathbf{i}_{\text{agg}}^{(1)}(r_0) = i_{\text{agg}}(r_0) = \sqrt{E} \sum_{i \in \Phi^{(\setminus 0)}} r_i^{-b} h_i s_i$; and vii) $\mathbf{v}^{(1)}(r_0) = v(r_0) = i_{\text{agg}}(r_0) + n$. The fading envelopes $|h_0|$ and $|h_i|$ for $i \in \Phi^{(\setminus 0)}$ are assumed to be i.i.d. and to follow a generic distribution with $\mathbb{E}\{|h_0|^2\} = \mathbb{E}\{|h_i|^2\} = \Omega$. As an example, Gamma [60, Sec. 2.2.1.4] and composite Gamma/Log-Normal [60, Sec. Sec. 2.2.3.1] fading channels are explicitly analyzed.

In this section, we provide a mathematical framework for computing the Average Symbol Error Probability (ASEP) of the demodulator in (2.5). The ASEP is defined as the symbol error probability averaged with respect to the distribution of the fading channels and of the spatial locations of the BSs. The proposed approach for computing the ASEP consists of four steps:

1. First, the statistical distribution of $i_{\text{agg}}(\cdot)$ is studied and a closed-form expression of its CF conditioned upon r_0 is derived with the aid of stochastic geometry (Section 2.3.1);
2. Then, the Pairwise Error Probability (PEP) conditioned upon the fading envelope (h_0) and the transmission distance (r_0) of BS_0 is computed with the aid of the Gil-Pelaez inversion theorem (Section 2.3.2);
3. Subsequently, the Average PEP (APEP) is obtained by removing the conditioning with respect to h_0 and r_0. The distribution of r_0 is computed by using the void probability theorem of PPPs [16, Th. 1.1.5] (Section 2.3.2);
4. Finally, the ASEP is computed from the APEP by using the NN approximation (Section

2.3.5).

As for the physical meaning of averaging the error probability with respect to the spatial positions of the BSs, the reader is referred to [24] for details.

2.3.1 Characteristic Function of the Other-Cell Interference

In this section, the CF of $i_{\text{agg}}(\cdot)$ conditioned upon r_0 is computed in closed-form for arbitrary fading models. The main result is summarized in *Theorem 2.1* and *Corollary 2.1*.

Theorem 2.1 *Let* $i_{\text{agg}}(r_0) = \sqrt{E}\sum_{i\in\Phi^{(\setminus 0)}} r_i^{-b} h_i s_i$. *By conditioning upon* r_0, *its CF can be formulated as follows:*

$$\psi_{i_{\text{agg}}}(\boldsymbol{\omega}; r_0) = \psi_{i_{\text{agg}}}(|\boldsymbol{\omega}|; r_0) = \exp\left\{-\lambda\pi r_0^2 \mathrm{T}\left(|\boldsymbol{\omega}|^2 r_0^{-2b} E\right)\right\} \tag{2.6}$$

where $\mathrm{T}(x) = p\Upsilon(x) - p$ *and:*

$$\begin{aligned}\Upsilon(x) &= \frac{1}{\mathsf{M}}\sum_{\chi=1}^{\mathsf{M}}\sum_{q=0}^{+\infty}\left(-\frac{1}{4}\right)^q \frac{1}{q!}\frac{\left(-1/b\right)_q}{\left(1-1/b\right)_q (1)_q}\left(x\left|\mu_\chi\right|^2\right)^q \mathbb{E}\left\{|h_i|^{2q}\right\} \\ &= \frac{1}{\mathsf{M}}\sum_{\chi=1}^{\mathsf{M}} \mathbb{E}_{|h_i|^2}\left\{{}_1F_2\left(-\frac{1}{b}; 1, 1-\frac{1}{b}; -\frac{x}{4}\left|\mu_\chi\right|^2 |h_i|^2\right)\right\}\end{aligned} \tag{2.7}$$

Proof*: See Appendix 2.8.1.* □

Corollary 2.1 *Let* $i_{\text{agg}}(r_0) = \sqrt{E}\sum_{i\in\Phi^{(\setminus 0)}} r_i^{-b} h_i s_i$. *Let a constant-envelope modulation be used, i.e.,* $|s_i|^2 = 1$ *for* $i \in \psi^{(\setminus 0)}$. *By conditioning upon* r_0, *its CF is equal to* $\psi_{i_{\text{agg}}}(\cdot;\cdot)$ *in* (2.6) *with* $\mathrm{T}(x) = p\Upsilon(x) - p$ *and:*

$$\begin{aligned}\Upsilon(x) &= \sum_{q=0}^{+\infty}\left(-\frac{1}{4}\right)^q \frac{1}{q!}\frac{\left(-1/b\right)_q}{\left(1-1/b\right)_q (1)_q} x^q \mathbb{E}\left\{|h_i|^{2q}\right\} \\ &= \mathbb{E}_{|h_i|^2}\left\{{}_1F_2\left(-\frac{1}{b}; 1, 1-\frac{1}{b}; -\frac{x}{4}|h_i|^2\right)\right\}\end{aligned} \tag{2.8}$$

Proof*: It follows from* (2.6) *with* $\left|\mu_\chi\right|^2 = 1$ *for* $\chi = 1, 2, \ldots, \mathsf{M}$. *This concludes the proof.* □

Remark 2.2 *A closed-form expression of the CF of the aggregate other-cell interference of SISO cellular networks is available in [61, Sec. III-C] as well. Similar to [61, Sec. III-C], the mathematical formulation in* (2.6) *is obtained with the aid of stochastic geometry. Several differences, however, between [61, Sec. III-C] and* (2.6) *exist. The most important of them is that* (2.6)

provides an exact and compact representation of the CF of the aggregate other-cell interference, while the mathematical development in [61, Sec. III-C] is based on a number of approximations, which are aimed to show differences and similarities with the Middleton Class A distribution. As such, [61, Sec. III-C] and (2.6) *are different and may serve for different purposes.* □

The results in *Theorem 2.1* and *Corollary 2.1* are general, since they are applicable to arbitrary fading distributions. However, the expectation with respect to the fading square envelope $|h_i|^2$ of the generic interfering channel needs to be computed in (2.7) and (2.8). In *Proposition 2.1* and *Proposition 2.2*, closed-form expressions of $\Upsilon(\cdot)$ for two channel models usually used for performance analysis, *i.e.*, Gamma [60, Sec. 2.2.1.4] and composite Gamma/Log-Normal [60, Sec. Sec. 2.2.3.1] distributions, are given. The propositions are formulated for arbitrary modulation schemes. From (2.8), they can be readily simplified for constant-envelope modulations.

Proposition 2.1 *Let $g_i = |h_i|^2$ follow a Gamma distribution with parameters (m, Ω), which we denote as $g_i \sim \text{Gamma}(m, \Omega)$ [60, Sec. 2.2.1.4]. Then, $\Upsilon(\cdot)$ in* (2.7) *has closed-form expression as follows:*

$$\Upsilon(x) = \frac{1}{\mathrm{M}} \sum_{\chi=1}^{\mathrm{M}} {}_2F_2\left(-\frac{1}{b}, m; 1, 1-\frac{1}{b}; -\frac{1}{4}\frac{\Omega}{m}\left|\mu_\chi\right|^2 x\right) \tag{2.9}$$

Proof*: From [60, Eq. 2.23], we obtain $\mathbb{E}_{|h_i|}\left\{|h_i|^{2q}\right\} = \Omega^q \Gamma\left(m+q\right)/\left(m^q \Gamma(m)\right)$. The proof follows by using the series representation of the generalized hypergeometric function [57, Ch. 5, Eq. 2]. This concludes the proof.* □

Proposition 2.2 *Let $g_i = |h_i|^2$ follow a Gamma distribution by conditioning upon its mean power, which follows a Log-Normal distribution, which we denote as $g_i \sim \text{Gamma/LogN}(m, \eta, \sigma^2)$ [60, Sec. 2.2.3.1]. Then, $\Upsilon(\cdot)$ in* (2.7) *has closed-form approximation as follows:*

$$\Upsilon(x) \approx \frac{1}{\mathrm{M}} \sum_{\chi=1}^{\mathrm{M}} \frac{1}{\sqrt{\pi}} \sum_{k=1}^{N_{\text{GHQ}}} w_k {}_2F_2\left(-\frac{1}{b}, m; 1, 1-\frac{1}{b}; -\frac{1}{4}\frac{\tilde{\tau}_k}{m}\left|\mu_\chi\right|^2 x\right) \tag{2.10}$$

where $\tilde{\tau}_k = 10^{\left(\sqrt{2}\sigma\tau_k+\eta\right)/10}$, and w_k and τ_k for $k = 1, 2, \ldots, N_{\text{GHQ}}$ are weights and abscissas of the Gauss-Hermite quadrature rule [56, Eq. 25.4.46], respectively.

Proof*: It follows by using the approximation of the Log-Normal distribution based on the Gauss-Hermite quadrature formula [7, Secs. D, E]. In particular, by applying the quadrature formula to [60, Eq. 2.57] and using [60, Eq. 2.23] we obtain $\mathbb{E}_{|h_i|}\left\{|h_i|^{2q}\right\} = \frac{\Gamma(m+q)}{(m^q\Gamma(m))\sqrt{\pi}} \sum_{k=1}^{N_{\text{GHQ}}} w_k \tilde{\tau}_k^q$. The rest follows by using the series representation of the generalized hypergeometric function [57, Ch. 5, Eq. 2]. This concludes the proof.* □

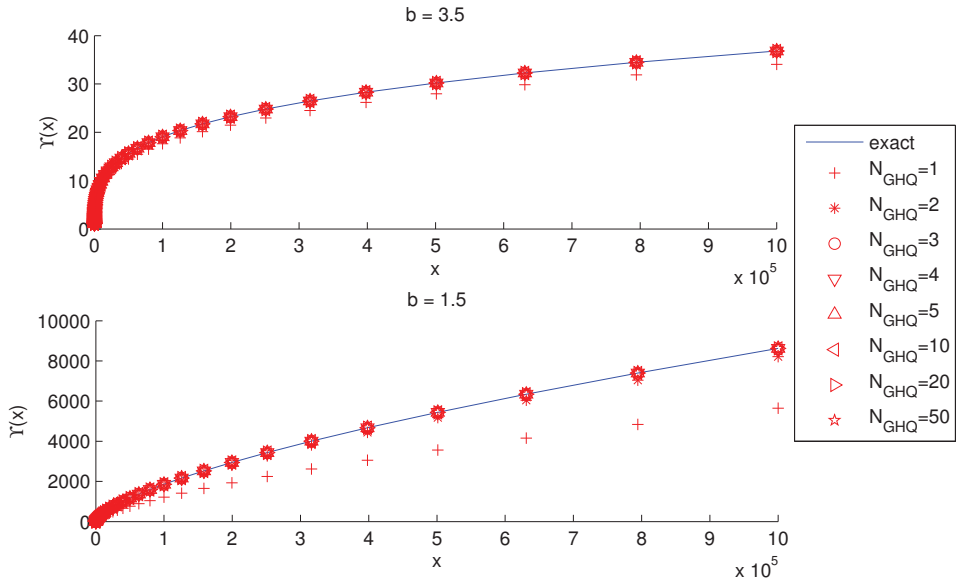

Figure 2.2: Illustration of the accuracy of the GHQ closed-form approximation in (2.10). The following parameters are considered: $m = 2$; $\sigma = 6$dB; $M = 16$ QAM; $b = 3.5$ (top) and $b = 1.5$ (bottom); and η is chosen as described in *Remark 2.3*. For consistency, similar parameters are considered in Section 2.6.

In Fig. 2.2, the accuracy of the closed-form approximation in (2.10) is studied, as a function of the number of points N_{GHQ}. The "exact" curves are obtained by numerically computing the two-fold integral related to the expectation in (2.7), which originates from the distribution of $g_i \sim \mathrm{Gamma/LogN}\left(m,\eta,\sigma^2\right)$ [60, Sec. 2.2.3.1]. The figure shows a good agreement between GHQ approximation and exact results. In particular, the accuracy increases as N_{GHQ} increases. From the figure, we note that $N_{\mathrm{GHQ}} = 3$ is a reasonable choice to get a good accuracy for the entire range of values of the function and to keep the computational complexity at a low level. For this reason, $N_{\mathrm{GHQ}} = 3$ is used in Section 2.6. It is worth noting that the hypergeometric function in (2.10) is computed by using the approximation discussed in Section 2.3.6.

Remark 2.3 *In Section 2.2, it is assumed that* $\mathbb{E}\left\{g_i\right\} = \mathbb{E}\left\{|h_i|^2\right\} = \Omega$. *As for the composite fading model of Proposition 2.2, this implies* $\eta = \kappa^{-1}\ln(\Omega) - (1/2)\kappa\sigma^2$ *with* $\kappa = 10^{-1}\ln(10)$ *[60, Eq. 2.59].* □

Remark 2.4 *In the present chapter, shadowing correlation is neglected for simplicity. However, it can be readily included in the system model by using the same approach as in [7, Sec. III-F]. In particular, the expectation in* (2.7) *can be computed similar to* (2.10) *by using the two-step approach in [7, Sec. III-F] and [7, Eq. 22]. The price to be paid is an increase of the computational complexity, since two GHQ summations need to be computed. The approach is applicable to scenarios with equi-correlated shadowing, as discussed and motivated in [7, Sec. III-F].* □

Remark 2.5 *In Proposition 2.2, it is assumed that a cell association criterion based on the shortest BS-to-MT distance is used even in the presence of Log-Normal shadowing. Accordingly,*

the CF of the aggregate other-cell interference is averaged with respect to the shadowing distribution. In the presence of shadowing, however, the cell association criterion may be modified by taking it into account. In this case, a cell association criterion based on the best received power may be used. For example, this is considered in [62] and [63]. It is interesting to note that the mathematical framework proposed in this section is applicable to this case study as well, by capitalizing on the results available in [62, Theorem 2] and [63, Lemma 1]. In particular, the proposed framework still holds by simply introducing a scaling factor in the density of BSs, which depends on the fractional moments of the shadowing distribution. This approach holds if the shadowing is assumed to be i.i.d. among the interfering links. □

Remark 2.6 *Closed-form expressions of the CF of* $i_{\text{agg}}(\cdot)$ *can be computed for a general class of fading distributions with the aid of the Meijer G-function. For a wide class of fading models, the PDF of* $g_i = |h_i|^2$ *can be formulated as* $f_{g_i}(\xi) = \mathscr{C}\xi^{\alpha} G_{\tilde{p},\tilde{q}}^{\tilde{m},\tilde{n}}\left(\mathscr{D}\xi^{\beta/\gamma}\middle|\begin{matrix}(\mathbf{a}_{\tilde{p}})\\(\mathbf{b}_{\tilde{q}})\end{matrix}\right)$ *[64]. With the aid of [58, Eq. 8.4.48.1], the expectation in* (2.7) *and* (2.8) *can be expressed in terms of the Meijer G-function by applying the Mellin-Barnes theorem [58, Eq. 2.24.1.1].* □

2.3.2 Average Pairwise Error Probability: Exact Analysis

By definition, the APEP is the probability that the actual transmitted symbol s_0 is decoded as $\hat{s}_0 = \bar{s}_0 \neq s_0$, by assuming that s_0 and $\bar{s}_0$ are the only two symbols of the constellation diagram. From (2.5), this occurs when $\Lambda(\tilde{s}_0 = \bar{s}_0) < \Lambda(\tilde{s}_0 = s_0)$. Since $\Lambda(\tilde{s}_0 = s_0) = 0$ from (2.5), the APEP reduces to the computation of $\text{APEP}(|\Delta_0|) = \Pr\{\Lambda(\tilde{s}_0 = \bar{s}_0) < 0\}$. We start by computing the APEP conditioned upon $|h_0|$ and r_0, which is denoted by $\text{PEP}(|\Delta_0|; |h_0|, r_0)$ (see *Lemma 2.1* in Appendix 2.8.2). Hence, the APEP is $\text{APEP}(|\Delta_0|) = \mathbb{E}_{|h_0|,r_0}\{\text{PEP}(|\Delta_0|; |h_0|, r_0)\}$. From (2.5), the APEP can be formulated as summarized in *Theorem 2.2*.

Theorem 2.2 *Let the demodulator in* (2.5). *Let* $\mathsf{SNR} = E/\mathcal{N}_0$ *denote the Signal-to-Noise-Ratio (SNR). The APEP can be formulated as* $\text{APEP}(|\Delta_0|) = \Pr\{\Lambda(\tilde{s}_0) < 0\} = \text{APEP}_{\text{N}}(|\Delta_0|) + \text{APEP}_{\text{NI}}(|\Delta_0|)$, *where* $\text{APEP}_{\text{N}}(\cdot)$ *and* $\text{APEP}_{\text{NI}}(\cdot)$ *are given in* (2.11)*:*

$$\begin{cases} \text{APEP}_{\text{N}}(|\Delta_0|) = \dfrac{1}{2\sqrt{\pi}} b |\Delta_0| \sqrt{\mathsf{SNR}} \displaystyle\int_0^{+\infty} x^{-(b+1)} \exp\left(-\pi\lambda x^2\right) \text{Q}_{\text{N}}(x; |\Delta_0|, \mathsf{SNR}, b)\, dx \\ \text{APEP}_{\text{NI}}(|\Delta_0|) = \dfrac{1}{2\pi} \displaystyle\int_0^{+\infty}\int_0^{+\infty} \frac{e^{-y}}{x} \exp\left\{-\frac{x y^b}{4(\pi\lambda)^b SNR}\right\} \left[1 - \exp\left\{-y\text{T}(x)\right\}\right] \text{Q}_{\text{NI}}(x; |\Delta_0|)\, dx dy \end{cases} \tag{2.11}$$

and the following short-hands have been introduced:

$$\begin{cases} \text{Q}_{\text{N}}(x; |\Delta_0|, \mathsf{SNR}, b) = \mathbb{E}_{|h_0|}\left\{|h_0| \exp\left\{-(1/4)\,\mathsf{SNR}\,|\Delta_0|^2\,|h_0|^2\,x^{-2b}\right\}\right\} \\ \text{Q}_{\text{NI}}(x; |\Delta_0|) = \mathbb{E}_{|h_0|}\left\{\sin\left((1/2)\,|\Delta_0|\,|h_0|\,x^{1/2}\right)\right\} \end{cases} \tag{2.12}$$

Proof*: See Appendix 2.8.3.* □

Theorem 2.2 provides an exact mathematical formulation of the APEP, which is applicable to arbitrary distributions of the fading envelope $|h_0|$. The expectations in (2.12) can be computed in closed-form for various fading models. In *Proposition 2.3* and *Proposition 2.4*, closed-form expressions of $\mathrm{Q}_{\mathrm{N}}(\cdot;\cdot,\cdot,\cdot)$ and $\mathrm{Q}_{\mathrm{NI}}(\cdot;\cdot,\cdot)$ are provided for Gamma [60, Sec. 2.2.1.4] and Gamma/Log-Normal [60, Sec. Sec. 2.2.3.1] channels.

Proposition 2.3 *Let $g_0 = |h_0|^2 \sim \mathrm{Gamma}(m,\Omega)$ [60, Sec. 2.2.1.4]. Let $\mathscr{K}_1 \geq 0$ and $\mathscr{K}_2 \geq 0$ be two non-negative constants. Let the expectations:*

$$\begin{cases} \mathscr{I}_1(\mathscr{K}_1) = \mathbb{E}_{g_0}\left\{\sqrt{g_0}\exp\left\{-\mathscr{K}_1 g_0\right\}\right\} \\ \qquad\quad = m^m\left(\Omega^m\Gamma(m)\right)^{-1}\Gamma(m+1/2)\left(\mathscr{K}_1+m/\Omega\right)^{-(m+1/2)} \\ \mathscr{I}_2(\mathscr{K}_2) = \mathbb{E}_{g_0}\left\{\sin\left(\mathscr{K}_2\sqrt{g_0}\right)\right\} \\ \qquad\quad = \sqrt{\Omega/m}\Gamma(m+1/2)\times\left(\Gamma(m)\right)^{-1}\mathscr{K}_2\times{}_1F_1\left(m+1/2;3/2,-(4m)^{-1}\Omega\mathscr{K}_2^2\right) \end{cases} \tag{2.13}$$

Then, $\mathrm{Q}_{\mathrm{N}}(x;|\Delta_0|,\mathsf{SNR},b) = \mathscr{I}_1\left((1/4)\,\mathsf{SNR}\,|\Delta_0|^2\,x^{-2b}\right)$ *and* $\mathrm{Q}_{\mathrm{NI}}(x;|\Delta_0|) = \mathscr{I}_2\left((1/2)\,|\Delta_0|\,x^{1/2}\right)$.

Proof*: $\mathscr{I}_1(\cdot)$ is computed with the aid of [65, Eq. 3.381.4] and $\mathscr{I}_2(\cdot)$ is computed with the aid of [65, Eq. 3.952.7] and of the Kummer's transformation ${}_1F_1(1-m;3/2,x)\exp\{-x\} = {}_1F_1(m+1/2;3/2,-x)$. The proof follows by direct inspection of $\mathscr{I}_1(\cdot)$, $\mathscr{I}_2(\cdot)$ and* (2.12)*. This concludes the proof.* □

Proposition 2.4 *Let $g_0 = |h_0|^2 \sim \mathrm{Gamma/LogN}\left(m,\eta,\sigma^2\right)$ [60, Sec. 2.2.3.1]. Let $\mathscr{K}_1 \geq 0$ and $\mathscr{K}_2 \geq 0$ be two non-negative constants. Let the expectations:*

$$\begin{cases} \mathscr{I}_1(\mathscr{K}_1) = \mathbb{E}_{g_0}\left\{\sqrt{g_0}\exp\left\{-\mathscr{K}_1 g_0\right\}\right\} \\ \qquad\quad \approx m^m\left(\Gamma(m)\right)^{-1}\times\Gamma\left(m+\frac{1}{2}\right)\frac{1}{2\sqrt{\pi}}\sum_{k=1}^{N_{\mathrm{GHQ}}} w_k\tilde{\tau}_k^{-m}\left(\mathscr{K}_1+m/\tilde{\tau}_k\right)^{-(m+1/2)} \\ \mathscr{I}_2(\mathscr{K}_2) = \mathbb{E}_{g_0}\left\{\sin\left(\mathscr{K}_2\sqrt{g_0}\right)\right\} \\ \qquad\quad \approx \Gamma(m+1/2)\left(\Gamma(m)\right)^{-1}\times\frac{\mathscr{K}_2}{\sqrt{\pi}}\sum_{k=1}^{N_{\mathrm{GHQ}}} w_k\sqrt{\frac{\tilde{\tau}_k}{m}}\,{}_1F_1\left(m+1/2;3/2,-\frac{\tilde{\tau}_k\mathscr{K}_2^2}{4m}\right) \end{cases} \tag{2.14}$$

Then, $\mathrm{Q}_{\mathrm{N}}(x;|\Delta_0|,\mathsf{SNR},b) = \mathscr{I}_1\left((1/4)\,\mathsf{SNR}\,|\Delta_0|^2\,x^{-2b}\right)$ *and* $\mathrm{Q}_{\mathrm{NI}}(x;|\Delta_0|) = \mathscr{I}_2\left((1/2)\,|\Delta_0|\,x^{1/2}\right)$.

Proof*: Consider the approximation of the Log-Normal distribution based on the Gauss-Hermite quadrature formula [7, Secs. D, E], i.e., $f_{g_0}(\xi) \approx \frac{m^m}{\Gamma(m)}\xi^{m-1}\frac{1}{\sqrt{\pi}}\sum_{k=1}^{N_{\mathrm{GHQ}}} w_k\tilde{\tau}_k^{-m}\exp\left\{-m\xi\tilde{\tau}_k^{-1}\right\}$. The proof follows by using mathematical steps similar to the proof of Proposition 2.3. This concludes the proof.* □

Remark 2.7 *The mathematical framework in [111] is a special case of Theorem 2.2 and Proposition 2.3 for* $m = 1$ *(Rayleigh fading).* □

2.3.3 Average Pairwise Error Probability: Asymptotic Analysis

In this section, we provide simplified mathematical frameworks in two limiting operating conditions: 1) *noise-limited, i.e.*, $\mathsf{SNR} \to 0$, and 2) *interference-limited, i.e.*, $\mathsf{SNR} \to +\infty$, cellular networks, where $\mathsf{SNR} = E/\mathcal{N}_0$. As discussed in [7, Sec. V-g], typical cellular networks operate in the interference-limited regime.

Corollary 2.2 *Let a noise-limited cellular network,* $\lim_{\mathsf{SNR}\to 0}\{\mathrm{APEP}(|\Delta_0|)\} = \mathrm{APEP}_{\mathrm{N}}^{(0)}(|\Delta_0|) = \mathrm{APEP}_{\mathrm{N}}(|\Delta_0|)$. *Let an interference-limited network,* $\lim_{\mathsf{SNR}\to +\infty}\{\mathrm{APEP}(|\Delta_0|)\} = \mathrm{APEP}_{\mathrm{NI}}^{(\infty)}(|\Delta_0|)$, *where:*

$$\mathrm{APEP}_{\mathrm{NI}}^{(\infty)}(|\Delta_0|) = \lim_{\mathsf{SNR}\to+\infty}\{\mathrm{APEP}_{\mathrm{NI}}(|\Delta_0|)\} = \frac{1}{2\pi}\int_0^{+\infty}\frac{1}{x}\frac{\mathrm{T}(x)}{1+\mathrm{T}(x)}\mathrm{Q}_{\mathrm{NI}}(x;|\Delta_0|,b)\,dx \tag{2.15}$$

Proof*: If follows from* (2.11) *and from the notable integral* $\int_0^{+\infty}\exp\{-y\}\left(1-\exp\{-\mathcal{K}y\}\right)dy = 1-(\mathcal{K}+1)^{-1}$ *for* $\mathcal{K}>0$. *This concludes the proof.* □

2.3.4 Average Pairwise Error Probability: Piecewise Single-Integral Bounds

The exact expression of the APEP in (2.11) requires the computation of a single and a two-fold integrals for obtaining $\mathrm{APEP}_{\mathrm{N}}(\cdot)$ and $\mathrm{APEP}_{\mathrm{NI}}(\cdot)$, respectively. On the other hand, $\mathrm{APEP}_{\mathrm{N}}^{(0)}(\cdot)$ and $\mathrm{APEP}_{\mathrm{NI}}^{(\infty)}(\cdot)$ are expressed in closed- and single-integral forms, respectively. Thus, they are simpler to be computed. In this section, we capitalize on the simple mathematical formulations of *Corollary 2.2* by providing an Upper-Bound (UB) and a Lower-Bound (LB) of the APEP. These bounds can serve as an easy-to-compute mathematical formulation for estimating the performance of cellular networks. They are summarized in *Proposition 2.5*.

Proposition 2.5 *Let the APEPs in Theorem 2.2 and Corollary 2.2. The bounds as follows hold:*

$$\mathrm{APEP}(|\Delta_0|) \gtrsim \mathrm{APEP}^{(\mathrm{LB})}(|\Delta_0|) = \max\left\{\mathrm{APEP}_{\mathrm{N}}^{(0)}(|\Delta_0|), \mathrm{APEP}_{\mathrm{NI}}^{(\infty)}(|\Delta_0|)\right\} \tag{2.16}$$

$$\begin{aligned}&\mathrm{APEP}(|\Delta_0|) \le \mathrm{APEP}^{(\mathrm{UB})}(|\Delta_0|)\\ &= \begin{cases}\mathrm{APEP}(|\Delta_0|)|_{E=0} = 1/2 & \text{if } \mathrm{APEP}_{\mathrm{N}}^{(0)}(|\Delta_0|) + \mathrm{APEP}_{\mathrm{NI}}^{(\infty)}(|\Delta_0|) \ge \mathrm{APEP}(|\Delta_0|)|_{E=0}\\ \mathrm{APEP}_{\mathrm{N}}^{(0)}(|\Delta_0|) + \mathrm{APEP}_{\mathrm{NI}}^{(\infty)}(|\Delta_0|) & \text{if } \mathrm{APEP}_{\mathrm{N}}^{(0)}(|\Delta_0|) + \mathrm{APEP}_{\mathrm{NI}}^{(\infty)}(|\Delta_0|) < \mathrm{APEP}(|\Delta_0|)|_{E=0}\end{cases}\end{aligned} \tag{2.17}$$

Proof*: See Appendix 2.8.4.* □

2.3.5 Nearest Neighbor Approximation of the Average Symbol Error Probability

From the APEP in *Theorem 2.2*, the ASEP can be obtained by using the NN approximation [55, p. 138]. In this paper, we propose the NN approximation for computing the ASEP from the APEP because of its simplicity and accuracy. The advantage is, in fact, that the ASEP is obtained by computing a single APEP for every symbol (μ_χ for $\chi = 1,2,\ldots,\mathsf{M}$) of the constellation diagram. By assuming equiprobable transmitted symbols, the NN approximation of the ASEP can be formulated as follows:

$$\text{ASEP} \approx \frac{1}{\mathsf{M}} \sum_{\chi=1}^{\mathsf{M}} N_{\Delta_{\min}}^{(\chi)} \text{APEP}\left(\left|\Delta_{\min}^{(\chi)}\right|\right) \tag{2.18}$$

where: i) $\left|\Delta_{\min}^{(\chi)}\right| = \min_{\mu_{\tilde{\chi}} \in \mathbb{M}} \left\{\left|\mu_{\tilde{\chi}} - \mu_\chi\right|, \mu_{\tilde{\chi}} \in \mathbb{M}, \tilde{\chi} \neq \chi\right\}$ is the minimum Euclidean distance among all pairs $\left(\mu_{\tilde{\chi}}, \mu_\chi\right)$ of symbols of the constellation diagram for $\mu_{\tilde{\chi}\neq\chi} \in \mathbb{M}$ and ii) $N_{\Delta_{\min}}^{(\chi)}$ is the number of nearest neighbors of μ_χ, *i.e.*, the number of points of the constellation diagram whose Euclidean distance from μ_χ is equal to $\left|\Delta_{\min}^{(\chi)}\right|$.

For some constellation diagrams, we may have $\left|\Delta_{\min}^{(\chi)}\right| = |\Delta_{\min}|$, which is independent of μ_χ. In this case, (2.18) reduces to $\text{ASEP} \approx N_{\Delta_{\min}}^{(\text{avg})} \text{APEP}\left(|\Delta_{\min}|\right)$, where $N_{\Delta_{\min}}^{(\text{avg})} = \left(1/\mathsf{M}\right) \sum_{\chi=1}^{\mathsf{M}} N_{\Delta_{\min}}^{(\chi)}$ is the average number of nearest neighbors of the constellation diagram. For example, $|\Delta_{\min}| = 2\sin\left(\pi/\mathsf{M}\right)$ with $N_{\Delta_{\min}}^{(\text{avg})} = 1$ if $\mathsf{M} = 2$ and $N_{\Delta_{\min}}^{(\text{avg})} = 2$ if $\mathsf{M} > 2$ for PSK modulation. If the standard square QAM with $\mathsf{M} = 16$ is considered, we have $|\Delta_{\min}| = 2/\sqrt{10}$ and $N_{\Delta_{\min}}^{(\text{avg})} = 3$. Similar results apply for different values of M.

Remark 2.8 *Another usual approach for estimating the ASEP from the APEP is the union-bound method [55], [60]. Our numerical results, however, have shown that the union-bound is less accurate than the NN approximation. This is due to the other-cell interference whose distribution significantly deviates from that of a Gaussian RV. The accuracy of the NN approximation is analyzed in Section 2.6.* □

2.3.6 On the Computation of Hypergeometric Functions: The Need for Approximations

In [7, Sec. III-B], it is shown that the calculation of some widely used special functions may lead to numerical instabilities when applied to the analysis of cellular networks based on the PPP-based abstraction model. The reason is related to the random spatial locations of the BSs and to the random distance of MT and serving BS (BS_0), which require the integration of the special functions over the whole positive real axis. Our analysis has shown that similar problems may arise when using the framework of *Theorem 2.2*. Similar to [7, Sec. III-B], the numerical accuracy depends on the mathematical software package being used. In order to avoid these issues, in this section we provide some efficient asymptotic approximations to the

computation of some special functions that may arise when using *Theorem 2.2*. The rationale behind the proposed approximations is similar to [7, Sec. III-B].

As an illustrative example, which is relevant to the present chapter, let us consider the mathematical frameworks for Gamma and Gamma/Log-Normal fading. From *Propositions 2.1-2.4*, it is apparent that two special functions need to be computed: $\mathscr{F}_{11}(x) = {}_1F_1\left(\alpha_1;\beta_1,-\mathscr{K}x\right)$ and $\mathscr{F}_{22}(x) = {}_2F_2\left(\alpha_1,\alpha_2;\beta_1,\beta_2;-\mathscr{K}x\right)$ for $\mathscr{K} > 0$ and $x \geq 0$. Our empirical trials based on commercially available mathematical software packages have shown that either numerical inaccuracies or long computational times can be expected if $\mathscr{K}x \gg 1$. For example, this arises when computing $\mathscr{F}_{22}(\cdot)$ for $\alpha_1 = -1/b$, $\alpha_2 = m$, $\beta_2 = 1-1/b$, *e.g.*, in (2.9), and either b or m are non-integer numbers. To circumvent this problem, the following asymptotic approximations are proposed:

$$\mathscr{F}_{11}(x) \overset{(a)}{\approx} \begin{cases} {}_1F_1\left(\alpha_1;\beta_1,-\mathscr{K}x\right) & \text{if } \mathscr{K}x < \aleph_\infty \\ \frac{\Gamma(\beta_1)}{\Gamma(\beta_1-\alpha_1)}(\mathscr{K}x)^{-\alpha_1} + \frac{\Gamma(\beta_1)}{\Gamma(\alpha_1)}\exp\{-\mathscr{K}x\}(-\mathscr{K}x)^{\alpha_1-\beta_1} & \text{if } \mathscr{K}x \geq \aleph_\infty \end{cases} \tag{2.19}$$

$$\mathscr{F}_{22}(x) \overset{(b)}{\approx} \begin{cases} {}_2F_2\left(\alpha_1,\alpha_2;\beta_1,\beta_2;-\mathscr{K}x\right) & \text{if } \mathscr{K}x < \aleph_\infty \\ \dfrac{\Gamma\left(\beta_1\right)\Gamma\left(\beta_2\right)\Gamma\left(\alpha_2-\alpha_1\right)}{\Gamma\left(\alpha_2\right)\Gamma\left(\beta_1-\alpha_1\right)\Gamma\left(\beta_2-\alpha_1\right)}(\mathscr{K}x)^{-\alpha_1} & \\ + \dfrac{\Gamma\left(\beta_1\right)\Gamma\left(\beta_2\right)\Gamma\left(\alpha_1-\alpha_2\right)}{\Gamma\left(\alpha_1\right)\Gamma\left(\beta_1-\alpha_2\right)\Gamma\left(\beta_2-\alpha_2\right)}(\mathscr{K}x)^{-\alpha_2} & \text{if } \mathscr{K}x \geq \aleph_\infty \\ + \dfrac{\Gamma\left(\beta_1\right)\Gamma\left(\beta_2\right)}{\Gamma\left(\alpha_1\right)\Gamma\left(\alpha_2\right)}\exp\{-\mathscr{K}x\}(-\mathscr{K}x)^{\alpha_1+\alpha_2-\beta_1-\beta_2} & \end{cases} \tag{2.20}$$

where (a) and (b) follow from [71] and [72], respectively.

The key parameter for the efficient computation of $\mathscr{F}_{11}(\cdot)$ and $\mathscr{F}_{22}(\cdot)$ is $\aleph_\infty$, which is a positive constant $\gg 1$. The choice of $\aleph_\infty$ depends on the mathematical software package being used for computing the generalized hypergeometric functions. In practice, $\aleph_\infty$ is the largest argument of the hypergeometric functions for which they can be efficiently computed. As an indication, the numerical results shown in Section 2.6 are obtained by setting $\aleph_\infty = 100$. As an example, Fig. 2.3 shows the accuracy of the approximations in (2.19) and (2.20) for $\aleph_\infty = 100$. It is worth mentioning that Fig. 2.3 is obtained by considering a set of parameters for which ${}_1F_1\left(\alpha_1;\beta_1,-\mathscr{K}x\right)$ and ${}_2F_2\left(\alpha_1,\alpha_2;\beta_1,\beta_2;-\mathscr{K}x\right)$ can be computed without resorting to the approximations in (2.19) and (2.20), otherwise it would have not been possible to demonstrate the accuracy of the approximations. The numerical results shown in Section 2.6 confirm the accuracy of the proposed approximations for those parameters for which ${}_1F_1\left(\alpha_1;\beta_1,-\mathscr{K}x\right)$ and ${}_2F_2\left(\alpha_1,\alpha_2;\beta_1,\beta_2;-\mathscr{K}x\right)$ cannot be computed as well.

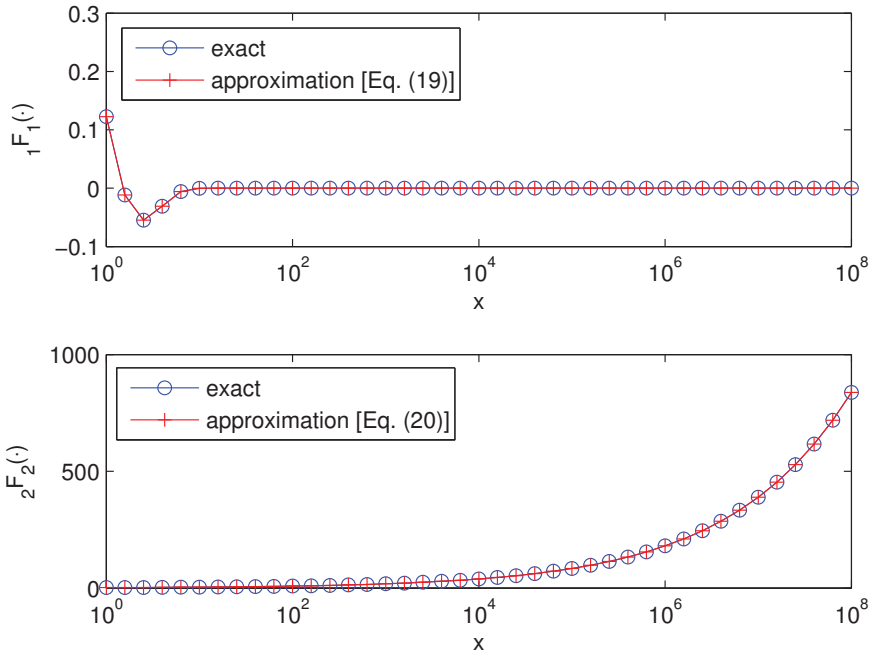

Figure 2.3: Accuracy of the approximations in (2.19) (top) and (2.20) (bottom). The parameters setup is: $b=3$; $m=2$; $\mathscr{K}=1$, where (top) $\alpha_1=m+1/2$ and $\beta_1=3/2$; (bottom) $\alpha_1=-1/b$, $\beta_1=1$, $\alpha_2=m$ and $\beta_2=1-1/b$. For consistency, similar parameters are considered in Section 2.6.

2.4 Downlink MIMO Cellular Networks

In this section, the error probability of MIMO cellular networks is studied by assuming an arbitrary number of antennas at the BSs, *i.e.*, N_t, and at the MT, *i.e.*, N_r. The mathematical analysis is based on the demodulator in (2.3). For mathematical tractability, i.i.d. Rayleigh fading on the interfering links is considered, *i.e.*, $\left|\mathbf{H}_i^{(r,t)}\right| \sim \text{Gamma}\,(1,\Omega)$ for $t=1,2,\ldots,N_t$, $r=1,2,\ldots,N_r$ and $i\in\Phi^{(\setminus 0)}$. On the other hand, the framework is general enough to be applicable to arbitrary fading models on the BS_0-to-MT link. As an example, explicit expressions of the error probability are provided under the assumption that it is Rayleigh distributed too, *i.e.*, $\left|\mathbf{H}_0^{(r,t)}\right| \sim \text{Gamma}\,(1,\Omega)$ for $t=1,2,\ldots,N_t$ and $r=1,2,\ldots,N_r$. The mathematical derivation shows that this latter scenario can be studied by capitalizing on the mathematical framework developed in Section 2.3 for SISO cellular networks and for transmission over Gamma fading.

2.4.1 Characteristic Function of the Other-Cell Interference at the Output of the Demodulator

In this section, we provide a closed-form expression of the CF of $\text{I}(\cdot)$ in (2.4), which is the other-cell interference at the output of the demodulator. The main result is given in *Theorem 2.3* and *Corollary 2.3*.

Theorem 2.3 *Let* $\mathrm{I}(r_0)=\sum_{r=1}^{N_r}\mathbf{i}_{\mathrm{agg}}^{(r)}(r_0)\sum_{t=1}^{N_t}\left(\mathbf{H}_0^{(r,t)}\boldsymbol{\Delta}_0^{(t)}\right)^H$. *Let the downlink channels* $\mathbf{H}_i$ *for* $i\in\Phi^{(\backslash 0)}$ *be i.i.d. Rayleigh distributed. By conditioning upon* r_0 *and upon* U *given in* (2.4)*, the CF of* $\mathrm{I}(\cdot)$ *can be formulated as follows:*

$$\psi_{\mathrm{I}}(\boldsymbol{\omega};r_0,\mathrm{U})=\psi_{\mathrm{I}}(|\boldsymbol{\omega}|;r_0,\mathrm{U})=\exp\left\{-\lambda\pi r_0^2\bar{\mathrm{T}}\left(|\boldsymbol{\omega}|^2 r_0^{-2b}E\mathrm{U}\right)\right\} \tag{2.21}$$

where $\bar{\mathrm{T}}(x)=p\bar{\Upsilon}(x)-p$ *and:*

$$\begin{aligned}\bar{\Upsilon}(x)&=\mathbb{E}_{\mathbf{s}_i}\left\{\sum_{q=0}^{+\infty}\left(-\frac{1}{4}\right)^q\frac{1}{q!}\frac{(-1/b)_q}{(1-1/b)_q}\left(\frac{\|\mathbf{s}_i\|^2}{N_t}\right)^q(\Omega x)^q\right\}\\&=\mathbb{E}_{\mathbf{s}_i}\left\{{}_1F_1\left(-\frac{1}{b};1-\frac{1}{b};-\frac{x}{4}\frac{\|\mathbf{s}_i\|^2}{N_t}\Omega\right)\right\}\end{aligned} \tag{2.22}$$

where $\mathbb{E}_{\mathbf{s}_i}\{\cdot\}$ *denotes the expectation computed with respect to the* N_t*-tuple of information symbols* $\mathbf{s}_i\in\mathbb{C}^{N_t\times 1}$*. Let* $g(\cdot)$ *be a generic function and* $\mathscr{K}>0$ *be a positive constant, this expectation can be formulated as follows:*

$$\mathbb{E}_{\mathbf{s}_i}\left\{g\left(\frac{\mathscr{K}}{N_t}\|\mathbf{s}_i\|^2\right)\right\}=\frac{1}{\mathsf{M}^{N_t}}\sum_{\chi_1=1}^{\mathsf{M}}\sum_{\chi_2=1}^{\mathsf{M}}\cdots\sum_{\chi_{N_t}=1}^{\mathsf{M}}g\left(\frac{\mathscr{K}}{N_t}\sum_{t=1}^{N_t}\left|\mu_{\chi_t}\right|^2\right) \tag{2.23}$$

Proof*: See Appendix 2.8.5.* □

Corollary 2.3 *Let* $\mathrm{I}(r_0)=\sum_{r=1}^{N_r}\mathbf{i}_{\mathrm{agg}}^{(r)}(r_0)\sum_{t=1}^{N_t}\left(\mathbf{H}_0^{(r,t)}\boldsymbol{\Delta}_0^{(t)}\right)^H$. *Let the downlink channels* $\mathbf{H}_i$ *for* $i\in\Phi^{(\backslash 0)}$ *be i.i.d. Rayleigh distributed. Let a constant-envelope modulation be used, i.e.,* $\left|\mathbf{s}_i^{(t)}\right|^2=1$ *for* $t=1,2,\ldots,N_t$ *and* $i\in\Phi^{(\backslash 0)}$*. By conditioning upon* r_0 *and* U *in* (2.4)*, the CF of* $\mathrm{I}(\cdot)$ *is* $\psi_{\mathrm{I}}(\cdot;\cdot,\cdot)$ *in* (2.21) *with* $\bar{\mathrm{T}}(x)=p\bar{\Upsilon}(x)-p$ *and:*

$$\bar{\Upsilon}(x)=\sum_{q=0}^{+\infty}\left(-\frac{1}{4}\right)^q\frac{1}{q!}\frac{(-1/b)_q}{(1-1/b)_q}(\Omega x)^q={}_1F_1\left(-\frac{1}{b};1-\frac{1}{b};-\frac{\Omega}{4}x\right) \tag{2.24}$$

Proof*: It follows from* (2.23) *and* $\mathbb{E}_{\mathbf{s}_i}\left\{g\left(\left(\mathscr{K}/N_t\right)\|\mathbf{s}_i\|^2\right)\right\}=g(\mathscr{K})$ *for constant-envelope modulations. This concludes the proof.* □

Remark 2.9 *By direct inspection, Theorem 2.3 with* $N_t=N_r=1$ *reduces to Theorem 2.1 with* $\Upsilon(\cdot)$ *in* (2.9) *for* $m=1$*, i.e., Rayleigh fading. Likewise, Theorem 2.3 with* $N_t=N_r=1$ *reduces to [111]. As far as the number of antennas* N_t *and* N_r *is concerned, Theorem 2.1 is a special case of Theorem 2.3. As far as the channel model is concerned, on the other hand, Theorem 2.1 is more general than Theorem 2.3. In fact, Theorem 2.3 is applicable only to Rayleigh fading, while Theorem 2.1 is applicable to general fading distributions.* □

2.4.2 Average Pairwise Frame Error Probability: Exact Analysis

In this section, we compute the error probability of the demodulator in (2.3) by capitalizing on the closed-form expression of the CF of the aggregate other-cell interference at the demodulator output. More specifically, in this section we are interested in computing the Average Pairwise Frame Error Probability ($\mathrm{APEP}^{(\mathrm{F})}$), which is defined as the probability that the actual transmitted vector $\mathbf{s}_0$ is decoded as $\hat{\mathbf{s}}_0 = \bar{\mathbf{s}}_0 \neq \mathbf{s}_0$, by assuming that $\mathbf{s}_0$ and $\bar{\mathbf{s}}_0$ are the only two information vectors possibly being transmitted. The rationale behind this definition, which is widely adopted in the literature [74], is that the typical MT is interested in decoding the entire information vector $\mathbf{s}_0$. Thus, an error occurs even if just one symbol $\mathbf{s}_0^{(t)}$ for $t = 1, 2, \ldots, N_t$ is not decoded correctly. Similar to the SISO cellular network setup, the $\mathrm{APEP}^{(\mathrm{F})}$ can be formulated as $\mathrm{APEP}^{(\mathrm{F})}(\boldsymbol{\Delta}_0) = \mathbb{E}_{\mathbf{H}_0, r_0}\left\{\mathrm{PEP}^{(\mathrm{F})}(\boldsymbol{\Delta}_0; \mathbf{H}_0, r_0)\right\}$. From (2.3), the $\mathrm{APEP}^{(\mathrm{F})}$ is summarized in *Theorem 2.4*.

Theorem 2.4 *Let the demodulator in* (2.3) *and* (2.4). *Let* $\mathsf{SNR} = E/\mathcal{N}_0$ *and* U *defined in* (2.4). *Then,* $\mathrm{APEP}^{(\mathrm{F})}$ *can be formulated as* $\mathrm{APEP}^{(\mathrm{F})}(\boldsymbol{\Delta}_0) = \Pr\{\Lambda(\tilde{\mathbf{s}}_0) < 0\} = \mathrm{APEP}_{\mathrm{N}}^{(\mathrm{F})}(\boldsymbol{\Delta}_0) + \mathrm{APEP}_{\mathrm{NI}}^{(\mathrm{F})}(\boldsymbol{\Delta}_0)$, *where* $\mathrm{APEP}_{\mathrm{N}}^{(\mathrm{F})}(\cdot)$ *and* $\mathrm{APEP}_{\mathrm{NI}}^{(\mathrm{F})}(\cdot)$ *are formulated in* (2.25), *shown at the bottom of the next page, and:*

$$\begin{cases} \mathrm{APEP}_{\mathrm{N}}^{(\mathrm{F})}(\boldsymbol{\Delta}_0) = \dfrac{1}{2\sqrt{\pi}} b \sqrt{\dfrac{\mathsf{SNR}}{N_t}} \displaystyle\int_0^{+\infty} x^{-(b+1)} \exp\left(-\pi\lambda x^2\right) \mathrm{Q}_{\mathrm{N}}^{(\mathrm{F})}\left(x; \boldsymbol{\Delta}_0, \dfrac{\mathsf{SNR}}{N_t}, b\right) dx \\ \mathrm{APEP}_{\mathrm{NI}}^{(\mathrm{F})}(\boldsymbol{\Delta}_0) = \dfrac{1}{2\pi} \displaystyle\int_0^{+\infty}\int_0^{+\infty} \dfrac{e^{-y}}{x} \exp\left\{-\dfrac{1}{4}\dfrac{N_t x y^b}{(\pi\lambda)^b SNR}\right\} \left[1 - \exp\left\{-y\overline{\mathrm{T}}(N_t x)\right\}\right] \mathrm{Q}_{\mathrm{NI}}^{(\mathrm{F})}(x; \Delta_0)\, dx dy \end{cases} \tag{2.25}$$

$$\begin{cases} \mathrm{Q}_{\mathrm{N}}^{(\mathrm{F})}\left(x; \boldsymbol{\Delta}_0, \mathsf{SNR}/N_t, b\right) = \mathbb{E}_{\mathrm{U}}\left\{\sqrt{\mathrm{U}} \exp\left\{-(1/4)\left(\mathsf{SNR}/N_t\right)\mathrm{U} x^{-2b}\right\}\right\} \\ \mathrm{Q}_{\mathrm{NI}}^{(\mathrm{F})}(x; \boldsymbol{\Delta}_0) = \mathbb{E}_{\mathrm{U}}\left\{\sin\left((1/2)\sqrt{\mathrm{U}} x^{1/2}\right)\right\} \end{cases} \tag{2.26}$$

Proof*: See Appendix 2.8.6.* □

Remark 2.10 *Theorem 2.3 and Theorem 2.4 hold for arbitrary fading distributions on the* BS_0*-to-MT link, since they are conditioned upon the RV* U *that depends only on* $\mathbf{H}_0$. □

As mentioned in *Remark 2.10, Theorem 2.4* holds for any $\mathbf{H}_0$. As an example, *Proposition 2.6* provides a closed-form expression of $\mathrm{Q}_{\mathrm{N}}^{(\mathrm{F})}(\cdot;\cdot,\cdot,\cdot)$ and $\mathrm{Q}_{\mathrm{NI}}^{(\mathrm{F})}(\cdot;\cdot)$ when the BS_0-to-MT links are i.i.d. Rayleigh distributed.

Proposition 2.6 *Let* $\mathrm{Q}_{\mathrm{N}}^{(\mathrm{F})}(\cdot;\cdot,\cdot,\cdot)$ *and* $\mathrm{Q}_{\mathrm{NI}}^{(\mathrm{F})}(\cdot;\cdot)$ *in* (2.26). *Let* $\left|\mathbf{H}_0^{(r,t)}\right| \sim \mathrm{Gamma}(1, \Omega)$ *for* $t = 1, 2, \ldots, N_t$ *and* $r = 1, 2, \ldots, N_r$. *Then,* $\mathrm{Q}_{\mathrm{N}}^{(\mathrm{F})}\left(x; \boldsymbol{\Delta}_0, \mathsf{SNR}/N_t, b\right) = \bar{\mathscr{F}}_1\left((1/4)\left(\mathsf{SNR}/N_t\right) x^{-2b}; \|\boldsymbol{\Delta}_0\|^2\right)$

and $\mathrm{Q}_{\mathrm{NI}}^{(\mathrm{F})}(x;\mathbf{\Delta}_0) = \bar{\mathscr{I}}_2\left((1/2)\,x^{1/2};\|\mathbf{\Delta}_0\|^2\right)$*, where, for arbitrary* $\mathscr{K}_1 > 0$ *and* $\mathscr{K}_2 > 0$ *positive constants, we have:*

$$\begin{cases} \bar{\mathscr{I}}_1\left(\mathscr{K}_1;\|\mathbf{\Delta}_0\|^2\right) = \mathbb{E}_{\mathrm{U}}\left\{\sqrt{\mathrm{U}}\exp\left\{-\mathscr{K}_1\mathrm{U}\right\}\right\} \\ \qquad\qquad = N_r^{N_r}\left[\left(\Omega N_r\|\mathbf{\Delta}_0\|^2\right)^{N_r}\Gamma(N_r)\right]^{-1}\Gamma(N_r+1/2)\times\left(\mathscr{K}_1+\left(\Omega\|\mathbf{\Delta}_0\|^2\right)^{-1}\right)^{-(N_r+1/2)} \\ \bar{\mathscr{I}}_2\left(\mathscr{K}_2;\|\mathbf{\Delta}_0\|^2\right) = \mathbb{E}_{\mathrm{U}}\left\{\sin\left(\mathscr{K}_2\sqrt{\mathrm{U}}\right)\right\} \\ \qquad\qquad = \sqrt{\Omega\|\mathbf{\Delta}_0\|^2}\Gamma(N_r+1/2)\left(\Gamma(N_r)\right)^{-1}\mathscr{K}_2 \\ \qquad\qquad\quad \times {}_1F_1\left(N_r+1/2;3/2,-(1/4)\,\Omega\|\mathbf{\Delta}_0\|^2\mathscr{K}_2^2\right) \end{cases} \tag{2.27}$$

Proof*: See Appendix 2.8.7.* □

Finally, we close this section with three comments about the computation of $\mathrm{APEP}^{(\mathrm{F})}$:

1. Based on the similarity of (2.11) and (2.12) with (2.25) and (2.26), asymptotic expressions similar to *Corollary 2.2* can be computed for MIMO cellular networks. In particular, *Corollary 2.2* can be readily generalized with the substitutions: $\mathsf{SNR} \to \mathsf{SNR}/N_t$, $\mathrm{T}(\cdot) \to \bar{\mathrm{T}}(\cdot)$, $\mathrm{Q}_{\mathrm{N}}(\cdot) \to \mathrm{Q}_{\mathrm{N}}^{(\mathrm{F})}(\cdot)$ and $\mathrm{Q}_{\mathrm{NI}}(\cdot) \to \mathrm{Q}_{\mathrm{NI}}^{(\mathrm{F})}(\cdot)$.

2. Based on similar arguments, piecewise single-integral bounds for MIMO cellular networks can be obtained from Section 2.3.4.

3. In Section 2.3.6, we have pointed out that the computation of some hypergeometric functions may either lead to numerical inaccuracies or may need too much time for some network setups. To avoid these issues, approximations based on asymptotic expansions of the hypergeometric functions have been proposed. These numerical problems do not arise, on the other hand, in MIMO cellular networks for propagation over Rayleigh fading channels. This originates from the fact that the particular form of the special functions for Rayleigh fading seems to be more numerically stable than for other fading distributions. This outcome is also in agreement with [111], where the error probability of SISO cellular networks over Rayleigh fading is studied and the authors did not experience any numerical issues with the computation of the special functions. However, these numerical issues are dependent on the mathematical software package that is used for the computation. Should numerical instabilities occur, the readers may apply the piecewise asymptotic approximation of (2.19) to MIMO cellular networks too.

2.4.3 Nearest Neighbor Approximation of the Average Frame Error Probability

Similar to Section 2.3.5, in this section we propose a mathematical framework to the computation of the Average Frame Error Probability (AFEP), which is based on the NN approx-

imation and on the computation of a single APEP$^{(\mathrm{F})}$. For ease of illustration, let us consider the Rayleigh fading case, where $\left|\mathbf{H}_0^{(r,t)}\right| \sim \text{Gamma}\,(1,\Omega)$ and $\left|\mathbf{H}_i^{(r,t)}\right| \sim \text{Gamma}\,(1,\Omega)$ for $t = 1,2,\ldots,N_t$, $r = 1,2,\ldots,N_r$ and $i \in \Phi^{(\backslash 0)}$. By direct inspection of (2.25)–(2.27) and with the aid of (2.19), it follows that APEP$^{(\mathrm{F})}$ depends only on $\|\boldsymbol{\Delta}_0\|^2$. In particular, it decreases as $\|\boldsymbol{\Delta}_0\|^2$ increases. In other words, the error probability depends on the Euclidean distance between pairs of N_t-dimensional vectors of the constellation diagram. Also, the larger the Euclidean distance the smaller the error probability. As a consequence, the AFEP can be computed from the pairs $(\mathbf{s}_0, \tilde{\mathbf{s}}_0)$ of the N_t-dimensional constellation diagram providing the smallest Euclidean distance $\|\boldsymbol{\Delta}_0\|^2$. Accordingly, the NN approximation of the AFEP can be formulated as follows:

$$\text{AFEP} \approx \frac{1}{\mathsf{M}^{N_t}} \sum_{\chi=1}^{\mathsf{M}^{N_t}} N^{(\chi)}_{\|\boldsymbol{\Delta}_{\min}\|^2} \text{APEP}^{(\mathrm{F})} \left(\left\| \boldsymbol{\Delta}^{(\chi)}_{\min} \right\|^2 \right) \tag{2.28}$$

where: i) $\left\| \boldsymbol{\Delta}^{(\chi)}_{\min} \right\|^2 = \min_{\boldsymbol{\mu}_{\tilde{\chi}} \in \mathbb{M}^{N_t \times 1}} \left\{ \left\| \boldsymbol{\mu}_{\tilde{\chi}} - \boldsymbol{\mu}_{\chi} \right\|^2, \boldsymbol{\mu}_{\tilde{\chi} \neq \chi} \in \mathbb{M}^{N_t \times 1}, \tilde{\chi} \neq \chi \right\}$ is the minimum Euclidean distance among all pairs $\left(\boldsymbol{\mu}_{\tilde{\chi}}, \boldsymbol{\mu}_{\chi} \right)$ of vectors of the N_t-dimensional constellation diagram $\mathbb{M}^{N_t \times 1}$ and ii) $N^{(\chi)}_{\|\boldsymbol{\Delta}_{\min}\|^2}$ is the number of nearest neighbors of $\boldsymbol{\mu}_{\chi}$. If $\left\| \boldsymbol{\Delta}^{(\chi)}_{\min} \right\|^2 = \|\boldsymbol{\Delta}_{\min}\|^2$ for every $\boldsymbol{\mu}_{\chi} \in \mathbb{M}^{N_t \times 1}$, then (2.28) simplifies to $\text{AFEP} \approx N^{(\text{avg})}_{\|\boldsymbol{\Delta}_{\min}\|^2} \text{APEP}^{(\mathrm{F})} \left(\|\boldsymbol{\Delta}_{\min}\|^2 \right)$ with $N^{(\text{avg})}_{\|\boldsymbol{\Delta}_{\min}\|^2} = \left(1/\mathsf{M}^{N_t}\right) \sum_{\chi=1}^{\mathsf{M}^{N_t}} N^{(\chi)}_{\|\boldsymbol{\Delta}_{\min}\|^2}$ being the average number of nearest neighbors of the constellation diagram. For some constellation diagrams, we may have $N^{(\chi)}_{\|\boldsymbol{\Delta}_{\min}\|^2} = N_{\|\boldsymbol{\Delta}_{\min}\|^2}$ for every $\boldsymbol{\mu}_{\chi} \in \mathbb{M}^{N_t \times 1}$, which implies $N^{(\text{avg})}_{\|\boldsymbol{\Delta}_{\min}\|^2} = N_{\|\boldsymbol{\Delta}_{\min}\|^2}$ and $\text{AFEP} \approx N_{\|\boldsymbol{\Delta}_{\min}\|^2} \text{APEP}^{(\mathrm{F})} \left(\|\boldsymbol{\Delta}_{\min}\|^2 \right)$.

For example, if the standard square QAM with M symbols is considered, we have:

- $\left(\|\boldsymbol{\Delta}_{\min}\|^2, N_{\|\boldsymbol{\Delta}_{\min}\|^2} \right) = (4,2)$ if $(\mathsf{M} = 2, N_t = 2)$;
- $\left(\|\boldsymbol{\Delta}_{\min}\|^2, N_{\|\boldsymbol{\Delta}_{\min}\|^2} \right) = (2,4)$ if $(\mathsf{M} = 4, N_t = 2)$;
- $\left(\|\boldsymbol{\Delta}_{\min}\|^2, N^{(\text{avg})}_{\|\boldsymbol{\Delta}_{\min}\|^2} \right) = (0.4,6)$ if $(\mathsf{M} = 16, N_t = 2)$;
- $\left(\|\boldsymbol{\Delta}_{\min}\|^2, N_{\|\boldsymbol{\Delta}_{\min}\|^2} \right) = (4,4)$ if $(\mathsf{M} = 2, N_t = 4)$;
- $\left(\|\boldsymbol{\Delta}_{\min}\|^2, N_{\|\boldsymbol{\Delta}_{\min}\|^2} \right) = (2,8)$ if $(\mathsf{M} = 4, N_t = 4)$.

It is worth noting that $N^{(\chi)}_{\|\boldsymbol{\Delta}_{\min}\|^2} \in \{4,5,6,7,8\}$ if $(\mathsf{M} = 16, N_t = 2)$. On the other hand, if PSK modulation is used, it is possible to show, by direct inspection of the constellation diagram, that $\|\boldsymbol{\Delta}_{\min}\|^2 = 4\sin^2\left(\pi/\mathsf{M}\right)$ for $\mathsf{M} \geq 2$ and $N_{\|\boldsymbol{\Delta}_{\min}\|^2} = N_t$ if $\mathsf{M} = 2$ and $N_{\|\boldsymbol{\Delta}_{\min}\|^2} = 2N_t$ if $\mathsf{M} \geq 4$. If $\mathsf{M} = 2$ and $\mathsf{M} = 4$, square QAM and PSK modulations provide the same results, as expected. For a general constellation diagram, *Remark 2.11* hold.

Remark 2.11 *Let $\boldsymbol{\mu}_{\chi} \in \mathbb{M}^{N_t \times 1}$ be the complex points of a generic N_t-dimensional constellation diagram. Then, $\left\| \boldsymbol{\Delta}_{\min}^{(\chi)} \right\|^2 = \left| \Delta_{\min}^{(\chi)} \right|^2$ and $N_{\|\boldsymbol{\Delta}_{\min}\|^2}^{(\chi)} = N_t N_{\Delta_{\min}}^{(\chi)}$, where $\left| \Delta_{\min}^{(\chi)} \right|$ and $N_{\Delta_{\min}}^{(\chi)}$ are defined in Section 2.3.5. This is because the minimization of the summation of N_t positive and identically distributed functions is equivalent to the minimization of each individual function, each of them having the same minimum.* □

2.5 Insights from the Mathematical Framework: Main Performance Trends

In this section, we summarize the main performance trends that can be inferred from the mathematical frameworks developed in the previous sections. Two case studies are considered, which correspond to noise-limited ($\mathsf{SNR} \to 0$) and interference-limited ($\mathsf{SNR} \to +\infty$) cellular networks. As a result, the performance trends are mainly derived from direct inspection of the asymptotic frameworks of Section 2.3.3.

Let us consider a SISO cellular network operating in the noise-limited regime. From *Corollary 2.2*, it follows that $\mathrm{APEP}(|\Delta_0|) \approx \mathrm{APEP}_{\mathrm{N}}(|\Delta_0|)$. It is worth nothing that $\mathrm{APEP}_{\mathrm{N}}(\cdot)$ is different from common mathematical frameworks in the absence of other-cell interference [60], as the BS_0-to-MT distance is a random variable that depends on the cell association criterion, which, in turn, depends on the density of BSs λ. However, the performance trends as a function of the SNR and of the path-loss exponent b are preserved. In addition, by direct inspection of $\mathrm{APEP}_{\mathrm{N}}(\cdot)$, the following conclusions can be drawn.

- *The diversity order of the APEP, $\mathscr{D}$, [75] depends only on* $\mathrm{Q}_{\mathrm{N}}^{(\infty)} = \mathrm{Q}_{\mathrm{N}}(\cdot; \mathsf{SNR} \to \infty)$. According to [75, Sec. II], the diversity order is defined as the slope of the APEP as a function of the SNR in a log-log scale. From (2.12), only $\mathrm{Q}_{\mathrm{N}}(\cdot;\cdot)$ depends on the SNR and, thus, it determines the diversity order. Let us assume that $\mathrm{Q}_{\mathrm{N}}^{(\infty)}$ can be formulated, according to [75, Sec. II], as $\mathrm{Q}_{\mathrm{N}}^{(\infty)} \approx \mathscr{K} \mathsf{SNR}^{-d}$, where $\mathscr{K}$ is a positive constant independent of the SNR. Then, from direct inspection of (2.12), the diversity order is equal to $\mathscr{D} = d - 1/2$. As an example, let us consider either Gamma or Gamma/Log-Normal fading. From direct inspection of (2.13) and (2.14), respectively, it follows that $d = m + 1/2$ for high-SNR. As a consequence, $\mathscr{D} = m$ in both cases.

- *The APEP decreases by increasing the BSs' density.* This follows directly from (2.11), which shows that the APEP decreases exponentially with the density, λ, of BSs.

- *The APEP increases by increasing the shadowing standard deviation.* Let us consider the Gamma/Log-Normal fading model in (2.14). The impact of the shadowing standard deviation depends on how η is chosen and if it depends on σ. If, as suggested in *Remark 2.3*, $\eta = \kappa^{-1} \ln(\Omega) - (1/2)\kappa\sigma^2$, then the analysis of (2.14) reveals that the APEP increases by increasing σ. Likewise, if η is independent of σ, *e.g.*, $\eta = 0$, it is possible to show that the APEP still increases by increasing σ. In fact, τ_k for $k = 1, 2, \ldots, N_{\mathrm{GHQ}}$ can take either

positive or negative values and the latter ones determine the behavior of (2.14) as σ increases. Furthermore, the larger m the more pronounced the impact of σ on the APEP.

Let us consider a SISO cellular network operating in the interference-limited regime. From *Corollary 2.2*, it follows that $\text{APEP}(|\Delta_0|) \approx \text{APEP}_{\text{NI}}^{(\infty)}(|\Delta_0|)$. Thus, the following conclusions can be drawn.

- *The APEP is independent of the SNR.* This follows from (2.15), which is independent of the SNR. This implies that an error-floor emerges for $\mathsf{SNR} \to \infty$ and that, as a result, the diversity order as a function of the SNR is, regardless of the fading model, equal to zero.
- *The APEP is independent of the BSs' density.* Similar to the low-SNR setup, this follows from (2.15), which is independent of λ.
- *Impact of the fading parameters.* Let us consider the impact of m for Gamma and Gamma/Log-Normal fading. From (2.15), two functions need to be analyzed: $f_1(m) = \frac{(p\Upsilon(x;m)-p)}{(p\Upsilon(x;m)-p+1)}$ and $f_2(m) = \text{Q}_{\text{NI}}(x;m)$. Also, it is known that ${}_pF_q\left(\mathbf{a}_p;\mathbf{b}_q;x\right)\big|_{x\to 0} \to 1$ [7, Sec. III-B]. As a result, $\Upsilon(x;m)|_{m\to+\infty} \to 1$ from (2.9) and (2.10). Thus, $f_1(m)\big|_{m\to+\infty} \to 0$. Likewise, $f_2(m)\big|_{m\to+\infty} \to m^{-1/2}$ from (2.13) and (2.14). In summary, we expect that the APEP decreases by increasing m. However, it is very difficult to study the monotonicity of the hypergeometric functions as a function of their many parameters. As for the impact of the shadowing standard deviation σ for Gamma/Log-Normal fading, a similar mathematical development can be used. In particular, from (2.10) and (2.14) we have to study $\tilde{\tau}_k$, whose impact on the APEP is opposite compared to m. By using arguments similar to the noise-limited regime, we expect that the APEP degrades by increasing σ.
- *The APEP decreases by increasing the path-loss exponent.* From (2.12) and (2.15), we note that only $\text{T}(\cdot)$ depends on b, which is a function of $\Upsilon(\cdot)$ in (2.7). By using the series representation [57, Ch. 5, Eq. 2] of the hypergeometric function in (2.7), it follows that the impact of b depends on the function $f_q(b) = \left(-1/b\right)_q \Big/ \left(1-1/b\right)_q$, where $q \geq 0$ is the index of the series expansion. Since $(x)_q = \Gamma\left(x+q\right)\Big/\Gamma(x)$, we obtain $f_q(b) = \left(1-qb\right)^{-1}$, which implies that $\left|f_q(\cdot)\right|$ decreases by increasing b for $q \geq 1$. In particular, $\Upsilon(x)|_{b\to+\infty} \to 1$, since only the term $q = 0$ of the series expansion has a contribution. The same conclusion can be obtained from (2.9) and (2.10), by noting that ${}_2F_2\left(-1/b, m; 1, 1-1/b; -\mathscr{K}x\right)\big|_{b\to+\infty} \to 1$. From (2.6), this implies $\text{T}(x)|_{b\to+\infty} \to 0$, which in turn implies $\text{APEP}_{\text{NI}}^{(\infty)}(|\Delta_0|)\Big|_{b\to+\infty} \to 0$ from (2.15). As a result, it is expected that the APEP decreases by increasing b.
- *The APEP decreases by decreasing the activity factor.* First of all, we note that $\text{T}(\cdot) \geq 0$, since (2.33) is non-negative by definition. Thus, from (2.6) we obtain $\Upsilon(x) \geq 1$. From (2.15), the impact of p on the APEP depends on the function $f\left(p\right) = \frac{(p\Upsilon(x)-p)}{(p\Upsilon(x)-p+1)}$. By studying the first- and second-order derivative of $f(\cdot)$ as a function of p and by taking into account that $\Upsilon(x) \geq 1$, it follows that $f(\cdot)$ is monotonically increasing with p. As a result, the APEP decreases as p decreases.

Let us now turn our attention to MIMO cellular networks. By direct comparison of (2.11) and (2.25), it follows that the performance trends of MIMO cellular networks in both noise- and interference-limited regimes are the same as those of SISO cellular networks, as a function of many system parameters, such as SNR, λ, b and p. Furthermore, in Appendix 2.8.7 it is proved that $\mathrm{U} \sim \mathrm{Gamma}\left(N_r, \Omega N_r \left\|\boldsymbol{\Delta}_0\right\|^2\right)$. Thus, we conclude that the impact of N_r is equivalent to the impact of m in SISO cellular networks. More specifically, N_r determines the diversity order in noise-limited scenarios. Likewise, the error probability decreases by increasing N_r in interference-limited scenarios. As the SNR increases, however, an error-floor emerges in the latter operating regime. The main difference between SISO and MIMO cellular networks consists in the impact of N_t. To better study the impact of N_t, *Corollary 2.4* and *Corollary 2.5* provide approximate closed-form expressions of (2.25). Similar results can be obtained for SISO cellular networks.

Corollary 2.4 *Let* $\left|\mathbf{H}_0^{(r,t)}\right| \sim \mathrm{Gamma}\left(1,\Omega\right)$ *for* $t = 1,2,\ldots,N_t$, $r = 1,2,\ldots,N_r$ *and* $\mathsf{SNR} \gg 1$. *Then:*

$$\mathrm{APEP}_{\mathrm{N}}^{(\mathrm{F})}\left(\left\|\boldsymbol{\Delta}_0\right\|\right) \approx \left(\frac{1}{4}\right)^{N_r+1/2} \frac{\left(\pi\lambda\right)^{-bN_r}}{\sqrt{\pi}} \times \frac{\Gamma\left(N_r+1/2\right)\Gamma\left(bN_r\right)}{\Gamma\left(N_r\right)} b\left(\frac{\mathrm{SNR}}{N_t}\Omega\left\|\boldsymbol{\Delta}_0\right\|^2\right)^{-N_r} \tag{2.29}$$

Proof*: It follows from* (2.25) *and* (2.27) *by taking into account that* $\mathscr{K}_1 + \left(\Omega\left\|\boldsymbol{\Delta}_0\right\|^2\right)^{-1} \approx \mathscr{K}_1$ *if* $\mathsf{SNR} \gg 1$. *The integral is computed in closed-form with the aid of [65, Eq. 3.326.2]. This concludes the proof.* □

Corollary 2.5 *Let* $\left|\mathbf{H}_0^{(r,t)}\right| \sim \mathrm{Gamma}\left(1,\Omega\right)$ *for* $t = 1,2,\ldots,N_t$, $r = 1,2,\ldots,N_r$ *and* $\mathsf{SNR} \gg 1$. *Then:*

$$\begin{aligned}
&\mathrm{APEP}_{\mathrm{NI}}^{(\mathrm{F},\infty)}\left(\left\|\boldsymbol{\Delta}_0\right\|\right) \\
&\quad\overset{(a)}{\leq} -\frac{p}{2} - \frac{p}{4\sqrt{\pi}}\frac{1}{b}\frac{1}{\Gamma\left(N_r\right)}\frac{\left\|\boldsymbol{\Delta}_0\right\|}{\sqrt{N_t}} \times G_{3,3}^{2,2}\left(\frac{\left\|\boldsymbol{\Delta}_0\right\|^2}{4N_t}\middle|\begin{matrix} 1/2-N_r & 1/2 & 1/2-1/b \\ 0 & -1/2-1/b & -1/2 \end{matrix}\right) \\
&\quad\overset{(b)}{\approx} -\frac{p}{2} + \frac{p}{\sqrt{\pi}}\frac{1}{b+2}\frac{\Gamma\left(N_r+1/2\right)}{\Gamma\left(N_r\right)}\frac{\left\|\boldsymbol{\Delta}_0\right\|}{\sqrt{N_t}} + \frac{p}{2\sqrt{\pi}}\Gamma\left(\frac{1}{2}+\frac{1}{b}\right)\frac{\Gamma\left(N_r-1/b\right)}{\Gamma\left(N_r\right)}\left(\frac{\left\|\boldsymbol{\Delta}_0\right\|^2}{4N_t}\right)^{-1/b}
\end{aligned} \tag{2.30}$$

Proof*: The bound in (a) originates from* (2.25) *and* $\mathsf{SNR} \gg 1$ *by using the same line of thought as* (2.15). *The integral is computed by using the upper-bound* $\bar{\mathrm{T}}\left(x\right)/\left(\bar{\mathrm{T}}\left(x\right)+1\right) \leq \bar{\mathrm{T}}\left(x\right)$, *which is accurate especially for low values of* p. *Finally, the integral is solved by using* (2.27) *and with the aid of [65, Eq. 7.612.1], [58, Eq. 8.4.45.1] and the Mellin-Barnes theorem [58, Eq. 2.24.1.1]. The asymptotic approximation in (b) follows from [76], by taking into account that, based on the NN approximation, the AFEP is dominated by the APEPs for which the condition* $\left\|\boldsymbol{\Delta}_0\right\|^2/4N_t \ll 1$ *holds. This concludes the proof.* □

From the NN approximation in Section 2.4.3 and with the aid of *Corollary 2.4* and *Corollary 2.5*,

the AFEP of MIMO cellular networks can be formulated as $\text{AFEP}_{\text{N}}^{(\text{F})} \approx \mathcal{K}_M N_t \text{APEP}_{\text{N}}^{(\text{F})}(\|\mathbf{\Delta}_0\|_{\min})$ and $\text{AFEP}_{\text{NI}}^{(\text{F},\infty)} \approx \mathcal{K}_M N_t \text{APEP}_{\text{NI}}^{(\text{F},\infty)}(\|\mathbf{\Delta}_0\|_{\min})$ for noise- and interference-limited regimes, respectively. For example, if PSK modulation is considered, we have: $\mathcal{K}_M = 1$ if $M = 2$; $\mathcal{K}_M = 2$ if $M \geq 4$ and $\|\mathbf{\Delta}_0\|_{\min} = 2\sin(\pi/M)$. In order to study the impact of N_t, let us consider MIMO systems that have to provide the same rate for arbitrary antenna configurations. The rate is defined as $\text{R} = N_t \log_2(M)$ bits per channel use (bpcu). Accordingly, $\|\Delta_0\|_{\min} = 2\sin\left(\pi 2^{-\text{R}/N_t}\right)$. Furthermore, as far as the density λ of BSs is concerned, two case studies are worth being investigated: 1) λ and N_t are independent of each other and 2) $\lambda = \lambda(N_t) = \lambda_0/N_t$, which implies that λ depends on N_t but their product is constant and equal to λ_0. The latter case study is of interest in order to compare MIMO cellular networks either with many single-antenna BSs or with a few multi-antenna BSs, but always keeping the same density of BSs antennas. This is, in fact, a key optimization problem in cellular networks [84]. While the mathematical study of the derivatives of (2.29) and (2.30), as a function of N_t, is possible, it turns out to be quite tedious as it depends on many system parameters. A simpler and more pragmatic way to proceed is to plot $\text{AFEP}_{\text{N}}^{(\text{F})}$ and $\text{AFEP}_{\text{NI}}^{(\text{F},\infty)}$ for typical cellular setups (the reader is referred to Section 2.6 for some examples) and to study the impact of N_t, by assuming a fixed rate R and $\|\Delta_0\|_{\min} = 2\sin\left(\pi 2^{-\text{R}/N_t}\right)$. The following trends emerge from this analysis:

- In noise-limited cellular networks, the AFEP is expected to decrease by increasing N_t if λ and N_t are independent of each other.
- In noise-limited cellular networks, the AFEP is expected to increase by increasing N_t if $\lambda N_t = \lambda_0$.
- In interference-limited cellular networks, the AFEP is independent of λ and it is expected to decrease by increasing N_t. The impact is more pronounced in symmetric MIMO setups having $N_t = N_r$, while it is less pronounced if $N_t > N_r$. In fact, increasing N_r is also beneficial in MIMO cellular networks.

These trends are substantiated in Section 2.6 with the aid of Monte Carlo simulations as well. In any case, the APEPs in (2.29) and (2.30) are sufficiently simple and depend on all the most important design parameters that the interested reader may readily plot them for comparing different MIMO setups of interest.

2.6 Numerical and Simulation Results

In this section, some numerical examples are shown in order to substantiate the accuracy of the proposed mathematical frameworks and to investigate the performance trends highlighted in Section 2.5. The following notation is used for SISO transmission: i) *MC* denotes the results obtained with the aid of Monte Carlo simulations; ii) *NN* denotes the results obtained with the aid of the NN approximation in Section 2.3.5 and of the exact APEP computed in Section 2.3.2; iii) *NN-LB* differs from *NN* because the LB of the APEP computed in Section 2.3.4 is

used; iv) *NN-UB* differs from *NN* because the UB of the APEP computed in Section 2.3.4 is used; and v) *NN-INF* differs from *NN* because the asymptotic expression of the APEP (interference-limited regime) computed in Section 2.3.3 is used. All mathematical frameworks are computed by using the approximations in Section 2.3.6 by setting $\aleph_\infty = 100$. We have verified that the same curves are obtained by using the exact expressions of the hypergeometric functions, when they can be computed efficiently (*i.e.*, if neither b nor m are non-integer numbers). As for MIMO transmission, the mathematical frameworks are replaced with those available in Section 2.4. In this case, no approximations are used for the computation of the hypergeometric functions. Monte Carlo simulations are obtained by using the procedure described in [7, Sec. V]. The only difference is that the error performance instead of the average rate is computed, by implementing the demodulator in (2.2). All Monte Carlo simulations are depicted by using "black" curves. Curves with different markers represent the mathematical frameworks. In all figures, the rate of MIMO systems is defined as $\mathrm{R} = N_t \log_2(M)$ bpcu. As for the composite Gamma/Log-Normal channel model, the results are obtained by setting $\eta = \kappa^{-1}\ln(\Omega) - (1/2)\kappa\sigma^2$ with $\kappa = 10^{-1}\ln(10)$, as discussed in *Remark 2.3*. The mathematical frameworks are obtained by setting $N_{\mathrm{GHQ}} = 3$.

Validation of the PPP-based Abstraction Model Before analyzing the accuracy of the mathematical frameworks against Monte Carlo simulations based on the PPP abstraction model for the locations of the BSs, in Fig. 2.4 we compare Monte Carlo simulations obtained by modeling the BS locations via grid-based and PPP-based abstraction models. A similar comparison is available in [6, Sec. V-A] for the coverage probability. In this section, we focus our attention on the error probability. The following notation is used in Fig. 2.4: i) *solid lines* show the results obtained with the aid of Monte Carlo simulations based on the PPP-based abstraction and ii) *dashes lines* show the results obtained with the aid of Monte Carlo simulations based on the grid-based abstraction. The latter results are obtained by using the same procedure as in [6, Sec. V-A] with three main differences: 1) instead of the SINR, the received signal in (2.1) is generated and the demodulator in (2.2) is applied at the MT; 2) either a Gamma or a Gamma/Log-Normal channel model is used; and 3) the error probability instead of the coverage probability is considered. By direct inspection of Fig. 2.4, we observe a reasonable agreement between the two abstraction models. As expected, and similar to [6, Sec. V-A], the PPP-based abstraction model provides a worst estimate of the error probability compared to the grid-based abstraction model, since interfering BSs may be arbitrarily close to each other. On the other hand, the main advantage of the PPP-based abstraction model lies in its mathematical tractability and in the design insights that can be inferred from the resulting mathematical frameworks.

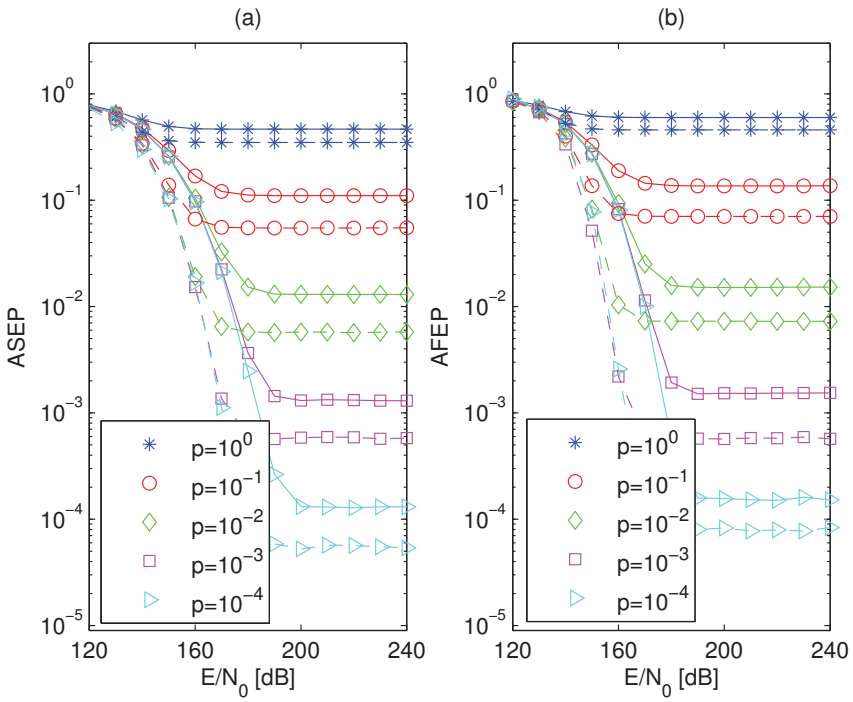

Figure 2.4: ASEP/AFEP of a $N_t \times N_r$ system against the reference SNR $E/\mathcal{N}_0$: comparison between PPP- (solid lines) and grid-based (dashed lines) abstraction models. Setup: (a) $N_t = 1$ and $N_r = 1$, QAM with $M = 16$, Gamma/Log-Normal channel model with $m = 2$ and $\sigma = 6$dB, $b = 3$ and $\lambda = 10^{-5}$. (b) $N_t = 2$ and $N_r = 2$, QAM with $M = 16$, Gamma channel model with $m = 1$ (Rayleigh fading), $b = 3$ and $\lambda = 10^{-5}$.

Validation of the Mathematical Frameworks In Figs. 2.5–2.7, the accuracy of the mathematical frameworks is compared against Monte Carlo simulations. We observe that a good accuracy is obtained for the analyzed system setups. In particular, the NN approximation provides an upper-bound of the simulated ASEP/AFEP. The accuracy for high-SNR increases by increasing the number of antennas at the receiver. The piecewise singe-integral bounds are accurate and simple to compute. However, they are less accurate in the two "corners" of the error probability curves. The accuracy in the corners increases by decreasing the activity factor p. In the figures, $p = 10^{-3}$ is shown since it provides reasonable values of the ASEP/AFEP for the cellular setup under analysis. The framework denoted by *NN-INF* confirms that the ASEP/AFEP is independent of λ in the interference-limited regime. For ease of illustration, in the next figures only the results denoted by *MC* ("black" curves) and *NN* (all the other curves) are shown.

Impact of Wireless Channel and Cellular Setup In Figs. 2.8–2.11, the error performance of SISO and MIMO transmissions is studied as a function of fading and shadowing conditions, as well as as a function of BSs density and activity factor. Overall, the performance trends are in agreement with the analysis of Section 2.5. More specifically, Fig. 2.8 shows that the fading severity m has a negligible impact on the ASEP and that, on the other hand, the shadowing standard deviation σ has a more important impact. As expected, the ASEP decreases by

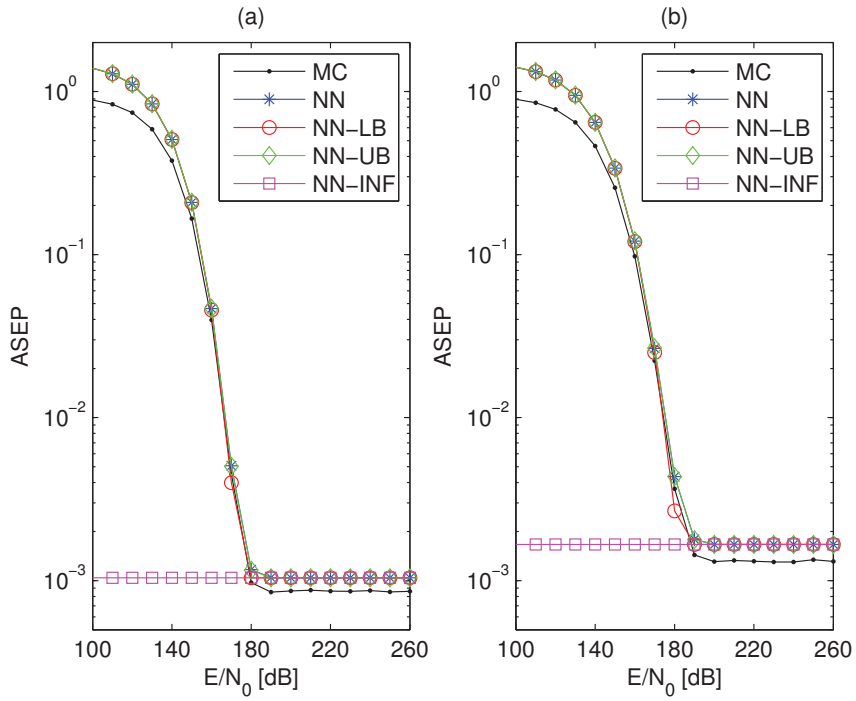

Figure 2.5: ASEP of a $N_t \times N_r = 1 \times 1$ system against the reference SNR $E/\mathcal{N}_0$. Setup: (a) QAM with $M = 16$, Gamma channel model with $m = 2$, $b = 3$, $\lambda = 10^{-5}$ and $p = 10^{-3}$. (b) QAM with $M = 16$, Gamma/Log-Normal channel model with $m = 2$ and $\sigma = 6$dB, $b = 3$, $\lambda = 10^{-5}$ and $p = 10^{-3}$.

increasing m and degrades by increasing σ. Figures 2.9 and 2.10 show the important impact that the path-loss exponent b has on the ASEP. The trend is different for noise- and interference-limited networks. The figures also confirm that the BS density λ affects the ASEP only in the noise-limited regime. In Fig. 2.11, the impact of the activity factor p is studied. The figure confirms the important impact of p on the achievable ASEP/AFEP, as it drastically reduces the net contribution of the other-cell interference. High values of p may need more sophisticated demodulators compared to the interference-unaware detector studied in the present chapter, in order to counteract the impact of other-cell interference. Although not shown due to space limitations, we have studied the accuracy of our framework for constant-envelop modulations (*e.g.*, PSK modulation) as well. Our results show that, in general, the mathematical frameworks are more accurate in this latter case.

Impact of Receive and Transmit Antennas In Figs. 2.12–2.14, we study how multiple antennas at the BSs and at the typical MT affect the error performance. In particular, Fig. 2.12 confirms that having multiple-antenna at the receiver leads to an improvement of the ASEP/AFEP. However, no receive diversity gain is obtained in the interference-limited regime. In Fig. 2.13, we study symmetric, *i.e.*, $N_t = N_r$, MIMO schemes and investigate two cellular network deployments: i) Fig. 2.13(a) shows the AFEP by assuming that the density λ of BSs is kept the same but the number of BSs antennas N_t is different and ii) Fig. 2.13(b) shows

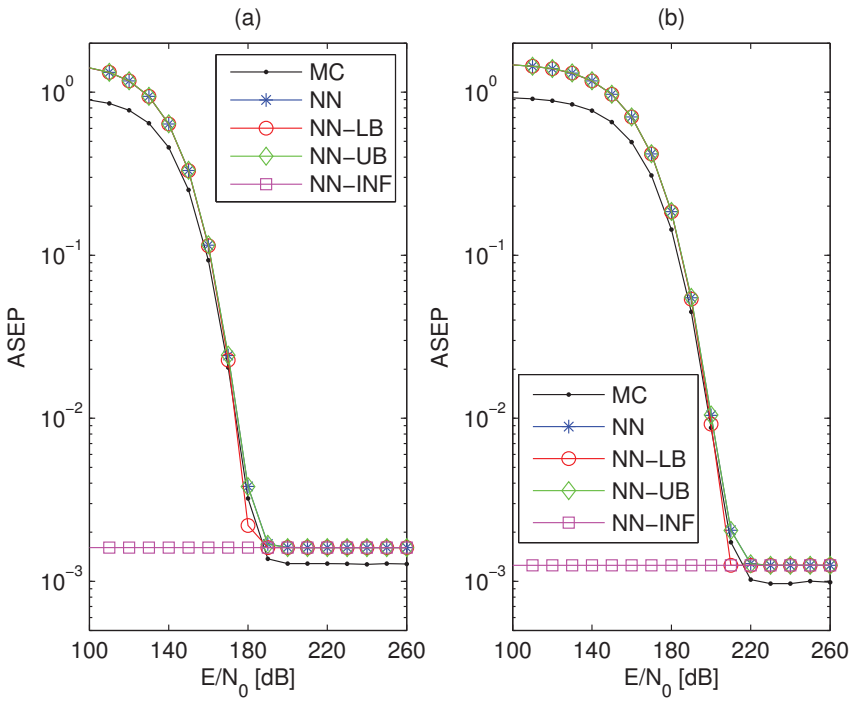

Figure 2.6: ASEP of a $N_t \times N_r = 1 \times 1$ system against the reference SNR $E/\mathcal{N}_0$. Setup: (a) QAM with $M = 16$, Gamma/Log-Normal channel model with $m = 2.5$ and $\sigma = 6$dB, $b = 3$, $\lambda = 10^{-5}$ and $p = 10^{-3}$. (b) QAM with $M = 16$, Gamma/Log-Normal channel model with $m = 2$ and $\sigma = 6$dB, $b = 2.5$, $\lambda = 10^{-5}$ and $p = 10^{-3}$.

the AFEP by assuming that the density of BSs antennas $\lambda_0 = N_t\lambda$ is kept the same and the BSs density λ depends on N_t. In this latter case, the fewer N_t the larger λ. The analysis of these two cellular setups is useful for understanding whether it is better either to increase the density of BSs and to use simple transmission schemes (SISO) or to reduce the density of BSs but to use more advanced transmission schemes (MIMO). Fig. 2.13 shows that the two setups provide a different AFEP only in the noise-limited regime. In particular, Fig. 2.13(b) illustrates that increasing N_t but reducing λ is not a good option. The reason is that the reliability of the useful link degrades because of the longer transmission distance, while the reduction of the other-cell interference has a negligible impact. In the interference-limited regime, on the other hand, both setups provide the same error-floor, since λ does not affect the AFEP. As a result, in this operating regime the density of BSs can be reduced as the number of antennas at the BSs increases. However, λ cannot be arbitrarily reduced by increasing N_t, since it has to be guaranteed that the system operates in the interference-limited regime. A similar study is performed in Fig. 2.14, but an asymmetric, *i.e.*, $N_t \neq N_r$, MIMO scheme is considered. As for the BSs against BSs antennas densification, trends similar to Fig. 2.13 are obtained. Also, as discussed in Section 2.5, Fig. 2.14(a) shows that increasing N_t provides a better AFEP if λ is kept constant. On the other hand, Fig. 2.14(b) shows that increasing N_t leads to a degradation and to an improvement of the AFEP if λ_0 is kept constant, in the noise- and interference-limited regime, respectively. However, the performance difference as a function of N_t is smaller compared to Fig. 2.13, since $N_t > N_r$ for some system setups.

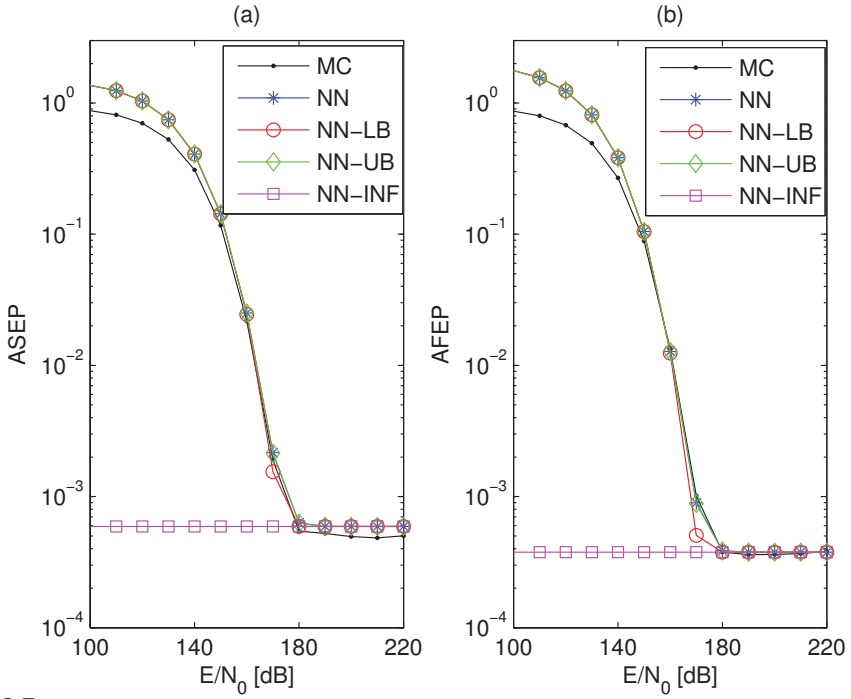

Figure 2.7: ASEP/AFEP of a $N_t \times N_r = N_t \times 2$ system against the reference SNR $E/\mathcal{N}_0$. Setup: (a) $N_t = 1$, QAM with $M = 16$, Gamma channel model with $m = 1$ (Rayleigh fading), $b = 3$, $\lambda = 10^{-5}$ and $p = 10^{-3}$. (b) $N_t = 2$, QAM with $M = 4$, Gamma channel model with $m = 1$ (Rayleigh fading), $b = 3$, $\lambda = 10^{-5}$ and $p = 10^{-3}$.

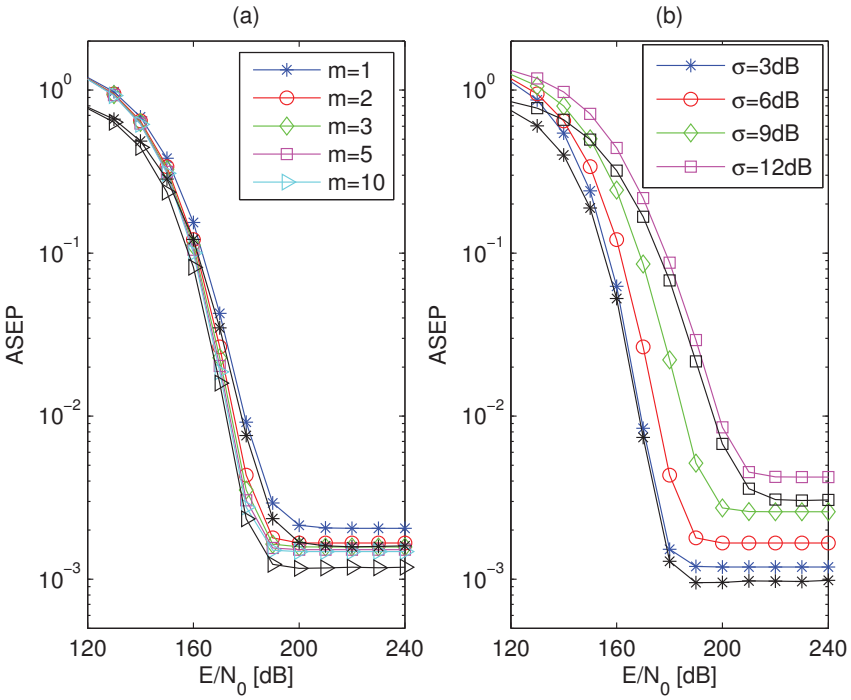

Figure 2.8: ASEP of a $N_t \times N_r = 1 \times 1$ system against the reference SNR $E/\mathcal{N}_0$. Setup: (a) QAM with $M = 16$, Gamma/Log-Normal channel model with $\sigma = 6$dB, $b = 3$, $\lambda = 10^{-5}$ and $p = 10^{-3}$. (b) QAM with $M = 16$, Gamma/Log-Normal channel model with $m = 2$, $b = 3$, $\lambda = 10^{-5}$ and $p = 10^{-3}$.

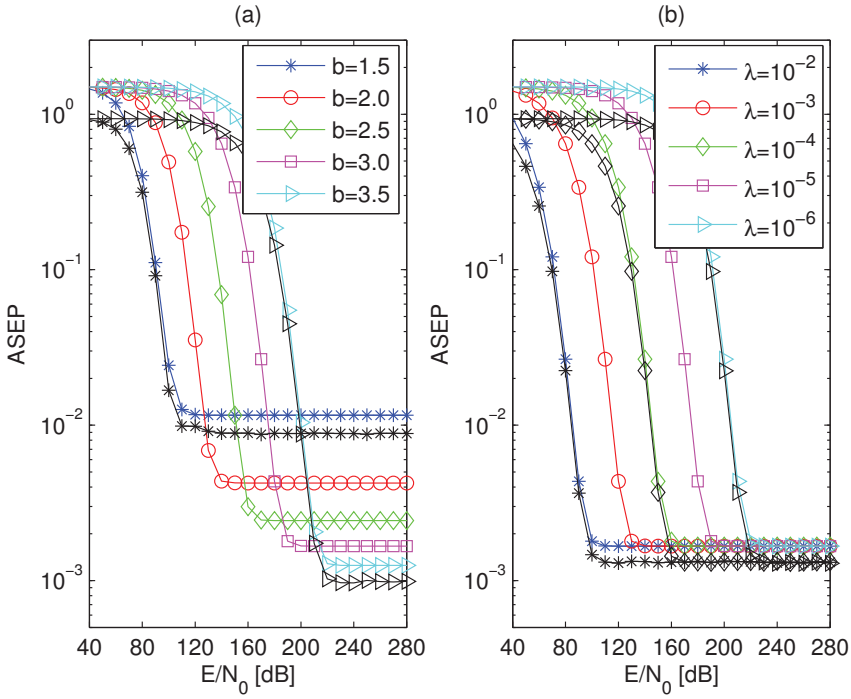

Figure 2.9: ASEP of a $N_t \times N_r = 1 \times 1$ system against the reference SNR $E/\mathcal{N}_0$. Setup: (a) QAM with $M = 16$, Gamma/Log-Normal channel model with $m = 2$ and $\sigma = 6$dB, $\lambda = 10^{-5}$ and $p = 10^{-3}$. (b) QAM with $M = 16$, Gamma/Log-Normal channel model with $m = 2$ and $\sigma = 6$dB, $b = 3$ and $p = 10^{-3}$.

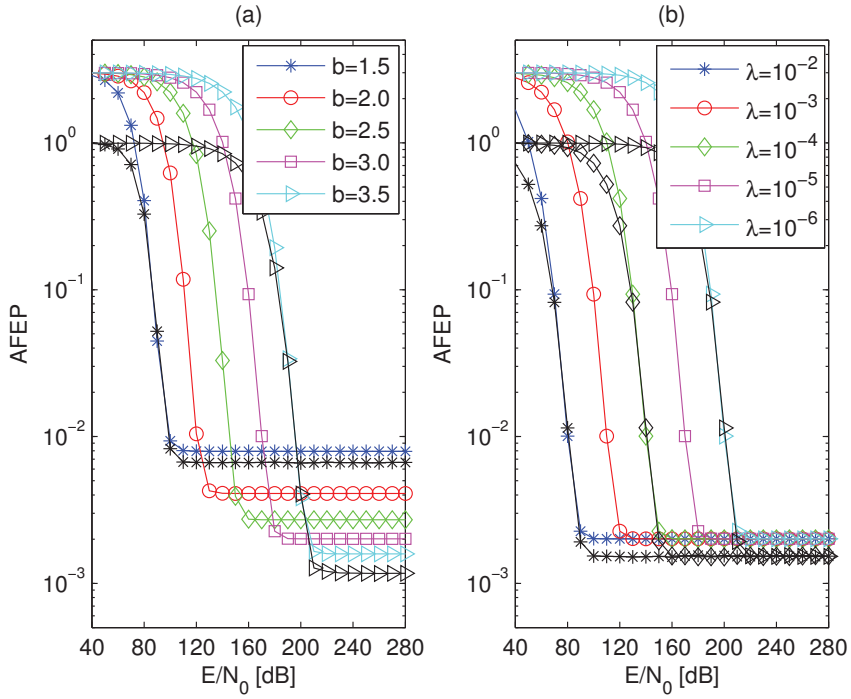

Figure 2.10: AFEP of a $N_t \times N_r = 2 \times 2$ system against the reference SNR $E/\mathcal{N}_0$. Setup: (a) QAM with $M = 16$, Gamma channel model with $m = 1$ (Rayleigh fading), $\lambda = 10^{-5}$ and $p = 10^{-3}$. (b) QAM with $M = 16$, Gamma channel model with $m = 1$ (Rayleigh fading), $b = 3$ and $p = 10^{-3}$.

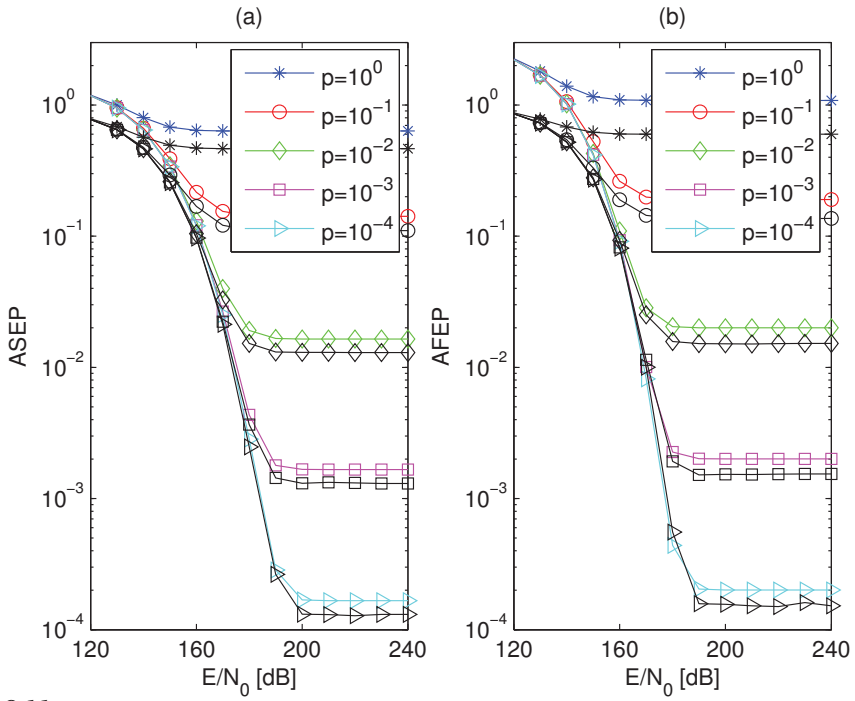

Figure 2.11: ASEP/AFEP of a $N_t \times N_r$ system against the reference SNR $E/\mathcal{N}_0$. Setup: (a) $N_t = 1$ and $N_r = 1$, QAM with $M = 16$, Gamma/Log-Normal channel model with $m = 2$ and $\sigma = 6$dB, $b = 3$ and $\lambda = 10^{-5}$. (b) $N_t = 2$ and $N_r = 2$, QAM with $M = 16$, Gamma channel model with $m = 1$ (Rayleigh fading), $b = 3$ and $\lambda = 10^{-5}$.

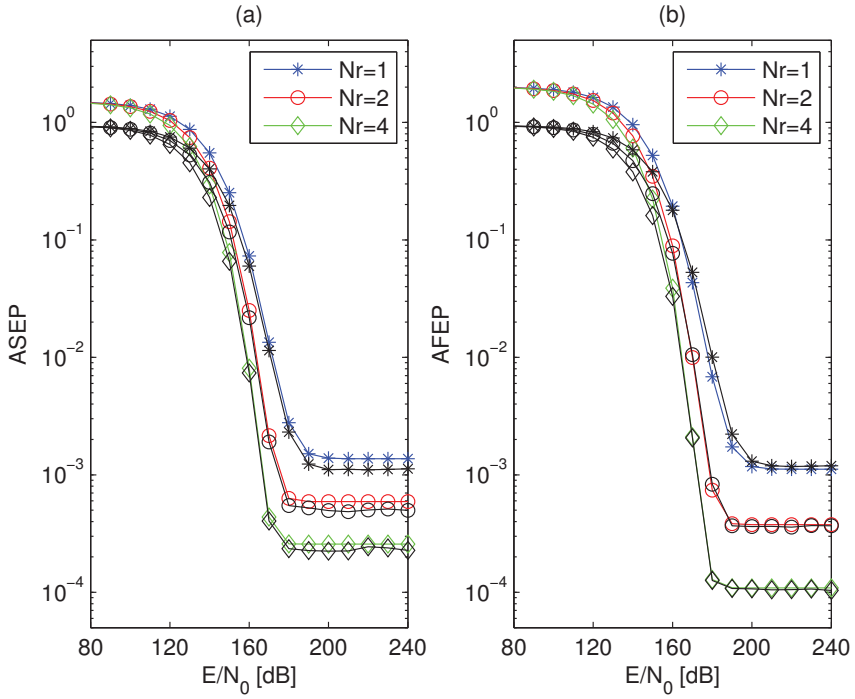

Figure 2.12: ASEP/AFEP of a $N_t \times N_r$ system against the reference SNR $E/\mathcal{N}_0$. Setup: (a) $N_t = 1$, QAM with $M = 16$, Gamma channel model with $m = 1$ (Rayleigh fading), $b = 3$, $\lambda = 10^{-5}$ and $p = 10^{-3}$. (b) $N_t = 2$, QAM with $M = 4$, Gamma channel model with $m = 1$ (Rayleigh fading), $b = 3$, $\lambda = 10^{-5}/2$ and $p = 10^{-3}$.

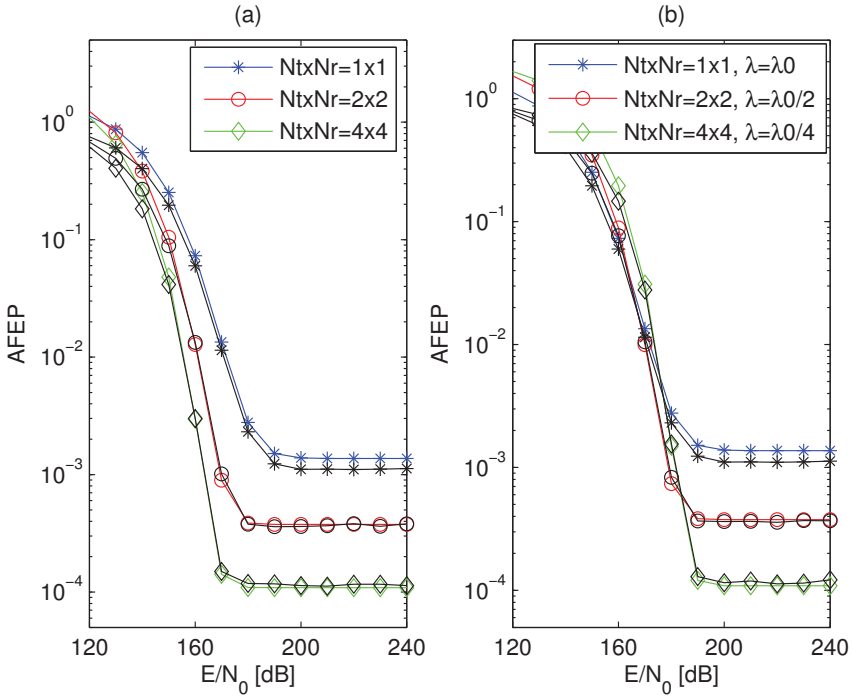

Figure 2.13: AFEP of a $N_t \times N_r$ system providing Rate = 4 bpcu against the reference SNR $E/\mathcal{N}_0$. Setup: (a) Gamma channel model with $m = 1$ (Rayleigh fading), $b = 3$, $\lambda = 10^{-5}$ and $p = 10^{-3}$. (b) Gamma channel model with $m = 1$ (Rayleigh fading), $b = 3$, $\lambda_0 = 10^{-5}$ and $p = 10^{-3}$.

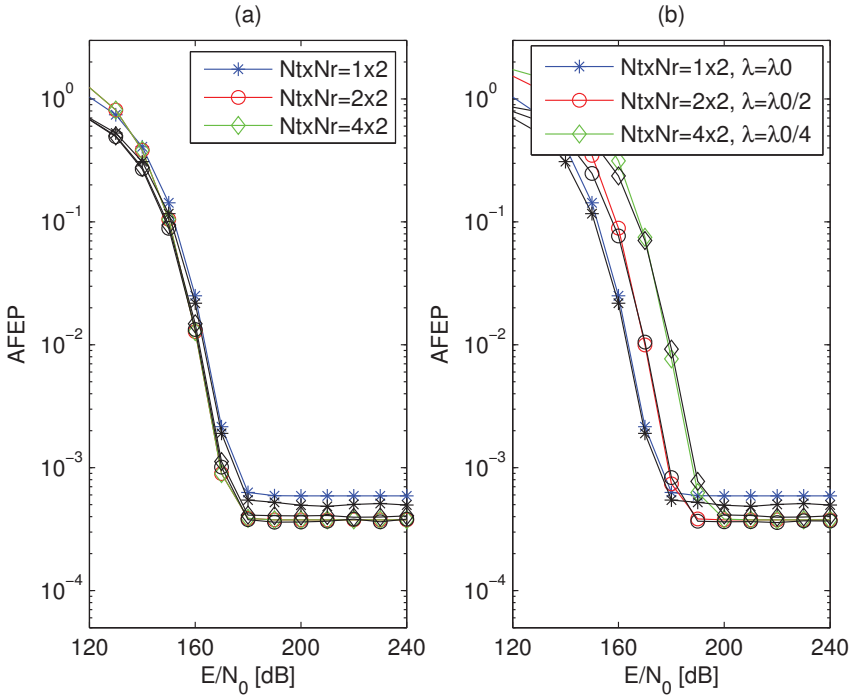

Figure 2.14: AFEP of a $N_t \times N_r = N_t \times 2$ system providing Rate = 4 bpcu against the reference SNR $E/\mathcal{N}_0$. Setup: (a) Gamma channel model with $m = 1$ (Rayleigh fading), $b = 3$, $\lambda = 10^{-5}$ and $p = 10^{-3}$. (b) Gamma channel model with $m = 1$ (Rayleigh fading), $b = 3$, $\lambda_0 = 10^{-5}$ and $p = 10^{-3}$.

2.7 Conclusion

In this chapter, new mathematical frameworks to the computation of the error probability of MIMO cellular networks have been proposed and have been substantiated with the aid of Monte Carlo simulations. Various frameworks have been developed, which provide a flexible trade-off between accuracy and computational complexity. Their analysis has revealed important performance trade-offs that may emerge depending on the SNR operating regime, the fading parameters and the number of antennas available at the BSs and MT. For example, it has been shown that MIMO transmission with $N_t = N_r$ allows one to reduce the density of BSs by increasing N_t without performance degradation in the interference-limited regime and with a small performance degradation in the noise-limited regime.

By using the property on the superposition of the independent PPPs (*Appendix Definition A.4*), the mathematical framework is readily applicable to the multi-tier heterogeneous cellular networks, which can be modeled as the superposition of many tiers of BSs having different transmit powers, densities, path-loss exponents, fading parameters and distributions, and flexible bias factors for various tier association schemes. And the positions of the BSs in each tier are modeled as points of an independent PPP.

2.8 Appendices

2.8.1 Proof of Theorem 2.1

Let $z_i = h_i s_i = |h_i||s_i| \exp\left\{j\left(\arg\{h_i\} + \arg\{s_i\}\right)\right\}$. The aggregate interference can be formulated as $i_{\text{agg}}(r_0) = \sqrt{E} \sum_{i \in \Phi^{(\backslash 0)}} r_i^{-b} h_i s_i = \sqrt{E} \sum_{i \in \Phi^{(\backslash 0)}} r_i^{-b} z_i$. By definition, the CF of $i_{\text{agg}}(\cdot)$ conditioned upon r_0, *i.e.*, $\psi_{i_{\text{agg}}}(\boldsymbol{\omega}; r_0)$, can be written as follows:

$$\begin{aligned}
&\psi_{i_{\text{agg}}}(\boldsymbol{\omega}; r_0) \\
&\quad = \mathbb{E}_{i_{\text{agg}}}\left\{\exp\left\{j\boldsymbol{\omega} i_{\text{agg}}(r_0)\right\}\right\} \\
&\quad \overset{(a)}{=} \sum_{k=0}^{+\infty} \underbrace{\left(\mathbb{E}_{z_i, r_i}\left\{\exp\left\{j\boldsymbol{\omega}\sqrt{E} r_i^{-b} z_i\right\}\right\}\right)^k}_{P_1(\boldsymbol{\omega}; k)} \underbrace{\frac{\left[p\lambda\pi\left(R_{\max}^2 - r_0^2\right)\right]^2}{k!} \exp\left\{-p\lambda\pi\left(R_{\max}^2 - r_0^2\right)\right\}}_{P_2(R_{\max}, r_0; k)} \Bigg|_{R_{\max} \to +\infty}
\end{aligned} \tag{2.31}$$

where (a) is obtained by using the same steps as those in [17, Sec. 3.2.2] and [24, Sec. II-C]. In particular, $P_1(\boldsymbol{\omega}; k)$ originates from the assumption that all the interfering BSs are identically distributed and $P_2(R_{\max}, r_0; k)$ originates from the definition of PPP and denotes the probability that k interfering BSs fall in the annular region with radii r_0 and $R_{\max}$ [16].

By taking into account that z_i is a circularly symmetric complex RV and by using the same steps as in [20, Secs. III-A, III-B], (2.31) can be formulated as follows:

$$\psi_{i_{\text{agg}}}(\boldsymbol{\omega}; r_0) = \psi_{i_{\text{agg}}}(|\boldsymbol{\omega}|; r_0) = \exp\left\{-2p\lambda\pi\mathbb{E}_{z_i^{(\text{re})}}\left\{\mathcal{T}_i\left(|\boldsymbol{\omega}|; r_0, z_i^{(\text{re})}\right)\right\}\right\} \tag{2.32}$$

where $z_i^{(\text{re})} = \text{Re}\{z_i\} = |h_i||s_i|\cos\left(\arg\{h_i\} + \arg\{s_i\}\right)$ and $\mathcal{T}_i(\cdot;\cdot,\cdot)$ is given in (2.33) as follows:

$$\begin{aligned}
\mathcal{T}_i\left(|\omega|; r_0, z_i^{(\text{re})}\right) &= |\omega|^{2/b} E^{1/b} b^{-1} \int_0^{|\omega|\sqrt{E} r_0^{-b}} \left[1 - \cos\left(t z_i^{(\text{re})}\right)\right] t^{-(1+2/b)}\, dt \\
&\overset{(a)}{=} \frac{r_0^2}{2}\left[-1 + {}_1F_2\left(-\frac{1}{b}; \frac{1}{2}, 1 - \frac{1}{b}; -\frac{1}{4}\frac{|\omega|^2 E}{r_0^{2b}}\left(z_i^{(\text{re})}\right)^2\right)\right] \\
&\overset{(b)}{=} \frac{r_0^2}{2}\left[-1 + \sum_{q=0}^{+\infty}\left(-\frac{1}{4}\right)^q \frac{1}{q!}\frac{(-1/b)_q}{(1/2)_q\left(1-1/b\right)_q}\left(\frac{|\omega|^2 E}{r_0^{2b}}\left(z_i^{(\text{re})}\right)^2\right)^q\right]
\end{aligned} \tag{2.33}$$

where (a) follows from [65, Eq. 3.771.3] and (b) is obtained by applying the series representation of the generalized hypergeometric function [57, Ch. 5, Eq. 2].

The CF in (2.6) follows by computing the expectation in (2.32), which from (2.33) implies the

need of computing the moments $\mathbb{E}_{z_i^{(\mathrm{re})}}\left\{\left(z_i^{(\mathrm{re})}\right)^{2q}\right\}$. This is possible as shown in what follows:

$$\begin{aligned}\mathbb{E}_{z_i^{(\mathrm{re})}}\left\{\left(z_i^{(\mathrm{re})}\right)^{2q}\right\} &= \mathbb{E}_{z_i^{(\mathrm{re})}}\left\{|h_i|^{2q}|s_i|^{2q}\cos^{2q}\left(\arg\{h_i\}+\arg\{s_i\}\right)\right\}\\ &\overset{(a)}{=} \mathbb{E}_{|h_i|,s_i}\left\{|h_i|^{2q}|s_i|^{2q}\,\mathbb{E}_{\arg\{h_i\}}\left\{\cos^{2q}\left(\arg\{h_i\}+\arg\{s_i\}\right)\right\}\right\}\\ &\overset{(b)}{=} \mathbb{E}_{|h_i|,s_i}\left\{|h_i|^{2q}|s_i|^{2q}\,\Gamma\left(q+1/2\right)/\left(\sqrt{\pi}\Gamma\left(q+1\right)\right)\right\}\\ &= \Gamma\left(q+1/2\right)/\left(\sqrt{\pi}\Gamma\left(q+1\right)\right)\mathbb{E}_{|h_i|}\left\{|h_i|^{2q}\right\}\mathbb{E}_{|s_i|}\left\{|s_i|^{2q}\right\}\end{aligned} \tag{2.34}$$

where (a) originates by noting that $|h_i|$ and $\arg\{h_i\}$ are assumed to be independent in system model of Section 2.2 and (b) follows from [66, Eq. 16] with the aid of some simplifications.

Finally, (2.6) follows from $\mathbb{E}_{|s_i|}\left\{|s_i|^{2q}\right\} = \left(1/\mathrm{M}\right)\sum_{\chi=1}^{\mathrm{M}}\left|\mu_\chi\right|^{2q}$ and some simplifications. The expression in terms of the hypergeometric function follows from the series representation in [57, Ch. 5, Eq. 2]. This concludes the proof.

2.8.2 Proof of Lemma 2.1

Lemma 2.1 *Let the demodulator in* (2.5)*. Then,* $\mathrm{PEP}\left(|\Delta_0|;h_0,r_0\right) = \Pr\left\{\Lambda\left(\tilde{s}_0\right)<0|\,h_0,r_0\right\}$ *can be formulated as follows:*

$$\mathrm{PEP}\left(|\Delta_0|;h_0,r_0\right) = \mathrm{PEP}\left(|\Delta_0|;|h_0|,r_0\right) = \mathrm{PEP}_{\mathrm{N}}\left(|\Delta_0|;|h_0|,r_0\right) + \mathrm{PEP}_{\mathrm{NI}}\left(|\Delta_0|;|h_0|,r_0\right) \tag{2.35}$$

where $\mathrm{PEP}_{\mathrm{N}}\left(\cdot;\cdot,\cdot\right)$ *and* $\mathrm{PEP}_{\mathrm{NI}}\left(\cdot;\cdot,\cdot\right)$ *are given in* (2.36) *as follows:*

$$\begin{cases}\mathrm{PEP}_{\mathrm{N}}\left(|\Delta_0|;|h_0|,r_0\right) = \dfrac{1}{2}-\dfrac{1}{\pi}\displaystyle\int_0^{+\infty}\sin\left(\frac{1}{2}r_0^{-b}\sqrt{E}|\Delta_0||h_0|\varpi\right)\varpi^{-1}\exp\left(-\frac{1}{4}\mathscr{N}_0\varpi^2\right)d\varpi\\ \mathrm{PEP}_{\mathrm{NI}}\left(|\Delta_0|;|h_0|,r_0\right) = \dfrac{1}{\pi}\displaystyle\int_0^{+\infty}\sin\left(\frac{1}{2}r_0^{-b}\sqrt{E}|\Delta_0||h_0|\varpi\right)\varpi^{-1}\exp\left(-\frac{1}{4}\mathscr{N}_0\varpi^2\right)\left[1-\psi_{i_{\mathrm{agg}}}\left(\varpi;r_0\right)\right]d\varpi\end{cases} \tag{2.36}$$

Proof*: By definition from* (2.5)*, the PEP can be formulated as follows:*

$$\begin{aligned}&\mathrm{PEP}\left(|\Delta_0|;h_0,r_0\right) = \Pr\left\{\Lambda\left(\tilde{s}_0\right)<0|\,h_0,r_0\right\}\\ &= \Pr\left\{\mathrm{Re}\left\{v\left(r_0\right)|h_0||\Delta_0|\exp\left\{-j\left(\arg\{h_0\}+\arg\{\Delta_0\}\right)\right\}\right\} < -\left(1/2\right)r_0^{-b}\sqrt{E}|\Delta_0|^2|h_0|^2\right\}\\ &\overset{(a)}{=} \Pr\left\{\mathrm{Re}\left\{v\left(r_0\right)\right\} < -\left(1/2\right)r_0^{-b}\sqrt{E}|\Delta_0||h_0|\right\}\\ &\overset{(b)}{=} F_{v^{(\mathrm{re})}}\left(-\left(1/2\right)r_0^{-b}\sqrt{E}|\Delta_0||h_0|\right)\overset{(c)}{=}\mathrm{PEP}\left(|\Delta_0|;|h_0|,r_0\right)\end{aligned} \tag{2.37}$$

where: (a) holds because $v(\cdot)$ is a circularly symmetric RV, $v(r_0)\exp\{-j(\arg\{h_0\}+\arg\{\Delta_0\})\} \overset{d}{=} v(r_0)$ [67]; (b) follows from the definition of CDF of the RV $v^{(\mathrm{re})}(r_0) = \mathrm{Re}\{v(r_0)\}$; and (c) emphasizes that the PEP depends only on the absolute value of h_0, i.e., $|h_0|$, while it is independent of the phase of h_0, as shown in the equality in (b).

By using the Gil-Pelaez inversion theorem [54] for computing $F_{v^{(\mathrm{re})}}(\cdot)$, (2.37) *simplifies as follows:*

$$\begin{aligned}\mathrm{PEP}(|\Delta_0|;|h_0|,r_0) &\overset{(a)}{=} \frac{1}{2}+\frac{1}{\pi}\int_0^{+\infty}\sin\left(-(1/2)\,r_0^{-b}\sqrt{E}|\Delta_0||h_0||\boldsymbol{\omega}|\right)|\boldsymbol{\omega}|^{-1}\psi_{v^{(\mathrm{re})}}(|\boldsymbol{\omega}|;r_0)\,d|\boldsymbol{\omega}| \\ &\overset{(b)}{=} \frac{1}{2}-\frac{1}{\pi}\int_0^{+\infty}\sin\left((1/2)\,r_0^{-b}\sqrt{E}|\Delta_0||h_0||\boldsymbol{\omega}|\right)|\omega|^{-1}\psi_{v}(|\boldsymbol{\omega}|;r_0)\,d|\boldsymbol{\omega}|\end{aligned} \tag{2.38}$$

where (a) originates from [68, Eq. 12], by noticing that $\mathrm{Re}\{\psi_{v^{(\mathrm{re})}}(|\boldsymbol{\omega}|;r_0)\} = \psi_{v^{(\mathrm{re})}}(|\boldsymbol{\omega}|;r_0)$ and $\mathrm{Im}\{\psi_{v^{(\mathrm{re})}}(|\boldsymbol{\omega}|;r_0)\} = 0$, i.e., $\psi_{v^{(\mathrm{re})}}(\cdot;\cdot)$ is a real function and (b) follows by taking into account that $\sin(\cdot)$ is an odd function and that $v(\cdot)$ is a circularly symmetric RV, i.e., $\psi_{v^{(\mathrm{re})}}(|\boldsymbol{\omega}|;r_0) = \psi_{v}(|\boldsymbol{\omega}|;r_0)$.

Since $v(r_0) = i_{\mathrm{agg}}(r_0)+n$, as well as $i_{\mathrm{agg}}(\cdot)$ and n are independent RVs, we have $\psi_v(|\boldsymbol{\omega}|;r_0) = \psi_n(|\boldsymbol{\omega}|)\,\psi_{i_{\mathrm{agg}}}(|\boldsymbol{\omega}|;r_0) \overset{(c)}{=} \psi_n(|\boldsymbol{\omega}|) - \psi_n(|\boldsymbol{\omega}|)\left[1-\psi_{i_{\mathrm{agg}}}(|\boldsymbol{\omega}|;r_0)\right]$, where $\psi_n(|\omega|) = \exp\left(-\frac{1}{4}\mathcal{N}_0|\omega|^2\right)$ is the CF of a Gaussian RV [69] and (c) follows from [70, Eq. 18]. Equation (2.35) *follows by inserting $\psi_v(\cdot;\cdot)$ in* (2.38)*. In particular, the addend $\mathrm{PEP}_{\mathrm{N}}$ is related to the factor $\psi_n(\cdot)$ and the addend $\mathrm{PEP}_{\mathrm{NI}}$ is related to the factor $\psi_n(\cdot)\left[1-\psi_{i_{\mathrm{agg}}}(\cdot;\cdot)\right]$, respectively. This concludes the proof.* □

2.8.3 Proof of Theorem 2.2

From *Lemma 2.1* in Appendix 2.8.2, the expectations $\mathrm{APEP}_{\mathrm{N}}(|\Delta_0|) = \mathbb{E}_{|h_0|,r_0}\{\mathrm{PEP}_{\mathrm{N}}(|\Delta_0|;|h_0|,r_0)\}$ and $\mathrm{APEP}_{\mathrm{NI}}(|\Delta_0|) = \mathbb{E}_{|h_0|,r_0}\{\mathrm{PEP}_{\mathrm{NI}}(|\Delta_0|;|h_0|,r_0)\}$ need to be computed. Equations (2.39) and (2.40) provide the mathematical steps to this end:

$$\begin{aligned}&\mathrm{APEP}_{\mathrm{N}}(|\Delta_0|) \\ &\overset{(a)}{=} \frac{1}{2}-2\lambda\mathbb{E}_{|h_0|}\left\{\int_0^{+\infty}\left[\int_0^{+\infty}\sin\left(\frac{1}{2}\xi^{-b}\sqrt{E}|\Delta_0||h_0|\varpi\right)\exp\left(-\frac{1}{4}\mathcal{N}_0\varpi^2\right)\frac{d\varpi}{\varpi}\right]\xi\exp\left\{-\pi\lambda\xi^2\right\}d\xi\right\} \\ &\overset{(b)}{=} \frac{1}{2}-\lambda\pi\mathbb{E}_{|h_0|}\left\{\int_0^{+\infty}\mathrm{erf}\left(2^{-1}\sqrt{\mathsf{SNR}}|\Delta_0||h_0|\xi^{-b}\right)\xi\exp\left\{-\pi\lambda\xi^2\right\}d\xi\right\}\end{aligned} \tag{2.39}$$

$$\mathrm{APEP}_{\mathrm{NI}}\left(|\Delta_0|\right) \overset{(a)}{=} 2\lambda \times \int_0^{+\infty}\int_0^{+\infty} \xi \exp\left\{-\pi\lambda\xi^2\right\} \mathbb{E}_{|h_0|}\left\{\sin\left(\frac{1}{2}\xi^{-b}\sqrt{E}|\Delta_0||h_0|\varpi\right)\right\} \exp\left(-\frac{1}{4}\mathrm{N}_0\varpi^2\right)\left[1-\psi_{i_{\mathrm{agg}}}(\varpi;\xi)\right]\frac{d\varpi}{\varpi}d\xi \tag{2.40}$$

where (a) follows since $f_{r_0}(\xi) = 2\pi\lambda\xi\exp\left(-\pi\lambda\xi^2\right)$ [6] and (b) follows by computing the integral in the square brackets with the aid of [65, Eq. 3.952.6]. The $\mathrm{APEP}_{\mathrm{N}}(\cdot)$ in (2.11) follows by applying the integration by part rule and the $\mathrm{APEP}_{\mathrm{NI}}(\cdot)$ in (2.11) follows from (2.6) and some changes of variable. This concludes the proof.

2.8.4 Proof of Proposition 2.5

Similar to *Corollary 2.2*, let a noise-limited cellular network, then $\lim_{\mathsf{SNR}\to 0}\{\mathrm{APEP}(|\Delta_0|)\} = \mathrm{APEP}_{\mathrm{N}}^{(0)}(|\Delta_0|) = \mathrm{APEP}_{\mathrm{N}}(|\Delta_0|)$. Also, let $\lim_{\mathsf{SNR}\to+\infty}\{\mathrm{APEP}(|\Delta_0|)\} = \mathrm{APEP}_{\mathrm{NI}}^{(\infty)}(|\Delta_0|)$.

The LB in (2.16) is obtained by taking into account that: 1) since $\mathrm{APEP}_{\mathrm{NI}}(|\Delta_0|) \geq 0$ for $\mathsf{SNR} \geq 0$, this implies that $\mathrm{APEP}(|\Delta_0|) \geq \mathrm{APEP}_{\mathrm{N}}(|\Delta_0|) = \mathrm{APEP}_{\mathrm{N}}^{(0)}(|\Delta_0|)$ and 2) since $\mathrm{APEP}_{\mathrm{N}}(|\Delta_0|) \geq 0$ for $\mathsf{SNR} \geq 0$, this implies that $\mathrm{APEP}(|\Delta_0|) \geq \mathrm{APEP}_{\mathrm{NI}}(|\Delta_0|) \approx \mathrm{APEP}_{\mathrm{NI}}^{(\infty)}(|\Delta_0|)$, where the last approximation holds for $\mathrm{APEP}_{\mathrm{NI}}^{(\infty)}(|\Delta_0|) > \mathrm{APEP}_{\mathrm{N}}^{(0)}(|\Delta_0|)$ (high-SNR). These two inequalities imply that: i) for low-SNR, *i.e.*, $\mathrm{APEP}_{\mathrm{N}}^{(0)}(|\Delta_0|) > \mathrm{APEP}_{\mathrm{NI}}^{(\infty)}(|\Delta_0|)$, we have $\mathrm{APEP}(|\Delta_0|) \gtrsim \mathrm{APEP}_{\mathrm{N}}^{(0)}(|\Delta_0|)$ and ii) for high-SNR, *i.e.*, $\mathrm{APEP}_{\mathrm{NI}}^{(\infty)}(|\Delta_0|) > \mathrm{APEP}_{\mathrm{N}}^{(0)}(|\Delta_0|)$, we have $\mathrm{APEP}(|\Delta_0|) \gtrsim \mathrm{APEP}_{\mathrm{NI}}^{(\infty)}(|\Delta_0|)$.

The UB in (2.17) is obtained by taking into account that: 1) $\mathrm{APEP}(|\Delta_0|) \leq \mathrm{APEP}(|\Delta_0|)|_{E=0} = 1/2$ by definition of APEP. This also follows from (2.35) and (2.36), since $\sin(\mathscr{K}E)|_{E=0} = 0$ for $\mathscr{K} > 0$. This condition applies to low-SNR, when the PEP is dominated by the AWGN and 2) $\mathrm{APEP}_{\mathrm{NI}}^{(\infty)}(|\Delta_0|) \geq \mathrm{APEP}_{\mathrm{NI}}(|\Delta_0|)$ for $\mathsf{SNR} \geq 0$, which follows from (2.11). This last inequality implies that, for high-SNR, $\mathrm{APEP}_{\mathrm{NI}}(|\Delta_0|)$ can be replaced by $\mathrm{APEP}_{\mathrm{NI}}^{(\infty)}(|\Delta_0|)$. Since low- and high-SNR conditions correspond to the inequalities $\mathrm{APEP}_{\mathrm{N}}^{(0)}(|\Delta_0|) + \mathrm{APEP}_{\mathrm{NI}}^{(\infty)}(|\Delta_0|) \geq \mathrm{APEP}(|\Delta_0|)|_{E=0}$ and $\mathrm{APEP}_{\mathrm{N}}^{(0)}(|\Delta_0|) + \mathrm{APEP}_{\mathrm{NI}}^{(\infty)}(|\Delta_0|) < \mathrm{APEP}(|\Delta_0|)|_{E=0}$, respectively, then (2.17) follows. This concludes the proof.

2.8.5 Proof of Theorem 2.3

By inserting $\mathbf{i}_{\mathrm{agg}}^{(r)}(r_0) = \sqrt{E/N_t}\sum_{i\in\Phi^{(\setminus 0)}} r_i^{-b}\sum_{\tilde{t}=1}^{N_t}\mathbf{H}_i^{(r,\tilde{t})}\mathbf{s}_i^{(\tilde{t})}$ of (2.1) in $\mathrm{I}(\cdot)$ of (2.4), the latter can be formulated as $\mathrm{I}(r_0) = \sqrt{E}\sum_{i\in\Phi^{(\setminus 0)}} r_i^{-b}\tilde{z}_i$, where $\tilde{z}_i = \sqrt{1/N_t}\sum_{r=1}^{N_r}\sum_{\tilde{t}=1}^{N_t}\sum_{t=1}^{N_t}\mathbf{H}_i^{(r,\tilde{t})}\mathbf{s}_i^{(\tilde{t})}\left(\mathbf{H}_0^{(r,t)}\mathbf{\Delta}_0^{(t)}\right)^H$. From Appendix 2.8.1, we note that $\mathrm{I}(\cdot)$ and $i_{\mathrm{agg}}(\cdot)$ have the same mathematical formulation. The only difference is that z_i in $i_{\mathrm{agg}}(\cdot)$ needs to be replaced by $\tilde{z}_i$ in $\mathrm{I}(\cdot)$. In addition, and similar to z_i, the RVs $\tilde{z}_i$ are still circularly symmetric and i.i.d. for $i \in \Phi^{(\setminus 0)}$. As a consequence, the CF of $\mathrm{I}(\cdot)$

can be formulated as shown in (2.32) and (2.33), by simply replacing $z_i^{(\mathrm{re})}$ with $\tilde{z}_i^{(\mathrm{re})} = \mathrm{Re}\{\tilde{z}_i\}$. Accordingly, the moments of $\tilde{z}_i^{(\mathrm{re})}$ conditioned upon $\mathbf{H}_0$ and $\mathbf{\Delta}_0$ need to be computed. Let us denote these conditioned moments by $\eta_q(\mathbf{H}_0, \Delta_0) = \mathbb{E}_{\tilde{z}_i|\mathbf{H}_0,\mathbf{\Delta}_0}\left\{\left(\tilde{z}_i^{(\mathrm{re})}\right)^{2q}\right\}$. Since $\mathbf{H}_i^{(r,t)} \sim \mathscr{CN}(0,\Omega)$, $\mathrm{Re}\left\{\mathbf{H}_i^{(r,t)}\right\} \sim \mathscr{CN}(0,\Omega/2)$. Thus, $\tilde{z}_i^{(\mathrm{re})}$ turns out to be a Gaussian RV by conditioning upon $\mathbf{H}_0$, $\mathbf{\Delta}_0$ and $\mathbf{s}_i$, which we denote by $\tilde{z}_i^{(\mathrm{re})} \sim \mathscr{N}_{|\mathbf{H}_0,\mathbf{\Delta}_0,\mathbf{s}_i}\left(0, (\Omega/2)\,\mathrm{U}\left(1/N_t\right)\sum_{\tilde{t}=1}^{N_t}\left|\mathbf{s}_i^{(\tilde{t})}\right|^2\right)$. Thus, from [73, Eq. 13] the moments can be computed as follows:

$$\eta_q(\mathbf{H}_0,\Delta_0) = \eta_q(\mathrm{U}) = \mathbb{E}_{\mathbf{s}_i}\left\{(-1)^q\frac{\sqrt{\pi}}{\Gamma\left(1/2-q\right)}\left(\frac{1}{N_t}\sum_{\tilde{t}=1}^{N_t}\left|\mathbf{s}_i^{(\tilde{t})}\right|^2\right)^q\Omega^q\mathrm{U}^q\right\} \tag{2.41}$$

The rest of the proof follows from the series representation of the generalized hypergeometric function [57, Ch. 5, Eq. 2] and from the identities $\sum_{\tilde{t}=1}^{N_t}\left|\mathbf{s}_i^{(\tilde{t})}\right|^2 = \|\mathbf{s}_i\|^2$ and ${}_2F_2\left(\frac{1}{2},\alpha;\frac{1}{2},\beta;-x\right) = {}_1F_1\left(\alpha;\beta;-x\right)$. This concludes the proof.

2.8.6 Proof of Theorem 2.4

The proof is similar to Appendix 2.8.2 and Appendix 2.8.3. By applying the Gil-Pelaez inversion theorem [54] to (2.3), $\mathrm{APEP}^{(\mathrm{F})}$ conditioned upon $\mathbf{H}_0$ and r_0 can be formulated, similar to (2.38), as follows:

$$\begin{aligned}&\mathrm{APEP}^{(\mathrm{F})}(\Delta_0;\mathbf{H}_0,r_0) = \mathrm{APEP}^{(\mathrm{F})}(\mathrm{U},r_0)\\ &= \frac{1}{2} - \frac{1}{\pi}\times\int_0^{+\infty}\sin\left((1/2)\,r_0^{-b}\sqrt{E/N_t}\mathrm{U}\,|\boldsymbol{\omega}|\right)|\boldsymbol{\omega}|^{-1}\times\psi_{\mathrm{N}^{(\mathrm{re})}}(|\boldsymbol{\omega}|;\mathrm{U})\,\psi_{\mathrm{I}^{(\mathrm{re})}}(|\boldsymbol{\omega}|;r_0,\mathrm{U})\,d\,|\boldsymbol{\omega}|\end{aligned} \tag{2.42}$$

where: i) $\mathrm{N}^{(\mathrm{re})} = \mathrm{Re}\{\mathrm{N}\} \sim \mathscr{N}\left(0,\left(\mathscr{N}_0/2\right)\mathrm{U}\right)$ follows from the AWGN assumption and from (2.4); ii) $\mathrm{I}^{(\mathrm{re})} = \mathrm{Re}\{\mathrm{I}\}$ is defined in (2.4); iii) $\psi_{\mathrm{N}^{(\mathrm{re})}}(|\boldsymbol{\omega}|;\mathrm{U}) = \psi_{\mathrm{N}}(|\boldsymbol{\omega}|;\mathrm{U})$ and $\psi_{\mathrm{I}^{(\mathrm{re})}}(|\boldsymbol{\omega}|;r_0,\mathrm{U}) = \psi_{\mathrm{I}}(|\boldsymbol{\omega}|;r_0,\mathrm{U})$, since N and I are circularly symmetric RVs; iv) $\psi_{\mathrm{N}}(|\omega|;\mathrm{U}) = \exp\left\{-\frac{1}{4}|\omega|^2\mathscr{N}_0\mathrm{U}\right\}$, since it is a Gaussian RV [69]; and v) $\psi_{\mathrm{I}}(\cdot;\cdot,\cdot)$ is given in (2.21). The rest of the proof is the same as in Appendices 2.8.2 and 2.8.3. This concludes the proof.

2.8.7 Proof of Proposition 2.6

Let us consider the RV $\mathrm{U} = \sum_{r=1}^{N_r}\left|\sum_{t=1}^{N_t}\mathbf{H}_0^{(r,t)}\mathbf{\Delta}_0^{(t)}\right|^2$ in (2.4). Since $\left|\mathbf{H}_0^{(r,t)}\right| \sim \mathrm{Gamma}(1,\Omega)$ and the channel phases are uniformly distributed, then $\mathbf{H}_0^{(r,t)} \sim \mathscr{CN}(0,\Omega)$ for $t = 1,2,\ldots,N_t$ and $r = 1,2,\ldots,N_r$. Thus, by conditioning upon $\mathbf{\Delta}_0$, we have $\sum_{t=1}^{N_t}\mathbf{H}_0^{(r,t)}\mathbf{\Delta}_0^{(t)} \sim \mathscr{CN}_{|\mathbf{\Delta}_0}\left(0,\Omega\,\|\mathbf{\Delta}_0\|^2\right)$. This implies that $\mathrm{U} \sim \mathrm{Gamma}\left(N_r,\Omega N_r\,\|\Delta_0\|^2\right)$. The rest of the proof follows by comparing (2.27) with (2.13). This concludes the proof.

3 Stochastic Geometry Modeling and Analysis of Downlink MIMO Cellular Networks Using the Gil-Pelaez Inversion Theorem

Chapter 3. Stochastic Geometry Modeling and Analysis of Downlink MIMO Cellular Networks Using the Gil-Pelaez Inversion Theorem

In this chapter, we introduce new mathematical frameworks to the computation of coverage probability and average rate of cellular networks by relying on a stochastic geometry abstraction modeling approach. With the aid of the Gil-Pelaez inversion formula, we prove that coverage and rate can be compactly formulated as a two-fold integral for arbitrary per-link power gains. In the interference-limited regime, single-integral expressions are obtained. The new mathematical frameworks are also applicable for the performance analysis of several important MIMO transmission schemes in downlink cellular networks. As one case study, Gamma distributed per-link power gains are investigated further and approximated closed-form expressions for coverage and rate in the interference-limited regime are obtained, which shed light on the impact of channel parameters and physical-layer transmission schemes. The other case study studies the service success probability of a typical MT in partially loaded cellular networks. Furthermore, the trends of coverage and rate on several important system parameters are discussed based on the mathematical frameworks and the accuracy of the mathematical analysis is substantiated through extensive Monte Carlo simulations for various cellular network setups.

The present chapter is organized as follows. *Section 3.1* introduces the motivations and contributions. In *Section 3.2*, the system model is introduced and the problem is formulated. In *Section 3.3*, several MIMO schemes fit the system model in *Section 3.2* have been visited. In *Section 3.4*, exact frameworks are provided for the computation of coverage and average rate. In *Section 3.5*, approximations are provided for the Gamma distributed per-link gains. In *Section 3.6*, a partially loaded downlink cellular network is studied with the aid of Gil-Pelaez inversion formula. In *Section 3.7*, numerical examples substantiating the mathematical findings are shown. Finally, *Section 3.8* concludes the present chapter.

3.1 Introduction 60

3.2 System Model 61

3.2.1 PPP-Based Cellular Networks Modeling 61

3.2.2 Problem Formulation 61

3.3 MIMO Transmission Schemes in Downlink Cellular Networks 62

3.3.1 Spatial Multiplexing and Per-Stream ZF Receiver 62

3.3.2 Orthogonal Space-Time Block Coding 63

3.3.3 Fixed Rate SVD Multiplexing 64

3.3.4 MIMO MRC 65

3.3.5 Selection Diversity and Combining 66

3.4 Gil-Pelaez Based Mathematical Frameworks to the Computations of Coverage and Rate . . . 67
3.4.1 Coverage Probability . . . 67
3.4.2 Average Rate . . . 68
3.5 Case Study: Coverage and Rate in Downlink Cellular Networks with Gamma Distributed Per-Link Power Gains . . . 68
3.5.1 Coverage Probability . . . 69
3.5.2 Average Rate . . . 70
3.6 Case Study: Service Success Probability in Partially Loaded Downlink Cellular Networks . . . 71
3.6.1 Modified System Model and Problem Formulation . . . 71
3.6.2 Load Modeling . . . 72
3.6.3 Service Success Probability . . . 74
3.7 Numerical and Simulation Results . . . 75
3.8 Conclusion . . . 78
3.9 Appendices . . . 80
3.9.1 Proof of Theorem 3.1 . . . 80
3.9.2 Proof of Proposition 3.6 . . . 80

3.1 Introduction

Besides the techniques to the mathematical modeling and performance evaluation of cellular networks based on stochastic geometry reported in [19] and summarized in *Section 1.2.2*, in this chapter, we introduce another technique to the computation of coverage and rate of cellular networks. The proposed approach is based on the Gil-Pelaez inversion formula [54]. The application of the Gil-Pelaez theorem to the analysis of wireless networks in the presence of interference is not new and various papers are available, *e.g.*, [39], [68]. These mathematical frameworks, however, are not based on a stochastic geometry abstraction modeling. In this context, to the best of the authors knowledge, the Gil-Pelaez theorem has been employed only in [21] and [111], where the error probability of cognitive radio and cellular networks is investigated, respectively. In this chapter, on the other hand, we are interested in the analysis of coverage and rate of cellular networks, which lead to a different and novel mathematical formulation. More specifically, we provide novel two-fold integral expressions for coverage and rate, which have a compact mathematical formulation and are applicable to arbitrary per-link power gains and path-loss exponents. In the interference-limited regime, exact single-integral expressions formulated in terms of generalized hypergeometric functions are provided. The developed mathematical frameworks are also applicable for several important MIMO transmissions in downlink cellular networks, including spatial multiplexing (SMX) and per-stream zero-forcing (ZF) [78, Section II.A.], orthogonal space-time block coding (OSTBC) [79, Section 3.4],[78, Section II.B.], fixed rate singular value decomposition (SVD) multiplexing [79, Section 3.2], MIMO MRC [81, 82, 83], selection diversity (SD) and combining [79, Section 3.5].

In one of the case studies, we focus our attention on fading channels and transmission schemes whose equivalent per-link power gains follow a Gamma distribution with arbitrary parameters. In this scenario, we provide approximated closed-form expressions for coverage and rate, whose accuracy is assessed with the aid of Monte Carlo simulations. The rationale of this choice originates from [37] and [30], where it is shown that the per-link power gains of a large class of multiple-antenna transmission schemes for transmission over Rayleigh fading channels can be approximated by a Gamma distribution with adequate parameters. In [37], the impact of the parameters of the Gamma distribution is investigated by relying on approximated expressions of the other-cell interference obtained through moment-matching methods. In [30], the same problem is solved with the aid of stochastic ordering. In [19, Sec. IV-H], it is shown that, in general, the analysis of multiple-antenna transmission schemes requires the computation of the derivatives of the MGF of the other-cell interference. In this Chapter, approximated but simple closed-form expressions for coverage and rate are provided, which provide insight on the achievable performance of cellular networks as a function of the parameters of the per-link power gains, *e.g.*, the multiple-antenna transmission scheme if Rayleigh fading is assumed.

In the other case study, we investigate the load modeling and service success probability of a typical MT in partially loaded downlink cellular networks. The mathematical formulation of

the load in cellular networks originates from [40, 41, 42, 43] and in this chapter we extend the analysis of load to the case where multiple resource blocks are available at each BS.

3.2 System Model

3.2.1 PPP-Based Cellular Networks Modeling

A bi-dimensional downlink cellular network deployment is considered, where a probe MT is located at the origin and the BSs are modeled as points of a homogeneous PPP, denoted by Φ, of density λ. The MT is served by the nearest BS (BS_0). Their distance is denoted by r_0, which is a RV having probability density function equal to $f_{r_0}(\xi) = 2\pi\lambda\xi \exp\left(-\pi\lambda\xi^2\right)$ [6]. Similar to [6, Sec. VI], full-frequency reuse is considered. Thus, the set of interfering BSs ($\Phi^{(\backslash 0)}$) is still a PPP of density λ. The distance from the ith interfering BS to the MT is denoted by $r_i > r_0$ for $i \in \Phi^{(\backslash 0)}$.

3.2.2 Problem Formulation

The SINR of this downlink cellular network can be formulated as follows:

$$\begin{aligned} \mathrm{SINR} &= \frac{\mathsf{P}\gamma_0 r_0^{-\alpha}}{\mathscr{N}_0 + \mathsf{P}\mathscr{I}_{agg}(r_0)} \\ \mathscr{I}_{agg}(r_0) &= \textstyle\sum_{i\in\Phi^{(\backslash 0)}} \gamma_i r_i^{-\alpha} \end{aligned} \tag{3.1}$$

where P is the equivalent transmit power of the BSs, $\mathscr{N}_0$ is the noise power, $\alpha > 2$ is the path-loss exponent, $\alpha = 2b$ with b denoting the amplitude path-loss exponent, $\mathscr{I}_{agg}(\cdot)$ is the aggregate other-cell interference, γ_0 and γ_i for $i \in \Phi^{(\backslash 0)}$ are the per-link power gains of intended and interfering links, which have an arbitrary distribution that usually depends on fading channel and transmission scheme [37], [30].

In this chapter, coverage probability ($\mathrm{P}_{\mathrm{cov}}$) and average rate ($\mathscr{R}$) are studied. They can be formulated as follows:

$$\mathrm{P}_{\mathrm{cov}}(\tau) = \Pr\{\mathrm{SINR} \geq \tau\} \tag{3.2}$$

$$\mathscr{R} = \mathbb{E}\{\ln(1+\mathrm{SINR})\} \overset{(a)}{=} \int_0^{+\infty} \mathrm{P}_{\mathrm{cov}}\left(\exp(t)-1\right) dt \overset{(b)}{=} -\int_0^{+\infty} \ln\left(1+y\right) \mathrm{P}_{\mathrm{cov}}^{(1)}\left(y\right) dy \tag{3.3}$$

where $\tau > 0$ is a reliability threshold, (a) follows from [19, Eq. (7)] and (b) follows by applying integration by parts, since $\mathrm{P}_{\mathrm{cov}}(\tau \to 0) = 1$ and $\mathrm{P}_{\mathrm{cov}}(\tau \to \infty) = 0$.

3.3 MIMO Transmission Schemes in Downlink Cellular Networks

Let a downlink MIMO cellular network deployed as in *Section 3.2*, where a probe MT equipped with N_r receive antennas is located at the origin and the BSs equipped with N_t receive antennas are modeled as points of a homogeneous PPP Φ of density λ. Let $\mathbf{H}_0$, $\mathbf{H}_i$, $\mathbf{G}_i$ be the $N_r \times N_t$ fading channel matrices from probe BS_0 to the probe MT_0, from interfering BS_i to the probe MT_0, and from interfering BS_i to its intended receiver respectively. More specifically, $\mathbf{H}_0 = \left[\mathbf{h}_{0,1}, \mathbf{h}_{0,2}, ...\mathbf{h}_{0,N_t}\right]$ with $\mathbf{h}_{0,t} = \left[\mathbf{H}_0^{(1,t)}, \mathbf{H}_0^{(2,t)}, ..., \mathbf{H}_0^{(N_r,t)}\right]^T$, and the same notation applies for $\mathbf{H}_i$ and $\mathbf{G}_i$. For simplicity the downlink channels are assumed to be i.i.d. Rayleigh fading channels with unit mean square value $\mathbb{E}\left\{\left|\mathbf{H}_0^{(r,t)}\right|^2\right\} = \mathbb{E}\left\{\left|\mathbf{H}_i^{(r,t)}\right|^2\right\} = \mathbb{E}\left\{\left|\mathbf{G}_i^{(r,t)}\right|^2\right\} = 1$ for $t = 1, 2, \ldots, N_t$, $r = 1, 2, \ldots, N_r$. $\mathbf{s}_0 = \left[\mathbf{s}_0^{(1)}, \mathbf{s}_0^{(2)}, ..., \mathbf{s}_0^{(N_t)}\right]$ and $\mathbf{s}_i = \left[\mathbf{s}_i^{(1)}, \mathbf{s}_i^{(2)}, ..., \mathbf{s}_i^{(N_t)}\right]$ denotes the transmit symbol vectors at the probe BS_0 and interfering BS_i, respectively.

In this section, five different MIMO transmission schemes are introduced, namely spatial multiplexing (SMX) and per-stream zero-forcing (ZF) [78, Section II.A.], orthogonal space-time block coding (OSTBC) [79, Section 3.4],[78, Section II.B.], fixed rate singular value decomposition (SVD) multiplexing [79, Section 3.2], MIMO MRC [81, 82, 83], selection diversity (SD) and combining[79, Section 3.5]. They cover a wide range of practical MIMO systems, including the open-loop and close-loop networks, single-stream and multi-stream transmissions, *etc.*, as summarized in *Table 3.1*, and performance analysis problem of these MIMO schemes in downlink cellular networks can be formulated as in (3.1) and can be solved by the Gil-Pelaez inversion approach introduced in this chapter.

Table 3.1: MIMO Transmission Schemes in Downlink Cellular Networks (MRT = Maximum Ratio Transmission; N_{ts}=Number of Time Slots).

Schemes	**Transmitter**	**Receiver**	**Single-Stream /Multi-Stream**	**Open-Loop /Close-Loop**	**Time Slot**
SMX-ZF	SMX	Per-stream ZF	Multi-Stream	Open-Loop	1
OSTBC	OSTBC code	Matched Filter	Multi-Stream	Open-Loop	N_{ts}
Fixed Rate SVD	SVD	SVD	Single-Stream	Close-Loop	1
MIMO MRC	MRT	MRC	Single-Stream	Close-Loop	1
SD & Combining	Best Antenna	MRC	Single-Stream	Close-Loop	1

3.3.1 Spatial Multiplexing and Per-Stream ZF Receiver

In an open-loop MIMO system, if spatial multiplexing is applied at the N_t-antenna transmitter, then N_t streams of data are interfering each other. The $N_r \times 1$ received signal vector $\mathbf{y}_{0,t} = \left[\mathbf{y}_{0,t}^{(1)}, \mathbf{y}_{0,t}^{(2)}, ..., \mathbf{y}_{0,t}^{(N_r)}\right]^T$ at N_r-antenna MT_0 from the t-th stream of N_t-antenna BS_0 in the dowlink

open-loop MIMO cellular networks can be formulated as follows:

$$\mathbf{y}_{0,t} = \underbrace{\sqrt{E/N_t}\, r_0^{-b}\mathbf{h}_{0,t}\mathbf{s}_0^{(t)}}_{\text{useful signal}} + \underbrace{\sum_{q=1,q\neq t}^{N_t}\sqrt{E/N_t}\, r_0^{-b}\mathbf{h}_{0,q}\mathbf{s}_0^{(q)}}_{\text{self interference}} + \underbrace{\sum_{i\in\Phi^{(\backslash 0)}}\sqrt{E/N_t}\, r_i^{-b}\mathbf{H}_i\mathbf{s}_i}_{\text{other cell Interference}} + \mathbf{n}_0 \quad (3.4)$$

The per-stream ZF receiver, multiplies the ZF vector $\mathbf{w}_{0,t}^H \in C^{1\times N_r}$ on $\mathbf{y}_{0,t}$ and the self-interference between streams is eliminated [78, Section II.A.]. $\mathbf{w}_{0,t}^H$ is the t-th row of the pseudo channel inverse $\left(\mathbf{H}_0^H\mathbf{H}_0\right)^{-1}\mathbf{H}_0^H \in C^{N_t\times N_r}$, and per stream output can be formulated as follows:

$$z_{0,t} = \mathbf{w}_{0,t}^H\mathbf{y}_{0,t} \quad (3.5)$$

Proposition 3.1 *Let the spatial multiplexing transmitter employed at the N_t-antenna BSs and the per-stream ZF receiver employed at the N_r-antenna MTs in an open-loop downlink MIMO cellular network, the SINR of $z_{0,t}$ in* (3.5) *at the output of the receiver can be formulated as in* (3.1) *with* $\mathrm{P} = E/N_t$, $\gamma_0 \sim \mathrm{Gamma}\left(N_r - N_t - 1, N_r - N_t - 1\right)$ *and* $\gamma_i \sim \mathrm{Gamma}\left(N_t, N_t\right)$.

Proof*: From* (3.4) *and* (3.5), $\gamma_{0,t} = 1/\left[\left(\mathbf{H}_0^H\mathbf{H}_0\right)^{-1}\right]_t$ *and* $\gamma_{i,t} = \left[\left(\mathbf{H}_0^H\mathbf{H}_0\right)^{-1}\mathbf{H}_0^H\left(\mathbf{H}_i\mathbf{H}_i^H\right)\mathbf{H}_0\left(\mathbf{H}_0^H\mathbf{H}_0\right)^{-1}\right]_t$ $/\left[\left(\mathbf{H}_0^H\mathbf{H}_0\right)^{-1}\right]_t$, *where* $[\cdot]_t$ *denotes the* (t,t)*-th element in a square matrix. The rest of proof follows from [78, Section II.A.] and the subscript* t *is dropped since each stream is identical.* □

3.3.2 Orthogonal Space-Time Block Coding

In an open-loop MIMO system, if OSTBC is applied, then N_s symbols are transmitted over N_{ts} time slots using $N_t \le N_r$ antennas [78, Section II.B.]. The code rate is $coderate = N_s/N_{ts}$. The received $N_r \times N_s$ signal matrix $\mathbf{Y}_0$ at MT_0 is as follows:

$$\mathbf{Y}_0 = \underbrace{\sqrt{E/N_t}\, r_0^{-b}\mathbf{H}_0\mathbf{X}_0}_{\text{useful signal}} + \underbrace{\sum_{i\in\bar{\Psi}_{\mathrm{RB}}^{\backslash 0}}\sqrt{E/N_t}\, r_i^{-b}\mathbf{H}_i\mathbf{X}_i}_{\text{other cell Interference}} + \mathbf{N}_0 \quad (3.6)$$

where $\mathbf{X}_0 = \sum_{q=1}^{N_s}\left(s_{0,q}\mathbf{A}_q + s_{0,q}^H\mathbf{B}_q\right)$ and $\mathbf{X}_i = \sum_{q=1}^{N_s}\left(s_{i,q}\mathbf{A}_q + s_{i,q}^H\mathbf{B}_q\right)$ are $N_t \times N_{ts}$ transmitted OSTBC code matrices at probe and interfering transmitters respectively, with $s_{0,q}$ and $s_{i,q}$ denoting the q-th transmitted symbol of probe and interfering transmitters respectively. For example,if Alamouti code is applied in a 2×2 OSTBC MIMO system, the code rate is then $coderate = N_s/N_{ts} = 1$, and $\mathbf{A}_1 = \begin{pmatrix}1 & 0\\ 0 & 0\end{pmatrix}, \mathbf{B}_1 = \begin{pmatrix}0 & 0\\ 0 & 1\end{pmatrix}$ and $\mathbf{A}_2 = \begin{pmatrix}0 & 0\\ 1 & 0\end{pmatrix}, \mathbf{B}_2 = \begin{pmatrix}0 & -1\\ 0 & 0\end{pmatrix}$. The fading channel matrices $\mathbf{H}_0$ and $\mathbf{H}_i$ are assumed to be consistent over N_{ts} time slots, $\mathbf{N}_0 \sim \mathscr{CN}\left(\mathbf{0}_{N_r\times N_{ts}}, \mathscr{N}_0\mathbf{I}_{N_r\times N_{ts}}\right)$ is the AWGN noise matrix.

Proposition 3.2 *Let OSTBC in an open-loop downlink MIMO cellular network as in* (3.6)*, the SINR of the data estimate for one symbol can be formulated as in* (3.1) *with* $\mathrm{P} = E/N_t$,

$\gamma_0 \sim \text{Gamma}(N_t N_r, N_t N_r)$ *and* $\gamma_i \sim \text{Gamma}(N_r, N_r)$.

Proof*: Let* $\bar{\mathbf{h}}_0 = vec(\mathbf{H}_0)$ *be the vectorization of the matrix* $\mathbf{H}_0$ *and* $\bar{\mathbf{h}}_i^{(k)}$ *be a permutation of entries in* $vec(\mathbf{H}_i)$ *depending on the block coding structure. Then* $\gamma_0 = \|\mathbf{H}_0\|^2$ *and* $\gamma_i = \sum_{k=1}^{N_r} \left(\bar{\mathbf{h}}_0^H / \left\|\bar{\mathbf{h}}_0\right\|\right) \bar{\mathbf{h}}_i^{(k)} s_i^{(k)}$*. The rest of proof follows by [79, Section 3.4] and [78, Section II.B.] and neglecting the correlation between each* $\left(\bar{\mathbf{h}}_0^H / \left\|\bar{\mathbf{h}}_0\right\|\right) \bar{\mathbf{h}}_i^{(k)} s_i^{(k)}$ *in* γ_i. □

3.3.3 Fixed Rate SVD Multiplexing

The MIMO channel can be decomposed into spatial modes by means of its SVD as follows:

$$\begin{aligned} &\mathbf{H}_0 = \mathbf{U}_0 \Sigma_0 \mathbf{V}_0^H, \mathbf{U}_0 \in C^{N_r \times N_r}, \Sigma_0 \in C^{N_r \times N_t}, \mathbf{V}_0 \in C^{N_t \times N_t} \\ &\mathbf{G}_i = \mathbf{U}_i \Sigma_i \mathbf{V}_i^H, \mathbf{U}_i \in C^{N_r \times N_r}, \Sigma_i \in C^{N_r \times N_t}, \mathbf{V}_i \in C^{N_t \times N_t} \end{aligned} \tag{3.7}$$

It is worth noting that $\mathbf{G}_i$ denotes the channel matrix from the ith interferer to its intended receiver. $\mathbf{U}_0, \mathbf{V}_0$ are unitary matrices, Σ_0 is the diagonal matrix of singular values, which are the square roots of eigenvalues of the Wishart matrix $\mathbf{H}_0 \mathbf{H}_0^H$. Meanwhile, let Λ_0 be the diagonal matrix of eigenvalues. The same notation holds for interfering links. If the number of non-zero eigenvalues is M, we can say MIMO spatial multiplexing has M spatial modes.

It is known that MIMO capacity can be achieved by SVD with full CSI (with power allocation). The system model is as [79, Chapter 3.2], the $N_r \times 1$ received signal vector $\mathbf{y}_0 = \left[\mathbf{y}_0^{(1)}, \mathbf{y}_0^{(2)}, ..., \mathbf{y}_0^{(N_r)}\right]^T$ at MT_0 can be formulated as follows:

$$\mathbf{y}_0 = \underbrace{\sqrt{E/N_t} r_0^{-b} \mathbf{H}_0 \mathbf{V}_0 \mathbf{s}_0}_{\text{useful signal}} + \underbrace{\sum_{i \in \Phi^{(\backslash 0)}} \sqrt{E/N_t} r_i^{-b} \mathbf{H}_i \mathbf{V}_i \mathbf{s}_i}_{\text{other cell Interference}} + \mathbf{n}_0 \tag{3.8}$$

The fixed rate SVD MIMO transmission scheme, multiplies unitary matrices $\mathbf{U}_0^H$ on $\mathbf{y}_0$, thus, the post-processing signal vector is:

$$\mathbf{z}_0 = \mathbf{U}_0^H \mathbf{y}_0 = \sqrt{E/N_t} r_0^{-b} \Sigma_0 \mathbf{s}_0 + \sum_{i \in \Phi^{(\backslash 0)}} \sqrt{E/N_t} r_i^{-b} \mathbf{U}_0^H \mathbf{H}_i \mathbf{V}_i \mathbf{s}_i + \mathbf{U}_0^H \mathbf{n}_0 \tag{3.9}$$

The fixed rate SVD scheme is achieved by randomly selecting one mode among all available modes [79, Eq. 4.8] as the probe link.

Proposition 3.3 *Let fixed rate SVD in a close-loop downlink MIMO cellular network as in* (3.8) *and* (3.9)*, randomly selecting one mode among all the* M *available modes, the SINR can be formulated as in* (3.1) *with* $\text{P} = E/N_t$*,* γ_0 *having its PDF given as follows in* (3.10) *and* $\gamma_i \sim \text{Gamma}(M, M)$.

$$f_{\gamma_0}(\phi) = \frac{1}{M} \sum_{k=0}^{M-1} \left(L_k(\phi)\right)^2 e^{-\phi} \tag{3.10}$$

where $L_k(\phi) = \sum_{i=0}^{k} \begin{pmatrix} k \\ k-i \end{pmatrix} \frac{(-\phi)^i}{i!}$.

Proof*: From* (3.8) *and* (3.9)*, for the interfering links,* $\gamma_i = \sum_{k=1}^{M} \left| \mathbf{u}^H \mathbf{H}_i \mathbf{v}_{i,k} s_{i,k} \right|^2$*, where* $\mathbf{u}$ *is the corresponding vector to the randomly selected mode (singular value); for the probe link, randomly selecting one mode among all the M available modes results in a unordered eigenvalue of a Wishart matrix. The rest of proof follows by [79, Eq. 4.13].* □

3.3.4 MIMO MRC

MIMO MRC [79, 80, 81], which performs maximum ratio transmission (MRT) at transmitter and MRC at receiver. The $N_r \times 1$ received signal vector $\mathbf{y}_0 = \left[\mathbf{y}_0^{(1)}, \mathbf{y}_0^{(2)}, ..., \mathbf{y}_0^{(N_r)} \right]^T$ at N_r-antenna MT_0 can be formulated as follows:

$$\mathbf{y}_0 = \underbrace{\sqrt{E/N_t} r_0^{-b} \mathbf{H}_0 \mathbf{w}_{T,0} s_0}_{\text{useful signal}} + \underbrace{\sum_{i \in \Phi^{(\backslash 0)}} \sqrt{E/N_t} r_i^{-b} \mathbf{H}_i \mathbf{w}_{T,i} s_i}_{\text{other cell Interference}} + \mathbf{n}_0 \tag{3.11}$$

where $\mathbf{w}_{T,i} = \mathbf{U}_i, \mathbf{w}_{T,0} = \mathbf{U}_0$ are MRT vectors applied at the transmitter side with $\mathbf{U}_0$ being the eigenvector corresponding to the largest eigenvalue $\lambda_{\max,0}$ of $\mathbf{F}_0 = \mathbf{H}_0^H \mathbf{H}_0$ and $\mathbf{U}_i$ being the eigenvector corresponding to the largest eigenvalue $\lambda_{\max,i}$ of of $\mathbf{F}_i = \mathbf{G}_i^H \mathbf{G}_i$. The MIMO MRC scheme, multiplies MRC vector $\mathbf{w}_{R,0}^H$ on $\mathbf{y}_0$, where $\mathbf{w}_{R,0} = \mathbf{H}_0 \mathbf{U}_0$, thus, the post-processing signal is:

$$z_0 = \mathbf{w}_{R,0}^H \mathbf{y}_0 \tag{3.12}$$

Proposition 3.4 *Let MRT being employed at the* N_t*-antenna BSs and MRC receiver being employed at the* N_r*-antenna MTs in a close-loop downlink MIMO cellular network, the SINR of* z_0 *in* (3.12) *at the output of the receiver can be formulated as in* (3.1) *with* $\mathrm{P} = E/N_t$*,* γ_0 *having its PDF given as follows in* (3.14) *and* $\gamma_i \sim \mathrm{Gamma}(1,1)$.

$$f_{\gamma_0}(x) = \frac{\sum_{v=1}^{q} \sum_{l=p-q}^{(p+q-2v)v} c_{v,l} x^l e^{-vx}}{\prod_{k=1}^{q} \Gamma(q-k+1) \Gamma(p-k+1)} \tag{3.13}$$

where $q = \min(N_t, N_r)$, $p = \max(N_t, N_r)$ *and* $c_{v,l}$ *is the coefficient of* $x^l e^{-vx}$.

Proof*: From* (3.11) *and* (3.12)*,* $\gamma_i = \left(1/\lambda_{\max,0}\right) \left| \mathbf{w}_{R,0}^H \mathbf{H}_i \mathbf{w}_{T,i} \right|^2$ *and it is a Rayleigh RV [80, Eq. 36].* γ_0 *is the largest eigenvalue* $\lambda_{\max,0}$ *of* $\mathbf{F}_0 = \mathbf{H}_0^H \mathbf{H}_0$*. And its PDF is available in [81, 82, 83], while its CDF is available in [80, Eq. 6].*

□

Remark 3.1 *The moment generating function of* γ_0 *is available in close-form as follows accord-*

ing to [83]:

$$\mathscr{M}_{\gamma_0}(s) = \frac{1}{\prod_{k=1}^{q}\Gamma(q-k+1)\Gamma(p-k+1)} \sum_{v=1}^{q} \sum_{l=p-q}^{(p+q-2v)v} \frac{d_{v,l}}{(1+s/v)^{l+1}} \tag{3.14}$$

where the coefficient $d_{v,l} = \left(l!/v^{l+1}\right) c_{v,l}$ *is available in [83, Table. I-IV]. For example, in a* 2×2 *MIMO MRC system,* $N_r = N_t = 2$*, the MGF of the* γ_0 *is as follows:*

$$\mathscr{M}_{\gamma_0}(s) = \frac{1}{\prod_{k=1}^{2}\Gamma(2-k+1)\Gamma(2-k+1)} \left(\frac{d_{1,0}}{(1+s)^1} + \frac{d_{1,1}}{(1+s)^2} + \frac{d_{1,2}}{(1+s)^3} + \frac{d_{2,0}}{(1+s/2)^1}\right)$$

where the coefficients $d_{1,0} = 2, d_{1,1} = -2, d_{1,2} = 2, d_{2,0} = -1$ *are from [83, Table. I].* □

3.3.5 Selection Diversity and Combining

Another single stream MIMO scheme is to perform MRC at receiver and select the best instantaneous channel (largest magnitude vector channel) at transmitter. The system model is as in [79, Section 3.5]. The $N_r \times 1$ received signal vector $\mathbf{y}_0 = \left[\mathbf{y}_0^{(1)}, \mathbf{y}_0^{(2)}, ..., \mathbf{y}_0^{(N_r)}\right]^T$ at N_r-antenna MT_0 can be formulated as follows:

$$\mathbf{y}_0 = \underbrace{\sqrt{E/N_t}\, r_0^{-b}\mathbf{h}_{0,t^\dagger} s_0}_{\text{useful signal}} + \underbrace{\sum_{i\in\Phi^{(!0)}} \sqrt{E/N_t}\, r_i^{-b}\mathbf{h}_{i,t^\dagger} s_i}_{\text{other cell Interference}} + \mathbf{n}_0 \tag{3.15}$$

Let $t^\dagger = arg\max_t \left(\left\|\mathbf{h}_{0,t}\right\|^2\right)$ denote the best channel selection. The SD - combing scheme, multiplies MRC vector $\mathbf{h}_{0,t^\dagger}^H$ on $\mathbf{y}_0$ at the receiver side, thus, the post-processing signal is:

$$z_0 = \mathbf{h}_{0,t^\dagger}^H \mathbf{y}_0 \tag{3.16}$$

Proposition 3.5 *Let best instantaneous channel selected at the* N_t*-antenna BSs and MRC receiver being employed at the* N_r*-antenna MTs in a close-loop downlink MIMO cellular network, the SINR of* z_0 *in* (3.16) *at the output of the receiver can be formulated as in* (3.1) *with* $\mathrm{P} = E/N_t$*,* γ_0 *having its CDF given as follows in* (3.17) *and* $\gamma_i \sim \mathrm{Gamma}(1,1)$*.*

$$F_{\gamma_0}(x) = \left(1 - e^{-x}\sum_{k=0}^{N_r-1}\frac{x^k}{k!}\right)^{N_t} = \left(1 - \frac{\Gamma[N_r, x]}{\Gamma[N_r]}\right)^{N_t} \tag{3.17}$$

Proof*: From* (3.15) *and* (3.16)*,* $\gamma_i = \left|\left(\mathbf{h}_{0,t^\dagger}^H / \left\|\mathbf{h}_{0,t^\dagger}\right\|\right)\mathbf{h}_{i,t^\dagger}\right|^2$ *and it is a Rayleigh RV [79].* $\gamma_0 = \left\|\mathbf{h}_{0,t^\dagger}\right\|^2$ *and its CDF is available in [79, Eq. 3.31].*

3.4 Gil-Pelaez Based Mathematical Frameworks to the Computations of Coverage and Rate

In this section, new mathematical frameworks to the computation of (3.1) and (3.2) are provided, by assuming that γ_0 and γ_i for $i \in \Phi^{(\backslash 0)}$ have an arbitrary distribution. For generality, and according to, *e.g.,* [37] and [30], the distributions of γ_0 and γ_i are different and independent. The interferers power gains γ_i for $i \in \Phi^{(\backslash 0)}$, on the other hand, are assumed to be independent but identically distributed.

3.4.1 Coverage Probability

Theorem 3.1 *Let* $\mathrm{P}_{\mathrm{cov}}(\cdot)$ *in* (3.2). *It can be formulated as:*

$$\mathrm{P}_{\mathrm{cov}}(\tau) = \frac{1}{2} - 2\lambda \int_0^{+\infty} \mathrm{Im}\left\{ \mathscr{M}_{\gamma_0}\left(j\frac{x}{\tau}\right) \mathscr{F}_{\mathrm{NI}}(x) \right\} \frac{dx}{x} \tag{3.18}$$

where $\mathscr{M}_{\gamma_0}$ *is the MGF function of* γ_0 *and the following functions are introduced:*

$$\mathscr{F}_{\mathrm{NI}}(x) = \int_0^{+\infty} y \exp\left(j y^{\alpha} x \frac{\mathscr{N}_0}{\mathsf{P}} \right) \exp\left(-\pi\lambda y^2 \Upsilon_{\mathrm{I}}(jx)\right) dy \tag{3.19}$$

$$\Upsilon_{\mathrm{I}}(z) = \mathbb{E}_{\gamma_i}\left\{ {}_1F_1\left(-\frac{2}{\alpha}; 1-\frac{2}{\alpha}; z\gamma_i\right) \right\} \tag{3.20}$$

Proof*: See Appendix 3.9.1.* □

Corollary 3.1 *Let* $\mathrm{P}_{\mathrm{cov}}(\cdot)$ *in* (3.2) *with* $\mathscr{N}_0 = 0$, *i.e.,* $\mathrm{P}_{\mathrm{cov}}^{[\infty]}(\cdot)$. *It can be formulated as:*

$$\mathrm{P}_{\mathrm{cov}}^{[\infty]}(\tau) = \frac{1}{2} - \frac{1}{\pi} \int_0^{+\infty} \mathrm{Im}\left\{ \frac{\mathscr{M}_{\gamma_0}\left(j\frac{x}{\tau}\right)}{\Upsilon_{\mathrm{I}}(jx)} \right\} \frac{dx}{x} \tag{3.21}$$

Proof*: It follows from* (3.19) *letting* $\mathscr{N}_0 = 0$ *and computing the integral using* $\int_0^{+\infty} t \exp\left(-kt^2\right) dt = 1/(2k)$. □

The computation of (3.18) and (3.21) requires a closed-form expression of the expectation in (3.20). *Remark 3.2* provides a general approach to solve this problem.

Remark 3.2 *Let* $\mathbb{E}_{\gamma_i}\{\gamma_i^k\} = \bar{\gamma}^k\left((\mathbf{p})_k/(\mathbf{q})_k\right)$ *for* $k = 1, 2, \ldots$, *where* $\mathbf{p} = (p_1, p_2, \ldots, p_N)$ *and* $\mathbf{q} = (q_1, q_2, \ldots, q_M)$ *are vectors with N and M real-valued entries, and* $(\mathbf{p})_k$ *and* $(\mathbf{q})_k$ *are short-hands for* $(\mathbf{p})_k = (p_1)_k (p_2)_k \cdots (p_N)_k$ *and* $(\mathbf{q})_k = (q_1)_k (q_2)_k \cdots (q_M)_k$. *Then, the following equalities*

hold:

$$\Upsilon_{\mathrm{I}}(z) \overset{(a)}{=} \sum_{k=0}^{+\infty} \frac{(-2/\alpha)_k (\mathbf{p})_k}{(1-2/\alpha)_k (\mathbf{q})_k} \frac{\left(z\bar{\gamma}\right)^k}{k!} \overset{(b)}{=} {}_{N+1}F_{M+1}\left(-\frac{2}{\alpha}, \mathbf{p}; 1-\frac{2}{\alpha}, \mathbf{q}; z\bar{\gamma}\right) \tag{3.22}$$

where (a) and (b) follow from the series representation of the hypergeometric function [57, Ch. 5, Eq. (2)]. The formulation $\mathbb{E}_{\gamma_i}\{\gamma_i^k\} = \bar{\gamma}^k \left((\mathbf{p})_k / (\mathbf{q})_k\right)$ *holds for a large number of fading distributions and transmission schemes. A general class of distributions is available in [64, Eq. (13)], whose moments can be computed using [58, Eq. (2.25.2.1)].* □

3.4.2 Average Rate

Theorem 3.2 *Let* $\mathscr{R}$ *in* (3.3)*. It can be formulated as:*

$$\mathscr{R} = -2\lambda \int_0^{+\infty} \mathrm{Im}\left\{ j\mathscr{F}_0(jx)\mathscr{F}_{\mathrm{NI}}(x)\right\} dx \tag{3.23}$$

where $\mathscr{F}_{\mathrm{NI}}(\cdot)$ *is defined in* (3.19) *and* $\mathscr{F}_0(\cdot)$ *is given as follows:*

$$\mathscr{F}_0(z) = \int_0^{+\infty} \frac{\ln(1+y)}{y^2} \mathscr{M}_{\gamma_0}^{(1)}\left(\frac{z}{y}\right) dy \tag{3.24}$$

Proof*: It follows from* (3.3) *by using* (3.18)*, since* $\mathrm{P}_{\mathrm{cov}}^{(1)}(y) = \left(\frac{2\lambda}{y^2}\right) \int_0^{+\infty} \mathrm{Im}\left\{ j\mathscr{M}_{\gamma_0}^{(1)}\left(j\left(\frac{x}{y}\right)\right)\mathscr{F}_{\mathrm{NI}}(x)\right\} dx$. □

Corollary 3.2 *Let* $\mathscr{R}$ *in* (3.3) *with* $\mathscr{N}_0 = 0$*, i.e.,* $\mathscr{R}^{[\infty]}$*. It can be formulated as:*

$$\mathscr{R}^{[\infty]} = -\frac{1}{\pi} \int_0^{+\infty} \mathrm{Im}\left\{ j \frac{\mathscr{F}_0(jx)}{\Upsilon_{\mathrm{I}}(jx)}\right\} dx \tag{3.25}$$

Proof*: It is the same as the proof of Corollary 3.1.* □

Remark 3.3 *The computation of* (3.24) *and* (3.25) *requires closed-form expressions for the first derivative of* $\mathscr{M}_{\gamma_0}(\cdot)$*. Luckily, they are available for many fading distributions. A summary can be found in [64, Tables II–V].* □

3.5 Case Study: Coverage and Rate in Downlink Cellular Networks with Gamma Distributed Per-Link Power Gains

In this section, we focus our attention on the case study where the power gains of intended and interfering links follow a Gamma distribution with arbitrary parameters, $\gamma_0 \sim \mathrm{Gamma}(m_0, \Omega_0)$

and $\gamma_i \sim \text{Gamma}(m_I, \Omega_I)$. This case study is meaningful because it finds application to the analysis of cellular networks for propagation over Rayleigh fading, which rely on multiple-antenna transmission schemes at the physical layer. The reader is referred to [37] and [30] for further details. In order to get insight on the impact of the multiple-antenna transmission scheme, the authors of [37] and [30] resort to approximated representations of the aggregate other-cell interference and to stochastic ordering analysis. In [19, Sec. IV-H], it is shown that an accurate analysis of this scenario would require the computation of the higher-order derivatives of the MGF of the aggregate other-cell interference. Unlike these papers, with the aid of the mathematical formulations in *Corollary 3.1* and *Corollary 3.2*, we propose approximated but closed-form expressions for coverage and rate. The obtained mathematical expressions are shown to provide relevant information on the impact of system parameters, which may offer a simple approach for comparing various multiple-antenna transmission schemes at the physical layer [37], [30]. In Section 4.6, we show that the performance trends obtained from the proposed mathematical frameworks are confirmed with the aid of Monte Carlo simulations.

By assuming $\gamma_0 \sim \text{Gamma}(m_0, \Omega_0)$ and $\gamma_i \sim \text{Gamma}(m_I, \Omega_I)$, *Corollary 3.1* and *Corollary 3.2* can be simplified as follows:

$$\text{P}_{\text{cov}}^{[\infty]}(\tau) \overset{(a)}{=} \frac{1}{2} - \frac{1}{\pi}\int_0^{+\infty} \text{Im}\left\{ \frac{\left(1 + j\tilde{\kappa}_0 x\right)^{-m_0}}{{}_2F_1\left(-\frac{2}{\alpha}, m_I; 1-\frac{2}{\alpha}; j\kappa_I x\right)} \right\} \frac{dx}{x} \tag{3.26}$$

$$\mathscr{R}^{[\infty]} \overset{(b)}{=} \frac{1}{\pi\Gamma(m_0)} \int_0^{+\infty} \text{Im}\left\{ \frac{G_{3,3}^{2,3}\left(j\kappa_0 x \middle| \begin{matrix} 1 & 1 & 1-m_0 \\ & 1 & 1 & 0 \end{matrix} \right)}{{}_2F_1\left(-\frac{2}{\alpha}, m_I; 1-\frac{2}{\alpha}; j\kappa_I x\right)} \right\} \frac{dx}{x} \tag{3.27}$$

where $\kappa_0 = \Omega_0/m_0$, $\tilde{\kappa}_0 = \kappa_0/\tau$ and $\kappa_I = \Omega_I/m_I$. Also, (a) is obtained by taking into account that $\mathscr{M}_{\gamma_0}(s) = (1+s\kappa_0)^{-m_0}$ [60, Eq. (2.22)], $\mathbb{E}_{\gamma_i}\left\{\gamma_i^k\right\} = \kappa_I^k (m_I)_k$ [60, Eq. (2.23)] and by applying *Remark 3.2*. The equality in (b) is obtained using similar mathematical steps. In addition, $\mathscr{F}_0(\cdot)$ is computed by taking into account that $\mathscr{M}_{\gamma_0}^{(1)}(s) = -\Omega_0 (1+s\kappa_0)^{-(m_0+1)}$ and by using [58, Eq. (8.4.2.5)], [58, Eq. (8.4.6.5)] and [58, Eq. (2.24.1.1)].

Approximated closed-form expressions of (3.26) and (3.27) are provided in *Proposition 3.6* and *Proposition 3.7*, respectively.

3.5.1 Coverage Probability

Proposition 3.6 *Let* $\text{P}_{\text{cov}}^{[\infty]}(\cdot)$ *in* (3.26). *The following holds:*

$$\text{P}_{\text{cov}}^{[\infty]}(\tau) \approx 1 - \left(1 + \frac{1}{2}\frac{1}{m_0}\frac{\Omega_0}{\Omega_I}(\alpha-2)\frac{1}{\tau}\right)^{-m_0} \tag{3.28}$$

Proof*: See Appendix 3.9.2.* □

Remark 3.4 *By direct inspection of* (3.28)*, the coverage probability has the following performance trends: i) it increases as* $\eta = \Omega_0 (\alpha - 2) \big/ (\tau \Omega_I)$ *increases; ii) it increases as* m_0 *increases; and iii) it is independent of* m_I*.* □

Remark 3.5 *Let* $\mathscr{K}_{\mathrm{P}_{\mathrm{cov}}} = \big(\Omega_0 \big/ \Omega_I\big)\big(1 \big/ (m_0 \tau)\big)$*. The accuracy of the approximation in* (3.28) *increases as* $\mathscr{K}_{\mathrm{P}_{\mathrm{cov}}}$ *increases. This follows by using the same line of thought as [75, Fig. 1]. In* (3.48)*, in fact, the first-order Taylor approximation of the hypergeometric function is used. As a consequence, this approximation is accurate when the numerator of the integrand function in* (3.26) *behaves more and more like a delta function at the origin. This occurs as* $\mathscr{K}_{\mathrm{P}_{\mathrm{cov}}}$ *increases.* □

3.5.2 Average Rate

Proposition 3.7 *Let* $\mathscr{R}^{[\infty]}$ *in* (3.27)*. The following holds:*

$$\mathscr{R}^{[\infty]} \approx \frac{1}{\Gamma(m_0)} G_{3,3}^{3,2}\left(\left(\frac{1}{2} \frac{1}{m_0} \frac{\Omega_0}{\Omega_I} (\alpha - 2) \right)^{-1} \middle| \begin{matrix} 0 & 0 & 1 \\ m_0 & 0 & 0 \end{matrix} \right) \tag{3.29}$$

Proof*: By inserting the first derivative of* (3.28) *in* (3.3)*,* $\mathscr{R}^{[\infty]}$ *is:*

$$\mathscr{R}^{[\infty]} \approx \kappa_{0I} \int_0^{+\infty} y^{m_0 - 1} \ln\big(1 + y\big) \big(y + \kappa_{0I} / m_0\big)^{-(m_0 + 1)} \, dy \tag{3.30}$$

where $\kappa_{0I} = (1/2)\big(\Omega_0 \big/ \Omega_I\big)(\alpha - 2)$*. The proof follows by computing the integral using [58, Eq. (8.4.2.5)], [58, Eq. (8.4.6.5)] and [58, Eq. (2.24.1.1)].* □

Remark 3.6 *By plotting the Meijer G-function in* (3.29) *as a function of* $\tilde{\eta} = (\Omega_0 / \Omega_I)(\alpha - 2)$ *and* m_0*, the same performance trends as for the coverage (Remark 3.4) hold.* □

Remark 3.7 *Let* $\mathscr{K}_{\mathrm{Rate}} = \big(\Omega_0 \big/ \Omega_I\big)\big(1 \big/ m_0\big)$*. The accuracy of the approximation in* (3.29) *increases as* $\mathscr{K}_{\mathrm{Rate}}$ *decreases. It follows similar to Remark 3.5, by taking into account that the Meijer G-function in the numerator of* (3.27) *behaves more and more like a delta function at the origin as* $\mathscr{K}_{\mathrm{Rate}}$ *decreases.* □

3.6 Case Study: Service Success Probability in Partially Loaded Downlink Cellular Networks

3.6.1 Modified System Model and Problem Formulation

Let the BSs of a downlink SISO/MIMO cellular network be deployed as in *Section 3.2*, in partially loaded networks [40, 41, 42, 43], each BS is assumed to have limited N_{RB} available resource blocks. Let $\lambda^{(\mathrm{MT})}$ be the deployment density of the MTs, which is also a PPP, the following two scenarios could happen: i) multiple MTs could be potentially associated with one BS. Due to limited resource blocks, only limited number of MTs can be served; ii) a few or no MTs are potentially associated with a BS and the resource blocks are not fully utilized. Thus, a BS may not be transmitting on some available resource blocks. The load is considered by introducing two probabilities: the MT selection probability on a random resource block $p^{(\mathrm{RB})}_{\mathrm{select}}$ and the BS inactive probability on a random resource block $p^{(\mathrm{RB})}_{\mathrm{inactive}}$. The mathematical formulations of these two probabilities are introduced in the next section.

Conditioning on the selection of the probe MT, on a random resource block, the conditional SINR of this partially loaded downlink cellular network can be formulated as follows:

$$\begin{aligned}&\mathrm{SINR}\big|\left(\text{MT being selected}\right)=\frac{\mathrm{P}/N_{\mathrm{RB}}\gamma_0 r_0^{-\alpha}}{\mathcal{N}_0+\mathrm{P}/N_{\mathrm{RB}}\tilde{\mathscr{I}}_{agg}(r_0)}\\&\tilde{\mathscr{I}}_{agg}(r_0)=\sum\nolimits_{i\in\tilde{\Phi}^{(\backslash 0)}}\gamma_i r_i^{-\alpha}\end{aligned}\tag{3.31}$$

where $\mathrm{P}/N_{\mathrm{RB}}$ is the equivalent transmit power of the BSs, equally allocated in all N_{RB} resource blocks, $\tilde{\mathscr{I}}_{agg}(\cdot)$ is the aggregate other-cell interference from the active set of interfering BSs on the random resource block $i\in\tilde{\Phi}^{(\backslash 0)}$, where the density of $\tilde{\Phi}^{(\backslash 0)}$ is a thinning version of the density of all BSs $\Phi^{(\backslash 0)}$, *i.e.*,

$$\tilde{\lambda}=\left(1-p^{(\mathrm{RB})}_{\mathrm{inactive}}\right)\lambda\tag{3.32}$$

In this section, conditional coverage probability ($\tilde{\mathrm{P}}_{\mathrm{cov}}$), which is the SINR coverage probability conditioning on the probe MT being selected, and service success probability ($\mathrm{P}_{\mathrm{service}}$), which is the probability that the cellular network succeeds in serving an arbitrary MT with the target SINR threshold, are studied. They can be formulated as follows:

$$\tilde{\mathrm{P}}_{\mathrm{cov}}(\tau)=\Pr\left\{\mathrm{SINR}\big|\left(\text{MT being selected}\right)\geq\tau\right\}\tag{3.33}$$

$$\mathrm{P}_{\mathrm{service}}(\tau)=p^{(\mathrm{RB})}_{\mathrm{select}}\times\tilde{\mathrm{P}}_{\mathrm{cov}}(\tau)\tag{3.34}$$

3.6.2 Load Modeling

This section is focused on the mathematical modeling of $p^{(\mathrm{RB})}_{\mathrm{select}}$ and $p^{(\mathrm{RB})}_{\mathrm{inactive}}$. Indeed, a special case study of $p^{(\mathrm{RB})}_{\mathrm{select}}$ and $p^{(\mathrm{RB})}_{\mathrm{inactive}}$ has been done in [40, 41, 42, 43] for one resource block. In this section, by relying on the similar steps, we extend the analysis to a general case with multiple resource blocks.

The load modeling starts from the property of Poisson Voronoi cell, which is exactly the network tessellation when shortest distance BS-to-MT cell association policy is applied in cellular networks. The PDF of the size of a typical Voronoi cell, normalized by $1/\lambda$, which has been obtained through the extensive Monte Carlo simulations [77] and widely used in the analysis of partially loaded cellular networks [40, 41, 42, 43], is given as follows:

$$f_X(x) = \frac{3.5^{3.5}}{\Gamma(3.5)} x^{2.5} e^{-3.5x} \tag{3.35}$$

where X is a RV denotes the cell size normalized by $1/\lambda$.

Lemma 3.1 *Let the random variable N denote the number of MTs in the Voronoi cell of a randomly chosen BS. Then, the probability mass function (PMF) of N is as follows:*

$$\Pr\{N = n\} = \frac{3.5^{3.5}\Gamma(3.5+n)\left(\lambda^{(\mathrm{MT})}/\lambda\right)^n}{\Gamma(3.5)\, n!\left(\lambda^{(\mathrm{MT})}/\lambda + 3.5\right)^{n+3.5}} \tag{3.36}$$

Proof*: The proof directly follows from [40, Lemma. 1].* □

Proposition 3.8 *The probability that a randomly chosen BS does not have any MT in its Voronoi cell is defined as $p^{(\mathrm{BS})}_{\mathrm{inactive}}$*

$$p^{(\mathrm{BS})}_{\mathrm{inactive}} = \Pr\{N = 0\} = \left(1 + 3.5^{-1}\lambda^{(\mathrm{MT})}/\lambda\right)^{-3.5} \tag{3.37}$$

Proof*: The proof directly follows from Lemma 3.1 and [40, Proposition. 1].* □

Remark 3.8 *From* (3.37)*, the BS inactive probability is a monotonically increasing function of the ratio $\lambda^{(\mathrm{MT})}/\lambda$, i.e., given $\lambda^{(\mathrm{MT})}$, a higher density of BSs λ results in a higher probability that a BS is inactive.* □

Proposition 3.9 *If N_{RB} resource blocks are available, on a randomly chosen resource block, the probability that a randomly chosen BS does not have any MT in its Voronoi cell is defined as $p^{(\mathrm{RB})}_{\mathrm{inactive}}$:*

$$p^{(\mathrm{RB})}_{\mathrm{inactive}} = \sum_{n=0}^{N_{\mathrm{RB}}} (1 - n/N_{\mathrm{RB}}) \Pr\{N = n\} \tag{3.38}$$

Proof*: Let n be the number of MTs located in a randomly chosen Vonoroi cell. If and only if* $n < N_{\mathrm{RB}}$*, there will be idle RBs, on which the BS is not transmitting. Given n MTs located in a BS coverage area, the probability that this BS is not transmitting on a random RB is* $1 - n/N_{\mathrm{RB}}$*. The rest of proof follows from the law of total probability.* □

Remark 3.9 *From* (3.38)*, the BS inactive probability is a monotonically increasing function of the number of resource blocks* N_{RB}*, i.e., given* $\lambda^{(\mathrm{MT})}/\lambda$*, more resource blocks at each BS results in a higher probability that a BS is inactive on a randomly selected resource block.* □

Lemma 3.2 *The PDF of the size of the Voronoi cell, to which a randomly chosen MT belongs, normalized by* $1/\lambda$*, is as follows:*

$$f_Y(y) = \frac{3.5^{4.5}}{\Gamma(4.5)} y^{3.5} e^{-3.5y} \tag{3.39}$$

where Y *is a RV that denotes the size of the Voronoi cell normalized by* $1/\lambda$*.*

Proof*: The proof directly follows from [40, Lemma. 2].* □

Lemma 3.3 *Let the random variable* N' *denote the number of other MTs in the Voronoi cell to which a randomly chosen MT belongs. Then, the PMF of* N' *is as follows:*

$$\Pr\{N' = n\} = \frac{3.5^{4.5}\Gamma(4.5+n)\left(\lambda^{(\mathrm{MT})}/\lambda\right)^n}{\Gamma(4.5)\, n!\left(\lambda^{(\mathrm{MT})}/\lambda + 3.5\right)^{n+4.5}} \tag{3.40}$$

Proof*: The proof directly follows from [40, Lemma. 3].* □

Proposition 3.10 *If only one resource blocks are available at each BS, the probability that a randomly chosen MT is assigned this resource block at a given time and is served by the nearest BS is defined as* $p_{\mathrm{select}}^{(\mathrm{BS})}$*:*

$$p_{\mathrm{select}}^{(\mathrm{BS})} = \frac{1}{\lambda^{(\mathrm{MT})}/\lambda}\left(1 - \left(1 + 3.5^{-1}\lambda^{(\mathrm{MT})}/\lambda\right)^{-3.5}\right) \tag{3.41}$$

Proof*: The proof directly follows from [40, Proposition. 2].* □

Remark 3.10 *From* (3.41)*, the MT selection probability is a monotonically decreasing function of the ratio* $\lambda^{(\mathrm{MT})}/\lambda$*, i.e., given* $\lambda^{(\mathrm{MT})}$*, a higher density of BSs* λ *results in a higher probability that a MT is selected.* □

Proposition 3.11 *If* N_{RB} *resource blocks are available at each BS, the probability that a randomly chosen MT is assigned a resource block at a given time and is served by the nearest BS is*

defined as $p_{\text{select}}^{(\text{RB})}$*:*

$$p_{\text{select}}^{(\text{RB})} = 1 - \left(\frac{3.5}{3.5+\lambda^{(\text{MT})}/\lambda}\right)^{4.5} \frac{\Gamma\left[4.5+N_{\text{RB}}\right]}{\Gamma\left(4.5\right)} \left(\frac{\lambda^{(\text{MT})}/\lambda}{3.5+\lambda^{(\text{MT})}/\lambda}\right)^{N_{\text{RB}}} \times \begin{pmatrix} {}_2F_1\left[1, 4.5+N_{\text{RB}}, 1+N_{\text{RB}}, \frac{\lambda^{(\text{MT})}/\lambda}{3.5+\lambda^{(\text{MT})}/\lambda}\right] / \Gamma\left[1+N_{\text{RB}}\right] \\ -N_{\text{RB}} \times {}_2F_1\left[1, 4.5+N_{\text{RB}}, 2+N_{\text{RB}}, \frac{\lambda^{(\text{MT})}/\lambda}{3.5+\lambda^{(\text{MT})}/\lambda}\right] / \Gamma\left[2+N_{\text{RB}}\right] \end{pmatrix} \tag{3.42}$$

Proof*: If* N_{RB} *resource blocks are available, the selection probability conditioning on* $N' = n < N_{\text{RB}}$ *should always be 1 because in this case all MTs can be served, and selection probability conditioning on* $N' = n \geq N_{\text{RB}}$ *should be* $N_{\text{RB}}/(n+1)$*. Thus, by law of total probability, we have*

$$\begin{aligned} p_{\text{select}}^{(\text{RB})} &= \sum_{n=0}^{N_{\text{RB}}-1} 1 \Pr\left\{N'=n\right\} + \sum_{n=N_{\text{RB}}}^{\infty} \frac{N_{\text{RB}}}{n+1} \Pr\left\{N'=n\right\} \\ &\overset{(a)}{=} \sum_{n=0}^{N_{\text{RB}}-1} 1 \int_0^{\infty} \Pr\left\{N'=n \middle| Y=y\right\} f_Y\left(y\right) dy \\ &\quad + \sum_{n=N_{\text{RB}}}^{\infty} \frac{N_{\text{RB}}}{n+1} \int_0^{\infty} \Pr\left\{N'=n \middle| Y=y\right\} f_Y\left(y\right) dy \end{aligned} \tag{3.43}$$

The rest of proof follows by inserting $\Pr\left\{N'=n \middle| Y=y\right\} = \frac{\left(y\lambda^{(\text{MT})}/\lambda_{BS}\right)^n}{n!} \exp\left(y\lambda^{(\text{MT})}/\lambda_{BS}\right)$ *[40, Proposition. 2] into* (3.43) *and compute the resulting integrals with the aid of [85].* □

Remark 3.11 *From* (3.43)*, the MT selection probability is a monotonically increasing function of the number of resource blocks* N_{RB}*, i.e., given* $\lambda^{(\text{MT})}/\lambda$*, more resource blocks at each BS results in a higher probability that a MT is selected.* □

3.6.3 Service Success Probability

Theorem 3.3 *Let* $\text{P}_{\text{service}}\left(\cdot\right)$ *be the probability that the cellular network succeeds in serving an arbitrary MT with the target SINR threshold. It can be formulated from* (3.34)*:*

$$\text{P}_{\text{service}}\left(\tau\right) = p_{\text{select}}^{(\text{RB})} \times \tilde{\text{P}}_{\text{cov}}\left(\tau\right) = p_{\text{select}}^{(\text{RB})} \left(\frac{1}{2} - 2\lambda \int_0^{+\infty} \text{Im}\left\{\mathscr{M}_{\gamma_0}\left(j\frac{x}{\tau}\right) \tilde{\mathscr{F}}_{\text{NI}}\left(x\right)\right\} \frac{dx}{x}\right) \tag{3.44}$$

where $\mathscr{M}_{\gamma_0}\left(\cdot\right)$ *is the MGF function of* γ_0 *and the following function is introduced:*

$$\widetilde{\mathscr{F}}_{\text{NI}}\left(x\right) = \int_0^{+\infty} y \exp\left(j y^{\alpha} x \frac{N_0}{P/N_{\text{RB}}}\right) \exp\left(-\pi\lambda y^2 + \pi\tilde{\lambda} y^2 \left(1 - \Upsilon_{\text{I}}\left(jx\right)\right)\right) dy \tag{3.45}$$

with the shorthand notation $\Upsilon_{\text{I}}\left(z\right) = \mathbb{E}_{\gamma_i}\left\{{}_1F_1\left(-\frac{2}{\alpha}; 1-\frac{2}{\alpha}; z\gamma_i\right)\right\}$*, as defined in* (3.20) *and the density of the active set of interfering BSs on the random resource block* $\tilde{\lambda} = \left(1 - p_{\text{inactive}}^{(\text{RB})}\right)\lambda$*, as defined in* (3.32)*.*

Proof*: The proof follows the steps in Theorem 3.1 with a thinning density* $\tilde{\lambda}$ *of interfering BSs. And the MGF function* $\mathscr{M}_{\gamma_0}\left(\cdot\right)$ *is available for various MIMO transmission schemes, as*

introduced in Section 3.2 . □

Corollary 3.3 *Let* $\mathrm{P}_{\text{service}}(\cdot)$ *in* (3.34) *with* $\mathcal{N}_0 = 0$*, i.e.,* $\mathrm{P}^{[\infty]}_{\text{service}}(\cdot)$*. It can be formulated as:*

$$\mathrm{P}^{[\infty]}_{\text{service}}(\tau) = p^{(\mathrm{RB})}_{\text{select}} \times \mathrm{P}^{[\infty]}_{\text{cov}}(\tau) = p^{(\mathrm{RB})}_{\text{select}} \left(\frac{1}{2} - \frac{1}{\pi} \int_0^{+\infty} \mathrm{Im} \left\{ \frac{\mathscr{M}_{\gamma_0}(jx/\tau)}{1 - \left(1 - p^{(\mathrm{RB})}_{\text{inactive}}\right)\left(1 - \Upsilon_{\mathrm{I}}(jx)\right)} \right\} \frac{dx}{x} \right) \tag{3.46}$$

Proof*: It directly follows from the close-form expression of the integral as stated in the proof of* (3.20) . □

Remark 3.12 $\mathrm{P}^{[\infty]}_{\text{service}}(\tau)$ *as in* (3.46) *is a monotonically increasing function of the number of resource blocks* N_{RB}*, i.e., given* $\lambda^{(\mathrm{MT})}/\lambda$*, more resource blocks at each BS results in a higher probability that a MT is being successfully served.* $\mathrm{P}^{[\infty]}_{\text{service}}(\tau)$ *as in* (3.46) *is a monotonically increasing function of the ratio* $\lambda^{(\mathrm{MT})}/\lambda$*, i.e., given* $\lambda^{(\mathrm{MT})}$*, a higher density of BSs* λ *results in a higher probability that a MT is being successfully served.*

Proof*: By assuming Gamma distributed per-link gains and following the similar steps as in the proof of* (3.28)*, we can obtain* $\mathrm{P}^{[\infty]}_{\text{service}}(\tau) \approx p^{(\mathrm{RB})}_{\text{select}} \times \left(1 - \left(1 + \frac{1}{1-p^{(\mathrm{RB})}_{\text{inactive}}} \frac{1}{2} \frac{1}{m_0} \frac{\Omega_0}{\Omega_I} (\alpha - 2) \frac{1}{\tau}\right)^{-m_0}\right)$*, which is a monotonically increasing function of* $p^{(\mathrm{RB})}_{\text{inactive}}$*. The rest of proof follows by noting the trends in Remark 3.8,3.9,3.10,3.11.* □

3.7 Numerical and Simulation Results

Validation of the Exact and Approximated Mathematical Frameworks In Fig. 3.1 and Fig. 3.2, numerical examples are shown to substantiate the proposed mathematical frameworks against Monte Carlo simulations, which are obtained as described in [7, Sec. V-a]. For simplicity, the interference-limited regime is analyzed, *i.e.*, $\mathcal{N}_0 = 0$ and the per-link power gains are Gamma distributed. The illustrations confirm that (3.26) and (3.27) are exact. They also show that (3.28) and (3.29) are fairly accurate. In particular, the expected accuracy discussed in *Remark 3.5* and *Remark 3.7* is confirmed. More importantly, (3.28) and (3.29) well reproduce the behavior of coverage and rate as a function of the system parameters, as discussed in *Remark 3.4* and *Remark 3.6*. This is, in fact, the main usefulness of these approximations. Furthermore, the figures show that the accuracy of (3.28) and (3.29) increases as α decreases. This is an important outcome, since Monte Carlo simulations are either less accurate or require more simulation time for small values of α. For $\alpha = 2.1$, in fact, it has not been possible to produce sufficiently accurate Monte Carlo results in Fig. 3.2.

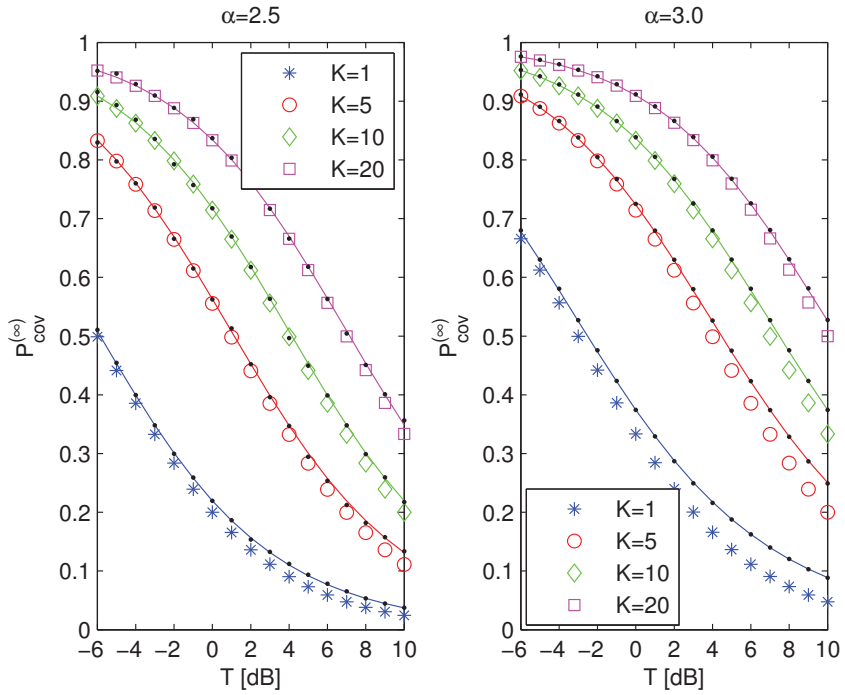

Figure 3.1: $P_{cov}^{[\infty]}(\cdot)$ as a function of T and $\mathscr{K} = (\Omega_0/\Omega_I)(1/m_0)$. Solid lines show (3.26), markers show (3.28) and "black dots" show Monte Carlo simulations.

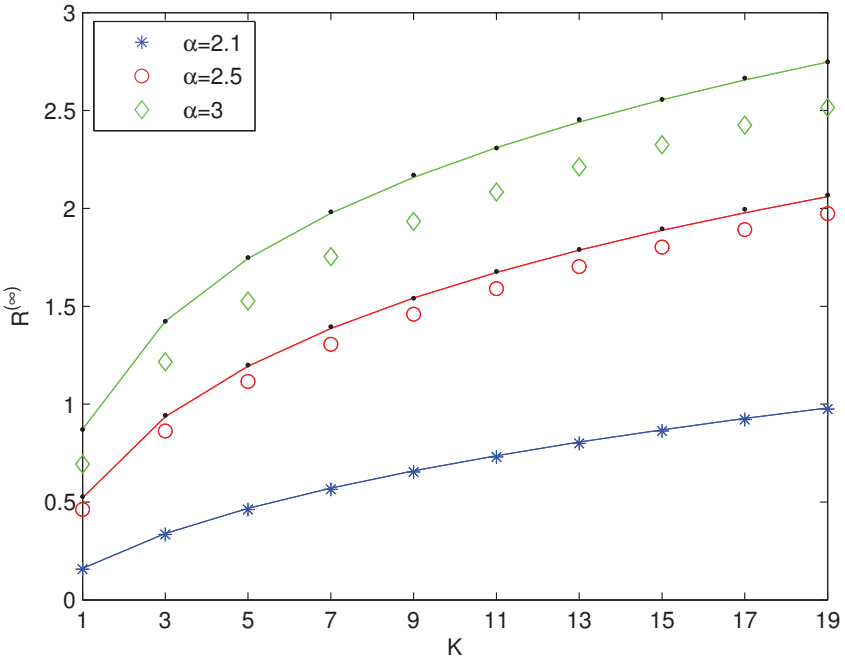

Figure 3.2: $\mathscr{R}^{[\infty]}$ as a function of $\mathscr{K} = (\Omega_0/\Omega_I)(1/m_0)$ and α. Solid lines show (3.27), markers show (3.29) and "black dots" show Monte Carlo simulations.

Impact of MIMO Transmission Schemes Fig. 3.4 validates the service success probabilities and the conditional coverage probabilities of different MIMO schemes discussed in *Section 3.3*. With current setup in Fig. 3.4, the MIMO scheme results in the best coverage and service success probability is MIMO MRC, while the worst is resulted from the transmission scheme employing SMX at the transmitter and per stream ZF at the receiver. If both the probe link and interfering link gains can be modeled as Gamma RV, the comparison of different MIMO schemes (for example, SMX - per stream ZF and OSTBC) can be done by the discussions in *Remark 3.4*.

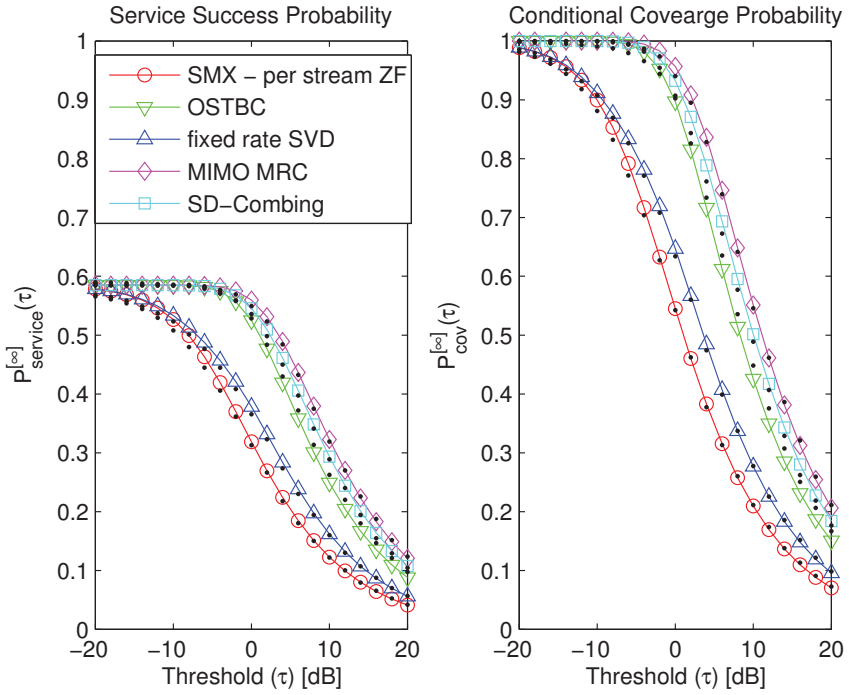

Figure 3.3: $\mathrm{P}^{[\infty]}_{\mathrm{service}}(\cdot)$ and $\mathcal{P}^{[\infty]}_{\mathrm{cov}}(\cdot)$ of different MIMO transmission schemes. Markers show *Corollary 3.3* and "black dots" show Monte Carlo simulations. Setup: $E/\mathcal{N}_0 \to \infty$, $N_{\mathrm{RB}} = 1$, $\lambda^{(\mathrm{MT})} = \lambda$, $\alpha = 2b = 4$, $N_r = N_t = 2$, OSTBC code is the Alamouti code as in *Section 3.3.2*.

Impact of the Load Fig. 3.4 shows the impact of the load, by observing two factors, the number of resource blocks N_{RB} and the ratio $\lambda^{(\mathrm{MT})}/\lambda$. As stated in *Remark 3.12*, $\mathrm{P}^{[\infty]}_{\mathrm{service}}(\tau)$ as in (3.46) is a monotonically increasing function of the number of resource blocks N_{RB}, *i.e.*, given $\lambda^{(\mathrm{MT})}/\lambda$, more resource blocks at each BS results in a higher probability that a MT is being successfully served. $\mathrm{P}^{[\infty]}_{\mathrm{service}}(\tau)$ as in (3.46) is a monotonically decreasing function of the ratio $\lambda^{(\mathrm{MT})}/\lambda$, *i.e.*, given $\lambda^{(\mathrm{MT})}$, a higher density of BSs λ results in a higher probability that a MT is being successfully served. This trends coincide the intuitions and they are supported by simulations as shown in Fig. 3.4.

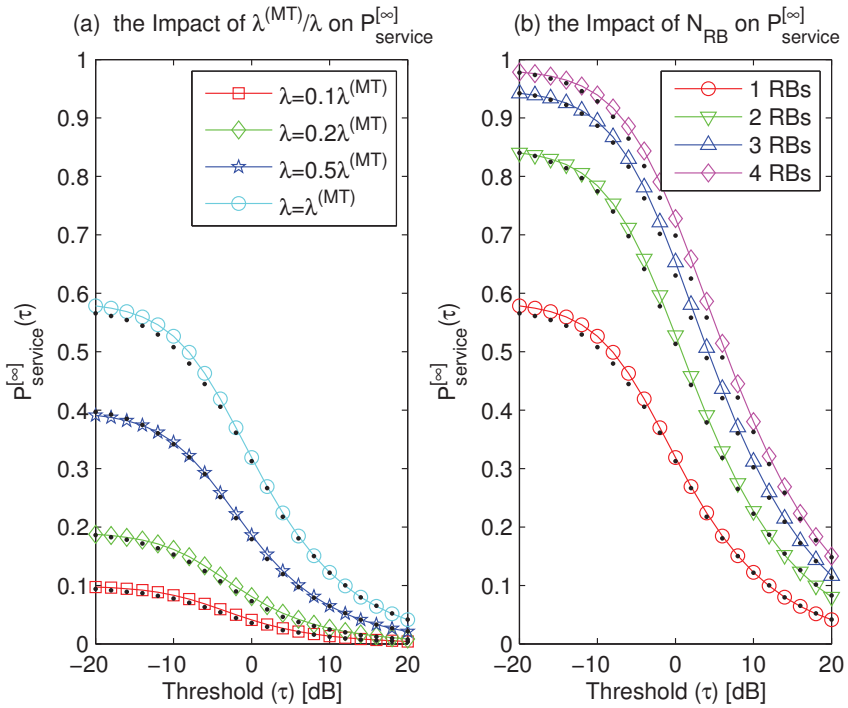

Figure 3.4: The impact of N_{RB} and $\lambda^{(\mathrm{MT})}/\lambda$ on $\mathrm{P}^{[\infty]}_{\mathrm{service}}(\cdot)$. Markers show *Corollary 3.3* and "black dots" show Monte Carlo simulations. Setup: $E/\mathcal{N}_0 \to \infty$, $\alpha = 2b = 4$, $N_r = N_t = 2$, SMX - per stream ZF MIMO transmission. (a) $N_{\mathrm{RB}} = 1$; (b) $\lambda^{(\mathrm{MT})} = \lambda$.

3.8 Conclusion

In this chapter, new mathematical expressions for coverage and rate of cellular networks are provided with the aid of the Gil-Pelaez inversion formula. The frameworks are shown to be general enough for the analysis of different fading channels and transmission schemes. Closed-form approximated expressions are proposed when the per–link power gains are distributed according to a Gamma distribution. Furthermore, partially loaded cellular systems are studied through the Gil-Pelaez inversion as well.

The mathematical frameworks are able to provide insights into the impacts of several importance parameters on trends of network performance including coverage, rate, load and service success probability, as well as the accuracy of proposed approximation when the per–link power gains are distributed according to a Gamma distribution ($\gamma_0 \sim \mathrm{Gamma}(m_0, \Omega_0)$ and $\gamma_i \sim \mathrm{Gamma}(m_I, \Omega_I)$). More specifically,

- the coverage probability and average rate increase as $\eta = \Omega_0(\alpha-2)/(\tau\Omega_I)$ and $\tilde{\eta} = (\Omega_0/\Omega_I)(\alpha-2)$ increase, respectively.
- The coverage probability and average rate increase as m_0 increases and are (almost) independent of m_I.

- The accuracy of the proposed approximation in terms of coverage probability and average rate increases as $\mathscr{K}_{\mathrm{P_{cov}}} = \left(\Omega_0/\Omega_I\right)\left(1/(m_0\tau)\right)$ increases and $\mathscr{K}_{\mathrm{Rate}} = \left(\Omega_0/\Omega_I\right)\left(1/m_0\right)$ decreases, respectively.
- The accuracy of the proposed approximation in terms of coverage probability and average rate increases as α decreases.
- The BS inactive probability and the MT selection probability increase as the number of resource blocks increases. They also increase as the ratio $\lambda^{(\mathrm{MT})}/\lambda$ increases.
- The service success probability $\mathrm{P}_{\mathrm{service}}^{[\infty]}(\tau)$ increases as the number of resource blocks increases. It also increases as the ratio $\lambda^{(\mathrm{MT})}/\lambda$ increases.

3.9 Appendices

3.9.1 Proof of Theorem 3.1

From (3.1) and (3.2), $\mathrm{P}_{\mathrm{cov}}(\cdot)$ can be formulated as follows:

$$\begin{aligned}\mathrm{P}_{\mathrm{cov}}(\tau) &= \int_0^{+\infty} \Pr\left\{ \mathscr{I}_{agg}(\xi) \leq \frac{\gamma_0 \xi^{-\alpha}}{\tau} - \frac{\mathscr{N}_0}{\mathsf{P}} \middle| \xi \right\} f_{r_0}(\xi)\, d\xi \\ &= \int_0^{+\infty} \mathbb{E}_{\gamma_0}\left\{ F_{\mathscr{I}_{agg}}\left(\frac{\gamma_0 \xi^{-\alpha}}{\tau} - \frac{\mathscr{N}_0}{\mathsf{P}} \right) \right\} f_{r_0}(\xi)\, d\xi \end{aligned} \tag{3.47}$$

where $F_{\mathscr{I}_{agg}}(z) = \Pr\left\{ \mathscr{I}_{agg}(\xi) \leq z \right\}$. $F_{\mathscr{I}_{agg}}(\cdot)$ can be formulated in terms of the CF of the aggregate other-cell interference, $\psi_{\mathscr{I}_{agg}}(\cdot)$, with the aid of the Gil-Pelaez inversion formula [54]. $\psi_{\mathscr{I}_{agg}}(\cdot)$ is available in [6, Eq. (4)]. The proof follows by re-writing [6, Eq. (4)] in terms of ${}_1F_1(\cdot;\cdot;\cdot)$, *i.e.*, $\psi_{\mathscr{I}_{agg}}(\omega;\xi) = \exp\left(\pi\lambda\xi^2\left[1 - \Upsilon_{\mathrm{I}}\left(j\omega\xi^{-\alpha}\right)\right]\right)$.

3.9.2 Proof of Proposition 3.6

From [57, Ch. 5, Eq. (2)], we have ${}_2F_1\left(-2/\alpha, m_I; 1-2/\alpha; j\kappa_I x\right) \approx 1 - j2\Omega_I(\alpha-2)^{-1}x$. Then, (3.26) can be approximated as follows:

$$\begin{aligned}\mathrm{P}_{\mathrm{cov}}^{[\infty]}(\tau) &\overset{(a)}{\approx} \frac{1}{2} - \frac{1}{2\pi j}\int_0^{+\infty}\left(\frac{\left(1 + j\tilde{\kappa}_0 x\right)^{-m_0}}{1 - j\tilde{\kappa}_I x} - \frac{\left(1 - j\tilde{\kappa}_0 x\right)^{-m_0}}{1 + j\tilde{\kappa}_I x} \right)\frac{dx}{x} \\ &\overset{(b)}{=} 1 - \frac{j}{2}\left(\frac{\left(-j\right)^{2m_0} - \left(j\right)^{2m_0}}{\left(\tilde{\kappa}_0 + \tilde{\kappa}_I\right)^{m_0}} \frac{\tilde{\kappa}_I^{m_0}}{\sin(\pi m_0)} \right)\end{aligned} \tag{3.48}$$

where $\tilde{\kappa}_I = 2\Omega_I(\alpha-2)^{-1}$, (a) follows from $\mathrm{Im}\{z\} = \left(2j\right)^{-1}\left(z - z^H\right)$ and (b) from $\ln(-1) = j\pi$ and [85] as shown in (3.49) as follow:

$$\begin{aligned}&\frac{1}{2\pi j}\int_0^{+\infty}\left(\frac{\left(1 + j\tilde{\kappa}_0 x\right)^{-m_0}}{1 - j\tilde{\kappa}_I x} - \frac{\left(1 - j\tilde{\kappa}_0 x\right)^{-m_0}}{1 + j\tilde{\kappa}_I x} \right)\frac{dx}{x} \\ &\quad= \frac{j}{2\pi}\tilde{\kappa}_0^{-2m_0}\left(\frac{\tilde{\kappa}_0 + \tilde{\kappa}_I}{\tilde{\kappa}_0}\right)^{-m_0}\left[\tilde{\kappa}_0^{2m_0}\ln(-1)\left(\frac{\tilde{\kappa}_0 + \tilde{\kappa}_I}{\tilde{\kappa}_0}\right)^{m_0}\right. \\ &\qquad\left. + \frac{\pi}{\sin(\pi m_0)}\left(\left(-j\tilde{\kappa}_0\right)^{m_0}\left(-j\tilde{\kappa}_I\right)^{m_0} - \left(j\tilde{\kappa}_0\right)^{m_0}\left(j\tilde{\kappa}_I\right)^{m_0}\right)\right]\end{aligned} \tag{3.49}$$

The proof follows since $\left(j/2\right)\left(\left(-j\right)^{2m_0} - \left(j\right)^{2m_0}\right)\Big/\sin(\pi m_0) = 1$.

4 Stochastic Geometry Modeling, System-Level Analysis and Optimization of Uplink Heterogeneous Cellular Networks with Multi-Antenna Base Stations

Chapter 4. Stochastic Geometry Modeling, System-Level Analysis and Optimization of Uplink Heterogeneous Cellular Networks with Multi-Antenna Base Stations

In this chapter, mathematical frameworks for system-level analysis and optimization of uplink heterogeneous cellular networks with multiple BSs antennas are introduced. MRC and OC at the BSs are studied and compared. A generalized cell association criterion and fractional power control mechanism are considered. The locations of each tier of BSs are modeled as points of homogeneous and independent Poisson point processes. With the aid of stochastic geometry, coverage and rate are formulated in integral but mathematically and computationally tractable expressions. Based on them, performance trends for small- and large-scale multi-antenna BSs are discussed. Coverage and rate are shown to highly depend on several parameters, including the path-loss exponent, the fractional power control compensation factor and the maximum transmit power of the mobile terminals. The gain of OC compared to MRC is shown to increase if a more aggressive power control is used and if the number of BSs antennas increases but is finite. For the same number of BSs antennas, OC is shown to reach the noise-limited asymptote faster than MRC. Based on the proposed frameworks, a heuristic algorithm for system-level optimization is proposed and its effectiveness is demonstrated with the aid of Monte Carlo simulations.

The rest of this chapter is organized as follows. In *Section 4.1*, the related work is reviewed and the major new contributions are summarized. In *Section 4.2*, the system model is introduced. In *Sections 4.3* and *4.4*, the mathematical frameworks for computing coverage and rate of MRC and OC demodulators are presented, respectively. In *Section 4.5*, system-level optimization is discussed and a heuristic algorithm for computing the optimal operating point is proposed. In Section *4.6*, frameworks and findings are validated with the aid of Monte Carlo simulations, as well as relevant performance trends are discussed. Finally, *Section 4.7* concludes this chapter.

4.1 Introduction 84

4.1.1 Challenges in Stochastic Geometry Modeling of the Uplink 84

4.1.2 Related Work 84

4.1.3 Contributions 85

4.2 System Model 86

4.2.1 PPP-Based Cellular Networks Modeling 87

4.2.2 Channel Modeling 87

4.2.3 Cell Association Modeling 88

4.2.4 Power Control Modeling 89

4.2.5 Signal Model and Demodulator 90

4.2.6 Problem Statement 92

4.2.7 Preliminaries 93

4.3 System-Level Analysis of Maximum Ratio Combining 95
4.3.1 Coverage Probability 96
4.3.2 Average Rate 99
4.3.3 Massive MIMO Regime 100
4.4 System-Level Analysis of Optimum Combining 102
4.4.1 Coverage Probability 103
4.4.2 Average Rate 107
4.4.3 Massive MIMO Regime 107
4.5 System-Level Optimization 109
4.6 Numerical and Simulation Results 110
4.7 Conclusion 117
4.8 Appendices 119
4.8.1 Proof of Proposition 4.1 119
4.8.2 Proof of Proposition 4.3 120

4.1 Introduction

4.1.1 Challenges in Stochastic Geometry Modeling of the Uplink

Modeling heterogeneous cellular networks by using stochastic geometry and point processes theories is now routinely adopted for system-level performance evaluation and optimization [15]. This approach, for example, has been successfully applied to for example, in single-tier downlink cellular networks [6, 29], multi-antenna cellular networks [30, 31], heterogeneous cellular networks [7, 32, 33, 35, 36, 42], and millimeter-wave cellular networks [44, 45, 46].The analysis of uplink cellular networks, however, has received much less attention compared to its downlink counterpart. The emergence of uplink intensive applications and services, *e.g.*, video chat/streaming, cloud-based storage/work, online gaming, etc. [86], however, has recently shifted the focus of researchers towards an accurate modeling, analysis and optimization of the uplink of heterogeneous cellular networks. This requires, however, to re-think the modeling and to develop new mathematical frameworks for analysis and optimization. This is due to the following main reasons:

- Power control plays a critical role for striking a flexible trade-off between coverage/rate and power consumption as a function of the location of the Mobile Terminals (MTs) within a cell [87]. The 3GPP, for example, adopts a fractional power control mechanism that depends on the path-loss and on the maximum transmit power of the MTs [88].

- Several modeling assumptions of the downlink do not hold anymore [89]. Uplink and downlink need to be considered as two different networks. Thus, the mathematical frameworks used for the downlink are not directly applicable to the uplink: new accurate and tractable abstraction models are needed.

- Due to the homogeneous transmit power of the MTs as opposed to the different tiers of BSs, optimizing the downlink may not necessarily result in an optimized uplink transmission [90]. The best serving BS, for example, may be different for the downlink and the uplink (decoupled downlink/uplink) [91].

4.1.2 Related Work

A few researchers have developed mathematically tractable yet accurate analytical frameworks for the uplink of heterogeneous cellular networks. The following contributions and limitations are worth being mentioned:

- In [92], the authors study two-tier cellular networks based on Code Division Multiple Access (CDMA) transmission. Small cell interference is modeled by relying on stochastic geometry modeling. Macro cell interference, however, is modeled by assuming a truncated Gaussian distribution (no PPP is used).

- In [47], the authors study single-tier cellular networks with fractional power control. For tractability, however, the BSs are assumed to be uniformly distributed in the Voronoi cells of their MTs.

- In [48], the authors study cellular networks with truncated channel inversion power control. For tractability, a cell association based on the smallest path-loss is considered. To compute the Laplace transform of the other-cell interference, some spatial constraints that originate from the cell association are neglected.

- In [49], the authors study two-tier cellular networks with power control and a biased cell association. The point process of the interfering MTs is modeled using a thinning approach based on curve fitting.

- In [50], the authors study multi-tier cellular networks with fractional power control and a weighted cell association. Similar to [49], a thinning-based approach for modeling the point process of the interfering MTs is used. The proposed method, however, does not require any fitting based on simulations. Also, the optimality of using a decoupled downlink/uplink association is mathematically assessed.

- In [51], the authors study, from a utility optimization standpoint, multi-tier cellular networks with fractional power control and a weighted cell association. To this end, a utility function based on the proportionally fair criterion is introduced and optimized. This utility function, however, is not directly related to coverage probability and average rate of multi-tier cellular networks.

- In [52], the authors study two-tier cellular networks to characterize the association probabilities of downlink and uplink transmissions. For tractability, however, power control is not taken into account.

- In [53], the authors generalize [52]. They study the rate of the typical MT and validate their findings against a real-world system-level simulator. For tractability, power control is not taken into account and some simplifications to compute the Laplace transform of the other-cell interference are made.

4.1.3 Contributions

Compared to these contributions, the present paper is different in several aspects. We focus our attention on multi-antenna BSs, while the aforementioned papers study single-antenna BSs. Maximum Ratio Combining (MRC) and Optimum Combining (OC) at the BSs are considered, and their coverage and rate are formulated in integral but mathematically and computationally tractable expressions. It is shown that the obtained frameworks reduce to simple closed-form formulas for some simplified, but relevant, setups. A multi-tier cellular network topology based on a weighted average received power cell association and fractional power control with maximum transmit power at the MTs is considered. The obtained mathematical frameworks

are used for system-level optimization as well, *e.g.*, to compute the best cell association weight and the best fractional power control compensation factor. Due to their relevance for future cellular network deployments, coverage and rate of massive (or large-scale) Multiple-Input-Multiple-Output (MIMO) systems [93], *i.e.*, with many BSs antennas, are studied. It is shown, in particular, that the fractional power control compensation factor plays an important role on the achievable performance of MRC and OC with large-scale antenna-arrays.

Our approach for modeling uplink heterogeneous cellular networks with multi-antenna BSs differs from those of [49] and [50]. In these papers, the point process of the actual interfering MTs in a tier of BSs is modeled as a thinned version of the potential interfering MTs of that tier of BSs, whose thinning probability depends on the tier association probability. The proposed modeling approach, on the other hand, is more similar to that of [48] and [51], where the thinning of [50] is not used. Our numerical results confirm that our approach offers the same accuracy as that of [50]. The framework in [50], however, assumes single-antenna transmission and no maximum transmit power constraint at the MTs. Compared to [48] and [51], important differences hold. We improve the accuracy of the approach proposed in [48], by taking into account that the distribution of the distance and of the transmit power of the typical MTs need to be normalized by the tier association probability (see, *e.g.*, [48, Eq. (30)]). Compared to [48], we consider a weighted average received power cell association and fractional power control. Compared to [51], we focus our attention on coverage and rate, instead of considering a modified utility function based on the proportionally fair criterion. This modified utility function, in fact, is not directly applicable to fading distributions different from Rayleigh (see, *e.g.*, [51, Eq. (28)]), which come into play if multiple-antenna BSs are considered.

4.2 System Model

A bi-dimensional uplink heterogeneous, *i.e.*, multi-tier, cellular network is considered, where the MTs act as transmitters and the BSs act as receivers. $\mathscr{K}$ tiers of BSs are available, where each tier is characterized by different transmission characteristics, *i.e.*, transmit-power, deployment density, etc. The MTs are equipped with a single transmit antenna, while the BSs of the kth tier are equipped with N_k receive antennas, for $k = 1,2,\ldots,\mathscr{K}$. Each BS of every tier is assumed to serve (*i.e.*, receive data in the uplink) a single MT in each of its available resource blocks. All BSs of every tier are assumed to be active, *i.e.*, saturated traffic conditions hold. Let $\lambda^{(\mathrm{MT})}$ and $\lambda_k^{(\mathrm{BS})}$ be the deployment densities of the MTs and of the kth tier of BSs. Saturated traffic conditions hold if $\lambda^{(\mathrm{MT})} \gg \sum_{k=1}^{\mathscr{K}} \lambda_k^{(\mathrm{BS})}$. In each resource block, as a result, the density of *active* MTs that are served by the kth tier of BSs is equal to $\bar{\lambda}_k^{(\mathrm{MT})} = \lambda_k^{(\mathrm{BS})}$ for $k = 1,2,\ldots,\mathscr{K}$. The set of active MTs that belong to (*i.e.*, are served by a BS of) the kth tier is denoted by $\bar{\Phi}_k^{(\mathrm{MT})}$ for $k = 1,2,\ldots,\mathscr{K}$.

4.2.1 PPP-Based Cellular Networks Modeling

The BSs of the kth tier are distributed according to $\mathscr{K}$ homogeneous and independent PPPs, $\Phi_k^{(\mathrm{BS})}$, of density $\lambda_k^{(\mathrm{BS})}$ for $k = 1,2,\ldots,\mathscr{K}$. The MTs are distributed according to another homogeneous and independent PPP, $\Phi^{(\mathrm{MT})}$, of density $\lambda^{(\mathrm{MT})}$. In general, $\bar{\Phi}_k^{(\mathrm{MT})} \subseteq \Phi^{(\mathrm{MT})}$ for $k = 1,2,\ldots,\mathscr{K}$. For mathematical tractability and in agreement with recent literature, *e.g.*, [48] and [51], the following modeling assumption is retained.

Assumption 4.1 *For each tier of BSs and in each resource block, the sets of active MTs, $\bar{\Phi}_k^{(\mathrm{MT})}$, are assumed to constitute $\mathscr{K}$ homogeneous and mutually independent PPPs of density $\bar{\lambda}_k^{(\mathrm{MT})}$ for $k = 1,2,\ldots,\mathscr{K}$. This implies that the locations of the active MTs (intra- and inter-tier) are mutually independent as well.* □

In practice, the sets $\bar{\Phi}_k^{(\mathrm{MT})}$ for $k = 1,2,\ldots,\mathscr{K}$ are not PPPs because of the criterion used for associating BSs and MTs (see Section 4.2.3) and of the constraint of having one active MT in each resource block. They, in fact, introduce some spatial dependencies among the locations of the active MTs. The accuracy of *Assumption 4.1* is substantiated in Section 4.6. It is shown, in particular, that *Assumption 4.1* is sufficiently accurate if all spatial constraints originating from the cell association criterion are duly taken into account.

4.2.2 Channel Modeling

The channel model takes path-loss, shadowing and fast-fading into account. The channels of all uplink links of same tier are assumed to be independent and identically distributed (i.i.d.). The uplink channels of different tiers are assumed to be independent and non-identically distributed (i.ni.d.).

Path-Loss

Let a generic BS of the kth tier, *i.e.*, $\mathrm{BS}_k \in \Phi_k^{(\mathrm{BS})}$. Let a generic MT, *i.e.*, $\mathrm{MT} \in \Phi^{(\mathrm{MT})}$. Let their transmission distance be $r_{\mathrm{BS}_k,\mathrm{MT}}$. The close-in path-loss model, $l(\cdot)$, is defined as $\ell\left(r_{\mathrm{BS}_k,\mathrm{MT}}\right) = \rho_0 r_{\mathrm{BS}_k,\mathrm{MT}}^{\alpha_k}$ [95], where ρ_0 denotes the free-space path-loss at a distance of one meter and $\alpha_k > 2$ denotes the power path-loss exponent. In particular, $\rho_0 = (4\pi/\nu)^2$, where ν is the transmission wavelength.

Shadowing

Each uplink link between $\mathrm{MT} \in \Phi^{(\mathrm{MT})}$ and $\mathrm{BS}_k \in \Phi_k^{(\mathrm{BS})}$ is subject to mid-scale fading, *i.e.*, shadowing. Let it be denoted by $S_{\mathrm{BS}_k,\mathrm{MT}}$. It is assumed to follow a log-normal distribution [96], whose PDF is $f_{S_{\mathrm{BS}_k,\mathrm{MT}}}(\xi) = 10\log_{10}(e)\Big/\left(\sqrt{2\pi\sigma_k^2}\xi\right)\exp\left(-\left(10\log_{10}(\xi)-\mu_k\right)^2\Big/\left(2\sigma_k^2\right)\right)$ [60], where μ_k and σ_k^2 are mean and variance (in dB) of the RV $10\log_{10}\left(S_{\mathrm{BS}_k,\mathrm{MT}}\right)$, respectively. In this paper, $\mu_k = 0$ dB is assumed.

Fast-Fading

Each uplink link between MT $\in \Phi^{(\mathrm{MT})}$ and $\mathrm{BS}_k \in \Phi_k^{(\mathrm{BS})}$ is subject to a complex channel gain, *i.e.*, fast-fading. Let it be denoted by $h_{\mathrm{BS}_k,\mathrm{MT}}$. It is assumed to follow a circularly symmetric complex Gaussian distribution with zero mean and variance Ω_k (Rayleigh fading). Hence, the power gain $\left|h_{\mathrm{BS}_k,\mathrm{MT}}\right|^2$ follows an exponential distribution with mean square value Ω_k. The PDF of $\left|h_{\mathrm{BS}_k,\mathrm{MT}}\right|^2$ is $f_{\left|h_{\mathrm{BS}_k,\mathrm{MT}}\right|^2}(\xi) = \left(1/\Omega_k\right)\exp\left(-\xi/\Omega_k\right)$ [60]. In this paper, $\Omega_k = 1$ is assumed.

4.2.3 Cell Association Modeling

A generalized cell association based on a weighted average received power criterion is considered [50]. Let the typical MT $\in \Phi^{(\mathrm{MT})}$. It is served by (*i.e.*, it is associated to) the BS of the κth tier defined as $\mathrm{BS}_{\mathrm{MT}} = \underset{\mathrm{BS}_\kappa \in \Phi_\kappa^{(\mathrm{BS})}}{\arg\min} \left\{ S_{\mathrm{BS}_\kappa,\mathrm{MT}}^{-1/\alpha_\kappa} r_{\mathrm{BS}_\kappa,\mathrm{MT}} \right\}$ if the following condition holds:

$$\begin{aligned} &\mathscr{T}_\kappa R_{\kappa,\mathrm{MT}}^{-\alpha_\kappa} > \mathscr{T}_k R_{k,\mathrm{MT}}^{-\alpha_k} && \text{for } k \neq \kappa = 1,2,\ldots,\mathscr{K} \\ &R_{k,\mathrm{MT}} = \min_{\mathrm{BS}_k \in \Phi_k^{(\mathrm{BS})}} \left\{ S_{\mathrm{BS}_k,\mathrm{MT}}^{-1/\alpha_k} r_{\mathrm{BS}_k,\mathrm{MT}} \right\} && \text{for } k = 1,2,\ldots,\mathscr{K} \end{aligned} \tag{4.1}$$

where $S_{\mathrm{BS}_k,\mathrm{MT}}$ and $r_{\mathrm{BS}_k,\mathrm{MT}}$ are shadowing and transmission distance of the MT-to-BS_k link, respectively, $\mathscr{T}_k$ is the cell association weight and $R_{k,\mathrm{MT}}$ is the *shortest generalized distance* from MT to any BSs of the kth tier, *i.e.*, $\mathrm{BS}_k \in \Phi_k^{(\mathrm{BS})}$. The distance $R_{k,\mathrm{MT}}$ is *generalized* because it accounts for shadowing as well.

Equation (4.1) encompasses several cell association criteria of interest. Let $\mathscr{Q}_k$ and $\mathscr{B}_k$ for $k = 1,2,\ldots,\mathscr{K}$ be the transmit power and the association bias of the BSs of the kth tier. The following holds:

- If $\mathscr{T}_k = 1$ for $k = 1,2,\ldots,\mathscr{K}$, this corresponds to the minimum path-loss cell association criterion that accounts for shadowing [63]. In this case, the highest received power in the uplink is ensured.
- If $\mathscr{T}_k = \mathscr{Q}_k$ for $k = 1,2,\ldots,\mathscr{K}$, this corresponds to the maximum received power cell association criterion in the downlink [33]. In this case, the highest received power in the downlink is ensured.
- If $\mathscr{T}_k = \mathscr{B}_k\mathscr{Q}_k$ for $k = 1,2,\ldots,\mathscr{K}$, this corresponds to the maximum biased received power cell association criterion in the downlink [7]. In this case, neither the highest received power in the uplink nor the highest received power in the downlink is ensured. But, a better load balancing may be achieved.

The association weights $\mathscr{T}_k$ can be optimized to maximize the performance, as discussed in Section 4.5.

4.2.4 Power Control Modeling

According to [88], a fractional power control mechanism is considered. Let us assume that a generic MT is served by a BS of the kth tier according to (4.1). For ease of notation, let us introduce the conditional RV $\tilde{R}_{k,\mathrm{MT}} = R_{k,\mathrm{MT}} \big| \mathscr{X}_k$ for $k = 1,2,\ldots,\mathscr{K}$, where $\mathscr{X}_k$ denotes the event "the MT is served by a BS of the kth tier". Equivalently, this conditional distance can be formulated as $\tilde{R}_{k,\mathrm{MT}} = R_{k,\mathrm{MT}} \big| \mathrm{MT} \in \bar{\Phi}_k^{(\mathrm{MT})}$. The RVs $R_{k,\mathrm{MT}}$ and $\tilde{R}_{k,\mathrm{MT}}$ have, in general, a different distribution, since $\tilde{R}_{k,\mathrm{MT}}$ takes (4.1) into account.

A *generalized* fractional power control mechanism is considered. Let the typical MT. By conditioning on MT being served by a BS of the kth tier according to (4.1), its transmit power is chosen as follows:

$$\tilde{\mathscr{P}}_{k,\mathrm{MT}} = \begin{cases} P_0 \tilde{R}_{k,\mathrm{MT}}^{\alpha_k \varepsilon} & \text{if } P_0 \tilde{R}_{k,\mathrm{MT}}^{\alpha_k \varepsilon} \leq P_{\max} \\ P_\infty & \text{otherwise} \end{cases} \tag{4.2}$$

where P_0 is the transmit power of MT before applying power control, $0 \leq \varepsilon \leq 1$ is the fractional power control compensation factor, $P_{\max}$ is the maximum transmit power at MT, and $P_\infty \leq P_{\max}$ is a fixed power level that is enforced if the transmit power after applying power control exceeds $P_{\max}$.

Equation (4.2) encompasses several power control schemes of interest. In particular, the following holds:

- If $P_\infty = P_{\max} = \infty$, fractional power control with unbounded transmit power is obtained [50].
- If $P_\infty = 0$ and $P_{\max} < \infty$, fractional power control with truncated transmit power is obtained [48].
- If $P_\infty = P_{\max} < \infty$, fractional power control with finite maximum transmit power is obtained [88].
- If $\epsilon = 0$, no power control is applied. If $\epsilon = 1$, power control based on channel inversion is applied.

These case studies provide a different trade-off in terms of performance and power consumption of the MTs [48], [50]. The fractional power control compensation factor, ϵ, may be optimized accordingly.

Remark 4.1 *Based on Assumption 4.1, the transmission distances of the active MTs are independent. Since each MT is assumed to choose, according to* (4.2)*, its transmit power independently of the others, this implies that the transmit powers of the active MTs can be assumed to be independent as well.* □

4.2.5 Signal Model and Demodulator

For ease of writing and presentation, the following notation and assumptions are considered:

- Based on *Assumption 4.1* and thanks to the Slivnyak theorem [16], the analysis is performed for a typical (MT, BS) pair. For every MT, its serving BS is chosen according to (4.1). The probe (or intended) uplink link is identified by the subscript "0". The typical MT is denoted by MT_0.

- The uplink links related to the interfering MTs, *i.e.*, all active MTs in a given resource block with the exception of MT_0, are identified by the subscript "i". The generic interfering MT is denoted by MT_i.

- The shortest generalized distances $R_{k,\mathrm{MT}}$ of probe and interfering MTs are denoted by $R_{k,0}$ and $R_{k,i}$. Likewise for $\tilde{R}_{k,\mathrm{MT}}$ (conditional shortest generalized distance) and $\tilde{\mathscr{P}}_{k,\mathrm{MT}}$ (conditional transmit power).

- Let the serving BS of MT_0 belong to the κth tier and let it be denoted by $\mathrm{BS}_{\mathrm{MT}_0}$. Then, $\mathrm{MT}_0 \in \bar{\Phi}_{\kappa}^{(\mathrm{MT})}$. Let a generic interfering MT be served by a BS that belongs to the kth tier. Then, $\mathrm{MT}_i \in \bar{\Phi}_{k}^{(\mathrm{MT})}$. Shadowing and fast-fading gains of the link from $\mathrm{MT}_i \in \bar{\Phi}_{k}^{(\mathrm{MT})}$ to $\mathrm{BS}_{\mathrm{MT}_0}$ are denoted by $S_{\kappa,k,i}$ and $h_{\kappa,k,i}$ for $k \neq \kappa$. If $k = \kappa$, *i.e.*, intra-tier interfering MTs are considered, the simplified notation $S_{\kappa,i}$ and $h_{\kappa,i}$ is used. From Section 4.2.2, the distribution of $S_{\kappa,k,i}$ and $h_{\kappa,k,i}$ depends on $\left(\mu_{\kappa}, \sigma_{\kappa}^2\right)$ and Ω_{κ}, *i.e.*, the tier (κ) of the serving BS of MT_0 ($\mathrm{BS}_{\mathrm{MT}_0}$) determines the parameters of the distribution.

- Likewise, the generalized (*i.e.*, that account for shadowing) distances from the interfering MTs, which belong to the kth tier, to the serving BS of MT_0 (*i.e.*, $\mathrm{BS}_{\mathrm{MT}_0}$), which belongs to the κth tier, are denoted by $D_{\kappa,k,i} = S_{\kappa,k,i}^{-1/\alpha_{\kappa}} r_{\kappa,i}$ for $k \neq \kappa$, where $r_{\kappa,i}$ is the distance between $\mathrm{MT}_i \in \bar{\Phi}_{k}^{(\mathrm{MT})}$ and $\mathrm{BS}_{\mathrm{MT}_0} \in \Phi_{\kappa}^{(\mathrm{BS})}$. If $k = \kappa$, *i.e.*, the interfering MTs are intra-tier, the simplified notation $D_{\kappa,i}$ is used. Unconditional and conditional shortest generalized distances from the interfering MTs to *their own* serving BSs, which are different from $\mathrm{BS}_{\mathrm{MT}_0}$, are denoted by $R_{k,i}$ and $\tilde{R}_{k,i}$. They are defined as discussed in Section 4.2.4.

Remark 4.2 *$D_{\kappa,k,i}$ is neither a conditional nor a shortest distance. The subscript κ accounts only for the fact that the shadowing parameters and the path-loss exponent in $D_{\kappa,k,i}$ are those of the κth tier.* □

Let the typical MT be served by a BS of the κth tier, *i.e.*, the conditioning upon $\mathscr{X}_{\kappa}$ holds. The received vector, $\mathbf{y}_{\kappa,0} = \left[y_{\kappa,0}^{(1)}, y_{\kappa,0}^{(2)}, \ldots, y_{\kappa,0}^{(N_{\kappa})}\right]^T$, at the N_{κ}-antenna probe BS, $\mathrm{BS}_{\mathrm{MT}_0}$, can be

formulated as follows:

$$\begin{aligned}\mathbf{y}_{\kappa,0} = &\sqrt{\tilde{\mathscr{P}}_{\kappa,0}\rho_0^{-1}\tilde{R}_{\kappa,0}^{-\alpha_k}}\mathbf{h}_{\kappa,0}x_{\kappa,0} + \mathbf{n}_{\kappa,0} + \sum_{\mathrm{MT}_i\in\tilde{\Phi}_\kappa^{(\mathrm{MT})}\setminus\mathrm{MT}_0}\sqrt{\tilde{\mathscr{P}}_{\kappa,i}\rho_0^{-1}D_{\kappa,i}^{-\alpha_\kappa}}\mathbf{h}_{\kappa,i}x_{\kappa,i}\mathbb{1}\left(D_{\kappa,i}>\tilde{R}_{\kappa,i}\right)\\ &+\sum_{k\neq\kappa=1}^{\mathscr{K}}\sum_{\mathrm{MT}_i\in\tilde{\Phi}_k^{(\mathrm{MT})}}\sqrt{\tilde{\mathscr{P}}_{k,i}\rho_0^{-1}D_{\kappa,k,i}^{-\alpha_\kappa}}\mathbf{h}_{\kappa,k,i}x_{k,i}\mathbb{1}\left(D_{\kappa,k,i}>\left(\left(\mathscr{T}_\kappa/\mathscr{T}_k\right)\tilde{R}_{k,i}^{\alpha_k}\right)^{1/\alpha_\kappa}\right)\end{aligned} \tag{4.3}$$

where, for $t=\{0,i\}$, $\mathbf{h}_{\kappa,k,t}=\left[h_{\kappa,k,t}^{(1)},h_{\kappa,k,t}^{(2)},\ldots,h_{\kappa,k,t}^{(N_\kappa)}\right]^T$ is the vector of fast-fading gains from the MTs to $\mathrm{BS}_{\mathrm{MT}_0}$, $\mathbf{n}_{\kappa,0}=\left[n_{\kappa,0}^{(1)},n_{\kappa,0}^{(2)},\ldots,n_{\kappa,0}^{(N_\kappa)}\right]^T$ is the vector of complex additive white Gaussian noise at $\mathrm{BS}_{\mathrm{MT}_0}$, and $x_{k,t}$ is the modulated symbol transmitted from the MTs. If $k=\kappa$, the notation $\mathbf{h}_{\kappa,t}$ is used. The distribution of each entry of $\mathbf{h}_{\kappa,k,t}$ is in Section 4.2.2. The elements of $\mathbf{n}_{\kappa,0}$ are i.i.d. and each of them follows a circularly symmetric complex Gaussian distribution with zero mean and variance equal to σ_N^2. The indicator functions, $\mathbb{1}(\cdot)$, in (4.3) take the geometric constraints introduced by the cell association criterion in (4.1) into account.

By inserting the generalized uplink power control of (4.2) in (4.3), the received vector can be formulated as:

$$\begin{aligned}\mathbf{y}_{\kappa,0} = &\sqrt{P_0\rho_0^{-1}\tilde{R}_{\kappa,0}^{\alpha_\kappa(\varepsilon-1)}}\mathbf{h}_{\kappa,0}x_{\kappa,0}\mathbb{1}\left(\tilde{R}_{\kappa,0}\leq\left(\frac{P_{\max}}{P_0}\right)^{1/(\alpha_\kappa\varepsilon)}\right)\\ &+\sqrt{P_\infty\rho_0^{-1}\tilde{R}_{\kappa,0}^{-\alpha_k}}\mathbf{h}_{\kappa,0}x_{\kappa,0}\mathbb{1}\left(\tilde{R}_{\kappa,0}>\left(\frac{P_{\max}}{P_0}\right)^{1/(\alpha_\kappa\varepsilon)}\right)+\mathbf{n}_{\kappa,0}\\ &+\sum_{\mathrm{MT}_i\in\tilde{\Phi}_\kappa^{(\mathrm{MT})}\setminus\mathrm{MT}_0}\sqrt{\frac{P_0\tilde{R}_{\kappa,i}^{\alpha_\kappa\varepsilon}}{\rho_0D_{\kappa,i}^{\alpha_\kappa}}}\mathbf{h}_{\kappa,i}x_{\kappa,i}\mathbb{1}\left(D_{\kappa,i}>\tilde{R}_{\kappa,i}\right)\mathbb{1}\left(\tilde{R}_{\kappa,i}\leq\left(\frac{P_{\max}}{P_0}\right)^{1/(\alpha_\kappa\varepsilon)}\right)\\ &+\sum_{\mathrm{MT}_i\in\tilde{\Phi}_\kappa^{(\mathrm{MT})}\setminus\mathrm{MT}_0}\sqrt{\frac{P_\infty}{\rho_0D_{\kappa,i}^{\alpha_\kappa}}}\mathbf{h}_{\kappa,i}x_{\kappa,i}\mathbb{1}\left(D_{\kappa,i}>\tilde{R}_{\kappa,i}\right)\mathbb{1}\left(\tilde{R}_{\kappa,i}>\left(\frac{P_{\max}}{P_0}\right)^{1/(\alpha_\kappa\varepsilon)}\right)\\ &+\sum_{k\neq\kappa=1}^{\mathscr{K}}\sum_{\mathrm{MT}_i\in\tilde{\Phi}_k^{(\mathrm{MT})}}\sqrt{\frac{P_0\tilde{R}_{k,i}^{\alpha_k\varepsilon}}{\rho_0D_{\kappa,k,i}^{\alpha_\kappa}}}\mathbf{h}_{\kappa,k,i}x_{k,i}\mathbb{1}\left(D_{\kappa,k,i}>\left(\left(\frac{\mathscr{T}_\kappa}{\mathscr{T}_k}\right)\tilde{R}_{k,i}^{\alpha_k}\right)^{1/\alpha_\kappa}\right)\mathbb{1}\left(\tilde{R}_{k,i}\leq\left(\frac{P_{\max}}{P_0}\right)^{1/(\alpha_k\varepsilon)}\right)\\ &+\sum_{k\neq\kappa=1}^{\mathscr{K}}\sum_{\mathrm{MT}_i\in\tilde{\Phi}_k^{(\mathrm{MT})}}\sqrt{\frac{P_\infty}{\rho_0D_{\kappa,k,i}^{\alpha_\kappa}}}\mathbf{h}_{\kappa,k,i}x_{k,i}\mathbb{1}\left(D_{\kappa,k,i}>\left(\left(\frac{\mathscr{T}_\kappa}{\mathscr{T}_k}\right)\tilde{R}_{k,i}^{\alpha_k}\right)^{1/\alpha_\kappa}\right)\mathbb{1}\left(\tilde{R}_{k,i}>\left(\frac{P_{\max}}{P_0}\right)^{1/(\alpha_k\varepsilon)}\right)\end{aligned} \tag{4.4}$$

At the N_κ-antenna probe BS, $\mathrm{BS}_{\mathrm{MT}_0}$, the symbol transmitted by the probe MT, MT_0, *i.e.*, $x_{\kappa,0}$ in (4.4), is estimated by applying a combiner whose weight vector is $\mathbf{w}_{\kappa,0}=\left[w_{\kappa,0}^{(1)},w_{\kappa,0}^{(2)},\ldots,w_{\kappa,0}^{(N_\kappa)}\right]^T$. Then, the output of the combiner is $z_{\kappa,0}=\mathbf{w}_{\kappa,0}^H\mathbf{y}_{\kappa,0}$. In Sections 4.3 and 4.4, $\mathbf{w}_{\kappa,0}$ is chosen based on MRC and OC criteria.

4.2.6 Problem Statement

Let $\mathrm{SINR}_{\kappa,0}$ be the Signal-to-Interference-plus-Noise-Ratio (SINR) associated to $z_{\kappa,0}$, assuming that $\mathrm{BS}_{\mathrm{MT}_0}$ belongs to the κth tier. Three performance metrics are of interest: coverage probability ($\mathsf{P}_{\mathrm{cov}}(\cdot)$), average rate ($\mathsf{R}$), and xth percentile rate ($\mathsf{R}_{x\mathrm{th}}$) of MT_0. Based on [109] and [53], they can be formulated as follows:

$$\mathsf{P}_{\mathrm{cov}}(\boldsymbol{\tau}) = \sum_{\kappa=1}^{\mathscr{K}} \Pr\left\{\mathrm{SINR}_{\kappa,0} > \tau_\kappa \middle| \mathscr{X}_\kappa\right\} \Pr\{\mathscr{X}_\kappa\} \tag{4.5}$$

$$\begin{aligned}
\mathsf{R} &= \mathrm{B_W} \sum_{\kappa=1}^{\mathscr{K}} \mathbb{E}_{\mathrm{SINR}_{\kappa,0}}\left\{\log_2\left(1+\mathrm{SINR}_{\kappa,0}\right)\middle|\mathscr{X}_\kappa\right\} \Pr\{\mathscr{X}_\kappa\} \\
&\overset{(a)}{=} \frac{\mathrm{B_W}}{\ln(2)} \sum_{\kappa=1}^{\mathscr{K}} \left(\int_0^{+\infty} \frac{\mathsf{P}_{\mathrm{cov}}(\tau_\kappa|\mathscr{X}_\kappa)}{\tau_\kappa+1} d\tau_\kappa \right) \Pr\{\mathscr{X}_\kappa\} \\
&\overset{(b)}{=} \frac{\mathrm{B_W}}{\ln(2)} \sum_{\kappa=1}^{\mathscr{K}} \left(-\int_0^{+\infty} \ln(\tau_\kappa+1)\, \mathsf{P}^{(1)}_{\mathrm{cov}}(\tau_\kappa|\mathscr{X}_\kappa)\, d\tau_\kappa \right) \Pr\{\mathscr{X}_\kappa\}
\end{aligned} \tag{4.6}$$

$$\begin{aligned}
&\mathsf{R}_{x\mathrm{th}} \middle| \left(\sum_{\kappa=1}^{\mathscr{K}} \Pr\left\{\mathrm{B_W}\log_2\left(1+\mathrm{SINR}_{\kappa,0}\right) < \mathsf{R}_{x\mathrm{th}} \middle| \mathscr{X}_\kappa\right\} \Pr\{\mathscr{X}_\kappa\} \right) = x\mathrm{th} \\
&\overset{(c)}{\Rightarrow} \mathsf{R}_{x\mathrm{th}} \middle| \sum_{\kappa=1}^{\mathscr{K}} \Pr\{\mathscr{X}_\kappa\} - \mathsf{P}_{\mathrm{cov}}\left(2^{\mathsf{R}_{x\mathrm{th}}/\mathrm{B_W}}-1\right) = x\mathrm{th}
\end{aligned} \tag{4.7}$$

where $\mathscr{X}_\kappa$ is the conditional event introduced in Section 4.2.4, $\boldsymbol{\tau} = [\tau_1, \tau_2, \ldots, \tau_{\mathscr{K}}]^T$ and τ_κ is the reliability threshold of the κth tier, $\mathrm{B_W}$ is the transmission bandwidth, $\mathsf{P}_{\mathrm{cov}}(\tau_\kappa|\mathscr{X}_\kappa) = \Pr\left\{\mathrm{SINR}_{\kappa,0} > \tau_\kappa \middle| \mathscr{X}_\kappa\right\}$, $\mathsf{P}^{(1)}_{\mathrm{cov}}(\tau_\kappa|\mathscr{X}_\kappa) = d\mathsf{P}_{\mathrm{cov}}(\tau_\kappa|\mathscr{X}_\kappa)/d\tau_\kappa$ is the first derivative of $\mathsf{P}_{\mathrm{cov}}(\cdot)$, (a) and (b) follow from [109, Eq. (3)], (c) from (4.5). Typically, $x = \{5, 50, 90\}$ correspond to the rates of cell-edge, median and cell-center MTs [53].

Remark 4.3 *If $P_\infty = 0$, the intended signal in* (4.4) *may be zero. Thus, the typical MT,* MT_0*, may be one of those in truncation outage [48], i.e., a MT whose transmit power after applying power control exceeds $P_{\max}$ and that is turned off for reducing its power consumption. Likewise, some interfering MTs in* (4.4) *may be turned off, resulting in less interference. Thanks to the indicator functions in* (4.4)*, the proposed frameworks for coverage/rate account for the MTs in truncation outage, both in terms of typical MT and interferers.* □

Remark 4.4 *The* xth *percentile rate in* (4.7) *is directly related to the coverage in* (4.5)*. It can be readily computed by using the Mathematica built-in function FindRoot. Examples are illustrated in Section 4.6.* □

4.2.7 Preliminaries

In this section, enabling results for facilitating the computation of coverage and rate are summarized.

Lemma 4.1 *Let the shortest generalized distance* $R_{k,t} = \min_{\mathrm{BS}_k \in \Phi_k^{(\mathrm{BS})}} \left\{ S_{\mathrm{BS}_k,t}^{-1/\alpha_k} r_{\mathrm{BS}_k,t} \right\}$ *for* $k = 1,2,\ldots,\mathscr{K}$ *and* $t = \{0,i\}$*. Its PDF, i.e.,* $f_{R_{k,t}}(\cdot)$ *and CCDF, i.e.,* $\bar{F}_{R_{k,t}}(\cdot)$*, can be formulated as follows:*

$$f_{R_{k,t}}(\xi) = 2\pi\lambda_k^{(S,\alpha)} \xi \exp\left(-\pi\lambda_k^{(S,\alpha)}\xi^2\right); \quad \bar{F}_{R_{k,t}}(\xi) = \exp\left(-\pi\lambda_k^{(S,\alpha)}\xi^2\right) \tag{4.8}$$

where $\lambda_k^{(S,\alpha)} = \lambda_k^{(BS)} \mathbb{E}\left\{ S_{BS_k,t}^{2/\alpha_k} \right\} = \lambda_k^{(BS)} \exp\left(\frac{(2/\alpha_k)}{10\log_{10}(e)}\mu_k + \frac{1}{2}\frac{(2/\alpha_k)^2}{(10\log_{10}(e))^2}\sigma_k^2 \right)$.

Proof*: It follows by applying the displacement theorem of PPPs [63, Sec. II-A] and the void probability theorem of PPPs [16], [63, Sec. IV-A]. The expectation* $\mathbb{E}\left\{ S_{\mathrm{BS}_k,t}^{2/\alpha_k} \right\}$ *follows from [60, Eq. (2.55)].* □

Lemma 4.2 *Let the cell association criterion in* (4.1)*. The probability,* $\mathscr{A}_\kappa = \Pr\{\mathscr{X}_\kappa\}$*, that a MT,* MT_t *for* $t = \{0,i\}$*, is served by a BS of the* κ *th tier, i.e.,* $\mathrm{MT}_t \in \bar{\Phi}_\kappa^{(\mathrm{MT})}$*, can be formulated as follows:*

$$\mathscr{A}_\kappa = \Pr\{\mathscr{X}_\kappa\} = 2\pi\lambda_\kappa^{(S,\alpha)} \int_0^{+\infty} \xi \exp\left(-\pi \sum_{k=1}^{\mathscr{K}} \lambda_k^{(S,\alpha)} \left(\mathscr{T}_k/\mathscr{T}_\kappa\right)^{2/\alpha_k} \xi^{2\alpha_\kappa/\alpha_k} \right) d\xi \tag{4.9}$$

where $\lambda_k^{(S,\alpha)} = \lambda_k^{(BS)} \exp\left(\frac{(2/\alpha_k)}{10\log_{10}(e)}\mu_k + \frac{1}{2}\frac{(2/\alpha_k)^2}{(10\log_{10}(e))^2}\sigma_k^2 \right)$ *for* $k = 1,2,\ldots,\mathscr{K}$.

Proof*: From* (4.1)*, by definition,* $\mathscr{A}_\kappa = \mathbb{E}_{R_{\kappa,t}}\left\{ \Pr\left\{ \bigcap_{k\neq\kappa=1}^{\mathscr{K}} R_{k,t} \geq \left(\left(\mathscr{T}_k/\mathscr{T}_\kappa\right) R_{\kappa,t}^{\alpha_\kappa}\right)^{1/\alpha_k} \middle| R_{\kappa,t} \right\} \right\}$*. By definition of PPP, the shortest generalized distances* $R_{k,t}$ *for* $k = 1,2,\ldots,\mathscr{K}$ *and* $t = \{0,i\}$ *are independent. Thus,* $\mathscr{A}_\kappa = \mathbb{E}_{R_{\kappa,t}}\left\{ \prod_{k\neq\kappa=1}^{\mathscr{K}} \bar{F}_{R_{k,t}}\left(\left(\left(\mathscr{T}_k/\mathscr{T}_\kappa\right) R_{\kappa,t}^{\alpha_\kappa}\right)^{1/\alpha_k} \right) \right\}$*. The proof follows from Lemma 4.1.* □

Corollary 4.1 *Let* $\mathscr{A}_\kappa$ *in* (4.9)*. If* $\alpha_k = \alpha$ *for* $k = 1,2,\ldots,\mathscr{K}$*, the following holds:*

$$\mathscr{A}_\kappa = \lambda_\kappa^{(S,\alpha)} \left(\sum_{k=1}^{\mathscr{K}} \lambda_k^{(S,\alpha)} \left(\mathscr{T}_k/\mathscr{T}_\kappa\right)^{2/\alpha} \right)^{-1} \tag{4.10}$$

where $\lambda_k^{(S,\alpha)} = \lambda_k^{(\mathrm{BS})} \exp\left((2/\alpha)\left(10\log_{10}(e)\right)^{-1}\mu_k + (1/2)(2/\alpha)^2\left(10\log_{10}(e)\right)^{-2}\sigma_k^2 \right)$.

Proof*: It immediately follows, by computing the integral, from Lemma 4.2.* □

Lemma 4.3 *Let the conditional shortest generalized distance* $\tilde{R}_{\kappa,t} = R_{\kappa,t} \big| \mathscr{X}_\kappa$ *for* $\kappa = 1,2,\ldots,\mathscr{K}$

and $t = \{0, i\}$. Its PDF can be formulated as follows:

$$f_{\tilde{R}_{\kappa,t}}(\xi) = 2\pi\left(\lambda_{\kappa}^{(S,\alpha)}/\mathscr{A}_{\kappa}\right)\xi \exp\left(-\pi \sum_{k=1}^{\mathscr{K}} \lambda_{k}^{(S,\alpha)}\left(\mathscr{T}_{k}/\mathscr{T}_{\kappa}\right)^{2/\alpha_{k}} \xi^{2\alpha_{\kappa}/\alpha_{k}}\right) \tag{4.11}$$

where $\mathscr{A}_{\kappa}$ is available in Lemma 4.2 and in Corollary 4.1 if $\alpha_{\kappa} = \alpha$ for $\kappa = 1, 2, \ldots, \mathscr{K}$.

Proof*: By definition, the CDF of $\tilde{R}_{k,t}$ is $F_{\tilde{R}_{\kappa,t}}(\xi) = \Pr\left\{\tilde{R}_{\kappa,t} \leq \xi \middle| \mathscr{X}_{\kappa}\right\}$. By applying the Bayes theorem, we have $F_{\tilde{R}_{\kappa,t}}(\xi) = \Pr\left\{\tilde{R}_{\kappa,t} \leq \xi \cap \mathscr{X}_{\kappa}\right\}/\Pr\{\mathscr{X}_{\kappa}\}$, where, by definition, $\Pr\left\{\tilde{R}_{\kappa,t} \leq \xi \cap \mathscr{X}_{\kappa}\right\} = \mathbb{E}_{R_{\kappa,t}}\left\{\Pr\left\{\bigcap_{k\neq\kappa=1}^{\mathscr{K}} R_{k,t} \geq \left(\left(\mathscr{T}_{k}/\mathscr{T}_{\kappa}\right) R_{\kappa,t}^{\alpha_{\kappa}}\right)^{1/\alpha_{k}} \mathbb{1}\left(R_{\kappa,t} \leq \xi\right) \middle| R_{\kappa,t}\right\}\right\}$. The proof follows from Lemma 4.2.* □

Corollary 4.2 *Let the PDF of $\tilde{R}_{\kappa,t}$ in* (4.11)*. Its CDF is equal to $F_{\tilde{R}_{\kappa,t}}(\xi) = \int_{0}^{\xi} f_{\tilde{R}_{\kappa,t}}(\zeta)\, d\zeta$. If $\alpha_{k} = \alpha$ for $k = 1, 2, \ldots, \mathscr{K}$, it can be formulated as follows:*

$$F_{\tilde{R}_{\kappa,t}}(\xi) = 1 - \exp\left(-\pi \sum_{k=1}^{\mathscr{K}} \lambda_{k}^{(S,\alpha)}\left(\mathscr{T}_{k}/\mathscr{T}_{\kappa}\right)^{2/\alpha} \xi^{2}\right) \tag{4.12}$$

Proof*: It immediately follows, by computing the integral, from Lemma 4.3 and by using Corollary 4.1.* □

Lemma 4.4 *Let the transmit power of the typical MT served by a BS of the κth tier be $\tilde{\mathscr{P}}_{\kappa,t}$ in* (4.2) *for $\kappa = 1, 2, \ldots, \mathscr{K}$ and $t = \{0, i\}$. Let $0 \leq P_{\infty} \leq P_{\max}$. The CDF of $\tilde{\mathscr{P}}_{\kappa,t}$, i.e., $F_{\tilde{\mathscr{P}}_{\kappa,t}}(\cdot)$, can be formulated as:*

$$F_{\tilde{\mathscr{P}}_{\kappa,t}}(\xi) = F_{\tilde{R}_{\kappa,t}}\left(\left(\min\left\{\xi, P_{\max}\right\}/P_{0}\right)^{1/(\alpha_{\kappa}\varepsilon)}\right) + \bar{F}_{\tilde{R}_{\kappa,t}}\left(\left(\frac{P_{\max}}{P_{0}}\right)^{1/(\alpha_{\kappa}\varepsilon)}\right)\mathbb{1}\left(\xi \geq P_{\infty}\right) \tag{4.13}$$

where $F_{\tilde{R}_{\kappa,t}}(\cdot)$ and $\bar{F}_{\tilde{R}_{\kappa,t}}(\cdot)$ are CDF and CCDF of $\tilde{R}_{\kappa,t}$, respectively, whose PDF, $f_{\tilde{R}_{\kappa,t}}(\cdot)$, follows from Lemma 4.3. If $\alpha_{k} = \alpha$ for $k = 1, 2, \ldots, \mathscr{K}$, $F_{\tilde{R}_{\kappa,t}}(\cdot)$ follows from Corollary 4.2.

Proof*: (4.2) can be written as $\tilde{\mathscr{P}}_{\kappa,t} = P_{0}\tilde{R}_{\kappa,t}^{\alpha_{k}\varepsilon}\mathbb{1}\left(\tilde{R}_{\kappa,t} \leq \left(\frac{P_{\max}}{P_{0}}\right)^{1/(\alpha_{\kappa}\varepsilon)}\right) + P_{\infty}\mathbb{1}\left(\tilde{R}_{\kappa,t} > \left(\frac{P_{\max}}{P_{0}}\right)^{1/(\alpha_{\kappa}\varepsilon)}\right)$. By definition, its CDF is equal to $F_{\tilde{\mathscr{P}}_{\kappa,t}}(\xi) = \Pr\left\{\tilde{\mathscr{P}}_{\kappa,t} \leq \xi\right\} \overset{(a)}{=} \Pr\left\{P_{0}\tilde{R}_{\kappa,t}^{\alpha_{k}\varepsilon} \leq \xi \cap \tilde{R}_{\kappa,t} \leq \left(\frac{P_{\max}}{P_{0}}\right)^{1/(\alpha_{\kappa}\varepsilon)}\right\}$ $+ \Pr\left\{P_{\infty} \leq \xi \cap \tilde{R}_{\kappa,t} > \left(\frac{P_{\max}}{P_{0}}\right)^{1/(\alpha_{\kappa}\varepsilon)}\right\}$, where (a) holds because the two indicator functions are mutually exclusive, i.e., the associated events are incompatible. The proof immediately follows from Lemma 4.3.* □

Lemma 4.5 *Let $D_{\kappa,k,i} = S_{\kappa,k,i}^{-1/\alpha_{\kappa}} r_{\kappa,i}$ for $k \neq \kappa = 1, 2, \ldots, \mathscr{K}$ be the generalized distances between the inter-tier interferers that belong to the kth tier, i.e., $\mathrm{MT}_{i} \in \bar{\Phi}_{k}^{(\mathrm{MT})}$, and the probe BS that belongs to the κth tier. Likewise, let $D_{\kappa,i} = S_{\kappa,i}^{-1/\alpha_{\kappa}} r_{\kappa,i}$ be the generalized distances*

between the intra-tier interferers that belong to the κth tier, i.e., $\mathrm{MT}_i \in \bar{\Phi}_{\kappa}^{(\mathrm{MT})} \backslash \mathrm{MT}_0$*, and the probe BS that belongs to the κth tier. Let Assumption 4.1 hold, i.e., $\bar{\Phi}_k^{(\mathrm{MT})}$ constitutes a PPP whose density is $\bar{\lambda}_k^{(\mathrm{MT})} = \lambda_k^{(\mathrm{BS})}$. Then, $\{D_{\kappa,k,i}\}_{\mathrm{MT}_i \in \bar{\Phi}_k^{(\mathrm{MT})}}$ constitutes a PPP in $\mathbb{R}^+$ whose density is $\bar{\lambda}_{\kappa,k}^{(S,\alpha)} = \lambda_k^{(\mathrm{BS})} \exp\left(\left(2/\alpha_\kappa\right) \left(10\log_{10}(e)\right)^{-1} \mu_\kappa + (1/2) \left(2/\alpha_\kappa\right)^2 \left(10\log_{10}(e)\right)^{-2} \sigma_\kappa^2 \right)$. Likewise, $\{D_{\kappa,i}\}_{\mathrm{MT}_i \in \bar{\Phi}_{\kappa}^{(\mathrm{MT})} \backslash \mathrm{MT}_0}$ constitutes a PPP in $\mathbb{R}^+$ whose density is $\bar{\lambda}_{\kappa}^{(S,\alpha)} = \bar{\lambda}_{\kappa,\kappa}^{(S,\alpha)}$.*

Proof*: It follows by applying the displacement theorem of PPPs [63, Sec. II-A] and [60, Eq. (2.55)].* □

Remark 4.5 *The density $\bar{\lambda}_k^{(S,\alpha)}$ of Lemma 4.5 is equal to $\lambda_k^{(S,\alpha)}$ in Lemmas 4.1, 4.2, i.e., $\bar{\lambda}_k^{(S,\alpha)} = \lambda_k^{(S,\alpha)}$.* □

Remark 4.6 *Except for Lemma 4.5, all lemmas and corollaries in Section 4.2.7 are exact. The BSs of each tier, in fact, constitute a PPP. Based on Assumption 4.1, on the other hand, the active MTs of each tier constitute an approximated PPP. Lemmas 4.1-4.4 and Corollaries 4.1, 4.2 depend only on the distribution of the BSs.* □

4.3 System-Level Analysis of Maximum Ratio Combining

Let us assume that a MRC demodulator is employed at the probe multi-antenna BS. As a result, $\mathbf{w}_{\kappa,0} = \mathbf{h}_{\kappa,0}$ [60, Ch. 11]. From (4.4), the SINR of $z_{\kappa,0} = \mathbf{w}_{\kappa,0}^H \mathbf{y}_{\kappa,0} = \mathbf{h}_{\kappa,0}^H \mathbf{y}_{\kappa,0}$ can be formulated as follows:

$$\mathrm{SINR}_{\kappa,0} = \mathscr{U}_{\kappa,0} \left(\sigma_N^2 + \mathscr{I}_{\kappa,\kappa}^{\backslash 0} + \sum_{k \neq \kappa = 1}^{\mathscr{K}} \mathscr{I}_{\kappa,k} \right)^{-1} \tag{4.14}$$

where the following short-hands have been introduced:

$$\begin{aligned}
\mathscr{U}_{\kappa,0} &= P_0 \rho_0^{-1} \tilde{R}_{\kappa,0}^{\alpha_\kappa(\varepsilon-1)} \gamma_{\kappa,0} \mathbb{1}\left(\tilde{R}_{\kappa,0} \leq \left(\frac{P_{\max}}{P_0} \right)^{1/(\alpha_\kappa \varepsilon)} \right) + P_\infty \rho_0^{-1} \tilde{R}_{\kappa,0}^{-\alpha_\kappa} \gamma_{\kappa,0} \mathbb{1}\left(\tilde{R}_{\kappa,0} > \left(\frac{P_{\max}}{P_0} \right)^{1/(\alpha_\kappa \varepsilon)} \right) \\
\mathscr{I}_{\kappa,\kappa}^{\backslash 0} &= \sum_{\mathrm{MT}_i \in \bar{\Phi}_{\kappa}^{(\mathrm{MT})} \backslash \mathrm{MT}_0} P_0 \rho_0^{-1} \tilde{R}_{\kappa,i}^{\alpha_\kappa \varepsilon} D_{\kappa,i}^{-\alpha_\kappa} \gamma_{\kappa,i} \mathbb{1}\left(D_{\kappa,i} > \tilde{R}_{\kappa,i} \right) \mathbb{1}\left(\tilde{R}_{\kappa,i} \leq \left(\frac{P_{\max}}{P_0} \right)^{1/(\alpha_\kappa \varepsilon)} \right) \\
&\quad + \sum_{\mathrm{MT}_i \in \bar{\Phi}_{\kappa}^{(\mathrm{MT})} \backslash \mathrm{MT}_0} P_\infty \rho_0^{-1} D_{\kappa,i}^{-\alpha_\kappa} \gamma_{\kappa,i} \mathbb{1}\left(D_{\kappa,i} > \tilde{R}_{\kappa,i} \right) \mathbb{1}\left(\tilde{R}_{\kappa,i} > \left(\frac{P_{\max}}{P_0} \right)^{1/(\alpha_\kappa \varepsilon)} \right) \\
\mathscr{I}_{\kappa,k} &= \sum_{\mathrm{MT}_i \in \bar{\Phi}_k^{(\mathrm{MT})}} P_0 \rho_0^{-1} \tilde{R}_{k,i}^{\alpha_k \varepsilon} D_{\kappa,k,i}^{-\alpha_\kappa} \gamma_{\kappa,k,i} \mathbb{1}\left(D_{\kappa,k,i} > \left(\left(\frac{\mathscr{T}_\kappa}{\mathscr{T}_k} \right) \tilde{R}_{k,i}^{\alpha_k} \right)^{1/\alpha_\kappa} \right) \mathbb{1}\left(\tilde{R}_{k,i} \leq \left(\frac{P_{\max}}{P_0} \right)^{1/(\alpha_k \varepsilon)} \right) \\
&\quad + \sum_{\mathrm{MT}_i \in \bar{\Phi}_k^{(\mathrm{MT})}} P_\infty \rho_0^{-1} D_{\kappa,k,i}^{-\alpha_\kappa} \gamma_{\kappa,k,i} \mathbb{1}\left(D_{\kappa,k,i} > \left(\left(\frac{\mathscr{T}_\kappa}{\mathscr{T}_k} \right) \tilde{R}_{k,i}^{\alpha_k} \right)^{1/\alpha_\kappa} \right) \mathbb{1}\left(\tilde{R}_{k,i} > \left(\frac{P_{\max}}{P_0} \right)^{1/(\alpha_k \varepsilon)} \right)
\end{aligned} \tag{4.15}$$

as well as the RVs $\gamma_{\kappa,0}=\left|\mathbf{h}_{\kappa,0}\right|^2\sim\text{Gamma}\left(N_\kappa,N_\kappa\Omega_\kappa\right)$, $\gamma_{\kappa,i}=\left|\left(\mathbf{h}_{\kappa,0}^H\Big/\left|\mathbf{h}_{\kappa,0}\right|\right)\mathbf{h}_{\kappa,i}\right|^2\sim\text{Gamma}\left(1,\Omega_\kappa\right)$ for $\text{MT}_i\in\bar{\Phi}_\kappa^{(\text{MT})}\backslash\text{MT}_0$, and $\gamma_{\kappa,k,i}=\left|\left(\mathbf{h}_{\kappa,0}^H\Big/\left|\mathbf{h}_{\kappa,0}\right|\right)\mathbf{h}_{\kappa,k,i}\right|^2\sim\text{Gamma}\left(1,\Omega_\kappa\right)$ for $\text{MT}_i\in\bar{\Phi}_k^{(\text{MT})}$. These latter RVs follow a Gamma distribution because the fast-fading is a circularly symmetric complex Gaussian RV (Section 4.2.2).

Based on (4.14), the following two sections provide frameworks for computing coverage and rate. From *Lemma 4.3* and *Corollary 4.2*, for ease of notation, we introduce the weighed PDF and CDF $f_{\tilde{R}_{\kappa,0}}^{(\mathscr{A}_\kappa)}(\xi)=\mathscr{A}_\kappa f_{\tilde{R}_{\kappa,0}}(\xi)=2\pi\lambda_\kappa^{(S,\alpha)}\xi\exp\left(-\pi\sum_{k=1}^{\mathscr{K}}\lambda_k^{(S,\alpha)}\left(\frac{\mathscr{T}_k}{\mathscr{T}_\kappa}\right)^{2/\alpha_k}\xi^{2\alpha_\kappa/\alpha_k}\right)$ and $F_{\tilde{R}_{\kappa,0}}^{(\mathscr{A}_\kappa)}(\xi)=\int_0^\xi f_{\tilde{R}_{\kappa,0}}^{(\mathscr{A}_\kappa)}(\zeta)\,d\zeta$.

4.3.1 Coverage Probability

Proposition 4.1 *Let the SINR in* (4.14) *for any non-negative* P_∞ *and* $P_{\max}$. *Let* $\psi_{\mathscr{I}_{\kappa,\kappa}^{\backslash 0}}(\cdot)$ *and* $\psi_{\mathscr{I}_{\kappa,k}}(\cdot)$ *be the CFs of* $\mathscr{I}_{\kappa,\kappa}^{\backslash 0}$ *and* $\mathscr{I}_{\kappa,k}$ *in* (4.15), *respectively. The coverage probability in* (4.5) *can be formulated as follows:*

$$\mathsf{P}_{\text{cov}}(\boldsymbol{\tau})=1/2-1/\pi\sum_{\kappa=1}^{\mathscr{K}}\int_0^{+\infty}\text{Im}\left\{\Psi_{\kappa,0}(\omega;\tau_\kappa)\exp\left(j\omega\sigma_N^2\right)\psi_{\mathscr{I}_{\kappa,\kappa}^{\backslash 0}}(\omega)\prod_{k\neq\kappa=1}^{\mathscr{K}}\psi_{\mathscr{I}_{\kappa,k}}(\omega)\right\}d\omega/\omega \quad (4.16)$$

where $\Psi_{\kappa,0}(\omega;\tau_\kappa)=\Psi_{\kappa,0}^{(P_0)}(\omega;\tau_\kappa)+\Psi_{\kappa,0}^{(P_\infty)}(\omega;\tau_\kappa)$, $\psi_{\mathscr{I}_{\kappa,\kappa}^{\backslash 0}}(\omega)=\psi_{\mathscr{I}_{\kappa,\kappa}^{\backslash 0}}^{(P_0)}(\omega)\,\psi_{\mathscr{I}_{\kappa,\kappa}^{\backslash 0}}^{(P_\infty)}(\omega)$, $\psi_{\mathscr{I}_{\kappa,k}}(\omega)=\psi_{\mathscr{I}_{\kappa,k}}^{(P_0)}(\omega)$ $\times\psi_{\mathscr{I}_{\kappa,k}}^{(P_\infty)}(\omega)$, *and the following short-hands have been introduced:*

$$\begin{aligned}
\Psi_{\kappa,0}^{(P_0)}(\omega;\tau_\kappa)&=\int_0^{\left(\frac{P_{\max}}{P_0}\right)^{1/(\alpha_\kappa\varepsilon)}}\left(1+j\omega P_0\rho_0^{-1}\tau_\kappa^{-1}\Omega_\kappa\xi^{\alpha_\kappa(\varepsilon-1)}\right)^{-N_\kappa}f_{\tilde{R}_{\kappa,0}}^{(\mathscr{A}_\kappa)}(\xi)\,d\xi\\
\Psi_{\kappa,0}^{(P_\infty)}(\omega;\tau_\kappa)&=\int_{\left(\frac{P_{\max}}{P_0}\right)^{1/(\alpha_\kappa\varepsilon)}}^{+\infty}\left(1+j\omega P_\infty\rho_0^{-1}\tau_\kappa^{-1}\Omega_\kappa\xi^{-\alpha_\kappa}\right)^{-N_\kappa}f_{\tilde{R}_{\kappa,0}}^{(\mathscr{A}_\kappa)}(\xi)\,d\xi\\
\psi_{\mathscr{I}_{\kappa,\kappa}^{\backslash 0}}^{(P_0)}(\omega)&=\exp\left(\pi\bar{\lambda}_\kappa^{(S,\alpha)}\int_0^{\left(\frac{P_{\max}}{P_0}\right)^{1/(\alpha_\kappa\varepsilon)}}\xi^2\Upsilon_\kappa\left(j\omega P_0\rho_0^{-1}\xi^{\alpha_\kappa(\varepsilon-1)}\right)f_{\tilde{R}_{\kappa,i}}(\xi)\,d\xi\right)\\
\psi_{\text{I}_{\kappa,\kappa}^{\backslash 0}}^{(P_\infty)}(\omega)&=\exp\left(\pi\bar{\lambda}_\kappa^{(S,\alpha)}\int_{\left(\frac{P_{\max}}{P_0}\right)^{1/(\alpha_\kappa\varepsilon)}}^{+\infty}\xi^2\Upsilon_\kappa\left(j\omega P_\infty\rho_0^{-1}\xi^{-\alpha_\kappa}\right)f_{\tilde{R}_{\kappa,i}}(\xi)\,d\xi\right)\\
\psi_{\mathscr{I}_{\kappa,k}}^{(P_0)}(\omega)&=\exp\left(\pi\bar{\lambda}_{\kappa,k}^{(S,\alpha)}\int_0^{\left(\frac{P_{\max}}{P_0}\right)^{1/(\alpha_k\varepsilon)}}\xi^{2\alpha_k/\alpha_\kappa}\left(\frac{\mathscr{T}_\kappa}{\mathscr{T}_k}\right)^{2/\alpha_\kappa}\Upsilon_\kappa\left(j\omega P_0\rho_0^{-1}\left(\frac{\mathscr{T}_k}{\mathscr{T}_\kappa}\right)\xi^{\alpha_\kappa(\varepsilon-1)}\right)f_{\tilde{R}_{k,i}}(\xi)\,d\xi\right)\\
\psi_{\mathscr{I}_{\kappa,k}}^{(P_\infty)}(\omega)&=\exp\left(\pi\bar{\lambda}_{\kappa,k}^{(S,\alpha)}\int_{\left(\frac{P_{\max}}{P_0}\right)^{1/(\alpha_k\varepsilon)}}^{+\infty}\xi^{2\alpha_k/\alpha_\kappa}\left(\frac{\mathscr{T}_\kappa}{\mathscr{T}_k}\right)^{2/\alpha_\kappa}\Upsilon_\kappa\left(j\omega P_\infty\rho_0^{-1}\left(\frac{\mathscr{T}_k}{\mathscr{T}_\kappa}\right)\xi^{-\alpha_\kappa}\right)f_{\tilde{R}_{k,i}}(\xi)\,d\xi\right)
\end{aligned} \quad (4.17)$$

where $\Upsilon_\kappa(x) = 1 - {}_2F_1\left(-2/\alpha_\kappa, 1; 1-2/\alpha_\kappa; \Omega_\kappa x\right)$. *The rest of the functions are defined in Section 4.2.7.*

Proof*: See Appendix I.* □

Remark 4.7 *The modeling approach most similar to ours is that of [48] (Section 4.1). Besides considering multi-antenna BSs, a generalized cell association and power control mechanism, the difference between [48] and Proposition 4.1 emerges from* (4.17)*. In* (4.17)*, the PDF of* $\tilde{R}_{k,i}$*,* $f_{\tilde{R}_{k,i}}(\cdot)$*, which appears in* $\psi_{\mathscr{I}_{\kappa,\kappa}^{\setminus 0}}(\cdot)$ *and* $\psi_{\mathscr{I}_{\kappa,k}}(\cdot)$*, is normalized by the association probability* $\mathscr{A}_\kappa$ *(see* (4.11)*). This is not the case of [48, Eq. (30)].* □

Corollary 4.3 *Let the SINR in* (4.14)*,* $\Psi_{\kappa,0}^{(P_0)}(\cdot;\cdot)$*,* $\psi_{\mathscr{I}_{\kappa,\kappa}^{\setminus 0}}^{(P_0)}(\cdot)$*,* $\psi_{\mathscr{I}_{\kappa,k}}^{(P_0)}(\cdot)$ *in* (4.17)*,* $P_\infty = 0$*. The coverage in* (4.5) *is:*

$$\begin{aligned}\mathsf{P}_{\mathrm{cov}}(\boldsymbol{\tau}) = {} & 1/2 \sum_{\kappa=1}^{\mathscr{K}} F_{\tilde{R}_{\kappa,0}^{(\mathscr{A}_\kappa)}}\left(\left(\frac{P_{\max}}{P_0}\right)^{1/(\alpha_\kappa \varepsilon)}\right) \\ & - 1/\pi \sum_{\kappa=1}^{\mathscr{K}} \int_0^{+\infty} \mathrm{Im}\left\{\Psi_{\kappa,0}^{(P_0)}(\omega;\tau_\kappa)\exp\left(j\omega\sigma_N^2\right)\psi_{\mathscr{I}_{\kappa,\kappa}^{\setminus 0}}^{(P_0)}(\omega)\prod_{k\neq\kappa=1}^{\mathscr{K}}\psi_{\mathscr{I}_{\kappa,k}}^{(P_0)}(\omega)\right\} d\omega/\omega\end{aligned} \tag{4.18}$$

Proof*: The proof is the same as that of Proposition 4.1 in Appendix I, by setting* $P_\infty = 0$*. Alternatively, by noting that* $1/2 - 1/\pi \int_0^{+\infty} Im\left\{\exp\left(j\omega\sigma_N^2\right)\psi_{\mathscr{I}_{\kappa,\kappa}^{\setminus 0}}(\omega)\prod_{k\neq\kappa=1}^{K}\psi_{\mathscr{I}_{\kappa,k}}(\omega)\right\}\frac{d\omega}{\omega} = 0$*,* (4.18) *follows from* (4.16)*.* □

Remark 4.8 *If* $P_\infty = 0$ *and* $P_{\max} < \infty$*, according to* (4.2)*, the MTs whose distance from their serving BSs is greater than* $R_{k,\max} = \left(\frac{P_{\max}}{P_0}\right)^{1/(\alpha_k\varepsilon)}$ *are in truncation outage. If they are typical MTs, their coverage is zero. Otherwise, their net impact to the other-cell interference is zero and the coverage increases. The reduction of the coverage due to the typical MTs in truncation outage corresponds to the first addend in* (4.18)*, i.e.,* $F_{\tilde{R}_{\kappa,0}^{(\mathscr{A}_\kappa)}}\left(\left(\frac{P_{\max}}{P_0}\right)^{1/(\alpha_\kappa\varepsilon)}\right) < \mathscr{A}_\kappa$ *if* $P_{\max} < \infty$*, and to the truncated integral* $\Psi_{\kappa,0}^{(P_0)}(\cdot;\cdot)$ *if* $P_{\max} < \infty$*. The increase of the coverage due to the reduced other-cell interference is related to the fact that only the truncated integrals* $\psi_{\mathscr{I}_{\kappa,\kappa}^{\setminus 0}}^{(P_0)}(\cdot)$ *and* $\psi_{\mathscr{I}_{\kappa,k}}^{(P_0)}(\cdot)$ *contribute to the CFs of the other-cell interference if* $P_{\max} < \infty$*.* □

Corollary 4.4 *Let the coverage in Proposition 4.1 and Corollary 4.3. If* $P_{\max} = \infty$*, it simplifies to* (4.18) *with* $\sum_{\kappa=1}^{\mathscr{K}} F_{\tilde{R}_{\kappa,0}^{(\mathscr{A}_\kappa)}}\left(\left(\frac{P_{\max}}{P_0}\right)^{1/(\alpha_\kappa\varepsilon)}\right) = 1$ *and by letting* $P_{\max} \to \infty$ *in* $\Psi_{\kappa,0}^{(P_0)}(\cdot;\cdot)$*,* $\psi_{\mathscr{I}_{\kappa,\kappa}^{\setminus 0}}^{(P_0)}(\cdot)$ *and* $\psi_{\mathscr{I}_{\kappa,k}}^{(P_0)}(\cdot)$*.*

Proof*: The proof is the same as that of Proposition 4.1 in Appendix I, by letting* $P_{\max} \to \infty$*. It is worth noting that, by definition of CDF,* $\sum_{\kappa=1}^{\mathscr{K}} F_{\tilde{R}_{\kappa,0}^{(\mathscr{A}_\kappa)}}\left(\left(\frac{P_{\max}}{P_0}\right)^{1/(\alpha_\kappa\varepsilon)}\right) = \sum_{\kappa=1}^{\mathscr{K}}\mathscr{A}_\kappa = 1$ *if* $P_{\max} \to \infty$*.* □

Remark 4.9 *Proposition 4.1 and Corollaries 4.3, 4.4 are formulated in terms of a two-fold integral, which can be efficiently computed by state-of-the-art computational programs. A two-fold integral is obtained in [50] too, even though single-antenna BSs, equal path-loss exponents, a simpler power control are considered.* □

From *Proposition 4.1* and *Corollaries 4.3, 4.4*, simplified frameworks for relevant system setups can be obtained. Some of them lead to minor simplifications and limited reduction of the computational complexity. Hence, they are not reported here. This includes, *e.g.*, full-channel inversion power control ($\varepsilon = 1$), no power control ($\varepsilon = 0$), interference-limited networks ($\sigma_N^2 = 0$), single-tier networks ($\mathcal{K} = 1$), heterogeneous networks where all tiers of BSs have the same path-loss exponent ($\alpha_k = \alpha$). In the following corollaries, we illustrate three case studies for which the number of nested integrals reduces to one or a closed-form expression is obtained.

Corollary 4.5 *Let the SINR in* (4.14)*,* $\alpha_k = \alpha$*,* $\varepsilon = 1$*,* $P_\infty = 0$*. The coverage is equal to* (4.18) *by setting* $\varepsilon = 1$*,* $\mathscr{A}_\kappa = \lambda_\kappa^{(S,\alpha)} \left(\sum_{k=1}^{\mathscr{K}} \lambda_k^{(S,\alpha)} \left(\frac{\mathscr{T}_k}{\mathscr{T}_\kappa} \right)^{2/\alpha} \right)^{-1}$*,* $F_{\tilde{R}_{\kappa,0}}^{(\mathscr{A}_\kappa)}(\xi) = \mathscr{A}_\kappa \left(1 - \exp\left(-\pi \left(\lambda_\kappa^{(S,\alpha)} \Big/ \mathscr{A}_\kappa \right) \xi^2 \right) \right)$*, and:*

$$
\begin{aligned}
&\Psi_{\kappa,0}^{(P_0)}(\omega;\tau_\kappa) = \left(1 + j\omega P_0 \rho_0^{-1} \tau_\kappa^{-1} \Omega_\kappa\right)^{-N_\kappa} F_{\tilde{R}_{\kappa,0}}^{(\mathscr{A}_\kappa)} \left(\left(\frac{P_{\max}}{P_0} \right)^{1/\alpha} \right) \\
&\psi_{\mathscr{I}_{\kappa,\kappa}^{\setminus 0}}^{(P_0)}(\omega) = \exp\left(\pi \bar{\lambda}_\kappa^{(S,\alpha)} \Upsilon_\kappa \left(j\omega P_0 \rho_0^{-1} \right) \mathcal{V}_\kappa(P_{\max}) \right) \\
&\psi_{\mathscr{I}_{\kappa,k}}^{(P_0)}(\omega) = \exp\left(\pi \bar{\lambda}_{\kappa,k}^{(S,\alpha)} \left(\frac{\mathscr{T}_\kappa}{\mathscr{T}_k} \right)^{2/\alpha} \Upsilon_\kappa \left(j\omega P_0 \rho_0^{-1} \left(\frac{\mathscr{T}_k}{\mathscr{T}_\kappa} \right) \right) \mathcal{V}_\kappa(P_{\max}) \right) \\
&\mathcal{V}_\kappa(P_{\max}) = \left(\frac{\pi \lambda_\kappa^{(S,\alpha)}}{\mathscr{A}_\kappa} \right)^{-1} - \left(\frac{\pi \lambda_\kappa^{(S,\alpha)}}{\mathscr{A}_\kappa} \right)^{-1} \exp\left(-\frac{\pi \lambda_\kappa^{(S,\alpha)}}{\mathscr{A}_\kappa} \left(\frac{P_{\max}}{P_0} \right)^{2/\alpha} \right) \\
&- \left(\frac{P_{\max}}{P_0} \right)^{2/\alpha} \exp\left(-\frac{\pi \lambda_\kappa^{(S,\alpha)}}{\mathscr{A}_\kappa} \left(\frac{P_{\max}}{P_0} \right)^{2/\alpha} \right)
\end{aligned}
\tag{4.19}
$$

Proof*: Since* $\alpha_k = \alpha$*,* (4.18) *holds. It follows from* (4.10)*,* (4.12)*, by computing the integrals in* (4.17)*.* □

Corollary 4.6 *Let the SINR in* (4.14)*,* $\alpha_k = \alpha$*,* $\varepsilon = 1$*,* $P_{\max} = \infty$*. The coverage in* (4.5) *can be formulated as in Corollary 4.5 by setting* $F_{\tilde{R}_{\kappa,0}}^{(\mathscr{A}_\kappa)}(P_{\max} \to \infty) = \mathscr{A}_\kappa$ *and* $\mathcal{V}_\kappa(P_{\max} \to \infty) = \left(\pi \lambda_\kappa^{(S,\alpha)} \Big/ \mathscr{A}_\kappa \right)^{-1}$*.*

Proof*: It immediately follows from Corollary 4.5 by noting that* P_∞ *is irrelevant if* $P_{\max} \to \infty$*.* □

Corollary 4.7 *Let the SINR in* (4.14)*,* $\varepsilon = 1$*,* $P_\infty = 0$*,* $N_\kappa = 1$*. The coverage in* (4.5) *can be*

formulated as:

$$P_{cov}(\tau)=\sum_{\kappa=1}^{K}\left(\exp\left(-P_0^{-1}\rho_0\tau_\kappa\Omega_\kappa^{-1}\sigma_N^2\right)\psi_{\mathscr{I}_{\kappa,\kappa}^{\backslash 0}}^{(P_0)}\left(jP_0^{-1}\rho_0\tau_\kappa\Omega_\kappa^{-1}\right)\right.$$
$$\left.\times\prod_{k\neq\kappa=1}^{K}\psi_{\mathscr{I}_{\kappa,k}}^{(P_0)}\left(jP_0^{-1}\rho_0\tau_\kappa\Omega_\kappa^{-1}\right)F_{\tilde{R}_{\kappa,0}}^{(A_\kappa)}\left(\left(\frac{P_{\max}}{P_0}\right)^{1/\alpha_\kappa}\right)\right) \tag{4.20}$$

where $F_{\tilde{R}_{\kappa,0}}^{(\mathscr{A}_\kappa)}(\cdot)$, $\psi_{\mathrm{I}_{\kappa,\kappa}^{\backslash 0}}^{(P_0)}(\cdot)$ *and* $\psi_{\mathrm{I}_{\kappa,k}}^{(P_0)}(\cdot)$ *are the same as in Proposition 4.1. If* $\alpha_k=\alpha$*, they can be formulated in closed-form as in Corollary 4.5. If* $P_{\max}\to\infty$*, they simplify as shown in Corollary 4.6.*

Proof*: If* $N_\kappa=1$ *for* $k=1,2,\ldots,\mathscr{K}$, $\gamma_{\kappa,0}\sim\text{Gamma}(1,\Omega_\kappa)$ *and* $\Pr\{\gamma_{\kappa,0}>\xi\}=\exp\left(-\xi/\Omega_\kappa\right)$*. Since* $\varepsilon=1$ *and* $P_\infty=0$, $\mathscr{U}_{\kappa,0}=P_0\rho_0^{-1}\gamma_{\kappa,0}\mathbb{1}\left(\tilde{R}_{\kappa,0}\leq\left(\frac{P_{\max}}{P_0}\right)^{1/\alpha_\kappa}\right)$*. Thus, the coverage is equal to*

$$\mathsf{P}_{\text{cov}}(\tau_\kappa|\mathscr{X}_\kappa)$$
$$=\mathbb{E}_{\tilde{R}_{\kappa,0},\mathscr{I}_{\kappa,\kappa}^{\backslash 0},\{\mathscr{I}_{\kappa,k}\}_{k\neq\kappa=1}^{K}}\left\{\exp\left(-\frac{\tau_\kappa}{P_0\rho_0^{-1}\Omega_\kappa}\left(\sigma_N^2+\mathscr{I}_{\kappa,\kappa}^{\backslash 0}+\sum_{k\neq\kappa=1}^{K}\mathscr{I}_{\kappa,k}\right)\right)\mathbb{1}\left(\tilde{R}_{\kappa,0}\leq\left(\frac{P_{\max}}{P_0}\right)^{1/\alpha_\kappa}\right)\middle|\mathscr{X}_\kappa\right\}.$$

The rest of the proof follows by computing the expectations in the last formula. □

Remark 4.10 *If* $\alpha_k=\alpha$*, the coverage in Corollary 4.7 is in closed-form. Under the same assumptions, a closed-form cannot be obtained by letting* $N_\kappa=1$ *in Corollaries 4.5, 4.6. The integral with respect to* ω *in* (4.18)*, in fact, has no closed-form. This is the reason why a different proof is provided for the single-antenna setup. By equating* (4.18) *and* (4.20)*, however, a closed-form for such an integral is now available.* □

4.3.2 Average Rate

An explicit expression of the rate is provided under the assumptions of *Proposition 4.1*. By using the same methodology, simplified frameworks can be obtained for the case studies discussed in the corollaries of Section 4.3.1. Further details are provided in *Remark 4.11* in what follows.

Proposition 4.2 *Let the SINR in* (4.14) *for any non-negative* P_∞ *and* $P_{\max}$*. Let* $\psi_{\mathscr{I}_{\kappa,\kappa}^{\backslash 0}}(\cdot)$ *and* $\psi_{\mathscr{I}_{\kappa,k}}(\cdot)$ *be the CFs of* $\mathscr{I}_{\kappa,\kappa}^{\backslash 0}$ *and* $\mathscr{I}_{\kappa,k}$ *in* (4.15)*, respectively. The average rate in* (4.6) *can be formulated as follows:*

$$\mathrm{R}=\mathrm{B_W}(\pi\ln(2))^{-1}\sum_{\kappa=1}^{\mathscr{K}}\int_0^{+\infty}\text{Im}\left\{\Lambda_{\kappa,0}(\omega;N_\kappa)\exp\left(j\omega\sigma_N^2\right)\psi_{\mathscr{I}_{\kappa,\kappa}^{\backslash 0}}(\omega)\prod_{k\neq\kappa=1}^{\mathscr{K}}\psi_{\mathscr{I}_{\kappa,k}}(\omega)\right\}d\omega/\omega \tag{4.21}$$

where $\psi_{\mathscr{I}_{\kappa,\kappa}^{\backslash 0}}(\cdot)$, $\psi_{\mathscr{I}_{\kappa,k}}(\cdot)$ *are defined in* (4.17) *and* $\Lambda_{\kappa,0}(\omega;N_\kappa)=\Lambda_{\kappa,0}^{(P_0)}(\omega;N_\kappa)+\Lambda_{\kappa,0}^{(P_\infty)}(\omega;N_\kappa)$ *with:*

$$\begin{aligned}
\mathcal{W}_{N_\kappa}(x) &= \sum_{m=2}^{N_\kappa} \frac{(-1)^m}{(N_\kappa+1-m)(x-1)^{m-1}} + \frac{(-1)^{N_\kappa+1}}{(x-1)^{N_\kappa}} \ln(x) + \sum_{m=1}^{N_\kappa-1} \frac{1}{m} + \ln(x) \\
\Lambda_{\kappa,0}^{(P_0)}(\omega; N_\kappa) &= \int_0^{\left(\frac{P_{\max}}{P_0}\right)^{1/(\alpha_\kappa \varepsilon)}} \mathcal{W}_{N_\kappa}\left(j\omega P_0 \rho_0^{-1} \Omega_\kappa \xi^{\alpha_\kappa(\varepsilon-1)}\right) f_{\tilde{R}_{\kappa,0}}^{(\mathscr{A}_\kappa)}(\xi)\, d\xi \\
\Lambda_{\kappa,0}^{(P_\infty)}(\omega; N_\kappa) &= \int_{\left(\frac{P_{\max}}{P_0}\right)^{1/(\alpha_\kappa \varepsilon)}}^{+\infty} \mathcal{W}_{N_\kappa}\left(j\omega P_\infty \rho_0^{-1} \Omega_\kappa \xi^{-\alpha_\kappa}\right) f_{\tilde{R}_{\kappa,0}}^{(\mathscr{A}_\kappa)}(\xi)\, d\xi
\end{aligned} \tag{4.22}$$

Proof*: It follows by inserting the first derivative of* (4.16) *in (b) of* (4.6)*, which leads to the integral* $\mathcal{W}_{N_\kappa}(x) = \int_0^{+\infty} \left(N_\kappa x/\tau^2\right) \ln(1+\tau)(1+x/\tau)^{-(N_\kappa+1)}\, d\tau$*. Its closed-form in* (4.22) *follows from the equality* $\mathcal{W}_{N_\kappa}(x) = N_\kappa x \int_0^{+\infty} \ln(1+\tau)(1+x\tau)^{-(N_\kappa+1)}\, d\tau - N_\kappa x \int_0^{+\infty} \ln(\tau)(1+x\tau)^{-(N_\kappa+1)}\, d\tau$*, whose closed-form expressions are obtained with the aid of the symbolic computational software program Mathematica and of [97].* □

Remark 4.11 *Similar to the coverage in Proposition 4.1, the rate in Proposition 4.2 is formulated in terms of two nested integrals, which can be efficiently computed by state-of-the-art symbolic software programs.* □

Remark 4.12 *Simplified expressions of the rate can be obtained from the corollaries in Section 4.3.1, by using the same approach as in Proposition 4.2 and, in particular, (b) in* (4.6)*. For some setups, a closed-form for* $\Lambda_{\kappa,0}(\cdot;\cdot)$*,* $\psi_{\mathscr{I}_{\kappa,\kappa}^{\setminus 0}}(\cdot)$ *and* $\psi_{\mathscr{I}_{\kappa,k}}(\cdot)$ *is available, which leads to a single integral formulation of the rate. The only exception is Corollary 4.7. In this case, a single integral expression can be obtained from (a) in* (4.6)*.* □

4.3.3 Massive MIMO Regime

In this section, a large number of BSs antennas is assumed. Pilot contamination [93] is neglected, since we are mainly interested in the impact of power control in massive MIMO [94]. Its analysis is postponed to future research. Due to space imitations, only the general system setup is analyzed.

Corollary 4.8 *Let the SINR in* (4.14) *for any non-negative* P_∞ *and* $P_{\max}$*. Let* $N_\kappa \gg 1$ *for* $\kappa = 1, 2, \ldots, \mathscr{K}$*. Then,* $\mathrm{SINR}_{\kappa,0}$ *linearly increases with* N_κ *and the coverage in* (4.5) *can be formulated as in* (4.16)*, where* $\psi_{\mathscr{I}_{\kappa,\kappa}^{\setminus 0}}(\cdot)$ *and* $\psi_{\mathscr{I}_{\kappa,k}}(\cdot)$ *are defined in* (4.17) *and* $\Psi_{\kappa,0}(\cdot;\cdot)$ *is replaced by the*

following function:

$$\begin{aligned}
&\Psi_{\kappa,0}(\omega;\tau_\kappa) \to \Psi_{\kappa,0}^{(N_\kappa\gg 1)}(\omega;\tau_\kappa) = \Psi_{\kappa,0}^{(N_\kappa\gg 1,P_0)}(\omega;\tau_\kappa) + \Psi_{\kappa,0}^{(N_\kappa\gg 1,P_\infty)}(\omega;\tau_\kappa)\\
&\Psi_{\kappa,0}^{(N_\kappa\gg 1,P_0)}(\omega;\tau_\kappa) = \int_0^{\left(\frac{P_{\max}}{P_0}\right)^{1/(\alpha_\kappa\varepsilon)}} \exp\left(-j\omega P_0\rho_0^{-1}\tau_\kappa^{-1}\Omega_\kappa N_\kappa\xi^{\alpha_\kappa(\varepsilon-1)}\right) f_{\tilde{R}_{\kappa,0}}^{(\mathscr{A}_\kappa)}(\xi)\,d\xi\\
&\Psi_{\kappa,0}^{(N_\kappa\gg 1,P_\infty)}(\omega;\tau_\kappa) = \int_{\left(\frac{P_{\max}}{P_0}\right)^{1/(\alpha_\kappa\varepsilon)}}^{+\infty} \exp\left(-j\omega P_\infty\rho_0^{-1}\tau_\kappa^{-1}\Omega_\kappa N_\kappa\xi^{-\alpha_\kappa}\right) f_{\tilde{R}_{\kappa,0}}^{(\mathscr{A}_\kappa)}(\xi)\,d\xi
\end{aligned} \tag{4.23}$$

Proof*: By virtue of the strong law of large numbers, we have* $\gamma_{\kappa,0} = \left|\mathbf{h}_{\kappa,0}\right|^2 \to N_\kappa\Omega_\kappa$ *if* $N_\kappa \gg 1$*. As a result,* $\mathscr{U}_{\kappa,0}$ *in* (4.15) *linearly increases with* N_κ*. Since* $\gamma_{\kappa,i}$ *and* $\gamma_{\kappa,k,i}$ *are independent of* N_κ*, the other-cell interference in* (4.15) *is independent of* N_κ *as well. This implies that* $\mathrm{SINR}_{\kappa,0}$ *in* (4.14) *linearly increases with* N_κ*. The coverage follows by using the same steps as the proof of Proposition 4.1 in Appendix I, but by replacing* $\gamma_{\kappa,0}$ *with its large-scale deterministic equivalent, i.e., its expected value equal to* $\gamma_{\kappa,0} \to N_\kappa\Omega_\kappa$*.* □

Corollary 4.9 *Let the SINR in* (4.14) *for any non-negative* P_∞ *and* $P_{\max}$*. Let* $N_\kappa \to \infty$ *for* $\kappa = 1,2,\ldots,\mathscr{K}$*. Let* $\mathscr{Z}(x) = \gamma_{\mathrm{EM}} + \ln(x) + U(1,1,x)$*. The average rate in* (4.6) *can be formulated as in* (4.21)*, where* $\psi_{\mathscr{I}_{\kappa,k}^{\setminus 0}}(\cdot)$ *and* $\psi_{\mathscr{I}_{\kappa,k}}(\cdot)$ *are defined in* (4.17) *and* $\Lambda_{\kappa,0}(\cdot;\cdot)$ *is replaced by the following function:*

$$\begin{aligned}
&\Lambda_{\kappa,0}(\omega;N_\kappa) \to \Lambda_{\kappa,0}^{(N_\kappa\gg 1)}(\omega) = \Lambda_{\kappa,0}^{(N_\kappa\gg 1,P_0)}(\omega) + \Lambda_{\kappa,0}^{(N_\kappa\gg 1,P_\infty)}(\omega)\\
&\Lambda_{\kappa,0}^{(N_\kappa\gg 1,P_0)}(\omega) = \int_0^{\left(\frac{P_{\max}}{P_0}\right)^{1/(\alpha_\kappa\varepsilon)}} \mathscr{Z}\left(j\omega P_0\rho_0^{-1}N_\kappa\Omega_\kappa\xi^{\alpha_\kappa(\varepsilon-1)}\right) f_{\tilde{R}_{\kappa,0}}^{(\mathscr{A}_\kappa)}(\xi)\,d\xi\\
&\Lambda_{\kappa,0}^{(N_\kappa\gg 1,P_\infty)}(\omega) = \int_{\left(\frac{P_{\max}}{P_0}\right)^{1/(\alpha_\kappa\varepsilon)}}^{+\infty} \mathscr{Z}\left(j\omega P_\infty\rho_0^{-1}N_\kappa\Omega_\kappa\xi^{-\alpha_\kappa}\right) f_{\tilde{R}_{\kappa,0}}^{(\mathscr{A}_\kappa)}(\xi)\,d\xi
\end{aligned} \tag{4.24}$$

Proof*: It follows from* (4.23)*, using steps similar to the proof of Proposition 4.2.* $\mathscr{Z}(\cdot)$ *originates by computing* $\mathscr{Z}(x) = x\int_0^{+\infty}\ln(1+\xi)\,\xi^{-2}\exp\left(-x/\xi\right)d\xi$ *with the aid of the software program Mathematica.* □

Remark 4.13 *As for the coverage, from* (4.17) *and* (4.23)*, the massive MIMO regime emerges if the number of BSs antennas,* N_κ*, satisfies the condition*

$$\eta_{\mathrm{cov}}(N_\kappa;\nu_\kappa) = \int_0^{+\infty}\left|\left(1+\xi^{-\nu_\kappa}\right)^{-N_\kappa} - \exp\left(-N_\kappa\xi^{-\nu_\kappa}\right)\right|^2 d\xi \ll 1$$

for $\nu_\kappa = \alpha_\kappa(1-\varepsilon)$ *and* $\nu_\kappa = \alpha_\kappa$*. By direct inspection of* $\eta_{\mathrm{cov}}(\cdot;\cdot)$*, we conclude that this error signal goes faster to zero as* ν_κ *(a non-negative parameter) increases. Thus, fewer BSs antennas are needed to enter into the massive MIMO regime as the path-loss exponent and the power control compensation factor increases and decreases, respectively. Similar comments and trends hold for the rate. By direct inspection of* (4.22) *and* (4.24)*, the error signal is, in this case, equal to* $\eta_{\mathrm{rate}}(N_\kappa;\nu_\kappa) = \int_0^{+\infty}\left|\mathscr{W}_{N_\kappa}(\xi^{-\nu_\kappa}) - \mathscr{Z}(N_\kappa\xi^{-\nu_\kappa})\right|^2 d\xi$*.* □

Remark 4.14 *By direct inspection of* (4.15)*, we conclude that* N_κ *does not affect the other-cell interference. It only affects the intended link. As a result,* N_κ *does not determine whether or not the MRC operates in the noise- or interference-limited regimes. This trend applies to both small- and large-scale MIMO systems. Let* $\upsilon_\kappa\left(P_{\max},P_0,P_\infty,\alpha_\kappa,\varepsilon\right)=\Pr\left\{\mathscr{I}_{\kappa,\kappa}^{\backslash 0}+\sum_{k\neq\kappa=1}^{\mathscr{K}}\mathscr{I}_{\kappa,k}\leq\sigma_N^2\right\}$*. The MRC operates in the noise- and interference-limited regimes if* $\upsilon_\kappa\left(P_{\max},P_0,P_\infty,\alpha_\kappa,\varepsilon\right)\to 1$ *and* $\upsilon_\kappa\left(P_{\max},P_0,P_\infty,\alpha_\kappa,\varepsilon\right)\to 0$*, respectively. The function* $\upsilon_\kappa\left(\cdot,\cdot,\cdot,\cdot,\cdot\right)$ *can be formulated as in* (4.16) *by letting* $\Psi_{\kappa,0}\left(\omega;\tau_\kappa\right)=1$*. It is independent of* N_κ*, but it highly depends on the quintuplet of parameters* $\left(P_{\max},P_0,P_\infty,\alpha_\kappa,\varepsilon\right)$*.* □

4.4 System-Level Analysis of Optimum Combining

Let us assume that an OC demodulator is employed at the probe BS. As a result, $\mathbf{w}_{\kappa,0}=\left(\mathbf{C}_{\kappa,0}+\sigma_N^2\mathbf{I}_{N_\kappa}\right)^{-1}\mathbf{h}_{\kappa,0}$, where

$$\tilde{\mathbf{C}}_{\kappa,0}=\mathbf{C}_{\kappa,0}+\sigma_N^2\mathbf{I}_{N_\kappa}=\mathbb{E}\left\{\left(\mathbf{y}_{\kappa,0}-\sqrt{\tilde{\mathscr{P}}_{\kappa,0}\rho_0^{-1}\tilde{R}_{\kappa,0}^{-\alpha_\kappa}}\mathbf{h}_{\kappa,0}x_{\kappa,0}\right)\left(\mathbf{y}_{\kappa,0}-\sqrt{\tilde{\mathscr{P}}_{\kappa,0}\rho_0^{-1}\tilde{R}_{\kappa,0}^{-\alpha_\kappa}}\mathbf{h}_{\kappa,0}x_{\kappa,0}\right)^H\right\}$$

is the $N_\kappa\times N_\kappa$ interference plus noise covariance matrix [60, Ch. 11]. From (4.4), $\mathbf{C}_{\kappa,0}$ can be written as follows:

$$\begin{aligned}\mathbf{C}_{\kappa,0}=&\sum_{\mathrm{MT}_i\in\tilde{\Phi}_\kappa^{(\mathrm{MT})}\backslash\mathrm{MT}_0}\frac{P_0\tilde{R}_{\kappa,i}^{\alpha_\kappa\varepsilon}}{\rho_0 D_{\kappa,i}^{\alpha_\kappa}}\mathbf{h}_{\kappa,i}\mathbf{h}_{\kappa,i}^H\left(D_{\kappa,i}>\tilde{R}_{\kappa,i}\right)\mathbb{1}\left(\tilde{R}_{\kappa,i}\leq\left(\frac{P_{\max}}{P_0}\right)^{1/(\alpha_\kappa\varepsilon)}\right)\\&+\sum_{\mathrm{MT}_i\in\tilde{\Phi}_\kappa^{(\mathrm{MT})}\backslash\mathrm{MT}_0}\frac{P_\infty}{\rho_0 D_{\kappa,i}^{\alpha_\kappa}}\mathbf{h}_{\kappa,i}\mathbf{h}_{\kappa,i}^H\left(D_{\kappa,i}>\tilde{R}_{\kappa,i}\right)\mathbb{1}\left(\tilde{R}_{\kappa,i}>\left(\frac{P_{\max}}{P_0}\right)^{1/(\alpha_\kappa\varepsilon)}\right)\\&+\sum_{k\neq\kappa=1}^{\mathscr{K}}\sum_{\mathrm{MT}_i\in\tilde{\Phi}_k^{(\mathrm{MT})}}\frac{P_0\tilde{R}_{k,i}^{\alpha_k\varepsilon}}{\rho_0 D_{\kappa,k,i}^{\alpha_\kappa}}\mathbf{h}_{\kappa,k,i}\mathbf{h}_{\kappa,k,i}^H\mathbb{1}\left(D_{\kappa,k,i}>\left(\left(\frac{T_\kappa}{T_k}\right)\tilde{R}_{k,i}^{\alpha_k}\right)^{1/\alpha_\kappa}\right)\mathbb{1}\left(\tilde{R}_{k,i}\leq\left(\frac{P_{\max}}{P_0}\right)^{1/(\alpha_k\varepsilon)}\right)\\&+\sum_{k\neq\kappa=1}^{\mathscr{K}}\sum_{\mathrm{MT}_i\in\tilde{\Phi}_k^{(\mathrm{MT})}}\frac{P_\infty}{\rho_0 D_{\kappa,k,i}^{\alpha_\kappa}}\mathbf{h}_{\kappa,k,i}\mathbf{h}_{\kappa,k,i}^H\mathbb{1}\left(D_{\kappa,k,i}>\left(\left(\frac{T_\kappa}{T_k}\right)\tilde{R}_{k,i}^{\alpha_k}\right)^{1/\alpha_\kappa}\right)\mathbb{1}\left(\tilde{R}_{k,i}>\left(\frac{P_{\max}}{P_0}\right)^{1/(\alpha_k\varepsilon)}\right)\end{aligned}\tag{4.25}$$

From (4.4), the SINR of $z_{\kappa,0}=\mathbf{w}_{\kappa,0}^H\mathbf{y}_{\kappa,0}=\left(\left(\mathbf{C}_{\kappa,0}+\sigma_N^2\mathbf{I}_{N_\kappa}\right)^{-1}\mathbf{h}_{\kappa,0}\right)^H\mathbf{y}_{\kappa,0}$ can be formulated as follows:

$$\begin{aligned}\mathrm{SINR}_{\kappa,0}=&P_0\rho_0^{-1}\tilde{R}_{\kappa,0}^{\alpha_\kappa(\varepsilon-1)}\mathbf{h}_{\kappa,0}^H\left(\mathbf{C}_{\kappa,0}+\sigma_N^2\mathbf{I}_{N_\kappa}\right)^{-1}\mathbf{h}_{\kappa,0}\mathbb{1}\left(\tilde{R}_{\kappa,0}\leq\left(\frac{P_{\max}}{P_0}\right)^{1/(\alpha_\kappa\varepsilon)}\right)\\&+P_\infty\rho_0^{-1}\tilde{R}_{\kappa,0}^{-\alpha_\kappa}\mathbf{h}_{\kappa,0}^H\left(\mathbf{C}_{\kappa,0}+\sigma_N^2\mathbf{I}_{N_\kappa}\right)^{-1}\mathbf{h}_{\kappa,0}\mathbb{1}\left(\tilde{R}_{\kappa,0}>\left(\frac{P_{\max}}{P_0}\right)^{1/(\alpha_\kappa\varepsilon)}\right)\end{aligned}\tag{4.26}$$

The SINR in (4.26) is a quadratic form in complex Gaussian vectors [98]. Based on this,

frameworks for computing coverage and rate are provided in what follows. A notation similar to the MRC is used.

4.4.1 Coverage Probability

Proposition 4.3 *Let the SINR in* (4.26) *for* $\sigma_N^2 > 0$ *and* $P_\infty > 0$. *The coverage in* (4.5) *can be formulated as:*

$$\begin{aligned}\mathsf{P}_{\mathrm{cov}}(\boldsymbol{\tau}) = &\sum_{\kappa=1}^{\mathscr{K}} \int_0^{\left(\frac{P_{\max}}{P_0}\right)^{1/(\alpha_\kappa \varepsilon)}} \mathscr{L}_\kappa\left(\xi^{\alpha_\kappa(\varepsilon-1)}; \tau_\kappa, P_0\right) f_{\tilde{R}_{\kappa,0}}^{(\mathscr{A}_\kappa)}(\xi)\, d\xi \\ &+ \sum_{\kappa=1}^{\mathscr{K}} \int_{\left(\frac{P_{\max}}{P_0}\right)^{1/(\alpha_\kappa \varepsilon)}}^{+\infty} \mathscr{L}_\kappa\left(\xi^{-\alpha_\kappa}; \tau_\kappa, P_\infty\right) f_{\tilde{R}_{\kappa,0}}^{(\mathscr{A}_\kappa)}(\xi)\, d\xi\end{aligned} \tag{4.27}$$

where, for $p \in \{P_0, P_\infty\}$, *the following short-hands have been introduced:*

$$\begin{aligned}\mathscr{L}_\kappa\left(x; \tau_\kappa, p\right) &= \exp\left(-\frac{\tau_\kappa \sigma_N^2}{p \rho_0^{-1} \Omega_\kappa x}\right) \sum_{l=1}^{N_\kappa} \frac{\mathscr{J}_{l,\kappa}^{(p)}(x; \tau_\kappa)}{(l-1)!} \left(\frac{\tau_\kappa \sigma_N^2}{p \rho_0^{-1} \Omega_\kappa x}\right)^{l-1} \\ \mathscr{J}_{l,\kappa}^{(p)}(x; \tau_\kappa) &= \prod_{k=1}^{K} \exp\left(-\bar{\lambda}_{\kappa,k}^{(S,\alpha)} \mathscr{O}_{\kappa,k}^{(p)}(x; \tau_\kappa)\right) \\ &\quad \times \left(1 + \sum_{m=1}^{N_\kappa - l} \sum_{m_1=0}^{m} \sum_{m_2=0}^{m} \cdots \sum_{m_K=0}^{m} \mathbb{1}\left(\sum_{k=1}^{K} m_k = m\right) \prod_{k=1}^{K} \frac{\left(\bar{\lambda}_{\kappa,k}^{(S,\alpha)} \mathscr{O}_{\kappa,k}^{(p)}(x; \tau_\kappa)\right)^{m_k}}{m_k!}\right) \\ \mathscr{O}_{\kappa,k}^{(p)}(x; \tau_\kappa) &= -\pi \left(\frac{\mathscr{T}_\kappa}{\mathscr{T}_k}\right)^{2/\alpha_\kappa} \int_0^{\left(\frac{P_{\max}}{P_0}\right)^{1/(\alpha_\kappa \varepsilon)}} \zeta^{2\alpha_k/\alpha_\kappa} \bar{\Upsilon}_\kappa\left(\left(\frac{\mathscr{T}_k}{\mathscr{T}_\kappa}\right)\left(P_0/p\right)\left(\zeta^{\alpha_k(\varepsilon-1)}/x\right)\tau_\kappa\right) f_{\tilde{R}_{k,i}}(\zeta)\, d\zeta \\ &\quad - \pi \left(\frac{\mathscr{T}_\kappa}{\mathscr{T}_k}\right)^{2/\alpha_\kappa} \int_{\left(\frac{P_{\max}}{P_0}\right)^{1/(\alpha_\kappa \varepsilon)}}^{+\infty} \zeta^{2\alpha_k/\alpha_\kappa} \bar{\Upsilon}_\kappa\left(\left(\frac{\mathscr{T}_k}{\mathscr{T}_\kappa}\right)\left(P_\infty/p\right)\left(\zeta^{-\alpha_k}/x\right)\tau_\kappa\right) f_{\tilde{R}_{k,i}}(\zeta)\, d\zeta\end{aligned} \tag{4.28}$$

and $\bar{\Upsilon}_\kappa(x) = 1 - {}_2F_1\left(-2/\alpha_\kappa, 1; 1 - 2/\alpha_\kappa; -x\right)$. *The rest of the functions are defined in Section 4.2.7.*

Proof*: See Appendix II.* □

Remark 4.15 *Similar to MRC, the coverage in* (4.28) *is formulated in terms of two nested integrals (see Remark 4.9). Simplified frameworks exist for some case studies, which are discussed in the following corollaries.* □

Corollary 4.10 *Let the SINR in* (4.26) *for* $\sigma_N^2 = 0$ *and* $P_\infty > 0$. *The coverage in* (4.5) *can be*

formulated as:

$$\begin{aligned}\mathrm{P}_{\mathrm{cov}}(\boldsymbol{\tau}) = &\sum_{\kappa=1}^{\mathscr{K}} \int_0^{\left(\frac{P_{\max}}{P_0}\right)^{1/(\alpha_\kappa \varepsilon)}} \mathscr{J}_{1,\kappa}^{(P_0)}\left(\xi^{\alpha_\kappa(\varepsilon-1)};\tau_\kappa\right) f_{\tilde{R}_{\kappa,0}}^{(\mathscr{A}_\kappa)}(\xi)\, d\xi \\ &+ \sum_{\kappa=1}^{\mathscr{K}} \int_{\left(\frac{P_{\max}}{P_0}\right)^{1/(\alpha_\kappa \varepsilon)}}^{+\infty} \mathscr{J}_{1,\kappa}^{(P_\infty)}\left(\xi^{-\alpha_\kappa};\tau_\kappa\right) f_{\tilde{R}_{\kappa,0}}^{(\mathscr{A}_\kappa)}(\xi)\, d\xi\end{aligned} \tag{4.29}$$

Proof: *It immediately follows from* (4.27)*, by letting* $\sigma_N^2 \to 0$. □

Corollary 4.11 *Let the SINR in* (4.26) *for* $\sigma_N^2 > 0$ *and* $P_\infty = 0$*. The coverage in* (4.5) *can be formulated as:*

$$\mathrm{P}_{\mathrm{cov}}(\boldsymbol{\tau}) = \sum_{\kappa=1}^{\mathscr{K}} \int_0^{\left(\frac{P_{\max}}{P_0}\right)^{1/(\alpha_\kappa \varepsilon)}} \mathscr{L}_\kappa\left(\xi^{\alpha_\kappa(\varepsilon-1)};\tau_\kappa,P_0\right) f_{\tilde{R}_{\kappa,0}}^{(\mathscr{A}_\kappa)}(\xi)\, d\xi \tag{4.30}$$

where $\mathscr{O}_{\kappa,k}^{(P_0)}(x;\tau_\kappa) = -\pi\left(\frac{\mathscr{T}_\kappa}{\mathscr{T}_k}\right)^{2/\alpha_\kappa} \int_0^{\left(\frac{P_{\max}}{P_0}\right)^{1/(\alpha_\kappa\varepsilon)}} \zeta^{2\alpha_k/\alpha_\kappa} \Upsilon_\kappa\left(\left(\frac{\mathscr{T}_k}{\mathscr{T}_\kappa}\right)\left(\zeta^{\alpha_k(\varepsilon-1)}/x\right)\tau_\kappa\right) f_{\tilde{R}_{k,i}}(\zeta)\, d\zeta$.

Proof: *The proof is the same as in Appendix II, by letting* $P_\infty = 0$. □

Remark 4.16 *It is worth emphasizing that the special cases in Corollary 4.10 and Corollary 4.11 cannot be obtained by numerically calculating* (4.27)*, since indeterminate expressions arise during the computation.* □

Corollary 4.12 *Let the SINR in* (4.26) *for* $\sigma_N^2 > 0$*,* $P_\infty > 0$*,* $N_\kappa = 1$ *for* $\kappa = 1,2,\ldots,\mathscr{K}$*. The coverage in* (4.5) *can be formulated as in* (4.27) *with*

$$\mathscr{L}_\kappa\left(x;\tau_\kappa,p\right) = \exp\left(-\tau_\kappa \sigma_N^2 \left(p\rho_0^{-1}\Omega_\kappa x\right)^{-1}\right) \prod_{k=1}^{\mathscr{K}} \exp\left(-\tilde{\lambda}_{\kappa,k}^{(S,\alpha)} \mathscr{O}_{\kappa,k}^{(p)}(x;\tau_\kappa)\right)$$

.

Proof: *It immediately follows from* (4.27)*, by letting* $N_\kappa = 1$ *for* $\kappa = 1,2,\ldots,\mathscr{K}$. □

Corollary 4.13 *Let the SINR in* (4.26) *for* $\sigma_N^2 > 0$*,* $P_\infty > 0$*, and* $\mathscr{K} = 1$*. The coverage in* (4.5) *is as follows:*

$$\begin{aligned}\mathrm{P}_{\mathrm{cov}}(\tau_1) = &\int_0^{\left(\frac{P_{\max}}{P_0}\right)^{1/(\alpha_1 \varepsilon)}} \mathscr{L}_1\left(\xi^{\alpha_1(\varepsilon-1)};\tau_1,P_0\right) f_{\tilde{R}_{1,0}}^{(\mathscr{A}_1)}(\xi)\, d\xi \\ &+ \int_{\left(\frac{P_{\max}}{P_0}\right)^{1/(\alpha_1 \varepsilon)}}^{+\infty} \mathscr{L}_1\left(\xi^{-\alpha_1};\tau_1,P_\infty\right) f_{\tilde{R}_{1,0}}^{(\mathscr{A}_1)}(\xi)\, d\xi\end{aligned} \tag{4.31}$$

where, for $p \in \{P_0, P_\infty\}$, $\mathscr{L}_1(\cdot;\cdot,\cdot)$ *and* $\mathscr{O}_{1,1}^{(p)}(\cdot;\cdot)$ *are defined in* (4.28) *and* $\mathscr{J}_{l,1}^{(p)}(\cdot;\cdot)$ *is as follows:*

$$\begin{aligned}\mathscr{J}_{l,1}^{(p)}(x;\tau_1) &= \exp\left(-\bar{\lambda}_{1,1}^{(S,\alpha)}\mathscr{O}_{1,1}^{(p)}(x;\tau_1)\right)\left(1+\sum_{m=1}^{N_\kappa-l}\frac{\left(\bar{\lambda}_{1,1}^{(S,\alpha)}\mathscr{O}_{1,1}^{(p)}(x;\tau_1)\right)^m}{m!}\right)\\ &\overset{(a)}{=} \frac{\Gamma\left(N_\kappa-l+1,\bar{\lambda}_{1,1}^{(S,\alpha)}\mathscr{O}_{1,1}^{(p)}(x;\tau_1)\right)}{\Gamma(N_\kappa-l+1)}\end{aligned} \tag{4.32}$$

Proof*: It immediately follows from* (4.27)*, by letting* $\mathscr{K}=1$*. The equality in (a) follows from the identity* $1+\sum_{m=1}^{M}x^m/m! = \sum_{m=0}^{M}x^m/m! = \exp(x)\left(\Gamma(M+1,x)/\Gamma(M+1)\right)$. □

Although simplified, the frameworks in *Corollaries 4.10-4.13* are still formulated in terms of two nested integrals. In what follows, special cases that lead to either single-integral or closed-forms are provided.

Corollary 4.14 *Let* $\varepsilon=1$ *and* $P_\infty=0$*. The coverage probability in* (4.5) *can be formulated as follows:*

$$\mathsf{P}_{\text{cov}}(\boldsymbol{\tau}) = \sum_{\kappa=1}^{\mathscr{K}}\left(\sum_{l=1}^{N_\kappa}\frac{\mathscr{J}_{l,\kappa}^{(P_0)}(1;\tau_\kappa)}{(l-1)!}\left(\frac{\tau_\kappa\sigma_N^2}{P_0\rho_0^{-1}\Omega_\kappa}\right)^{l-1}\right)\exp\left(-\frac{\tau_\kappa\sigma_N^2}{P_0\rho_0^{-1}\Omega_\kappa}\right)F_{\tilde{R}_{\kappa,0}}^{(\mathscr{A}_\kappa)}\left(\left(\frac{P_{\max}}{P_0}\right)^{1/(\alpha_\kappa\varepsilon)}\right) \tag{4.33}$$

where $\mathscr{O}_{\kappa,k}^{(P_0)}(1;\tau_\kappa) = -\pi\left(\frac{\mathscr{T}_\kappa}{\mathscr{T}_k}\right)^{2/\alpha_\kappa}\bar{\Upsilon}_\kappa\left(\left(\frac{\mathscr{T}_k}{\mathscr{T}_\kappa}\right)\tau_\kappa\right)\int_0^{\left(\frac{P_{\max}}{P_0}\right)^{1/(\alpha_\kappa\varepsilon)}}\zeta^{2\alpha_k/\alpha_\kappa}f_{\tilde{R}_{k,i}}(\zeta)\,d\zeta$.

Proof*: It immediately follows from Corollary 4.11, by letting* $\varepsilon=1$. □

Corollary 4.15 *Let* $\varepsilon=1$ *and* $P_{\max}\to\infty$*. The coverage probability in* (4.5) *can be formulated as follows:*

$$\mathsf{P}_{\text{cov}}(\boldsymbol{\tau}) = \sum_{\kappa=1}^{\mathscr{K}}\mathscr{A}_\kappa\left(\sum_{l=1}^{N_\kappa}\frac{\mathscr{J}_{l,\kappa}^{(P_0)}(1;\tau_\kappa)}{(l-1)!}\left(\frac{\tau_\kappa\sigma_N^2}{P_0\rho_0^{-1}\Omega_\kappa}\right)^{l-1}\right)\exp\left(-\frac{\tau_\kappa\sigma_N^2}{P_0\rho_0^{-1}\Omega_\kappa}\right) \tag{4.34}$$

where $\mathscr{O}_{\kappa,k}^{(P_0)}(1;\tau_\kappa) = -\pi\left(\frac{\mathscr{T}_\kappa}{\mathscr{T}_k}\right)^{2/\alpha_\kappa}\bar{\Upsilon}_\kappa\left(\left(\frac{\mathscr{T}_k}{\mathscr{T}_\kappa}\right)\tau_\kappa\right)\int_0^{+\infty}\zeta^{2\alpha_k/\alpha_\kappa}f_{\tilde{R}_{k,i}}(\zeta)\,d\zeta$.

Proof*: It is similar to the proof of Corollary 4.14, by taking into account that* $F_{\tilde{R}_{\kappa,0}}^{(\mathscr{A}_\kappa)}(P_{\max}\to\infty) = \mathscr{A}_\kappa$. □

Remark 4.17 *The single-integrals in Corollary 4.14 and Corollary 4.15 are ready-computable, since they involve no special functions. They correspond, in fact, to the CDF of* $\tilde{R}_{\kappa,0}$ *and to the fractional moments of* $\tilde{R}_{k,i}$. □

Corollary 4.16 *Let $\alpha_\kappa = \alpha$ for $\kappa = 1,2,\ldots,\mathscr{K}$, $\varepsilon = 1$ and $P_\infty = 0$. Let $\mathscr{V}_\kappa(\cdot)$ in* (4.19)*. The coverage probability in* (4.5) *can be formulated as in Corollary 4.14 with*

$$\mathscr{A}_\kappa = \lambda_\kappa^{(S,\alpha)} \left(\sum_{k=1}^{\mathscr{K}} \lambda_k^{(S,\alpha)} \left(\frac{\mathscr{T}_k}{\mathscr{T}_\kappa} \right)^{2/\alpha} \right)^{-1}, \; F_{\tilde{R}_{\kappa,0}}^{(\mathscr{A}_\kappa)}(\xi) = \mathscr{A}_\kappa \left(1 - \exp\left(-\pi \left(\lambda_\kappa^{(S,\alpha)} / \mathscr{A}_\kappa \right) \xi^2 \right) \right)$$

and

$$\mathscr{O}_{\kappa,k}^{(P_0)}(1;\tau_\kappa) = -\pi \left(\frac{\mathscr{T}_\kappa}{\mathscr{T}_k} \right)^{2/\alpha} \bar{\Upsilon}_\kappa \left(\left(\frac{\mathscr{T}_k}{\mathscr{T}_\kappa} \right) \tau_\kappa \right) \mathscr{V}_\kappa(P_{\max}).$$

Proof*: It follows from Corollary 4.14 by using* (4.10)-(4.12) *and by computing the integrals in closed-form.* □

Corollary 4.17 *Let $\alpha_\kappa = \alpha$ for $\kappa = 1,2,\ldots,\mathscr{K}$, $\varepsilon = 1$ and $P_{\max} \to \infty$. The coverage in* (4.5) *can be formulated as in Corollary 4.15 with*

$$\mathscr{O}_{\kappa,k}^{(P_0)}(1;\tau_\kappa) = -\left(\frac{\mathscr{T}_\kappa}{\mathscr{T}_k} \right)^{2/\alpha} \bar{\Upsilon}_\kappa \left(\left(\frac{\mathscr{T}_k}{\mathscr{T}_\kappa} \right) \tau_\kappa \right) \left(\sum_{k=1}^{\mathscr{K}} \lambda_k^{(S,\alpha)} \left(\frac{\mathscr{T}_k}{\mathscr{T}_\kappa} \right)^{2/\alpha} \right)^{-1}.$$

Proof*: It follows from Corollary 4.15, similar to the proof of Corollary 4.16 and Corollary 4.6.* □

Corollary 4.18 *Let $\alpha_\kappa = \alpha$, $\varepsilon = 1$, $P_\infty = 0$, $N_\kappa = 1$ and $\mathscr{V}_\kappa(\cdot)$ in* (4.19)*. The coverage in* (4.5) *is:*

$$\mathsf{P}_{\mathrm{cov}}(\boldsymbol{\tau}) = \sum_{\kappa=1}^{\mathscr{K}} \exp\left(-\tau_\kappa \sigma_N^2 \left(P_0 \rho_0^{-1} \Omega_\kappa \right)^{-1} \right) \left(\prod_{k=1}^{\mathscr{K}} \exp\left(-\bar{\lambda}_{\kappa,k}^{(S,\alpha)} \mathscr{O}_{\kappa,k}^{(P_0)}(1;\tau_\kappa) \right) \right) F_{\tilde{R}_{\kappa,0}}^{(\mathscr{A}_\kappa)} \left(\left(\frac{P_{\max}}{P_0} \right)^{1/\alpha} \right) \tag{4.35}$$

where $F_{\tilde{R}_{\kappa,0}}^{(\mathscr{A}_\kappa)}(\cdot)$ and $\mathscr{O}_{\kappa,k}^{(P_0)}(1;\cdot)$ are the same as in Corollary 4.16. If $P_{\max} \to \infty$, (4.35) *still holds by letting $F_{\tilde{R}_{\kappa,0}}^{(\mathscr{A}_\kappa)}(P_{\max} \to \infty) = \mathscr{A}_\kappa$ with $\mathscr{A}_\kappa$ given in Corollary 4.16 and with $\mathscr{O}_{\kappa,k}^{(P_0)}(1;\cdot)$ given in Corollary 4.17.*

Proof*: It immediately follows from Corollary 4.12, Corollary 4.16 and Corollary 4.17.* □

Remark 4.18 *If $N_\kappa = 1$, MRC and OC reduce to the same demodulator. We expect, thus, that the coverage in, e.g., Corollaries 4.7, 4.18, are the same. By direct comparison of* (4.20) *and* (4.35)*, for $P_{\max} < \infty$ and $P_{\max} \to \infty$, we observe that they coincide if $\alpha_k = \alpha$. This substantiates the correctness of our analysis. Mathematically proving this equivalence for every system setup is, on the other hand, not straightforward. The numerical computation of the frameworks for MRC and OC confirms, in fact, that this holds in general.* □

4.4.2 Average Rate

As for MRC, *Proposition 4.2* provides, in general, a two-fold integral for computing the average rate. This is possible by capitalizing on the equality (b) in (4.6), which allows us to compute, in closed-form, the integral with respect to τ_κ. This is not possible, unfortunately, for OC. In this case, the most efficient approach for computing the average rate is to use the equality (a) in (4.6). Based on propositions and corollaries in Section 4.4.1, this implies that the average rate is formulated in terms of a three-, two- or one-fold integral, depending on the setup. We have verified for many setups, however, that the integrals are efficiently computable with the aid of state-of-the-art computational software. We are currently researching on different approaches for computing the average rate of OC more efficiently. It is worth mentioning, however, that average rate and 50th percentile rate, *i.e.*, the median, are very close to each other. Thus, the average rate may be replaced by the 50th percentile rate, which can be computed more efficiently, as discussed in *Remark 4.4*.

4.4.3 Massive MIMO Regime

The framework in *Proposition 4.3* is applicable to any N_κ, and, thus, it holds for $N_\kappa \gg 1$ as well. Simplified but accurate frameworks for large but finite values of N_κ are difficult to be obtained, because N_κ appear in both $\mathscr{L}_\kappa(\cdot;\cdot,\cdot)$ and $\mathscr{J}_{l,\kappa}^{(p)}(\cdot;\cdot)$ of (4.28). In this section, thus, we focus our attention on the converge, as a function of various parameters, of the OC demodulator towards its noise-limited regime. This is, in fact, the ultimate objective of massive MIMO: reducing, as much as possible, the impact of the other-cell interference. To facilitate this study, *Corollary 4.19* provides the coverage of OC in the absence of other-cell interference.

Corollary 4.19 *Let the SINR in* (4.26) *for* $\sigma_N^2 > 0$, $P_\infty > 0$, *and* $\mathbf{C}_{\kappa,0} = \mathbf{0}_{N_\kappa}$, *i.e., the system is noise-limited. The coverage probability in* (4.5) *can be formulated as in* (4.27), *where:*

$$\mathscr{L}_\kappa\left(x;\tau_\kappa,p\right) = \exp\left(-\frac{\tau_\kappa\sigma_N^2}{p\rho_0^{-1}\Omega_\kappa x}\right)\sum_{l=1}^{N_\kappa}\frac{1}{(l-1)!}\left(\frac{\tau_\kappa\sigma_N^2}{p\rho_0^{-1}\Omega_\kappa x}\right)^{l-1} \overset{(a)}{=} \Gamma\left(N_\kappa, \frac{\tau_\kappa\sigma_N^2}{p\rho_0^{-1}\Omega_\kappa x}\right)\Big/\Gamma(N_\kappa) \tag{4.36}$$

If, in addition, $N_\kappa \gg 1$, *the coverage probability in* (4.5) *can be formulated as follows:*

$$\begin{aligned} P_{cov}^{(N_\kappa\gg1)}(\tau) = \sum_{\kappa=1}^{K}\Bigg\{ & F_{\tilde{R}_{\kappa,0}}^{(A_\kappa)}\left(\min\left\{\left(\frac{P_{\max}}{P_0}\right)^{1/(\alpha_\kappa\varepsilon)}, \left(\frac{\tau_\kappa\sigma_N^2}{P_0\rho_0^{-1}N_\kappa\Omega_\kappa}\right)^{1/\alpha_\kappa(\varepsilon-1)}\right\}\right) \\ & + \left(F_{\tilde{R}_{\kappa,0}}^{(A_\kappa)}\left(\left(\frac{\tau_\kappa\sigma_N^2}{P_\infty\rho_0^{-1}N_\kappa\Omega_\kappa}\right)^{-1/\alpha_\kappa}\right) - F_{\tilde{R}_{\kappa,0}}^{(A_\kappa)}\left(\left(\frac{P_{\max}}{P_0}\right)^{1/(\alpha_\kappa\varepsilon)}\right)\right) \\ & \times\mathbb{1}\left(\left(\frac{\tau_\kappa\sigma_N^2}{P_\infty\rho_0^{-1}N_\kappa\Omega_\kappa}\right)^{-1/\alpha_\kappa} > \left(\frac{P_{\max}}{P_0}\right)^{1/(\alpha_\kappa\varepsilon)}\right)\Bigg\} \end{aligned} \tag{4.37}$$

Proof*: In the noise-limited regime,* $\bar{\lambda}_{\kappa,k}^{(S,\alpha)}=0$ *holds. Then* $\mathscr{J}_{l,\kappa}^{(p)}(x;\tau_\kappa)=1$ *and* (4.36) *follows from* $\sum_{m=1}^{M} x^{m-1}\big/(m-1)!=\exp(x)\left(\Gamma(M,x)/\Gamma(M)\right)$. (4.37) *follows from* (4.26) *setting* $\mathbf{C}_{\kappa,0}=\mathbf{0}_{N_\kappa}$ *and by virtue of the law of large numbers, since* $\mathbf{h}_{\kappa,0}^{H}\left(\sigma_N^2\mathbf{I}_{N_\kappa}\right)^{-1}\mathbf{h}_{\kappa,0}\to(N_\kappa\Omega_\kappa)\big/\sigma_N^2$ *if* $N_\kappa\gg 1$ *holds.* □

Remark 4.19 *The coverage of OC in* (4.36) *and* (4.37) *is formulated in terms of a single-integral, which reduces to a closed-form if* $\alpha_\kappa=\alpha$ *(see Corollary 4.2). The average rate can be efficiently computed from (a) in* (4.6)*. Also,* (4.36) *and* (4.37) *are applicable to MRC too, since the SINRs* (4.14) *and* (4.26) *are the same if* $\bar{\lambda}_{\kappa,k}^{(S,\alpha)}=0$. □

Remark 4.20 *In the noise-limited regime, from the proof of Corollary 4.19,* $\mathscr{J}_{l,\kappa}^{(p)}(x;\tau_\kappa)=1$ *holds. Then, the gap, as a function of the system setup, from the noise-limited asymptote of OC can be quantified by studying* $\mathscr{J}_{l,\kappa}^{(p)}(\cdot;\cdot)$ *for non-zero values of* $\bar{\lambda}_{\kappa,k}^{(S,\alpha)}$*. By direct inspection of* $\mathscr{J}_{l,\kappa}^{(p)}(\cdot;\cdot)$ *in* (4.28)*, the following holds. 1)* $\mathscr{J}_{l,\kappa}^{(p)}(x;\tau_\kappa)\to 1$ *as* $\mathscr{O}_{l,\kappa}^{(p)}(x;\tau_\kappa)\to 0$*. This occurs if* $\bar{\Upsilon}_\kappa(x)\to 0$*, which implies* ${}_2F_1\left(-2/\alpha_\kappa,1;1-2/\alpha_\kappa;-x\right)\to 1$*. From* (4.28)*, we conclude that OC converges faster to the noise-limited (i.e., massive MIMO) regime as the path-loss exponent and the power control compensation factor increases and decreases, respectively. 2) Consider the worst-case scenario of an interference-limited setup, i.e.,* $\sigma_N^2=0$*. Also, assume* $\mathscr{K}=1$ *for simplicity. From Corollary, 4.10 and Corollary 4.13, the coverage depends on* N_κ *only through the function* $\mathscr{J}_{1,1}^{(p)}(x;\tau_1)=\Gamma\left(N_1,\bar{\lambda}_{1,1}^{(S,\alpha)}\mathscr{O}_{1,1}^{(p)}(x;\tau_1)\right)\Big/\Gamma(N_1)$*. As expected, hence, OC approaches the massive MIMO regime as* N_1 *increases, since* $\Gamma\left(N_1,y\right)/\Gamma(N_1)\to 1$ *if* $N_1\gg 1$ *for every* y*. The speed of convergence depends on the ratio of upper-incomplete Gamma and Gamma functions. For a fixed* N_1*, the massive MIMO regime is reached faster as* $\mathscr{O}_{1,1}^{(p)}(x;\tau_1)\to 0$*, which is in agreement with 1). These trends hold for* $\sigma_N^2>0$ *and* $\mathscr{K}>1$ *as well. In the presence of other-cell interference, in fact, only a few terms of the summation of* $\mathscr{L}_\kappa(\cdot;\cdot,\cdot)$ *in* (4.28) *provide a contribution and, thus,* (4.32) *still converges to 1 as* N_κ *increases.* □

Remark 4.21 *By comparing Corollary 4.8 and Remark 4.20, it is apparent that MRC and OC have similar trends as a function of the path-loss exponent and of the power control compensation factor. Coverage and rate, in addition, increase as* N_κ *increases. As for MRC, the convergence towards the noise-limited regime is independent of* N_κ*. As for OC, on the other hand, it depends on* N_κ*. In the presence of strong other-cell interference, thus, we expect that OC outperforms MRC for a finite (small or large) number of receive antennas. Since the mathematical frameworks of MRC and OC are quite different, this gain cannot be quantified in a mathematically compact form, as a function of the quintuplet* $(P_{\max},P_0,P_\infty,\alpha_\kappa,\varepsilon)$*. It can be readily obtained, however, by plotting* (4.16) *and* (4.27)*. Numerical examples are illustrated in Section 4.6.* □

4.5 System-Level Optimization

The mathematical frameworks introduced in Sections 4.3 and 4.4, despite being formulated, for the most general system setup, in integral forms, constitute accurate utility functions for system-level optimization. The importance of having them from a network utility optimization standpoint is discussed in [51]. Unlike [51], however, the utility functions introduced in this paper are directly formulated in terms of coverage and rate. In general terms, let $\mathbf{o} = \{o_1, o_2, \ldots, o_N\}$ be the N-tuple of parameters to be optimized, where $o_n \in \{P_{\max}, P_0, P_\infty, \varepsilon, \mathcal{T}_\kappa, \ldots\}$ for $n = 1, 2, \ldots, N$. Likewise, let $\mathbf{f}$ be the set of fixed (given) parameters that are not to be optimized. Since $\mathsf{P}_{\text{cov}}(\boldsymbol{\tau}) = \mathsf{P}_{\text{cov}}(\boldsymbol{\tau}; \mathbf{o}; \mathbf{f})$ and $\mathsf{R} = \mathsf{R}(\mathbf{o}; \mathbf{f})$, the network-level optimization problem can be formulated as $\mathbf{o}_{\text{opt}} = \arg\max_{\mathbf{o}} \{\mathsf{P}_{\text{cov}}(\boldsymbol{\tau}; \mathbf{o}; \mathbf{f})\}$ and $\mathbf{o}_{\text{opt}} = \arg\max_{\mathbf{o}} \{\mathsf{R}(\mathbf{o}; \mathbf{f})\}$ for coverage and rate, respectively. A similar optimization problem can be formulated for the xth percentile rate. Based on their mathematical expressions in Sections 4.3 and 4.4, similar to [51], this optimization problem does not have, in general, a closed-form solution and it is, in general, not convex. To make the computation of the optimum fast and accurate, *i.e.*, to avoid local maxima, we propose a pragmatic yet accurate algorithm for system-level optimization. To be concrete, we introduce the main idea by considering a two-tier, *i.e.*, $\mathcal{K} = 2$, cellular network and we focus our attention on the optimization of the cell association weights $\mathcal{T}_1$ and $\mathcal{T}_2$ in (4.1), while keeping all the other parameters fixed. A similar optimization problem is studied in [50] and [51], but under different assumptions. Let $\hat{\mathcal{T}} = \mathcal{T}_2 / \mathcal{T}_1$, then $\mathbf{o} = \{\mathcal{T}_1, \mathcal{T}_2\} = \hat{\mathcal{T}}$. We propose the following algorithm for computing the optimal value of $\hat{\mathcal{T}}$, *i.e.*, $\mathbf{o}_{\text{opt}} = \hat{\mathcal{T}}_{\text{opt}}$:

1. Identify the range where the optimum, $\hat{\mathcal{T}}_{\text{opt}}$, is likely to belong to, *i.e.*, $\hat{\mathcal{T}} \in \left[\hat{\mathcal{T}}_{\min}, \hat{\mathcal{T}}_{\max}\right]$. This range can be identified with the aid of the association probability $\mathscr{A}_1$ in (4.9). More specifically, $\left(\hat{\mathcal{T}}_{\min}, \hat{\mathcal{T}}_{\max}\right)$ can be computed by solving the equations $\mathscr{A}_1\left(\hat{\mathcal{T}}_{\min}\right) = 0.99$ and $\mathscr{A}_1\left(\hat{\mathcal{T}}_{\max}\right) = 0.01$. Outside this range, in fact, the typical MT is always served by one of the two tiers of BSs almost surely. For example, these solutions can be found with the aid of the NSolve function in Mathematica.

2. Plot the utility function of interest, *i.e.*, coverage or rate, as a function of $\hat{\mathcal{T}} \in \left[\hat{\mathcal{T}}_{\min}, \hat{\mathcal{T}}_{\max}\right]$ with a coarse step size $\hat{\mathcal{T}}_{\text{step}}$. Based on 3GPP documents, $\hat{\mathcal{T}}_{\text{step}}$ may be of the order of 2 dB or 3 dB [99].

3. Compute the optimum of the utility function based on the set of available points. Let denote it by $\hat{\mathcal{T}}_{\text{opt}}^{(0)}$. In the range $\hat{\mathcal{T}} \in \left[\hat{\mathcal{T}}_{\text{opt}}^{(0)} - \hat{\mathcal{T}}_{\text{step}}, \hat{\mathrm{T}}_{\text{opt}}^{(0)} + \hat{\mathcal{T}}_{\text{step}}\right]$, the utility function is, in general, concave.

4. Solve the optimization problem $\hat{\mathcal{T}}_{\text{opt}} = \underset{\hat{\mathcal{T}} \in \left[\hat{\mathcal{T}}_{\text{opt}}^{(0)} - \hat{\mathcal{T}}_{\text{step}}, \hat{\mathcal{T}}_{\text{opt}}^{(0)} + \hat{\mathcal{T}}_{\text{step}}\right]}{\arg\max} \left\{\mathsf{F}\left(\hat{\mathcal{T}}\right)\right\}$, where $\mathsf{F}\left(\hat{\mathcal{T}}\right) = \mathsf{P}_{\text{cov}}\left(\boldsymbol{\tau}; \hat{\mathcal{T}}\right)$, $\mathsf{F}\left(\hat{\mathcal{T}}\right) = \mathsf{R}\left(\hat{\mathcal{T}}\right)$ or $\mathsf{F}\left(\hat{\mathcal{T}}\right) = \mathsf{R}_{x\text{th}}\left(\hat{\mathcal{T}}\right)$, which has a unique solution. The optimum can be found using the FindMaximum function in Mathematica, by setting the initial point to $\hat{\mathcal{T}}_{\text{opt}}^{(0)}$.

Remark 4.22 *If the number of parameters to be jointly optimized is greater than one, i.e., $N > 1$, the optimization may be computationally intensive. In this case, an iterative approach may be used. Assume, e.g., $N = 2$. First, the optimal solution for o_1 may be computed by keeping o_2 fixed. Then, the optimal solution for o_2 may be computed by assuming o_1 fixed and equal to the optimal value of the previous step. This is iterated until convergence, i.e., the optimal o_1 and o_2 do not change from an iteration to another.* □

In Section 4.6, the effectiveness of this approach is validated for various setups. The important role played by several parameters, *e.g.*, the path-loss exponent, the power control compensation factor, is discussed.

4.6 Numerical and Simulation Results

In this section, numerical examples to validate the accuracy of our mathematical frameworks and to study the trade-offs that emerge in uplink heterogeneous cellular networks with multi-antenna BSs are illustrated.

Setup System-level Monte Carlo simulations are performed by carefully reproducing the system model of Section 4.2. It is worth mentioning, however, that *Assumption 4.1* is not enforced in the system-level simulator and that it is used only for developing the mathematical frameworks. To ensure saturated traffic conditions, the density of MTs is appropriately chosen, as discussed in Section 4.2. For each available MT, the cell association in (4.1) is applied and the transmit power is set according to (4.2). The probe link is assumed to be, without loss of generality, that corresponding to the MT that is closest to the origin. This allows us to speed up the simulations and to avoid border effects that originate from the practical need of considering a finite simulation area. This does not bias the validation of the proposed approach, since the probe link is different for each spatial realization and our results are obtained by averaging with respect to a large number of realizations. Finally, the SINRs in (4.14) and (4.26) for MRC and OC, respectively, are computed.

For simplicity, single- and two-tier cellular networks are analyzed. As for single-tier networks, unless otherwise stated, the following setup is considered: $\lambda_1^{(\mathrm{BS})} = 5$ BSs/Km^2, $\alpha_1 = 3.5$, $\rho_0 = 40$ dB, $P_{\max} = P_\infty = 30$ dBm and $P_{\max} = \infty$, $\mathrm{B_W} = 10$ MHz, $P_0 = P_0(\mathrm{B_W}) + 10\log_{10}(\mathrm{B_W})$ with $P_0(\mathrm{B_W}) = -100$ dBm/Hz, $\sigma_N^2 = \mathcal{N}_0 + 10\log_{10}(\mathrm{B_W})$ dBm with $\mathcal{N}_0 = -174$ dBm/Hz, $\varepsilon \in [0,1]$, $\mu_1 = 0$ dB, $\sigma_1 = 8$ dB, $\Omega_1 = 1$ and $N_1 = 4$. As for two-tier networks, the parameters are in the captions of the figures. The parameters of tier-2 are the same as those of tier-1, except for the BSs density and for the path-loss exponent.

Framework Validation In Fig. 4.1, we validate the accuracy of the PPP approximation in *Assumption 4.1*. To this end, we exploit the void probability theorem of homogeneous PPPs [16,

Th. 1.1.5], which states that a point process Φ of density λ is a homogeneous PPP *if and only if*, for any region of area A, the equality $\Pr\{\Phi(\mathsf{A})=\emptyset\}=\exp(-\lambda\mathsf{A})$ holds. Assuming *Assumption 4.1* true, the following holds: $\Pr\left\{\bar{\Phi}_k^{(\mathrm{MT})}(\mathsf{A})=\emptyset\right\}\approx\exp\left(-\bar{\lambda}_k^{(\mathrm{MT})}\mathsf{A}\right)$ for $k=1,2,\ldots,\mathscr{K}$. To test the accuracy of *Assumption 4.1*, we compare this mathematical expression of the void probability against that obtained via Monte Carlo simulations. Once all the MTs are associated with their serving BSs, in particular, we consider a region of area A centered at the origin and of radius R_A, *i.e.*, $\mathsf{A}=\pi\mathsf{R}_\mathsf{A}^2$. This assumption does not bias our analysis and avoids border effects. The probability that no nodes fall in this ball of area A is computed as a function of R_A. Theoretical (based on *Assumption 4.1*) and empirical void probabilities are illustrated in Fig. 4.1. It confirms that the gap is relatively small. More importantly, the shape of the void probability is well captured by *Assumption 4.1*. This substantiates its adoption for system-level performance evaluation of uplink heterogeneous cellular networks.

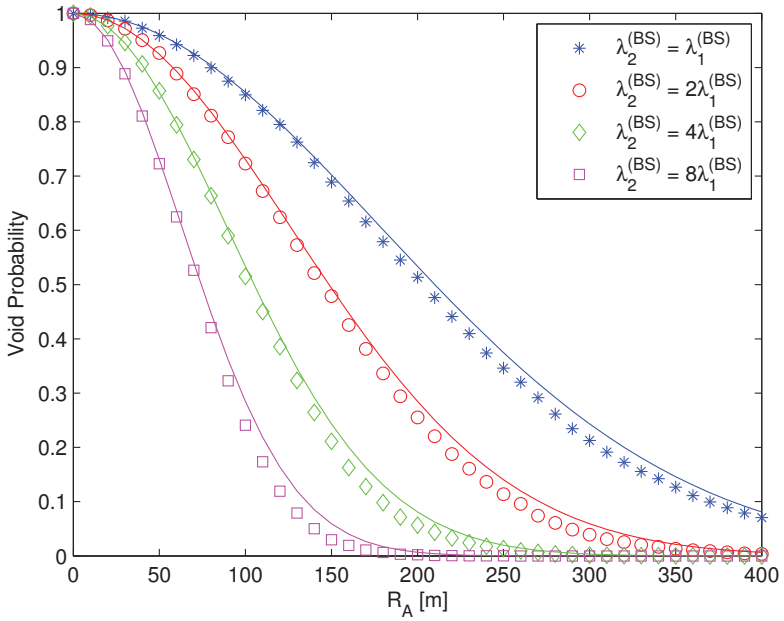

Figure 4.1: Void probability of an area A of radius R_A centered at the origin ($\mathsf{A}=\pi\mathsf{R}_\mathsf{A}^2$). Solid lines show the mathematical framework based on *Assumption 4.1* and markers show Monte Carlo simulations. Setup: $\mathscr{K}=2$, $\alpha=\alpha_1=\alpha_2=3.5$ and $\lambda_1^{(\mathrm{BS})}=5$ BSs/Km^2. Other parameters are in Section 4.6. The void probability of $\bar{\Phi}_2^{(\mathrm{MT})}$ is shown. If $\lambda_2^{(\mathrm{BS})}=\lambda_1^{(\mathrm{BS})}$, the void probabilities of $\bar{\Phi}_1^{(\mathrm{MT})}$ and $\bar{\Phi}_2^{(\mathrm{MT})}$ coincide.

In Fig. 4.2, we test the accuracy of our proposed frameworks for computing the coverage against other frameworks for the analysis of uplink cellular networks available in the literature. In particular, [48] and [50] are considered as a reference. The same setups as in [48] and [50] are used. Fig. 4.2 confirms that our frameworks are as accurate as [48] and [50], but ours are more general and account for multi-antenna BSs.

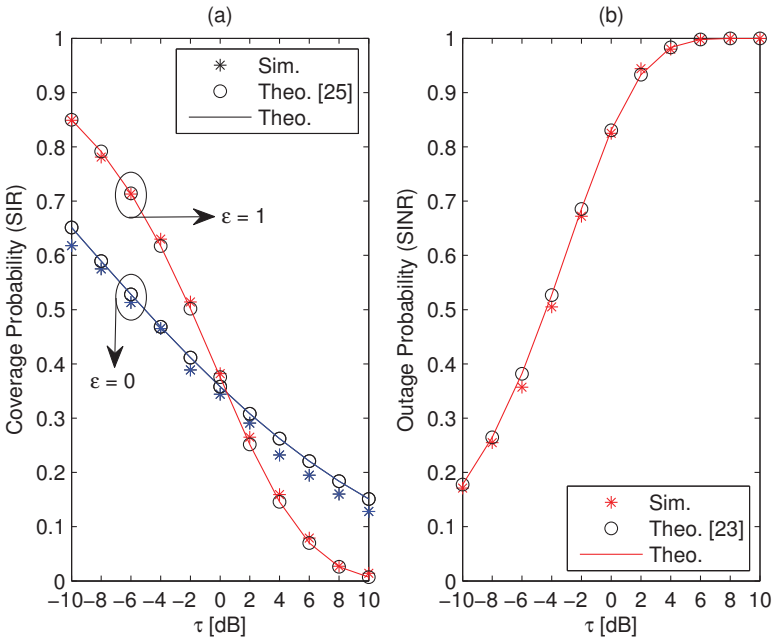

Figure 4.2: Validation of the proposed mathematical frameworks against those in [50] (a) and [48] (b). "Sim." corresponds to Monte Carlo simulations, "Theo." to the proposed framework and "Theo. [.]" to the frameworks in [50] and [48]. The setups are the same as in [50] and [48]: (a) two-tier network, $\lambda_1^{(\mathrm{BS})} = 5$ BSs/Km^2, $\lambda_2^{(\mathrm{BS})} = 6\lambda_1^{(\mathrm{BS})}$, $\alpha_1 = \alpha_2 = 3.5$, $P_{\max} = \infty$, $P_0(\mathrm{B_W}) = -80$ dBm/Hz, $\hat{\mathcal{T}} = \mathcal{T}_2/\mathcal{T}_1 = -20$ dB, $\rho_0 = 40$ dB, $\mathrm{B_W} = 10$ MHz, $\mu_1 = \mu_2 = 0$ dB, $\sigma_1 = \sigma_2 = 8$ dB, $\Omega_1 = \Omega_2 = 1$, $N_1 = N_2 = 1$, $\tau_1 = \tau_2 = \tau$, interference-limited setup (SINR = SIR = Signal-to-Interference-Ratio); and (b) one-tier network, $\lambda_1^{(\mathrm{BS})} = 2$ BSs/Km^2, $\alpha_1 = 4$, $P_{\max} = 30$ dBm, $P_0 = -90$ dBm, $\rho_0 = 0$ dB, $\sigma_N^2 = -90$ dBm, $\varepsilon = 1$, $\Omega_1 = 1$, $N_1 = 1$, there is no shadowing. In (b), "outage = 1 - coverage".

Impact of Power Control In Figs. 4.3 and 4.4, we study the impact of ε on the achievable rate. To analyze its impact for different locations of the typical MT within a cell, the xth percentile rate is considered. In particular, $x = 5$ and $x = 90$ correspond to cell-edge and cell-center MTs. $x = 50$ corresponds to the median rate within a cell, which, as shown in Figs. 4.3 and 4.4, is close to the average rate. Figures 4.3 and 4.4 confirm that ε and $P_{\max}$ strongly affect the rate for every x. Also, they show that, in general, an optimal value, $\varepsilon_{\mathrm{opt}}$, of ε exists. The figures report such $\varepsilon_{\mathrm{opt}}$ obtained by using the optimization algorithm in Section 4.5. The figures illustrate several interesting trends: i) the rate increases as the typical MT moves from the cell-edge to the cell-center, as expected; ii) OC usually outperforms MRC, as expected. We note, however, that the gain is more noticeable for large values of ε; iii) the optimal values of ε for MRC and OC are similar; and, more importantly, iv) the impact of ε is significantly different for $P_{\max} = \infty$ (Fig. 4.3) and $P_{\max} = 30$ dBm (Fig. 4.4). The reason is as follows. If $P_{\max} = \infty$, the rate tends to initially increase as ε increases, since the received power of the intended link increases. This trend holds until a critical value of ε is reached: once this occurs, the negative impact of the other-cell interference tends to be more pronounced, compared to increase of the received power. This is more evident for cell-center MTs, *i.e*, if $x = 90$. If $P_{\max} < \infty$, on the other hand, the impact of the other-cell interference is implicitly kept under control. Consider,

for example, cell-center MTs. As ε increases, the typical MT keeps increasing its transmit power, which unlikely reaches $P_{\max}$, since it is close to its serving BS. The interfering MTs, on the other hand, increase their transmit power until a given value of ε. Once this occurs, they reach $P_{\max}$ and do not increase their transmit power anymore. Because of that, the rate increases with ε and its optimal value is likely to be close to one. This trend does no hold for cell-edge MTs: due to their large distance towards their serving BS, they are likely to transmit at $P_{\max}$ too. Thus, the trend is more similar to the setup $P_{\max}=\infty$. It is worth noting that ε_{opt} is different for cell-center and cell-edge MTs. This brings to our attention that intra-cell power control may be adopted to provide a more uniform quality of service to all MTs within a cell.

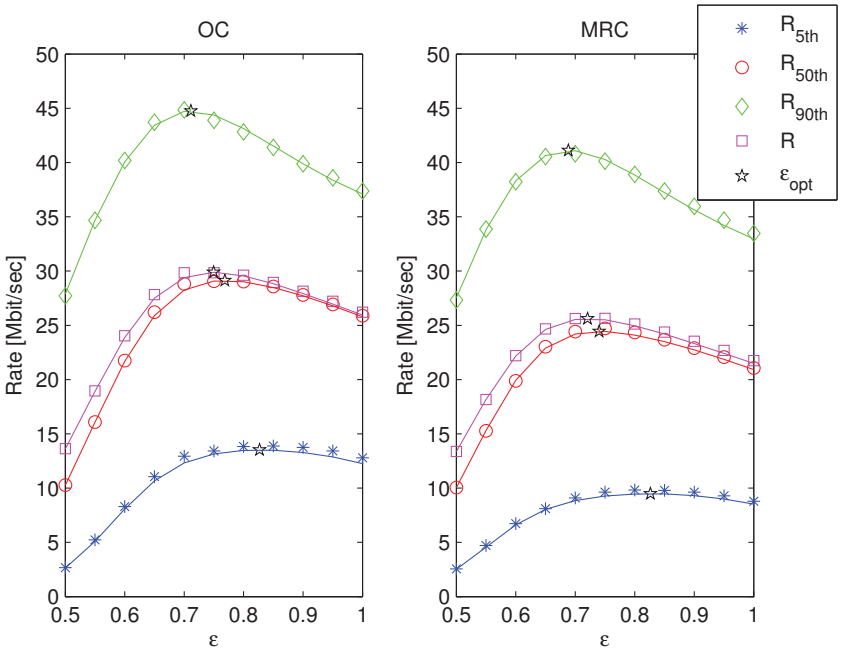

Figure 4.3: Percentile and average rate of OC and MRC as a function of ε. Solid lines show the proposed framework and markers show Monte Carlo simulations. Setup: single-tier network and $P_{\max}=\infty$. Other parameters are in Section 4.6. ★ denotes the rate corresponding to ε_{opt} computed as discussed in Section 4.5.

In Fig. 4.5, we study the average power consumption of the typical MT by assuming the same setup as in Figs. 4.3 and 4.4. We note that the average power consumption for $P_{\max}=\infty$ and $P_{\max}=30$ dBm is different only for large values of ε. This highlights the non-intuitive trend that having a finite limit of $P_{\max}$ has a beneficial impact on both the average rate, which increases, and on the average power consumption, which does not increase without any bounds. The reason is as follows. In interference-limited cellular networks, keeping the other-cell interference under control is critical: letting the MTs increase, without bound, their transmit power by increasing ε, on the other hand, boosts the other-cell interference. Identifying the optimal operating point as a function of the quintuplet of parameters $(P_{\max}, P_0, P_\infty, \alpha_\kappa, \varepsilon)$ is, however, a non-trivial problem. The proposed mathematical frameworks provide a flexible tool towards this end.

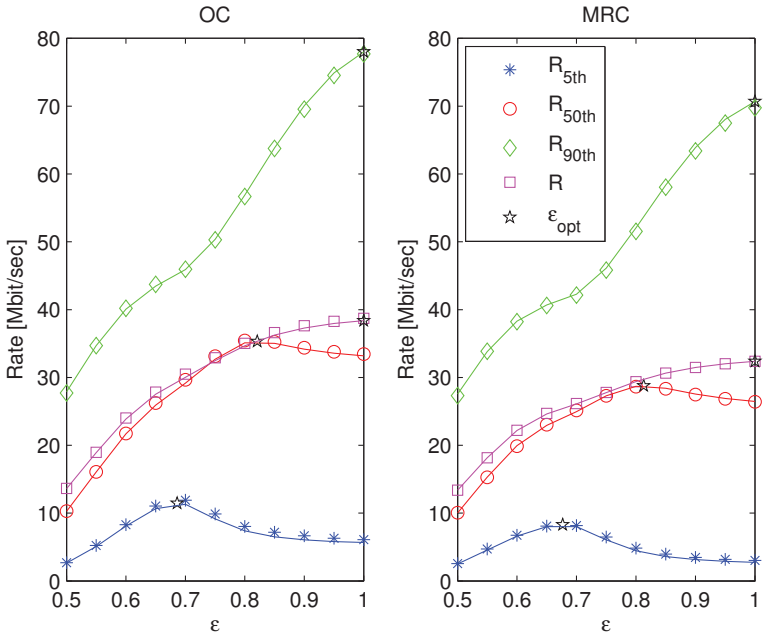

Figure 4.4: Percentile and average rate of OC and MRC as a function of ε. Solid lines show the proposed framework and markers show Monte Carlo simulations. Setup: single-tier network and $P_{\max} = 30$ dBm. Other parameters are in Section 4.6. ★ denotes the rate corresponding to ε_{opt} computed as discussed in Section 4.5.

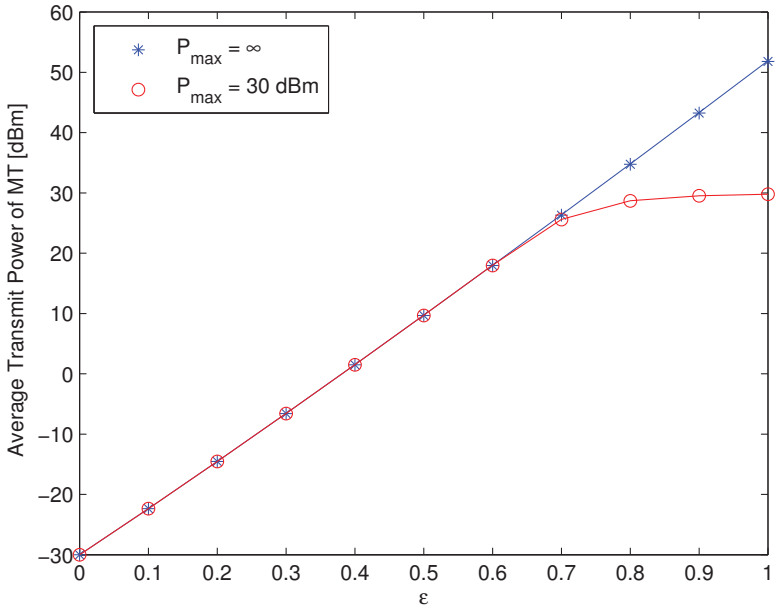

Figure 4.5: Average transmit power of the typical MT as a function of ε. Solid lines show the proposed mathematical framework and markers show Monte Carlo simulations. The framework is obtained by computing the expectation from the CDF in *Lemma 4.4*: $\mathbb{E}\{\tilde{\mathscr{P}}_{1,0}\} = \int_0^\infty \left(1 - F_{\tilde{\mathscr{P}}_{1,0}}(x)\right) dx$. The setup is the same as in Fig. 4.3 and Fig. 4.4 for $P_{\max} = \infty$ and $P_{\max} = 30$ dBm, respectively.

Impact of Receive Antennas (N_1): MRC versus OC Figures 4.6 and 4.7 confirm the trends in *Remarks 4.13, 4.14, 4.20, 4.21*: i) the rate increases as N_1 increases; ii) for small values of ε, MRC and OC provide similar rates. This is because the system is close to be noise-limited and there is no difference between MRC and OC. As ε increases, the other-cell interference becomes dominant and OC outperforms MRC; iii) MRC is incapable of reaching the noise-limited regime for large values of ε and if $N_1 < \infty$, since the other-cell interference is independent of N_1; and iv) as N_1 increases, OC reaches the noise-limited regime faster for smaller values of ε. In conclusion, OC is to be preferred to MRC if ε is not too small.

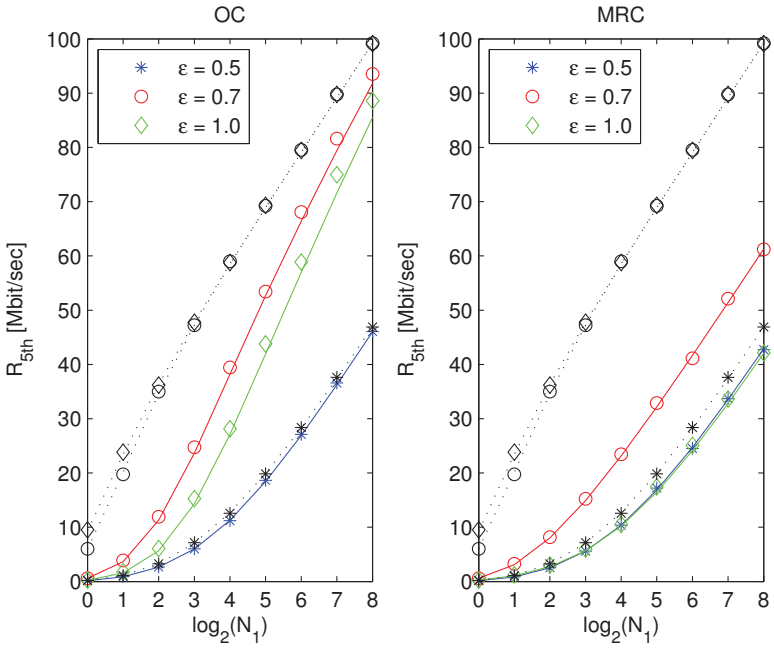

Figure 4.6: 5th percentile rate of OC and MRC as a function of the number of receive antennas (N_1). Solid lines show the proposed mathematical framework and markers show Monte Carlo simulations. Dotted lines (computed by using *Corollary 4.19*) and related markers show the noise-limited asymptote, *i.e.*, the other-cell interference is neglected. Setup: single-tier network and $P_{\max} = 30$ dBm. Other parameters are in Section 4.6. The optimal setup corresponding to ε_{opt} can be computed as discussed in Section 4.5. It turns out to be close to 0.7 for both MRC and OC. Thus, it is not shown for ease of readability.

System-Level Optimization Finally, we show numerical results obtained by applying the optimization algorithm of Section 4.5 to a two-tier cellular network. The objective is to compute the optimal values of $\hat{\mathcal{T}}$ and ε. For simplicity, the iterative algorithm in *Remark 4.22* is used. The optimal pair $(\hat{\mathcal{T}}_{\text{opt}}, \varepsilon_{\text{opt}})$ is provided in Table 4.1 and the corresponding rate is shown in Fig. 4.8. The main takeaway message is that the optimal operating point heavily depends on the path-loss exponents and that it is different for cell-center and cell-edge MTs. The results in Table 4.1 can be explained as follows. The other-cell interference decreases as the path-loss exponent increases. Thus, the best operating setup is obtained by letting the

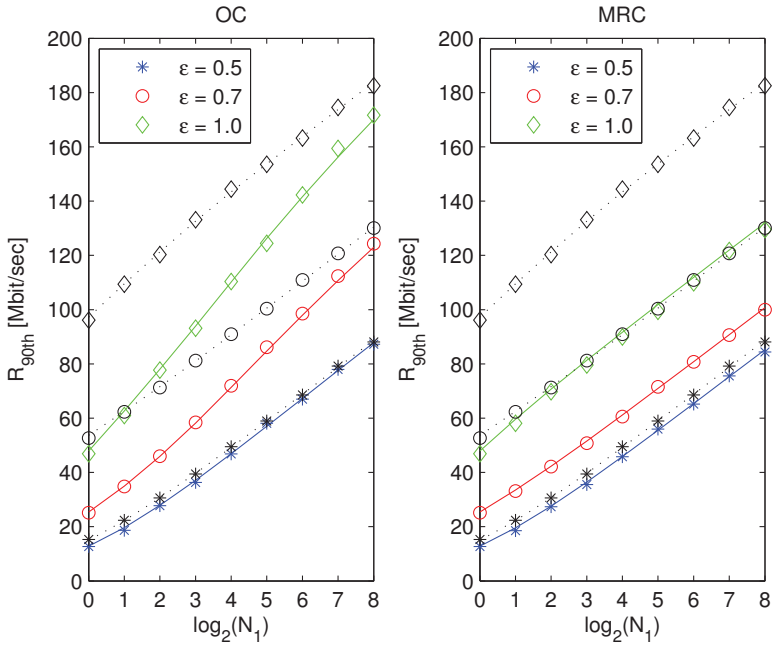

Figure 4.7: 90th percentile rate of OC and MRC as a function of the number of receive antennas (N_1). Setup: same as in Fig. 4.6. ε_{opt} turns out to be 1 for both MRC and OC.

MTs to be served by the tier with the biggest path-loss exponent. If the path-loss exponents of the two tiers are the same, the best setup is to force the cell-center MTs to be served by the tier with the smallest density of BSs (tier-1 in our case, *i.e.*, $\hat{\mathcal{T}}_{\text{opt}} \ll 1$) and the cell-edge MTs to be served by the BS providing the smallest path-loss with shadowing (*i.e.*, $\hat{\mathcal{T}}_{\text{opt}} = 1$). In our system model, in fact, each BS has a MT to serve (saturated traffic conditions). If $\hat{\mathcal{T}}_{\text{opt}} \ll 1$, the MTs served by tier-2 need to be very close to their serving BSs, to compensate for the small value of $\mathcal{T}_2$. As for cell-center MTs, this implies that they have a good probe link and are subject to a small other-cell interference, since the other MTs of tier-2 are close to their serving BSs as well. The MTs tagged to tier-1, on the other hand, may be far from their serving BSs but the number of active MTs is smaller than that in tier-2, since $\lambda_1^{(\text{BS})} < \lambda_2^{(\text{BS})}$. For cell-center MTs, in any case, this distance is not that large. As for cell-edge MTs, things are different: the rate increases by guaranteeing a high-quality intended link and by making power control less aggressive. This is usually realized by serving these MTs via the BS providing the smallest path-loss with shadowing (in agreement with [50]) and by keeping $\varepsilon < 1$.

In general, it is very difficult to "guess" the trends of uplink heterogeneous cellular networks. They, in fact, depend on a large number of parameters and may be different for cell-center and cell-edge MTs (see, *e.g.*, $\text{R}_{5\text{th}}$ in Table 4.1 for $(\alpha_1, \alpha_2) = (3.75, 3.25)$). The proposed mathematical frameworks are, however, accurate and flexible enough for identifying the optimal operating point at an affordable computational complexity.

Table 4.1: Optimal pair $(\hat{\mathcal{T}}_{\text{opt}}, \varepsilon_{\text{opt}})$ corresponding to the case studies of Fig. 4.8. The setup is the same as that in Fig. 4.8.

	$(\alpha_1, \alpha_2) = (3.5, 3.5)$	$(\alpha_1, \alpha_2) = (3.25, 3.75)$	$(\alpha_1, \alpha_2) = (3.75, 3.25)$
$\mathsf{R}_{5\text{th}}$	$(0\,\text{dB}, 0.765)$	$(36\,\text{dB}, 0.704)$	$(36\,\text{dB}, 0.799)$
R	$(-41.795\,\text{dB}, 1)$	$(36\,\text{dB}, 1)$	$(-47.923\,\text{dB}, 1)$
$\mathsf{R}_{90\text{th}}$	$(-42.223\,\text{dB}, 1)$	$(36\,\text{dB}, 1)$	$(-54\,\text{dB}, 1)$

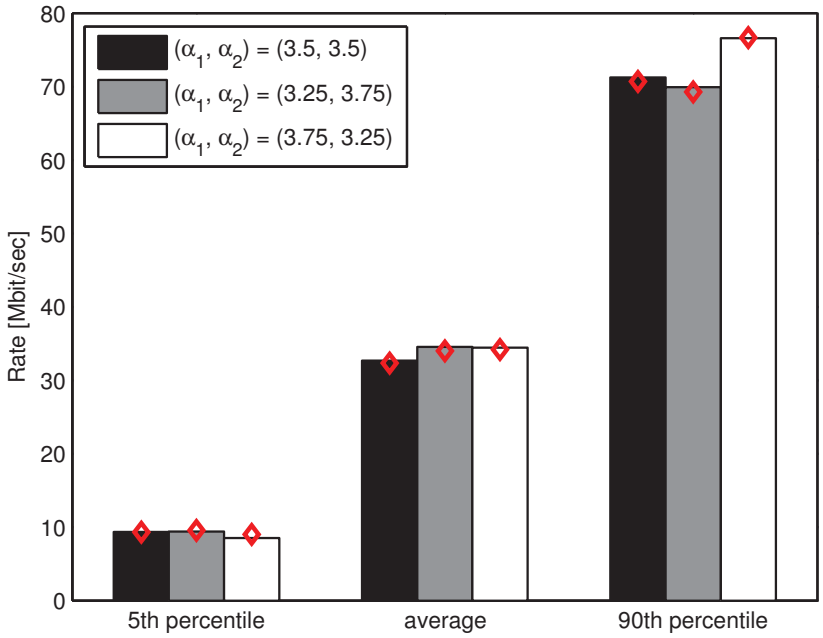

Figure 4.8: Percentile and average rate of a two-tier cellular network corresponding to the optimal pair $(\hat{\mathcal{T}}_{\text{opt}}, \varepsilon_{\text{opt}})$. These optimal parameters are provided in Table 4.1 and are computed by using the iterative algorithm discussed in *Remark 4.22*, by setting $\hat{\mathcal{T}}_{\text{min}} = -54$dB, $\hat{\mathcal{T}}_{\text{max}} = 36$dB and $\varepsilon \in [0,1]$ as the search space. The marker shows the corresponding rates obtained by using Monte Carlo simulations. Setup: two-tier network, $\lambda_2^{(\text{BS})} = 4\lambda_1^{(\text{BS})}$, MRC and $P_{\text{max}} = 30$ dBm. Other parameters are in Section 4.6. Except for $\lambda_2^{(\text{BS})}$ and α_2, all the other parameters of tier-2 are the same as those of tier-1.

4.7 Conclusion

Mathematical frameworks for computing coverage and rate of uplink heterogeneous cellular networks with multiple BSs antennas are introduced. They are formulated in terms of integral but mathematically and computationally tractable expressions, which reduce to closed-form formulas for some particular but relevant system setups. Coverage and rate are shown to depend on a large number of system parameters, which leads to a non-trivial optimization

of the uplink of cellular networks. The proposed frameworks provide an analytical tool that facilitates analysis and design of cellular systems by avoiding system-level simulations, whose complexity, computational time and accuracy depend on the system setup being considered. More specifically,

- For both MRC and OC receivers, the coverage and rate performance improves as the number of BSs antennas increases.
- For both MRC and OC receivers, fewer BSs antennas are needed to enter into the massive MIMO regime as the path-loss exponent and the power control compensation factor increases and decreases, respectively.
- OC outperforms MRC when the other-cell interference becomes dominant and the gain is more noticeable as the power control mechanism becomes more aggressive, for example, with larger values of ε and the number of BSs antennas increases but is finite.
- OC reaches the noise-limited regime by increasing the number of BSs antennas and MRC is incapable of reaching the noise-limited regime for large values of ε when the number of BSs antennas increases but is finite.
- The optimum power control compensation factor to maximize the coverage and rate performance exists and can be found by the proposed numerical optimization method. It is usually different and sensitive to other system parameters, like $P_{\max}$.
- The optimum power control compensation factors to maximize the cell-edge and cell-center performance are usually different. Thus, intra-cell power control mechanisms may be adopted for providing a more uniform quality of service to every MT within a cell.
- In multi-tier uplink heterogeneous cellular networks, optimal pair $\left(\hat{\mathcal{T}}_{\text{opt}}, \varepsilon_{\text{opt}}\right)$ exists and can be obtained by the proposed iterative optimization algorithm.
- The optimal pair usually heavily depends on the path-loss exponents and it is different for cell-center and cell-edge MTs.
- If the path-loss exponents of the two tiers are different, the best operating setup is to be served by the tier with the biggest path-loss exponent.
- If the path-loss exponents of the two tiers are the same, the best setup is to force the cell-center MTs to be served by the tier with the smallest density of BSs and the cell-edge MTs to be served by the BS providing the smallest path-loss with shadowing.

4.8 Appendices

4.8.1 Proof of Proposition 4.1

Let the SINR in (4.14). Let us introduce the notation $\mathscr{U}_{\kappa,0} = \mathscr{U}_{\kappa,0}\left(\tilde{R}_{\kappa,0}, \gamma_{\kappa,0}\right) = \mathscr{U}_{\kappa,0}^{(P_0)}\left(\tilde{R}_{\kappa,0}, \gamma_{\kappa,0}\right) + \mathscr{U}_{\kappa,0}^{(P_\infty)}\left(\tilde{R}_{\kappa,0}, \gamma_{\kappa,0}\right)$, where $\mathscr{U}_{\kappa,0}^{(P_0)}\left(\tilde{R}_{\kappa,0}, \gamma_{\kappa,0}\right) = P_0 \rho_0^{-1} \tilde{R}_{\kappa,0}^{\alpha_\kappa(\varepsilon-1)} \gamma_{\kappa,0} \mathbb{1}\left(\tilde{R}_{\kappa,0} \leq \left(\frac{P_{\max}}{P_0}\right)^{1/(\alpha_\kappa \varepsilon)}\right)$ as well as $\mathscr{U}_{\kappa,0}^{(P_\infty)}\left(\tilde{R}_{\kappa,0}, \gamma_{\kappa,0}\right) = P_\infty \rho_0^{-1} \tilde{R}_{\kappa,0}^{-\alpha_\kappa} \gamma_{\kappa,0} \mathbb{1}\left(\tilde{R}_{\kappa,0} > \left(\frac{P_{\max}}{P_0}\right)^{1/(\alpha_\kappa \varepsilon)}\right)$. Let $\mathscr{A}_\kappa = \Pr\{\mathscr{X}_\kappa\}$. Since the events $\mathbb{1}\left(\tilde{R}_{\kappa,0} \leq \left(\frac{P_{\max}}{P_0}\right)^{1/(\alpha_\kappa \varepsilon)}\right)$ and $\mathbb{1}\left(\tilde{R}_{\kappa,0} > \left(\frac{P_{\max}}{P_0}\right)^{1/(\alpha_\kappa \varepsilon)}\right)$ are incompatible, from (4.5), we have:

$$
\begin{aligned}
&\mathsf{P}_{\mathrm{cov}}(\boldsymbol{\tau}) \\
&= \sum_{\kappa=1}^{\mathscr{K}} \mathscr{A}_\kappa \mathbb{E}_{\tilde{R}_{\kappa,0}} \left\{ \mathbb{E}_{\gamma_{\kappa,0}} \left\{ \Pr\left\{ \mathscr{I}_{\kappa,\kappa}^{\backslash 0} + \sum_{k \neq \kappa = 1}^{\mathscr{K}} \mathscr{I}_{\kappa,k} < \mathscr{U}_{\kappa,0}^{(P_0)}\left(\tilde{R}_{\kappa,0}, \gamma_{\kappa,0}\right) \middle/ \tau_\kappa - \sigma_N^2 \middle| \mathscr{X}_\kappa, \tilde{R}_{\kappa,0}, \gamma_{\kappa,0} \right\} \right\} \right\} \\
&+ \sum_{\kappa=1}^{\mathscr{K}} \mathscr{A}_\kappa \mathbb{E}_{\tilde{R}_{\kappa,0}} \left\{ \mathbb{E}_{\gamma_{\kappa,0}} \left\{ \Pr\left\{ \mathscr{I}_{\kappa,\kappa}^{\backslash 0} + \sum_{k \neq \kappa = 1}^{\mathscr{K}} \mathscr{I}_{\kappa,k} < \mathscr{U}_{\kappa,0}^{(P_\infty)}\left(\tilde{R}_{\kappa,0}, \gamma_{\kappa,0}\right) \middle/ \tau_\kappa - \sigma_N^2 \middle| \mathscr{X}_\kappa, \tilde{R}_{\kappa,0}, \gamma_{\kappa,0} \right\} \right\} \right\}
\end{aligned}
\tag{4.38}
$$

From (4.38), (4.16) follows by applying the Gil-Pelaez inversion theorem [54]. In particular, the expectation with respect to $\gamma_{\kappa,0} \sim \mathrm{Gamma}(N_\kappa, N_\kappa \Omega_\kappa)$ follows from the identity $\mathscr{M}_{\gamma_{\kappa,0}}(s) = \mathbb{E}_{\gamma_{\kappa,0}}\left\{\exp\left(-s\gamma_{\kappa,0}\right)\right\} = \left(1 + s/\Omega_\kappa\right)^{-N_\kappa}$. The identity

$$
\mathbb{E}_{\tilde{R}_{\kappa,0}} \left\{ \mathbb{1}\left(\tilde{R}_{\kappa,0} \leq \left(\frac{P_{\max}}{P_0}\right)^{1/(\alpha_\kappa \varepsilon)}\right) \right\} + \mathbb{E}_{\tilde{R}_{\kappa,0}} \left\{ \mathbb{1}\left(\tilde{R}_{\kappa,0} > \left(\frac{P_{\max}}{P_0}\right)^{1/(\alpha_\kappa \varepsilon)}\right) \right\} = 1
$$

is used as well. Finally, it is taken into account that the other-cell interferences of different tiers of BSs are independent. To complete the proof, the CFs of $\mathscr{I}_{\kappa,\kappa}^{\backslash 0}$ and $\mathscr{I}_{\kappa,k}$ are computed in what follows. Let $\mathscr{I}_{\kappa,\kappa}^{\backslash 0}$ in (4.15). Let us introduce the RVs $\mathscr{I}_{\kappa,\kappa}^{\backslash 0,P_0}$ and $\mathscr{I}_{\kappa,\kappa}^{\backslash 0,P_\infty}$ such that $\mathscr{I}_{\kappa,\kappa}^{\backslash 0} = \mathscr{I}_{\kappa,\kappa}^{\backslash 0,P_0} + \mathscr{I}_{\kappa,\kappa}^{\backslash 0,P_\infty}$, where:

$$
\begin{aligned}
\mathscr{I}_{\kappa,\kappa}^{\backslash 0,P_0} &= \sum_{\mathrm{MT}_i \in \tilde{\Phi}_\kappa^{(\mathrm{MT})} \backslash \mathrm{MT}_0} P_0 \rho_0^{-1} \tilde{R}_{\kappa,i}^{\alpha_\kappa \varepsilon} D_{\kappa,i}^{-\alpha_\kappa} \gamma_{\kappa,i} \mathbb{1}\left(D_{\kappa,i} > \tilde{R}_{\kappa,i}\right) \mathbb{1}\left(\tilde{R}_{\kappa,i} \leq \left(\frac{P_{\max}}{P_0}\right)^{1/(\alpha_\kappa \varepsilon)}\right) \\
\mathscr{I}_{\kappa,\kappa}^{\backslash 0,P_\infty} &= \sum_{\mathrm{MT}_i \in \tilde{\Phi}_\kappa^{(\mathrm{MT})} \backslash \mathrm{MT}_0} P_\infty \rho_0^{-1} D_{\kappa,i}^{-\alpha_\kappa} \gamma_{\kappa,i} \mathbb{1}\left(D_{\kappa,i} > \tilde{R}_{\kappa,i}\right) \mathbb{1}\left(\tilde{R}_{\kappa,i} > \left(\frac{P_{\max}}{P_0}\right)^{1/(\alpha_\kappa \varepsilon)}\right)
\end{aligned}
\tag{4.39}
$$

By definition of CF, the following holds:

$$
\psi_{\mathscr{I}_{\kappa,\kappa}^{\backslash 0}}(\omega) = \mathbb{E}_{\mathscr{I}_{\kappa,\kappa}^{\backslash 0}}\left\{\exp\left\{j\omega \mathscr{I}_{\kappa,\kappa}^{\backslash 0}\right\}\right\} \overset{(a)}{=} \mathbb{E}_{\mathscr{I}_{\kappa,\kappa}^{\backslash 0,P_0}}\left\{\exp\left\{j\omega \mathscr{I}_{\kappa,\kappa}^{\backslash 0,P_0}\right\}\right\} \mathbb{E}_{\mathscr{I}_{\kappa,\kappa}^{\backslash 0,P_\infty}}\left\{\exp\left\{j\omega \mathscr{I}_{\kappa,\kappa}^{\backslash 0,P_\infty}\right\}\right\} \tag{4.40}
$$

where (a) follows from *Assumption 4.1, i.e.*, the set of active MTs is a PPP and their locations are independent. Let us focus our attention on $\mathbb{E}_{\mathscr{I}_{\kappa,\kappa}^{\backslash 0,P_0}}\left\{\exp\left\{j\omega \mathscr{I}_{\kappa,\kappa}^{\backslash 0,P_0}\right\}\right\}$. The following equalities

hold:

$$\begin{aligned}
&\mathbb{E}_{\mathscr{I}_{\kappa,\mathcal{K}}^{\setminus 0,P_0}}\left\{\exp\left\{j\omega\mathscr{I}_{\kappa,\mathcal{K}}^{\setminus 0,P_0}\right\}\right\}\\
&\overset{(b)}{=}\exp\left(-2\pi\bar{\lambda}_{\kappa}^{(S,\alpha)}\mathbb{E}_{\tilde{R}_{\kappa,i},\gamma_{\kappa,i}}\left\{\mathbb{1}\left(\tilde{R}_{\kappa,i}\leq\left(\frac{P_{\max}}{P_0}\right)^{1/(\alpha_\kappa\varepsilon)}\right)\int_{\tilde{R}_{\kappa,i}}^{+\infty}\left(1-\exp\left(j\omega\frac{P_0\tilde{R}_{\kappa,i}^{\alpha_\kappa\varepsilon}}{\rho_0 y^{\alpha_\kappa}}\gamma_{\kappa,i}\right)\right)ydy\right\}\right)\\
&\overset{(c)}{=}\exp\left(\pi\bar{\lambda}_{\kappa}^{(S,\alpha)}\mathbb{E}_{\tilde{R}_{\kappa,i},\gamma_{\kappa,i}}\left\{\tilde{R}_{\kappa,i}^2\left(1-{}_1F_1\left(-\frac{2}{\alpha_\kappa};1-\frac{2}{\alpha_\kappa};j\omega\frac{P_0\tilde{R}_{\kappa,i}^{\alpha_\kappa\varepsilon}}{\rho_0\tilde{R}_{\kappa,i}^{\alpha_\kappa}}\right)\right)\right\}\mathbb{1}\left(\tilde{R}_{\kappa,i}\leq\left(\frac{P_{\max}}{P_0}\right)^{1/(\alpha_\kappa\varepsilon)}\right)\right)\\
&\overset{(d)}{=}\exp\left(\pi\bar{\lambda}_{\kappa}^{(S,\alpha)}\mathbb{E}_{\tilde{R}_{\kappa,i}}\left\{\tilde{R}_{\kappa,i}^2\left(1-{}_2F_1\left(-\frac{2}{\alpha_\kappa},1;1-\frac{2}{\alpha_\kappa};j\omega\frac{P_0}{\rho_0}\Omega_\kappa\tilde{R}_{\kappa,i}^{\alpha_\kappa(\varepsilon-1)}\right)\right)\mathbb{1}\left(\tilde{R}_{\kappa,i}\leqslant\left(\frac{P_{\max}}{P_0}\right)^{1/(\alpha_\kappa\varepsilon)}\right)\right\}\right)
\end{aligned}\tag{4.41}$$

where (b) follows from *Assumption 4.1* and *Lemma 4.5*, by applying the Probability Generating Functional Theorem (PGFL) [16], (c) follows with the aid of the notable integral

$$\int_{\tilde{R}_{\kappa,i}}^{+\infty}\left(1-\exp\left(j\omega\mathscr{C}\tilde{R}_{\kappa,i}^{\upsilon_\kappa}y^{-\alpha_\kappa}\right)\right)ydy=\left(\tilde{R}_{\kappa,i}^2\big/2\right)\left({}_1F_1\left(-\frac{2}{\alpha_\kappa};1-\frac{2}{\alpha_\kappa};j\omega P_0\rho_0^{-1}\tilde{R}_{\kappa,i}^{\alpha_\kappa(\varepsilon-1)}\gamma_{\kappa,i}\right)-1\right),$$

and (d) follows from $\gamma_{\kappa,i}\sim\text{Gamma}\,(1,\Omega_\kappa)$ and the equality $\mathbb{E}_{\gamma_{\kappa,i}}\left\{{}_1F_1\left(-2/\alpha_\kappa;1-2/\alpha_\kappa;\mathscr{C}\gamma_{\kappa,i}\right)\right\}$ $={}_2F_1\left(-2/\alpha_\kappa,1;1-2/\alpha_\kappa;\mathscr{C}\Omega_\kappa\right)$ [109, Eq. (8)]. The second term can be computed using the same approach. Similar steps can be applied for the computation of the CF of $\mathscr{I}_{\kappa,k}$. The proof follows with the aid of some algebraic manipulations and simplifications.

4.8.2 Proof of Proposition 4.3

Consider a given spatial realization of BSs and MTs. Assume that the probe MT is served by the κth tier of BSs. Let $N_{I,\kappa}=\text{card}\left\{\bar{\Phi}_{\kappa}^{(\text{MT})}\setminus\text{MT}_0\right\}$ and $N_{I,k}=\text{card}\left\{\bar{\Phi}_{k}^{(\text{MT})}\right\}$ be the number of intra- and inter-tier interferers for $k\neq\kappa=1,2,\ldots,\mathcal{K}$, respectively. Let $\mathbb{E}_{\text{PPP}}\{\cdot\}$ denote the expectation with respect to the entire spatial realization of interfering MTs, *i.e.*, with respect to the RVs $N_{I,\kappa}$, $\tilde{R}_{\kappa,i}$, $\tilde{R}_{k,i}$, $D_{\kappa,i}$, $D_{\kappa,k,i}$ and $\tilde{R}_{\kappa,0}$. Let $\mathbb{E}_{\text{PPP}\setminus\tilde{R}_{\kappa,0}}\{\cdot\}$ denote the same expectation, but by keeping $\tilde{R}_{\kappa,0}$ fixed. In Rayleigh fading channels, the coverage probability of OC can be formulated as $\mathsf{P}_{\text{cov}}(\tau_\kappa|\mathscr{X}_\kappa,\text{PPP})=\mathscr{L}_\kappa\left(\tilde{R}_{\kappa,0}^{\alpha_\kappa(\varepsilon-1)};\tau_\kappa,P_0\middle|\text{PPP}\right)+\mathscr{L}_\kappa\left(\tilde{R}_{\kappa,0}^{-\alpha_\kappa};\tau_\kappa,P_\infty\middle|\text{PPP}\right)$ [98, Eqs. (11)-(13)], where:

$$\mathscr{L}_\kappa\left(x;\tau_\kappa,p\middle|\text{PPP}\right)=\exp\left(-\frac{\tau_\kappa\sigma_N^2}{p\rho_0^{-1}\Omega_\kappa x}\right)\sum_{l=1}^{N_\kappa}\frac{\mathscr{J}_{l,\kappa}^{(p)}(x;\tau_\kappa|\text{PPP})}{(l-1)!}\left(\frac{\tau_\kappa\sigma_N^2}{p\rho_0^{-1}\Omega_\kappa x}\right)^{l-1}\tag{4.42}$$

$$\mathscr{J}_{l,\kappa}^{(p)}(x;\tau_\kappa|\text{PPP})=\begin{cases}1 & \text{if}\quad N_\kappa\geq\sum_{k=1}^{\mathcal{K}}N_{I,k}+l\\ \left(1+\sum_{m=1}^{N_\kappa-l}\vartheta_m^{(p)}\tau_\kappa^m\right)/\Upsilon_\kappa^{(p)}(x;\tau_\kappa) & \text{if}\quad N_\kappa<\sum_{k=1}^{\mathcal{K}}N_{I,k}+l\end{cases}\tag{4.43}$$

as well as $\mathrm{Y}_{\kappa}^{(p)}(x;\tau_{\kappa}) = \prod_{k=1}^{\mathscr{K}}\prod_{i=1}^{N_{I,k}}\left(1+\tilde{\mathscr{I}}_{\kappa,k,i}^{(P_0)}\left(p\rho_0^{-1}x\right)^{-1}\tau_{\kappa}\right)\left(1+\tilde{\mathscr{I}}_{\kappa,k,i}^{(P_{\infty})}\left(p\rho_0^{-1}x\right)^{-1}\tau_{\kappa}\right)$, $\vartheta_r^{(p)}$ is the coefficient of τ_{κ}^r in $\mathrm{Y}_{\kappa}^{(p)}(\cdot;\cdot)$, and, letting $D_{\kappa,k,i} = D_{\kappa,i}$ for $k=\kappa$, the following two short-hands are introduced:

$$\begin{aligned}
\tilde{\mathscr{I}}_{\kappa,k,i}^{(P_0)} &= P_0\rho_0^{-1}\tilde{R}_{k,i}^{\alpha_k\varepsilon}D_{\kappa,k,i}^{-\alpha_{\kappa}}\mathbb{1}\left(D_{\kappa,k,i} > \left(\left(\frac{\mathscr{T}_{\kappa}}{\mathscr{T}_k}\right)\tilde{R}_{k,i}^{\alpha_k}\right)^{1/\alpha_{\kappa}}\right)\mathbb{1}\left(\tilde{R}_{k,i} \leq \left(\frac{P_{\max}}{P_0}\right)^{1/(\alpha_k\varepsilon)}\right)\\
\tilde{\mathscr{I}}_{\kappa,k,i}^{(P_{\infty})} &= P_{\infty}\rho_0^{-1}D_{\kappa,k,i}^{-\alpha_{\kappa}}\mathbb{1}\left(D_{\kappa,k,i} > \left(\left(\frac{\mathscr{T}_{\kappa}}{\mathscr{T}_k}\right)\tilde{R}_{k,i}^{\alpha_k}\right)^{1/\alpha_{\kappa}}\right)\mathbb{1}\left(\tilde{R}_{k,i} > \left(\frac{P_{\max}}{P_0}\right)^{1/(\alpha_k\varepsilon)}\right)
\end{aligned} \tag{4.44}$$

The rest of the proof consists of two steps: 1) computing the conditional expectation $\mathbb{E}_{\mathrm{PPP}\setminus\tilde{R}_{\kappa,0}}\{\cdot\}$ and 2) computing the expectation with respect to $\tilde{R}_{\kappa,0}$. The latter step follows immediately with the aid of $f_{\tilde{R}_{\kappa,0}}(\cdot)$ in (4.8) and it leads to the integral in (4.27). Thus, only the first step is discussed in what follows. From (4.42) and (4.43), it boils down to the computation of $\mathscr{J}_{l,\kappa}^{(p)}(x;\tau_{\kappa}) = \mathbb{E}_{\mathrm{PPP}\setminus\tilde{R}_{\kappa,0}}\left\{\mathscr{J}_{l,\kappa}^{(p)}(x;\tau_{\kappa}|\,\mathrm{PPP})\right\}$. For simplicity, let us denote the expectation with respect to the number of interferers, their distances towards their serving BSs and their distances towards the probe BS by $\mathbb{E}_{\mathbf{N_I}}\{\cdot\}$, $\mathbb{E}_{\tilde{\mathbf{R}}}\{\cdot\}$ and $\mathbb{E}_{\mathbf{D}}\{\cdot\}$, respectively. It is worth noting that $\mathrm{Y}_{\kappa}^{(p)}(\cdot;\cdot)$ and $\vartheta_m^{(p)}$ depend on $(\mathbf{N_I},\tilde{\mathbf{R}},\mathbf{D})$, *i.e.*, $\mathrm{Y}_{\kappa}^{(p)}(x;\tau_{\kappa}) = \mathrm{Y}_{\kappa}^{(p)}\left(x;\tau_{\kappa};\mathbf{N_I},\tilde{\mathbf{R}},\mathbf{D}\right)$ and $\vartheta_m^{(p)} = \vartheta_m^{(p)}\left(\mathbf{N_I},\tilde{\mathbf{R}},\mathbf{D}\right)$. As a result, we have $\mathscr{J}_{l,\kappa}^{(p)}(x;\tau_{\kappa}) = \mathbb{E}_{\mathbf{N_I}}\left\{\mathbb{E}_{\tilde{\mathbf{R}},\mathbf{D}}\left\{\mathscr{J}_{l,\kappa}^{(p)}\left(x;\tau_{\kappa}|\,\mathbf{N_I},\tilde{\mathbf{R}},\mathbf{D}\right)\right\}\right\} = \mathbb{E}_{\mathbf{N_I}}\left\{\mathscr{J}_{l,\kappa}^{(p)}(x;\tau_{\kappa}|\,\mathbf{N_I})\right\}$, where $\mathscr{J}_{l,\kappa}^{(p)}(x;\tau_{\kappa}|\,\mathbf{N_I}) = \mathbb{E}_{\tilde{\mathbf{R}},\mathbf{D}}\left\{\mathscr{J}_{l,\kappa}^{(p)}\left(x;\tau_{\kappa}|\,\mathbf{N_I},\tilde{\mathbf{R}},\mathbf{D}\right)\right\}$. From (4.43), we obtain $\mathscr{J}_{l,\kappa}^{(p)}(x;\tau_{\kappa}|\,\mathbf{N_I}) = \mathbb{1}\left(N_{\kappa} \geq \sum_{k=1}^{\mathscr{K}}N_{I,k}+l\right) + \bar{\mathscr{J}}_{l,\kappa}^{(p)}(x;\tau_{\kappa}|\,\mathbf{N_I})\,\mathbb{1}\left(N_{\kappa} < \sum_{k=1}^{\mathscr{K}}N_{I,k}+l\right)$, where:

$$\begin{aligned}
&\bar{\mathscr{J}}_{l,\kappa}^{(p)}(x;\tau_{\kappa}|\,\mathbf{N_I})\\
&= \mathbb{E}_{\tilde{\mathbf{R}},\mathbf{D}}\left\{1\Big/\mathrm{Y}_{\kappa}^{(p)}\left(x;\tau_{\kappa};\mathbf{N_I},\tilde{\mathbf{R}},\mathbf{D}\right)\right\} + \sum_{m=1}^{N_{\kappa}-l}\tau_{\kappa}^m\mathbb{E}_{\tilde{\mathbf{R}},\mathbf{D}}\left\{\vartheta_m^{(p)}\left(\mathbf{N_I},\tilde{\mathbf{R}},\mathbf{D}\right)\Big/\mathrm{Y}_{\kappa}^{(p)}\left(x;\tau_{\kappa};\mathbf{N_I},\tilde{\mathbf{R}},\mathbf{D}\right)\right\}\\
&\overset{(a)}{=} \prod_{k=1}^{\mathscr{K}}\left(\Delta_{\kappa,k}^{(p)}(x;\tau_{\kappa})\right)^{N_{I,k}} + \sum_{m=1}^{N_{\kappa}-l}\tau_{\kappa}^m\left[\sum_{m_1=0}^{m}\sum_{m_2=0}^{m}\cdots\sum_{m_{\mathscr{K}}=0}^{m}\mathbb{1}\left(\sum_{k=1}^{\mathscr{K}}m_k=m\right)\prod_{k=1}^{\mathscr{K}}\frac{\mathrm{X}_{\kappa,k,m_k}^{(p)}\left(x;\tau_{\kappa};N_{I,k}\right)}{m_k!}\right]
\end{aligned} \tag{4.45}$$

with

$$\begin{aligned}
\mathrm{X}_{\kappa,k,m_k}^{(p)}\left(x;\tau_{\kappa};N_{I,k}\right) &= \left((N_{I,k})!/(N_{I,k}-m_k)!\right)\left(1-\Delta_{\kappa,k}^{(p)}(x;\tau_{\kappa})\right)^{m_k}\left(\Delta_{\kappa,k}^{(p)}(x;\tau_{\kappa})\right)^{N_{I,k}-m_k}\\
\Delta_{\kappa,k}^{(p)}(x;\tau_{\kappa}) &= \mathbb{E}_{\tilde{R}_{k,i},D_{\kappa,k,i}}\left\{1\Big/\Delta_{\kappa,k,i}^{(p)}\left(x;\tau_{\kappa};\tilde{R}_{k,i},D_{\kappa,k,i}\right)\right\}\\
\Delta_{\kappa,k,i}^{(p)}\left(x;\tau_{\kappa};\tilde{R}_{k,i},D_{\kappa,k,i}\right) &= \left(1+\tilde{\mathscr{I}}_{\kappa,k,i}^{(P_0)}\left(p\rho_0^{-1}x\right)^{-1}\tau_{\kappa}\right)\times\left(1+\tilde{\mathscr{I}}_{\kappa,k,i}^{(P_{\infty})}\left(p\rho_0^{-1}x\right)^{-1}\tau_{\kappa}\right)
\end{aligned}.$$

The equality in (a) follows because, by virtue of *Assumption 4.1*, $\tilde{R}_{k,i}$ and $D_{\kappa,k,i}$ are i.i.d. within a given tier of BSs and are independent among different tiers of BSs. In (4.45), $(\tilde{R}_{k,i},D_{\kappa,k,i})$ denotes the generic pair of distances. To complete the proof, two expectations need to be

computed:

$$\mathscr{J}_{l,\kappa}^{(p)}(x;\tau_\kappa)=\mathbb{E}_{\mathbf{N_I}}\left\{\mathscr{J}_{l,\kappa}^{(p)}(x;\tau_\kappa|\mathbf{N_I})\right\};\ \Delta_{\kappa,k}^{(p)}(x;\tau_\kappa)=\mathbb{E}_{\tilde{R}_{k,i},D_{\kappa,k,i}}\left\{1\Big/\Delta_{\kappa,k,i}^{(p)}\left(x;\tau_\kappa;\tilde{R}_{k,i},D_{\kappa,k,i}\right)\right\}.$$

Let us start with the first. By virtue of *Assumption 4.1* and *Lemma 4.5*, the interfering MTs of the kth tier constitute a PPP of density $\bar{\lambda}_{\kappa,k}^{(S,\alpha)}$ for $k=1,2,\ldots,\mathscr{K}$. Let a generic area S_k, this implies that the number of interferers $N_{I,k}$ has distribution equal to $\Pr\{N_{I,k}\in\mathsf{S}_k\}=\exp\left(-\bar{\lambda}_{\kappa,k}^{(S,\alpha)}\mathsf{S}_k\right)\left(\bar{\lambda}_{\kappa,k}^{(S,\alpha)}\mathsf{S}_k\right)^{N_{I,k}}\Big/\left(N_{I,k}!\right)$. Furthermore, $N_{I,k}$ for $k=1,2,\ldots,\mathscr{K}$ are independent, which implies that their joint probability is the product of their marginal probabilities, *i.e.*, $\Pr\{\mathbf{N_I}|\mathbf{S}\}=\prod_{k=1}^{\mathscr{K}}\Pr\{N_{I,k}\in\mathsf{S}_k\}$. Without loss of generality, each area S_k is assumed to be an annular region with inner and outer radii equal to $D_{\min}$ and $D_{\max}$, repetitively, *i.e.*, $\mathsf{S}_k=\pi\left(D_{\max}^2-D_{\min}^2\right)$. Regardless of the spatial constraints originating from the cell association criterion in (4.1), *i.e.*, the indicator functions in (4.25), each area S_k can be arbitrary large. The inner radius $D_{\min}$, however, needs to be chosen such that $D_{\min}>\left(\left(\frac{\mathscr{T}_\kappa}{\mathscr{T}_k}\right)\tilde{R}_{k,i}^{\alpha_k}\right)^{1/\alpha_\kappa}$. In this proof, first we assume that it is finite and then we let it go to infinity, *i.e.*, $\mathsf{S}_k\to\infty$. Based on *Assumption 4.1* and *Lemma 4.5*, in addition, $D_{\kappa,k,i}$ is uniformly distributed in S_k and its PDF is equal to $f_{D_{\kappa,k,i}}(\xi)=\left(2\pi\xi/\mathsf{S}_k\right)\mathbb{1}(\xi\in\mathsf{S}_k)$. Based on this, it is apparent that $\Delta_{\kappa,k}^{(p)}(\cdot;\cdot)$ and $\mathsf{X}_{\kappa,k,m_k}^{(p)}(\cdot;\cdot;\cdot)$ in (4.45) depend on S_k, *i.e.*, $\Delta_{\kappa,k}^{(p)}(x;\tau_\kappa)=\Delta_{\kappa,k}^{(p)}(x;\tau_\kappa;\mathsf{S}_k)$ and $\mathsf{X}_{\kappa,k,m_k}^{(p)}\left(x;\tau_\kappa;N_{I,k}\right)=\mathsf{X}_{\kappa,k,m_k}^{(p)}\left(x;\tau_\kappa;N_{I,k};\mathsf{S}_k\right)$. To compute $\mathbb{E}_{\mathbf{N_I}}\left\{\mathscr{J}_{l,\kappa}^{(p)}(x;\tau_\kappa|\mathbf{N_I})\right\}$, based on (4.45), the following expectations need to be computed:

$$\begin{aligned}
\Xi_1(\mathbf{S})&=\mathbb{E}_{\mathbf{N_I}}\left\{\mathbb{1}\left(N_\kappa\geq\sum_{k=1}^{\mathscr{K}}N_{I,k}+l\right)\right\}=\sum_{N_{I,1}=0}^{+\infty}\sum_{N_{I,2}=0}^{+\infty}\cdots\sum_{N_{I,\mathscr{K}}=0}^{+\infty}\mathbb{1}\left(N_\kappa\geq\sum_{k=1}^{\mathscr{K}}N_{I,k}+l\right)\prod_{k=1}^{\mathscr{K}}\Pr\{N_{I,k}\in\mathsf{S}_k\}\\
\Xi_2(\mathbf{S})&=\mathbb{E}_{\mathbf{N_I}}\left\{\prod_{k=1}^{\mathscr{K}}\left(\Delta_{\kappa,k}^{(p)}(x;\tau_\kappa;\mathsf{S}_k)\right)^{N_{I,k}}\mathbb{1}\left(N_\kappa<\sum_{k=1}^{\mathscr{K}}N_{I,k}+l\right)\right\}\\
&=\sum_{N_{I,1}=0}^{+\infty}\sum_{N_{I,2}=0}^{+\infty}\cdots\sum_{N_{I,K}=0}^{+\infty}\mathbb{1}\left(N_\kappa<\sum_{k=1}^{\mathscr{K}}N_{I,k}+l\right)\prod_{k=1}^{\mathscr{K}}\left(\Delta_{\kappa,k}^{(p)}(x;\tau_\kappa;\mathsf{S}_k)\right)^{N_{I,k}}\Pr\{N_{I,k}\in\mathsf{S}_k\}\\
\Xi_3(\mathbf{S})&=\mathbb{E}_{\mathbf{N_I}}\left\{\prod_{k=1}^{\mathscr{K}}\mathsf{X}_{\kappa,k,m_k}^{(p)}\left(x;\tau_\kappa;N_{I,k};\mathsf{S}_k\right)\mathbb{1}\left(N_\kappa<\sum_{k=1}^{\mathscr{K}}N_{I,k}+l\right)\right\}\\
&=\sum_{N_{I,1}=0}^{+\infty}\sum_{N_{I,2}=0}^{+\infty}\cdots\sum_{N_{I,\mathscr{K}}=0}^{+\infty}\mathbb{1}\left(N_\kappa<\sum_{k=1}^{\mathscr{K}}N_{I,k}+l\right)\prod_{k=1}^{\mathscr{K}}\mathsf{X}_{\kappa,k,m_k}^{(p)}\left(x;\tau_\kappa;N_{I,k};\mathsf{S}_k\right)\Pr\{N_{I,k}\in\mathsf{S}_k\}
\end{aligned}\tag{4.46}$$

The expectations in (4.46) can be computed in closed-form with the aid of the identities $\sum_{n=0}^{N}x^n/n!=\exp(x)\,\Gamma(N+1,x)/\Gamma(N+1)$, $\sum_{n=N+1}^{+\infty}x^n/n!=\exp(x)-\exp(x)\,\Gamma(N+1,x)/\Gamma(N+1)$ and long algebraic manipulations. Due to space limitations, the details are not reported. The

final results are as follows:

$$\begin{aligned}\Xi_2(\mathbf{S}) &\overset{(b)}{=} \prod_{k=1}^{\mathscr{K}} \exp\left(-\bar{\lambda}_{\kappa,k}^{(S,\alpha)} \bar{\Delta}_{\kappa,k}^{(p)}(x;\tau_\kappa;\mathsf{S}_k)\right) \\ \Xi_3(\mathbf{S}) &\overset{(c)}{=} \prod_{k=1}^{\mathscr{K}} \exp\left(-\bar{\lambda}_{\kappa,k}^{(S,\alpha)} \bar{\Delta}_{\kappa,k}^{(p)}(x;\tau_\kappa;\mathsf{S}_k)\right) \prod_{k=1}^{\mathscr{K}} \left(\bar{\lambda}_{\kappa,k}^{(S,\alpha)} \bar{\Delta}_{\kappa,k}^{(p)}(x;\tau_\kappa;\mathsf{S}_k)\right)^{m_k}\end{aligned} \tag{4.47}$$

and $\Xi_1(\mathbf{S})|_{\mathsf{S}_1\to\infty,\mathsf{S}_2\to\infty,\ldots\mathsf{S}_{\mathscr{K}}\to\infty} \overset{(a)}{=} 0$, where $\bar{\Delta}_{\kappa,k}^{(p)}(x;\tau_\kappa;\mathsf{S}_k) = \mathsf{S}_k\left(1-\Delta_{\kappa,k}^{(p)}(x;\tau_\kappa;\mathsf{S}_k)\right)$. In (a), the limit with respect to the areas S_k for $k=1,2,\ldots,\mathscr{K}$ is computed already. This limit needs, on the other hand, to be computed in (b) and (c), *i.e.*, $\Xi_2 = \Xi_2(\mathbf{S})|_{\mathsf{S}_1\to\infty,\mathsf{S}_2\to\infty,\ldots\mathsf{S}_{\mathscr{K}}\to\infty}$ and $\Xi_3 = \Xi_3(\mathbf{S})|_{\mathsf{S}_1\to\infty,\mathsf{S}_2\to\infty,\ldots\mathsf{S}_{\mathscr{K}}\to\infty}$. So, the last step is to compute $\bar{\Delta}_{\kappa,k}^{(p)}(x;\tau_\kappa;\mathsf{S}_k)\Big|_{\mathsf{S}_k\to\infty}$ with $\Delta_{\kappa,k}^{(p)}(x;\tau_\kappa;\mathsf{S}_k) = \mathbb{E}_{\tilde{R}_{k,i},D_{\kappa,k,i}}\left\{1\Big/\Delta_{\kappa,k,i}^{(p)}\left(x;\tau_\kappa;\tilde{R}_{k,i},D_{\kappa,k,i};\mathsf{S}_k\right)\right\}$. The only expectation that needs to be explicitly computed is that with respect to $D_{\kappa,k,i}$, while that with respect to $\tilde{R}_{k,i}$ corresponds to the integral $\mathscr{O}_{\kappa,k}^{(p)}(\cdot;\cdot)$ in (4.28). The following equalities hold:

$$\begin{aligned}&\mathsf{S}_k\left(1-\mathbb{E}_{D_{\kappa,k,i}}\left\{1\Big/\Delta_{\kappa,k,i}^{(p)}\left(x;\tau_\kappa;\tilde{R}_{k,i},D_{\kappa,k,i};\mathsf{S}_k\right)\right\}\right) \\ &\overset{(a)}{=} \mathsf{S}_k\left(\int_{\xi\in\mathsf{S}_k}\left(2\pi\xi/\mathsf{S}_k\right)\left(1-1\Big/\Delta_{\kappa,k,i}^{(p)}\left(x;\tau_\kappa;\tilde{R}_{k,i},\xi;\mathsf{S}_k\right)\right)d\xi\right) \\ &\overset{(b)}{=} -\pi\left(\frac{\mathscr{T}_\kappa}{\mathscr{T}_k}\right)^{2/\alpha_\kappa}\tilde{R}_{k,i}^{2\alpha_k/\alpha_\kappa}\left(1-{}_2F_1\left(-2/\alpha_\kappa,1,1-2/\alpha_\kappa;-\left(\frac{\mathscr{T}_k}{\mathscr{T}_\kappa}\right)\left(P_0/p\right)\left(\tilde{R}_{k,i}^{\alpha_k(\varepsilon-1)}\Big/x\right)\tau_\kappa\right)\right) \\ &\quad -\pi\left(\frac{\mathscr{T}_\kappa}{\mathscr{T}_k}\right)^{2/\alpha_\kappa}\tilde{R}_{k,i}^{2\alpha_k/\alpha_\kappa}\left(1-{}_2F_1\left(-2/\alpha_\kappa,1,1-2/\alpha_\kappa;-\left(\frac{\mathscr{T}_k}{\mathscr{T}_\kappa}\right)\left(P_\infty/p\right)\left(\tilde{R}_{k,i}^{-\alpha_k}\Big/x\right)\tau_\kappa\right)\right)\end{aligned} \tag{4.48}$$

where (a) follows by definition of expectation with the aid of $f_{D_{\kappa,k,i}}(\xi) = \left(2\pi\xi/\mathsf{S}_k\right)\mathbb{1}(\xi\in\mathsf{S}_k)$ and by taking into account that $\int_{\xi\in\mathsf{S}_k}\left(2\pi\xi/\mathsf{S}_k\right)d\xi = 1$, (b) follows from (4.44) and by computing the integral with the aid of the identity

$$\int_x^{+\infty}\left(1-\left(1+b\xi^{-\nu}\right)^{-1}\right)\xi d\xi = \left(x^2/2\right)\left(1-{}_2F_1\left(-2/\nu,1,1-2/\nu;-bx^{-\nu}\right)\right).$$

The equality in (a) highlights that S_k cancels out. To get (b), in addition, the indicator function $\mathbb{1}\left(D_{\kappa,k,i} > \left(\left(\frac{\mathscr{T}_\kappa}{\mathscr{T}_k}\right)\tilde{R}_{k,i}^{\alpha_k}\right)^{1/\alpha_\kappa}\right)$ in (4.44) is taken into account, which implies $\xi\in\mathsf{S}_k \Rightarrow \xi \geq \left(\left(\frac{\mathscr{T}_\kappa}{\mathscr{T}_k}\right)\tilde{R}_{k,i}^{\alpha_k}\right)^{1/\alpha_\kappa}$. As a result, the limit $\mathsf{S}_k\to\infty$ does not have to be explicitly computed. The proof follows by inserting (4.47) and (4.48) in (4.46).

5 Conclusion and Future Work

This chapter closes the thesis with general conclusions in *Section 5.1* and summaries of future work in *Section 5.2*.

5.1 Conclusion 126

5.2 Future Work 126

5.2.1 Millimeter Wave Cellular Networks 127

5.2.2 Interference-Aware Uplink Power Control Schemes 129

5.2.3 Non-PPP Abstraction Models 130

5.1 Conclusion

Using PPP-based abstraction model and the tools provided by the stochastic geometry, this thesis performs mathematical modeling, analysis and optimization in both downlink and uplink cellular networks. More specially,

- in *chapter 2*, new mathematical frameworks to the computation of the error probability of MIMO cellular networks have been proposed for the first time and have been substantiated with the aid of Monte Carlo simulations. The frameworks are applicable for SISO cellular networks with arbitrary fading channels and spatial multiplexing MIMO cellular networks with Rayleigh fading channels in the interfering links. Exact and approximated frameworks have been developed to provide a flexible trade-off between accuracy and computational complexity. Their analysis has provided insights on the impact of SNR operating regime, the fading parameters and the number of antennas available at the BSs and MT on trends and trade-offs of the error performance.

- In *chapter 3*, new mathematical expressions for coverage and rate of cellular networks are provided with the aid of the Gil-Pelaez inversion formula. The frameworks are shown to be general enough for the analysis of different fading channels and MIMO transmission schemes. Furthermore, a partially loaded cellular networks has been studied with a little modification of the developed frameworks.

- In *chapter 4*, new mathematical frameworks for computing coverage and rate of uplink heterogeneous cellular networks with multiple BSs antennas are introduced. The mathematical frameworks show that coverage and rate depend on a large number of system parameters, which leads to a non-trivial optimization of the uplink cellular networks. Important findings include that different trends for cell-edge and cell-center MTs as a function of the power control compensation factor. Thus, intra-cell power control mechanisms may be adopted for providing a more uniform quality of service to every MT within a cell. In the interference-limited regime, OC is shown to outperform MRC as the power control mechanism becomes more aggressive and the number of BSs antennas increases but is finite.

5.2 Future Work

Many topics of interest in the field of stochastic geometry analysis of wireless and cellular networks remain open. Relying on the findings in this thesis, some of them can be readily solved. For example,

- Coverage, rate and error performance studies in the uplink/downlink heterogeneous MIMO cellular networks, which should be direct applications of mathematical findings and approaches in *Chapter2*, *Chapter3* and *Chapter4*.

- The joint optimization of uplink/downlink heterogeneous MIMO cellular networks, which should provide a deeper understanding on the uplink/downlink decoupling association as mentioned in [49, 50, 52, 53].

Some topics are related to the computational complicity, for example,

- The designs of interference-aware receiver structures. The receiver in *Chapter2* is interference-unaware. To design better receivers which are aware of the network interference, according to the simple rule of receiver design from detection and estimation theory, *e.g.*, maximum likelihood rule, requires the knowledge of the joint statistics of other-cell interference plus noise across different and correlated antennas. Although the other-cell interference in cellular networks has been correctly modeled by its CF, joint statistics, especially the joint PDF, is complicated and usually involving multi-fold integrals because it has to be computed by inverting multivariate CF and unfortunately is without any close-form solution.
- More insightful simplified/approximated mathematical frameworks towards the network designs. As developed in this thesis, commonly single-, double- , even three-fold integrals need to be numerically computed to evaluate the system performance, depending on different studied scenarios, and special functions like Hypergeometric functions and Meijer G-functions are often involved.

Besides these topics, in what follows are the possible directions to exploit the power of stochastic geometry analysis.

5.2.1 Millimeter Wave Cellular Networks

Millimeter Wave (mmWave) is believed to be one of the candidate technologies for the next generation mobile communications. The large bandwidth from 3GHz to 300GHz makes it very attractive [100, 101]. mmWave networks have been studied mainly based on the simulations and field measurements, only recently, mathematical modeling and analysis based on PPP-abstraction models and stochastic geometry has been reported in [44, 45, 46]. The major differences of mmWave networks from the conventional microwave networks are: i) the beamforming gain provided by the transmit and receive antenna arrays; 2) the propagation experiencing Line-Of-Sight (LOS) and Non-Line-Of-Sight (NLOS) links need to be appropriately modeled and may have different distributions, due to the more prominent impact of spatial blockages at mmWave frequencies. These differences prevent us to directly reuse the stochastic geometry frameworks developed for microwave transmissions. In the rest of this section, we do a review on the current state of and propose possibilities for the future work.

- Beamforming Gain Modeling. A simple model of beamforming gain can be modeled as

follows:

$$G_q(\theta) = \begin{cases} G_q^{\max} \text{if} |\theta| \leq \omega_q \text{ (mainlope)} \\ G_q^{\min} \text{if} |\theta| > \omega_q \text{ (sidelope)} \end{cases}, q \in (\text{BS}, \text{MT})$$

On the intended link, we have the maximum gain because BS will detect and align the antennas, which means $G^0 = G_{\text{BS}}^{\max} G_{\text{MT}}^{\max}$, On the non-intended link, the orientation is assumed to be random, so that G^i is a random variable with PDF available in [46]. Generalization of the antenna gain by more realistic models (for example, multiple slope model) can be one of the future work.

- Link State Modeling. The probabilities of occurrence as a function of distance r can be formulated as:

$$\begin{aligned} p_{OUT}(r) &= \max\{0, 1 - \gamma_{OUT} \exp(-\delta_{OUT} r)\} \\ p_{LOS}(r) &= \big(1 - p_{OUT}(r)\big) \gamma_{LOS} \exp(-\delta_{LOS} r) \\ p_{NLOS}(r) &= \big(1 - p_{OUT}(r)\big) \big(1 - \gamma_{LOS} \exp(-\delta_{LOS} r)\big) \end{aligned}$$

This distance dependence leads to difficulties in the mathematical formulations. Thus, ball approximations of link state have been used for simplifications. For example, one ball approximation can be described as follows [44]:

$$p_{LOS}(r) = \begin{cases} \tilde{p}_{LOS}^{[0,D_1]}, \text{if} r \leq D_1 \\ \tilde{p}_{LOS}^{[D_1,\infty]}, \text{if} r > D_1 \end{cases}, p_{NLOS}(r) = \begin{cases} \tilde{p}_{NLOS}^{[0,D_1]}, \text{if} r \leq D_1 \\ \tilde{p}_{NLOS}^{[D_1,\infty]}, \text{if} r > D_1 \end{cases}$$
$$\tilde{p}_{LOS}^{[0,D_1]} + \tilde{p}_{NLOS}^{[0,D_1]} = 1, \tilde{p}_{LOS}^{[D_1,\infty]} + \tilde{p}_{NLOS}^{[D_1,\infty]} = 1, \text{NO outage status}$$

And the BSs in LOS status and BSs in NLOS status can be modeled as thinning PPPs with different densities inside and outside the ball of radius D_1, which simplifies the system because it is then equivalent to a heterogeneous microwave network with different path loss models in each tier. Similarly, a two ball approximation has been used in [46]. Generalization of the ball approximation (for example, multiple ball approximation) can be one of the future work.

- Path Loss Modeling. The unbounded power-decay path loss model is used as $l_s(r) = (\kappa_s r)^{2b_s}, s \in (LOS, NLOS)$. It is readily to be extended to the advanced path-loss models, for example, a bounded path loss function for the link in state s can be expressed as

$$l_s(r) = \begin{cases} (\kappa_s D_0)^{2b_s}, r \leq D_0 \\ (\kappa_s r)^{2b_s}, r > D_0 \end{cases}$$

where κ is pre-defined constant, b is the amplitude path loss exponent and D_0 is introduced to avoid the singularity in the unbounded path loss model.

- Optimization Problems. It has been reported in [46] that the noise-limited approximation of mmWave cellular networks is accurate for a regular density of BSs deployments,

however, it may not be sufficiently accurate for ultra-dense network deployments and for sub-gigahertz transmission bandwidths. The future work can be on the mathematical optimization of the density of the BSs deployments.

5.2.2 Interference-Aware Uplink Power Control Schemes

As being said in *Chapter 4*, power control plays an important role in the trade-off between the coverage and rate and the power consumption of the MTs. The fractional power control mechanism that depends on the path-loss and on the maximum transmit power of the MTs introduced by 3GPP [88] has been studied in *Chapter 4*. In addition, some recent papers propose uplink power control schemes which consider the management of uplink inter-cell interference in order to improve the uplink performance [102, 103].

Let a general MT in a heterogeneous uplink cellular networks, conditioning on this MT being served by a BS of the kth tier and its transmit power $\mathscr{P}_{k,\mathrm{MT}}$, an interference-aware fractional power control mechanism can be introduced as follows:

$$\tilde{\mathscr{P}}_{k,\mathrm{MT}} = \begin{cases} P_0 \tilde{R}_{k,\mathrm{MT}}^{\alpha_k \varepsilon}, \text{ if } P_0 \tilde{R}_{k,\mathrm{MT}}^{\alpha_k \varepsilon} \leq P_{\max} \text{and} P_0 \tilde{R}_{k,\mathrm{MT}}^{\alpha_k \varepsilon} \tilde{\Lambda}_{k,\mathrm{MT}}^{-\alpha^{(I)}} \leq P_0^{(I)} \\ P_0^{(I)} \tilde{\Lambda}_{k,\mathrm{MT}}^{\alpha^{(I)}}, \text{ if } P_0 \tilde{R}_{k,\mathrm{MT}}^{\alpha_k \varepsilon} \tilde{\Lambda}_{k,\mathrm{MT}}^{-\alpha^{(I)}} > P_0^{(I)} \text{and} P_0^{(I)} \tilde{\Lambda}_{k,\mathrm{MT}}^{\alpha^{(I)}} \leq P_{\max} \\ P_\infty, \text{ if } P_0 \tilde{R}_{k,\mathrm{MT}}^{\alpha_k \varepsilon} > P_{\max} \text{and} P_0^{(I)} \tilde{\Lambda}_{k,\mathrm{MT}}^{\alpha^{(I)}} > P_{\max} \end{cases}$$

where the notation is kept consistent with the one in *Chapter 4*. In addition, $P_0^{(I)}$ denotes uplink interference PSD target, $\tilde{\Lambda}_{k,\mathrm{MT}} = \Lambda_{k,\mathrm{MT}} \big| \mathscr{X}_k$ denotes the generalized distance from a MT to its most interfered BS conditioning on this MT being served by a tier k BS, with $\Lambda_{k,\mathrm{MT}}$ denotes the generalized distance from a generic MT to its most interfered BS in the kth tier. $\alpha_k^{(I)}$ is the path loss exponent from a MT served by a tier k BS to its most interfered BS, which can be in tier k or in tier $\kappa \neq k = 1,2,...,\mathscr{K}$, *i.e.*, $\alpha_k^{(I)} = \alpha_k$ if the most interfered BS is in tier k and $\alpha_k^{(I)} = \alpha_\kappa$ if the most interfered BS is in tier $\kappa \neq k = 1,2,...,\mathscr{K}$. If a single tier network (tier κ) assumed, $\alpha_k^{(I)} = \alpha_\kappa$ and the most interfered BS is the one with the second smallest generalized distance from the MT to BSs.

The interference awareness in uplink power control allows one to keep under control the interference level caused by the MTs that transmit at very high power in order to compensate for a high path-loss. This approach is beneficial for reducing the power consumption of the MTs and the aggregate other-cell interference of the entire network.

A recent paper [115] demonstrates the advantages of interference-aware power control by extensive system-level Monte Carlo simulations. Some results from [115] are available in *Appendix B*. For example, in a single tier uplink cellular network with dual-antenna MRC receivers at BSs and parameters $\varepsilon = 1$, $P_{\max} = 70$ [dBm], $P_0^{(I)} = -100$ [dBm/Hz], compared to the fractional power control, the interference awareness leads to a 20%, 6% and 47% increase in average rate, 5th percentile rate and 90th percentile rate, respectively, as well as a 18%

reduction in MT power consumptions.

The above mentioned paper [115] also shows a non-trivial dependence of the coverage and rate performance on the quadruplet of parameters $(\varepsilon, N_R, P_{\max}, P_0^{(I)})$ which highlights the challenge of optimizing uplink cellular networks by relying only on numerical simulations. Thus, developing a mathematical framework based on stochastic geometry, is highly appreciated to solve the optimization problems of these networks.

To do the system analysis mathematically, the joint PDF of $\tilde{R}_{\kappa,\mathrm{MT}}$ and $\tilde{\Lambda}_{\kappa,\mathrm{MT}}$ needs to be characterized since they are correlated RVs. By relying on the properties of PPP, the joint PDF of $R_{\kappa,\mathrm{MT}}$ and $\Lambda_{\kappa,\mathrm{MT}}$ can be introduced as a starting point [104, 105]:

$$\begin{aligned} f_{R_{\kappa,\mathrm{MT}},\Lambda_{\kappa,\mathrm{MT}}}(x,y) &= \lim_{(\Delta x,\Delta y)\to(0,0)} \frac{\Pr\{x \le R_{\kappa,\mathrm{MT}} \le x+\Delta x, y \le \Lambda_{\kappa,\mathrm{MT}} \le y+\Delta y\}}{\Delta x \Delta y}, y > x \\ &= 4\pi^2 \left(\lambda_{\kappa}^{(S,\alpha)}\right)^2 x y \exp\left(-\pi \lambda_{\kappa}^{(S,\alpha)} y^2\right), y > x \end{aligned}$$

Future work could be carried out on the further investigations of mathematical formulations of uplink heterogeneous cellular networks based on this joint PDF and the efficient computation approaches for the additional-fold integrals led by the joint PDF.

5.2.3 Non-PPP Abstraction Models

By leveraging its nice statistic properties, the PPP-based abstraction model has been widely used to model the spatial deployments in wireless and cellular networks due to its mathematical tractability and modeling accuracy [15], however, it has some fundamental limitations. The PPP-based abstraction model assumes the mutual independence among all points in the point process, where two points could be arbitrarily close to each other. It is then not suitable for networks with repulsion, where the locations of points are spatially correlated.

In [19], the authors define other popular PPs used in modeling wireless communications systems and show the analogy between the PPs and the networks they model.

- *BPP*: A Binomial Point Process (BPP) can model the random patterns produced by a fixed number of points (N) in a set $\mathscr{B} \subset \mathbb{R}^d$with a finite Lebesgue measure $L(\mathscr{B}) < \infty$. Let $\prod = \{x_i; i = 1,2,3,...\}$ and $\prod \subset \mathscr{B}$, then $\prod$ is a BPP if the number of points inside a compact set $b \subseteq \mathscr{B}$ is a binomial random variable, and the numbers of points in disjoint sets are related via a multinomial distribution. If the total number of nodes is known and the service area is finite, then the BPP can be used to abstract the network.
- *HCPP*: A Hard Core Point Process (HCPP) is a repulsive point process where no two points of the process coexist with a separating distance less than a predefined hard core parameter r_h. A PP $\prod = \{x_i; i = 1,2,3,...\} \subset \mathbb{R}^d$ is an HCPP if and only if $\|x_i - x_j\| \ge r_h, \forall x_i, x_j \in \prod, i \ne j$ where $r_h \ge 0$ is a predefined hard core parameter. If there is a minimum distance separating the nodes due to some physical constrains, due to network

planning, or due to the MAC layer behavior, then a repulsive point process such as the Matérn HCPP can be used for modeling their spatial locations. The Matérn HCPP conditions on having a minimum distance between any two points of the process, and is obtained by applying dependent thinning to a PPP. That is, starting from a PPP, the HCPP is obtained by assigning a random mark uniformly distributed in $[0,1]$ to each point in the PPP, then deleting all points that coexist within a distance less than the hard core parameter from another point with a lower mark. Hence, only the points that have the lowest mark within their neighborhood distance are retained. As a result, no two points with a separation less than a predefined hard core parameter will coexist in the constructed HCPP.

- *PCP*: A Poisson Cluster Process (PCP) can model the random patterns produced by random clusters. The Poisson cluster process is constructed from a parent PPP $\prod = \{x_i; i = 1,2,3,...\}$ by replacing each point $x_i \in \prod$ with a cluster of points M_i, $\forall x_i \in \prod$, where the points in M_i are independently and identically distributed in the spatial domain. The PCP is used to model a network if the nodes are clustered according to certain social behavior or by the MAC protocol.

Although some of the above mentioned point process models can lead to a more realistic modeling than the PPP, the main problem is the mathematical tractability. To overcome this accuracy vs. mathematical complexity trade-off, the authors of [14] introduce the concept of "deployment gain", which allows one to carry out the analysis based on the mathematically-tractable PPP-based abstraction model, subject to a correction factor (*i.e.*, the deployment gain) that can be estimated and taken into account for a better and more accurate system design and optimization.

Until very recently, the Ginibre point process (GPP) is introduced to model the wireless networks with repulsion [106]. The GPP is one of the main examples of determinantal point processes that can be used to model random phenomena where repulsion is observed, which is a soft-core model compared to HCPP. In [106], the authors derive the mean and variance of the interference using two different approaches: the Palm measure approach and the reduced second moment approach, and then provide approximations of the interference distribution. They also find that the fitted β-GPP, which is between PPP and GPP and can closely model the deployment of actual base stations in terms of the coverage probability and other statistics.

Another notable work is [107]. The authors investigate the impact of spatial and temporal correlation on the performance in heterogeneous cellular networks which are modeled by non-PPP abstraction models. They use massive MIMO to understand the impact of spatial correlation, and use the random medium access protocol to examine the temporal correlation. Eventually, they use cooperative relay networks to illustrate the spatial-temporal correlation.

Future work could be on: i) more in-depth investigations of available statistic point processes which are more realistic than PPP while still tractable; ii) finding reasonable fittings of typical cellular networks by the approaches introduced in [14, 106]; iii) developing network

interference statistics with non-PPP abstraction models by accounting the spatial-temporal correlations identified in [107].

A Basic Properties of the Poisson Point Process

In this Appendix, the definitions, properties, and theorems related to Poisson Point Process are introduced. More information and detailed proofs can be found in notable books on stochastic geometry analysis in wireless communications and networks [16, 17, 18].

Let $\mathbb{S}$ be the set of all sequences of points in a d-dimensional Euclidean space $\mathbb{R}^d$, such that any sequence ϕ belonging to $\mathbb{S}$:

- is finite, *i.e.*, has only a finite number of points in any bounded subset of $\mathbb{R}^d$;
- is simple, *i.e.*, $x \neq y, \forall x, y \in \phi$.

A spatial point process Φ is a random, finite or countably-infinite collection of points in the space $\mathbb{R}^d$, without accumulation points.

Definition and Characterizations Consider a finite non-null measure Λ on the space $\mathbb{R}^d$.

Definition A.1 *The Poisson point process Φ of intensity measure Λ is defined by means of its finite-dimensional distributions:*

$$\Pr\{\Phi(A_1) = n_1, \Phi(A_2) = n_2, \ldots, \Phi(A_k) = n_k\} = \prod_{i=1}^{k} \exp(-\Lambda(A_1)) \frac{\Lambda(A_1)^{n_i}}{n_i!}$$

for every $k = 1, 2, \ldots$ and all bounded, mutually disjoint sets A_i for $i = 1, 2, \ldots, k$. If $\Lambda(dx) = \lambda dx$ is a multiple of Lebesgue measure (i.e. volume) in $\mathbb{R}^d$, we call Φ a homogeneous Poisson point process and $lambda$ is its intensity parameter. □

Definition A.2 *The Laplace functional $\mathscr{L}$ of a point process Φ is defined by the following formula:*

$$\mathscr{L}_\Phi(f) = \mathbb{E}\left\{\exp\left(-\int_{\mathbb{R}^d} f(x)\,\Phi(dx)\right)\right\}$$

where f runs over the set of all non-negative functions on $\mathbb{R}^d$. □

Laplace Functional A complete characterization of the distribution of a Point Process is given by its Laplace functional, which plays a similar role as the characteristic function for random variables.

Proposition A.1 *The Laplace functional $\mathscr{L}$ of a Poisson point process Φ intensity measure Λ is:*

$$\mathscr{L}_{\Phi}(f) = \exp\left(-\int_{\mathbb{R}^d}\left(1-\exp\left(-f(x)\right)\right)\Lambda(dx)\right)$$

where f runs over the set of all non-negative functions on $\mathbb{R}^d$. □

Probability Generating Functional The Probability Generating Functional (PGFL) is the equivalent of the Moment Generating Functional for Point Processes.

Definition A.3 *Let $v(x):\mathbb{R}^d \to [0,+\infty)$ be a measurable function. The PGFL of a Point Process Φ is defined by the following formula:*

$$\mathscr{G}[v] = E_{\Phi}\left\{\prod_{x\in\Phi} v(x)\right\}$$

□

Proposition A.2 *The PGFL of a Poisson point process Φ intensity measure Λ is:*

$$\mathscr{G}[v] = \exp\left(-\int_{\mathbb{R}^d}\left(1-\exp\left(-v(x)\right)\right)\Lambda(dx)\right)$$

□

PPP-invariant Operations The most attractive property of a Poisson Point Process is that many transformations and operations on it preserve the Poisson law. The concepts of superposition and thinning of a PPP are now introduced, concluding this section with the displacement theorem which involves the transformation of the Point Process from one Euclidean space to another one.

Superposition

Definition A.4 *The superposition of different Point Processes is defined as the sum $\Phi = \sum_{\mathbf{k}} \Phi_{\mathbf{k}}$, and it is still a Point Process if $\sum_k \mathbb{E}\{\Phi_k(\cdot)\}$ is a locally finite measure.* □

Proposition A.3 *The superposition of independent Poisson Point Processes with intensity measures Λ_k is a Poisson Point Process with intensity measure $\sum_k \Lambda_k$ if and only if the latter is a locally finite measure* □

Thinning

Definition A.5 *The thinning of a Point Process Φ with the retention function $p : \mathbb{R}^d \to [0,1]$ is a Point Process given by:*

$$\Phi^p(A) = \sum_k \epsilon_k \delta_{x_k}(A)$$

where the RVs $\{\epsilon_k\}$ are independent given Φ with $\Pr\{\epsilon_k = 1|\Phi\} = 1 - \Pr\{\epsilon_k = 0|\Phi\} = p(x_k)$ and $A \subset \mathbb{R}^d$. □

Proposition A.4 *The thinning of a Poisson Point Process with intensity measures Λ and the retention function p is a Poisson Point Process having intensity measure $p\Lambda$ with $(p\Lambda)(A) = \int_A p(x)\Lambda(dx)$.* □

Displacement Theorem Consider a probability kernel $p(x,B)$ from $\mathbb{R}^d$ to $\mathbb{R}^{d'}$, where $d' \geq 1$.

Theorem A.1 *The transformation of the Poisson Point Process with intensity measures Λ by a probability kernel p is the Poisson Point Process with intensity measure $\Lambda'(A) = \int_{\mathbb{R}^d} p(x,A)\Lambda(dx)$ and $A \subset \mathbb{R}^d$.* □

Palm Theory Palm theory formalizes the notion of the conditional distribution of a general point process given it has a point at some location. Note that for a point process without a fixed atom at this particular location, the probability of the condition is equal to 0 and the basic discrete definition of the conditional probability does not apply. We first define two measures associated with a general point process.

Definition A.6 *The mean measure of a Point Process Φ is the measure*

$$M(A) = \mathbb{E}\{\Phi(A)\}$$

on $\mathbb{R}^d$. The reduced Campbell measure of Φ is the measure

$$C^!(A \times Y) = \mathbb{E}\left\{\int_A \mathbb{1}(\Phi - \epsilon_x \in Y)\,\Phi(dx)\right\}$$

on $\mathbb{R}^d \times \mathbb{M}$, where $Y \subset \mathbb{M}$ and $\mathbb{M}$ denotes the set of point measures. □

Note that $M(A)$ is simply the mean number of points of Φ in A. The reduced Campbell measure $C^!(A \times Y)$ is a refinement of this mean measure; it gives the expected number of points of Φ in A such that when removing a particular point from Φ, the resulting configuration satisfies property Y. The fact that one measure is a refinement of the other, or more formally, that $C^!(\cdot \times Y)$ for each Y is absolutely continuous with respect to $M(\cdot)$, allows us to express the former as an integral of some function $\mathbb{P}^!_x$, called the Radon–Nikodym derivative with respect to the latter:

$$C^!(A \times Y) = \int_A P^!_x M(dx)$$

for all $A \subset \mathbb{R}^d$. The function $P^!_x = P^!_x(Y)$ depends on Y.

Definition A.7 *Given a point process with a locally finite mean measure, the distribution $P^!_x(\cdot)$ is called the reduced Palm distribution of Φ given a point at x.* □

Slivnyak–Mecke Theorem Slivnyak–Mecke Theorem is fundamental for the characterization of a Poisson Point Process, and has deep implications on the computational complexity for the evaluation of the aggregate interference or other performance metrics. Consider a probability kernel $p(x, B)$ from $\mathbb{R}^d$ to $\mathbb{R}^{d'}$, where $d' \geq 1$.

Theorem A.2 *Let Φ be a Poisson Point Process with intensity measures Λ. For Λ almost all $x \in \mathbb{R}^d$,*

$$\mathbb{P}^!_x(\cdot) = \Pr\{\Phi \in \cdot\}$$

that is, the reduced Palm distribution of the Poisson Point Process is equal to its (original) distribution. □

Definition A.8 *For a Poisson point process Φ one can take $\Phi^!_x = \Phi$ and $\Phi_x = \Phi + \epsilon_x$ for all $x \in \mathbb{R}^d$.* □

B Simulation Results: Interference–Aware Power Control in Uplink Cellular Networks

In this Appendix, simulation results of different uplink setups are considered in order to shed light on the effect of interference-unaware/aware fractional power control as a function of important system parameters, such as the fractional compensation factor ε, maximum MT transmit power $P_{\max}$, interference target $P_0^{(I)}$, receive-antenna number N_R and demodulators at BSs. More details are available in the author's recent conference paper [115].

- P. Guan and M. Di Renzo, " Stochastic Geometry Analysis of Uplink Cellular Networks with Multi-Antenna Base Stations and Interference-Aware Fractional Power Control", *2015 IEEE International Conference on Computing, Management and Telecommunications (ComManTel)*, to appear, Dec. 2015.

If an interference-unaware scheme is used, the transmit power of the typical MT can be formulated as follows:

$$\mathscr{P}_{\mathrm{MT}} = \begin{cases} P_0 R_{\mathrm{MT}}^{\alpha\varepsilon}, \text{ if } P_0 R_{\mathrm{MT}}^{\alpha\varepsilon} \leqslant P_{\max} \\ P_{\max}, \text{ otherwise} \end{cases}$$

where notation from *Chapter 4* is used.

If an interference-aware scheme is used, the transmit power of the typical MT can be formulated as follows.

$$\mathscr{P}_{\mathrm{MT}} = \begin{cases} P_0 R_{\mathrm{MT}}^{\alpha\varepsilon}, \text{ if } P_0 R_{\mathrm{MT}}^{\alpha\varepsilon} \leqslant P_{\max} \text{ and } P_0 R_{\mathrm{MT}}^{\alpha\varepsilon} \Lambda_{\mathrm{MT}}^{-\alpha} \leqslant P_0^{(I)} \\ P_0^{(I)} \Lambda_{\mathrm{MT}}^{\alpha}, \text{ if } P_0 R_{\mathrm{MT}}^{\alpha\varepsilon} \Lambda_{\mathrm{MT}}^{-\alpha} > P_0^{(I)} \text{ and } P_0^{(I)} \Lambda_{\mathrm{MT}}^{\alpha} \leqslant P_{\max} \\ P_{\max}, \text{ if } P_0 R_{\mathrm{MT}}^{\alpha\varepsilon} > P_{\max} \text{ and } P_0^{(I)} \Lambda_{\mathrm{MT}}^{\alpha} > P_{\max} \end{cases}$$

where $P_0^{(I)}$ denotes the maximum PSD interference level at the BS that experiences the largest interference, and Λ_{MT} denotes the generalized distance from the MT to this latter BS. In the

considered system model, Λ_{MT} denotes the second smallest generalized distance from the MT to any BSs in the network. The interference-aware power control scheme allows one to keep under control the interference level caused by the MTs that transmit at very high power in order to compensate for a high path-loss. This approach is beneficial for reducing the power consumption of the MTs and the aggregate other-cell interference of the entire network.

Let the legend "FPC" and "FPCIA" denote the fractional power control and interference–aware power control in the figures, respectively. The simulation parameters are listed in Table B.1.

Table B.1: Simulation Parameters: Interference–Aware Power Control in Uplink Cellular Networks

Bandwidth	Bw = 10 [MHz]
Free-space path-loss at 1 meter	$\rho_0 = 40$ [dB]
Path-loss exponent	$\alpha = 3.5$
BS density	$\lambda_{\mathrm{BS}} = 5$ BSs/Km^2
MT density	$\lambda_{\mathrm{MT}} = 100 \times \lambda_{\mathrm{BS}}$
Noise spectral density	$\sigma_N^2 = -174$ [dBm/Hz]
P_0	$P_0 = -80$ [dBm/Hz]
Shadowing parameters	$(\mu, \sigma) = (0, 8)$
Fast-fading parameters	$\Omega = 1$
Fractional factor ε	0 to 1
Max. MT power $P_{\max}$	20 to 70 [dBm] & ∞
Interference target $P_0^{(I)}$	-130 to -80 [dBm/Hz]
Receive-antenna number N_R	1, 2, 4, 8

In Fig.B.1(a)–(c), mean and standard deviation (std.) of the power consumption, $\mathscr{P}_{\mathrm{MT}}$, of the typical MT as a function of ε, $P_{\max}$ and $P_0^{(I)}$ are studied, respectively. The figure shows that the mean of $P_{\max}$ is an increasing function of ε, $P_{\max}$ and $P_0^{(I)}$. Also, it highlights that the benefits of interference-aware power control are more visible for large values of ε and $P_{\max}$, as well as for low values of $P_0^{(I)}$.

In Fig.B.2, the coverage probability of the typical MT is illustrated. It shows that uplink cellular networks tend to be noise- (SINR $\approx$ SNR) and interference-limited (SINR $\approx$ SIR) if ε is small and large, respectively. It confirms that the coverage increases as the number of receive antennas increases. Finally, it highlights that interference-aware power control seems to be more useful for cell-center MTs, since a larger gain is observed for large reliability thresholds.

In Fig.B.3–B.4, the impact of interference-unaware/aware power control is studied as a function of the demodulator being used and of the number of receive antennas N_R. In general, the rate increases as N_R increases and the gain of OC demodulation compared with MRC demodulation increases with NR as well. The impact of interference-aware power control is different for cell-edge (5th percentile) and cell-center (90th percentile) MTs. Usually, it is more beneficial for cell-center MTs. In Fig. B.4, in particular, it is shown that the optimal power control compensation factor ε may be different for cell-edge and cell-center users. This suggests that different ε factors may be used within a given cell for providing a better quality of experience to all the MTs in the network.

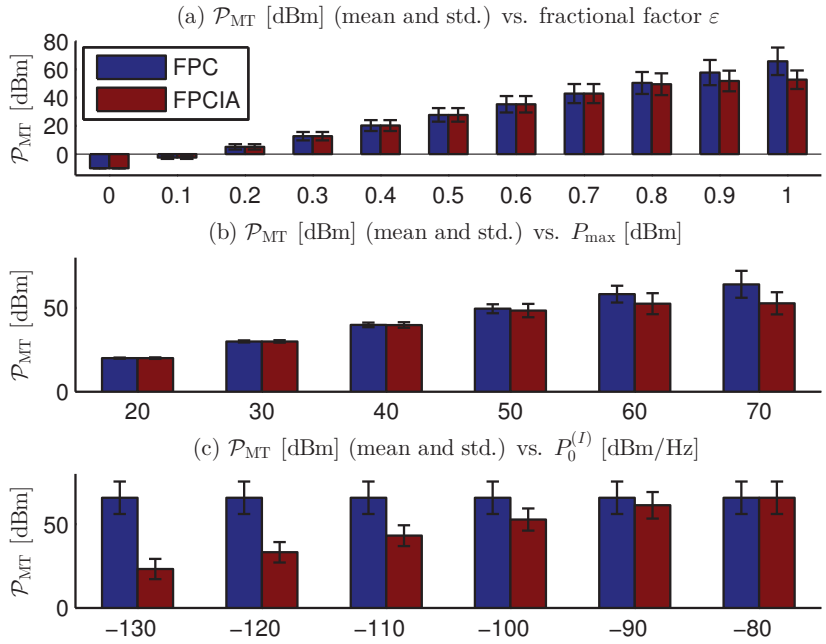

Figure B.1: MT transmit power $\mathcal{P}_{\mathrm{MT}}$ (mean and std.) against (a) ε, (b) $P_{\max}$ and (c) $P_0^{(I)}$, respectively. Setup: (a) $P_{\max}=\infty$, $P_0^{(I)}=-100$ [dBm/Hz], (b) $\varepsilon=1$, $P_0^{(I)}=-100$ [dBm/Hz], (c) $\varepsilon=1$, $P_{\max}=\infty$.

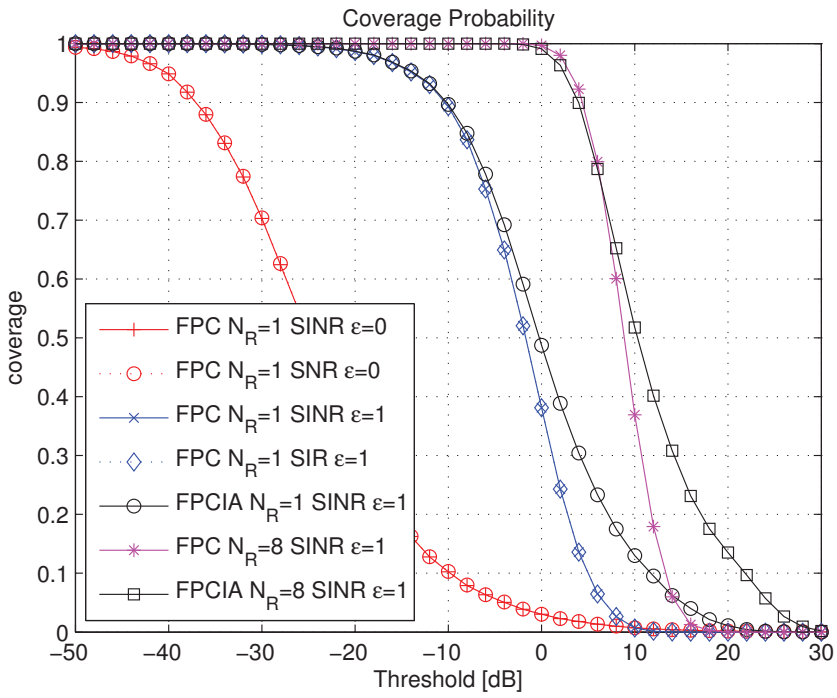

Figure B.2: Coverage Probability against reliability threshold. Setup: MRC, $P_{\max}=\infty$, $P_0^{(I)}=-100$ [dBm/Hz].

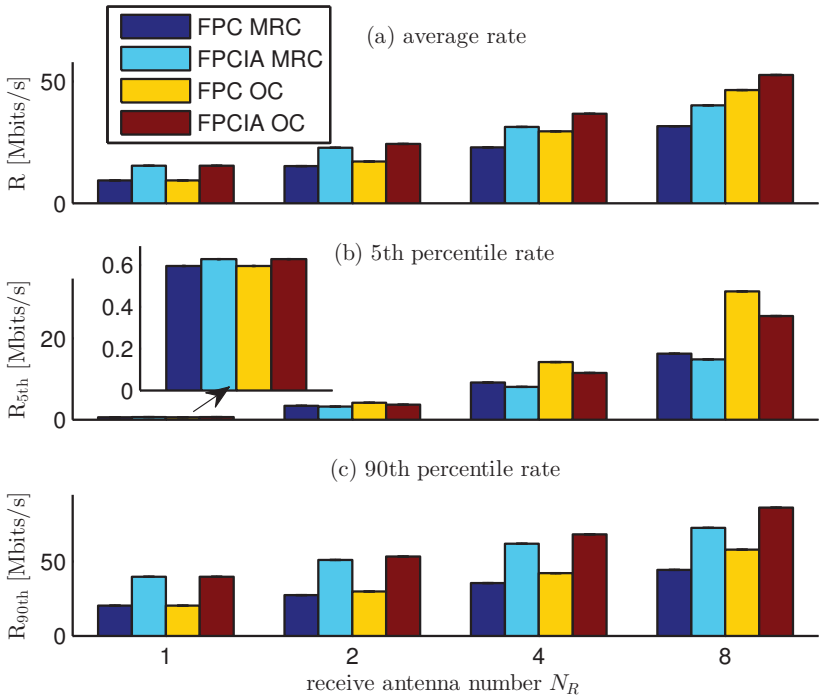

Figure B.3: (a) Average rate, (b) 5^{th} percentile rate and (c) 90^{th} percentile rate against N_R. Setup: MRC, $\varepsilon = 1$, $P_{\max} = \infty$, $P_0^{(I)} = -100$ [dBm/Hz].

In Fig.B.5–B.6, the impact of the maximum transmit power of the MTs, $P_{\max}$, and of the interference constraint $P_0^{(I)}$ is studied. The figures show, again, that cell-edge and cell-center MTs have different performance trends. As far as cell-edge MTs are concerned (5th percentile), in particular, the rate increases as $P_{\max}$ and $P_0^{(I)}$ increase. Furthermore, Fig. 6 confirms that setting $P_0^{(I)} = P_0$ eliminates the effect of interference awareness in the power control.

All in all, the figures show that several parameters affect the achievable performance of uplink cellular networks. If the system is adequately optimized, in particular, interference-aware power control may enhance the achievable performance. For example, if a MRC with $N_R = 2$ is used, and $\varepsilon = 1$, $P_{\max} = 70$ [dBm], $P_0^{(I)} = -100$ [dBm/Hz] is assumed, interference-aware power control leads to a 20%, 6% and 47% increase in average rate, 5^{th} percentile rate and 90^{th} percentile rate, respectively, as well as a 18% reduction in MT power consumptions.

In this Appendix, the numerical examples confirm the importance of power control for enhancing coverage and rate of cellular networks, as well as that different performance trends emerge for cell-edge and cell-center MTs. In particular, different power control compensation factors may be needed for different MTs in order to provide a more uniform quality of experience across the cell. The achievable performance shows a non-trivial dependence on the quadruplet of parameters $(\varepsilon, N_R, P_{\max}, P_0^{(I)})$, which highlights the challenge of optimizing uplink cellular networks by relying only on numerical simulations.

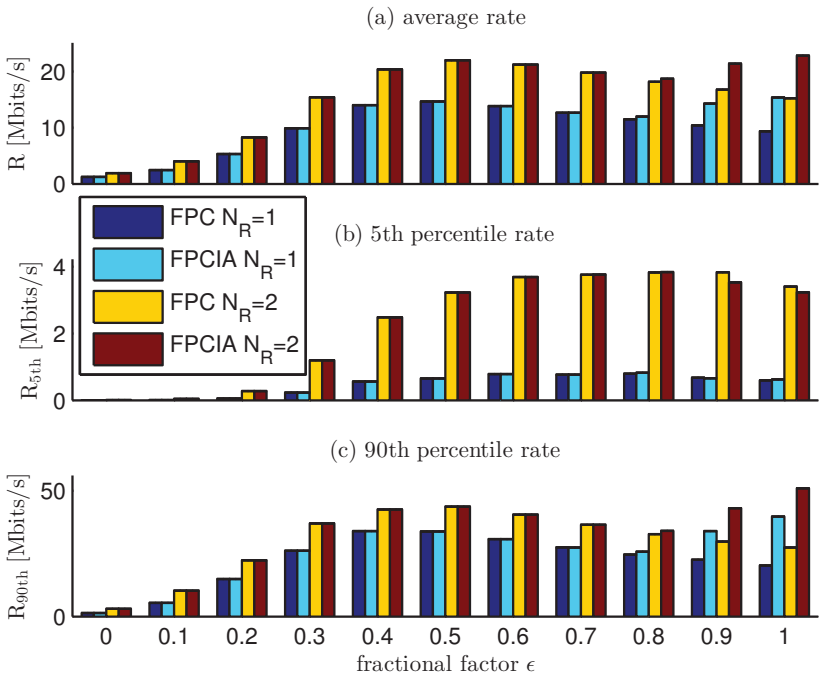

Figure B.4: (a) Average rate, (b) 5^{th} percentile rate and (c) 90^{th} percentile rate against ε. Setup: MRC, $P_{\max} = \infty$, $P_0^{(I)} = -100$ [dBm/Hz].

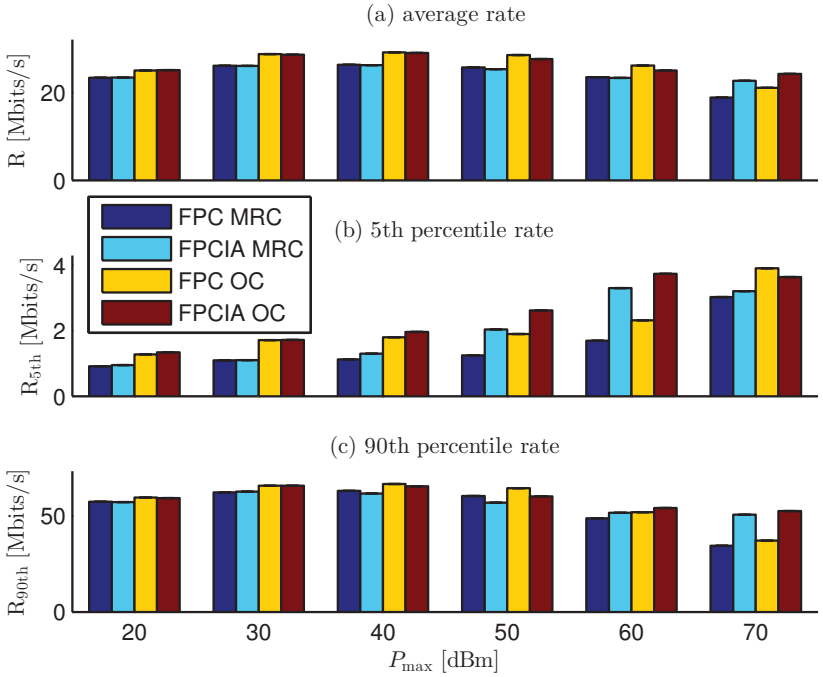

Figure B.5: (a) Average rate, (b) 5^{th} percentile rate and (c) 90^{th} percentile rate against $P_{\max}$. Setup: $\varepsilon = 1$, $P_0^{(I)} = -100$ [dBm/Hz], $N_R = 2$.

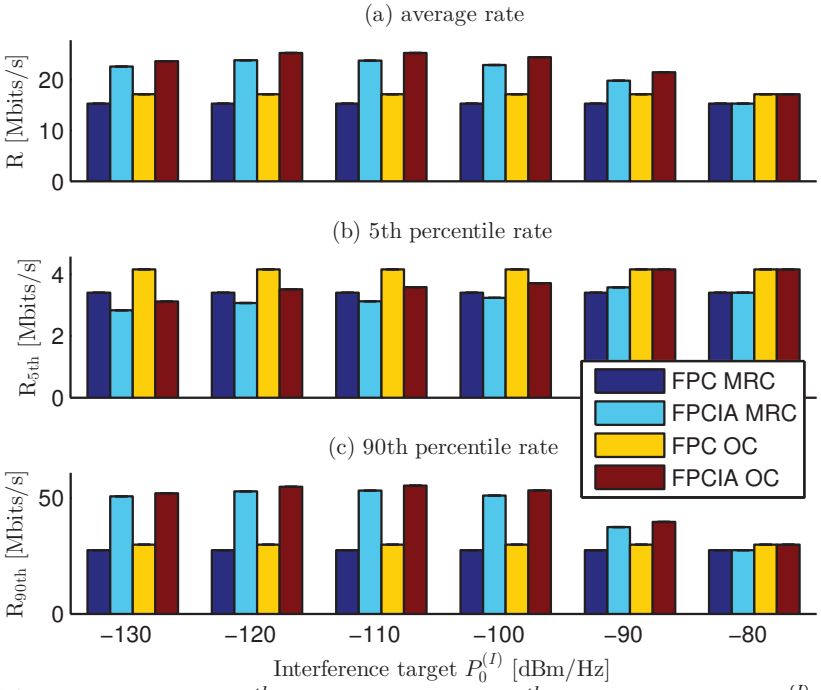

Figure B.6: (a) Average rate, (b) 5^{th} percentile rate and (c) 90^{th} percentile rate against $P_0^{(I)}$. Setup: $\varepsilon = 1$, $P_{\max} = \infty$, $N_R = 2$.

Bibliography

[1] 3GPP TR 36.913, "Requirements for further advancements for Evolved Universal Terrestrial Radio Access (E-UTRA) ", *V10.0.0*,2011 [Online]. Available: http://www.3gpp.org/DynaReport/36913.htm.

[2] Parkvall, S.; Dahlman, E.; Furuskar, A.; Jading, Y.; Olsson, M.; Wanstedt, S.; Zangi, K., "LTE-Advanced - Evolving LTE towards IMT-Advanced", *IEEE Vehicular Technology Conference Fall*, vol., no., pp.1-5, 21-24 Sept. 2008.

[3] A. D. Wyner, "Shannon-theoretic approach to a Gaussian cellular multiple-access channel", *IEEE Transactions on Information Theory*, vol. 40, no. 11, pp.1713–1727, Nov. 1994.

[4] C. B. Chae, I. Hwang, R. W. Heath, and V. Tarokh, "Interference Aware-Coordinated Beamforming System in a Two-Cell Environment", *Technical Report*, Harvard University, 2009. [Online]. Available: http://dash.harvard.edu/handle/1/3293263.

[5] V. H. Macdonald, "The cellular concept", *Bell System Technical Journal*, vol. 58, no. 1, pp. 15–41, Jan. 1979.

[6] J. G. Andrews, F. Baccelli, and R. K. Ganti, "A tractable approach to coverage and rate in cellular networks", *IEEE Transactions on Communications*, vol. 59, no. 11, pp. 3122–3134, Nov. 2011.

[7] M. Di Renzo, A. Guidotti, and G. E. Corazza, "Average rate of downlink heterogeneous cellular networks over generalized fading channels – A stochastic geometry approach", *IEEE Transactions on Communications*, vol. 61, no. 7, pp. 3050–3071, July 2013.

[8] J. Xu, J. Zhang, and J. G. Andrews, "On the accuracy of the Wyner model in cellular networks", *IEEE Transactions on Wireless Communications*, vol. 10, no. 9, pp. 3098–3109, Sep. 2011.

[9] Gilhousen, K.S.; Jacobs, I.M.; Padovani, R.; Viterbi, A.J.; Weaver, L.A., Jr.; Wheatley, C.E., III, "On the capacity of a cellular CDMA system", *IEEE Transactions on Vehicular Technology*, vol.40, no.2, pp.303,312, May 1991.

[10] F. Baccelli, M. Klein, M. Lebourges, and S. Zuyev, "Stochastic geometry and architecture of communication networks", *Telecommunication Systems*, vol. 7, no. 1, pp. 209–227, 1997.

[11] P. Fleming, A. L. Stolyar, and B. Simon, "Closed-form expressions for other-cell interference in cellular CDMA", *Technical Report*, University of Colorado at Boulder, Dec. 1997. [Online]. Available:http://ccm.ucdenver.edu/reports/rep116.pdf.

[12] T. X. Brown, "Cellular performance bounds via shotgun cellular systems", *IEEE Journal on Selected Areas in Communications*, vol. 18, no. 11, pp. 2443–2455, Nov. 2000.

[13] C.-H. Lee, C.-Y. Shihet, and Y.-S. Chen, "Stochastic geometry based models for modeling cellular networks in urban areas", *Springer Wireless Networks*, 10 pages, Oct. 2012.

[14] A. Guo and M. Haenggi, "Spatial stochastic models and metrics for the structure of base stations in cellular networks", *IEEE Transactions on Wireless Communications*, vol. 12, no. 11, pp. 5800–5821, Nov. 2013.

[15] W. Lu and M. Di Renzo, "Stochastic geometry modeling of cellular networks: Analysis, simulation and experimental validation", *ACM International Conference on Modeling, Analysis and Simulation of Wireless and Mobile Systems*, submitted. [Online]. Available: http://arxiv.org/pdf/1506.03857v1.pdf.

[16] F. Baccelli and B. Blaszczyszyn, *Stochastic Geometry and Wireless Networks, Part I: Theory, Part II: Applications*, Now Publishers, Sep. 2009.

[17] M. Haenggi and R. K. Ganti, *Interference in Large Wireless Networks*, Foundations and Trends in Networking, vol. 3, no. 2, pp 127–248, 2009.

[18] M. Haenggi, *Stochastic Geometry for Wireless Networks*, Cambridge University Press, Nov. 2012.

[19] H. ElSawy, E. Hossain, and M. Haenggi, "Stochastic geometry for modeling, analysis, and design of multi-tier and cognitive cellular wireless networks: A survey", *IEEE Communications Surveys & Tutorials*, vol. 15, no. 3, pp. 996–1019, 3rd quarter 2013.

[20] M. Z. Win, P. C. Pinto, and L. A. Shepp, "A mathematical theory of network interference and its applications", *Proceedings of the IEEE*, vol. 97, no. 2, pp. 205–230, Feb. 2009.

[21] A. Rabbachin, T. Q. S. Quek, S. Hyundong, and M. Z. Win, "Cognitive network interference", *IEEE Journal on Selected Areas in Communications*, vol. 29, no. 2, pp. 480–493, Feb. 2011.

[22] X. Ge, K. Huang, C.-X. Wang, X. Hong, and X. Yang, "Capacity analysis of a multi-cell multi-antenna cooperative cellular network with co-channel interference", *IEEE Transactions on Wireless Communications*, vol. 10, no. 10, pp. 3298–3309, Oct. 2011.

[23] A. Guidotti, V. Buccigrossi, M. Di Renzo, G. E. Corazza, and F. Santucci, "Outage and symbol error probabilities of dual-hop AF relaying in a Poisson field of interferers", *IEEE Wireless Communications and Networking Conference*, pp. 1–6, Apr. 2013.

[24] M. Di Renzo, C. Merola, A. Guidotti, F. Santucci, and G. E. Corazza, "Error performance of multi-antenna receivers in a Poisson field of interferers: A stochastic geometry approach", *IEEE Transactions on Communications*, vol. 61, no. 5, pp. 2025–2047, May 2013.

[25] A. Chopra and B. L. Evans, "Outage probability for diversity combining in interference-limited channels", *IEEE Transactions on Wireless Communications*, vol. 12, no. 2, pp. 550–560, Feb. 2013.

[26] R. Tanbourgi, H. S. Dhillon, J. G. Andrews, and F. K. Jondral, "Effect of spatial interference correlation on the performance of maximum ratio combining", *IEEE Transactions on Wireless Communications*, vol. 13, no. 6, pp. 3307–3316, June 2014.

[27] M. Di Renzo and W. Lu, "End-to-end error probability and diversity analysis of AF-based dual-hop cooperative relaying in a Poisson field of interferers at the destination", *IEEE Transactions on Wireless Communications*, vol.14, no.1, pp.15-32, Jan. 2015.

[28] M. Di Renzo and W. Lu, "On the diversity order of selection combining dual-branch dual-hop AF relaying in a Poisson field of interferers at the destination", *IEEE Transactions on Vehicular Technology*, vol.64, no.4, pp.1620-1628, April 2015

[29] M. Di Renzo and W. Lu, "The equivalent-in-distribution (EiD)-based approach: On the analysis of cellular networks using stochastic geometry", *IEEE Communications Letters*, vol. 18, no. 5, pp. 761–764, May 2014.

[30] H. S. Dhillon, M. Kountouris, and J. G. Andrews, "Downlink MIMO hetnets: Modeling, ordering results and performance analysis", *IEEE Transactions on Wireless Communications*, vol. 12, no. 10, pp. 5208–5222, Oct. 2013.

[31] M. Di Renzo and W. Lu, "Stochastic geometry modeling and performance evaluation of MIMO cellular networks using the equivalent-in-distribution (EiD)-based approach", *IEEE Transactions on Communications*, vol. 63, no. 3, pp. 977–996, Mar. 2015.

[32] S. Mukherjee, "Distribution of downlink SINR in heterogeneous cellular networks", *IEEE Journal on Selected Areas in Communications*, vol. 30, no. 3, pp. 575–585, Apr. 2012.

[33] H. S. Dhillon, R. K. Ganti, F. Baccelli, and J. G. Andrews, "Modeling and analysis of K-tier downlink heterogeneous cellular networks", *IEEE Journal on Selected Areas in Communications*, vol. 30, no. 3, pp. 550–560, Apr. 2012.

[34] S. Mukherjee, "Downlink SINR distribution in a heterogeneous cellular wireless network with max-SINR connectivity", *IEEE Annual Allerton Conference on Communication, Control, and Computing*, pp. 1–8, Sep. 2011.

[35] S. Mukherjee, "Downlink SINR distribution in a heterogeneous cellular wireless network with biased cell association", *IEEE International Conference on Communications – Workshop Small Cell Wireless Networks*, pp. 1–7, June 2012.

[36] H.-S. Jo, Y. J. Sang, P. Xia, and J. G. Andrews, "Heterogeneous cellular networks with flexible cell association: A comprehensive downlink SINR analysis", *IEEE Transactions on Wireless Communications*, vol. 11, no. 10, pp. 3484–3495, Oct. 2012.

[37] R. W. Heath Jr., M. Kountouris, and T. Bai, "Modeling heterogeneous network interference using Poisson point processes", *IEEE Transactions on Signal Processing*, vol. 61, no. 16, pp. 4114–4126, Aug. 2013.

[38] M. C. Valenti, D. Torrieri, and S. Talarico, "A direct approach to computing spatially averaged outage probability", *IEEE Communications Letters*, vol 18, no. 7, pp. 1103–1106, July 2014.

[39] A. Annamalai, C. Tellambura, and V. K. Bhargava, "Simple and accurate methods for outage analysis in cellular mobile radio systems – A unified approach", *IEEE Transactions on Communications*, vol. 49, no. 2, pp. 303–316, Feb. 2001.

[40] Yu, Seung Min, and Seong-Lyun Kim, " Downlink capacity and base station density in cellular networks", *11th International Symposium on Modeling & Optimization in Mobile, Ad Hoc & Wireless Networks (WiOpt)*, vol., no., pp.119-124, 13-17 May 2013.

[41] H. S. Dhillon, R. K. Ganti, and J. G. Andrews, "Load-aware modeling and analysis of heterogeneous cellular networks", *IEEE Transactions on Wireless Communications*, vol. 12, no. 4, pp. 1666–1677, Apr. 2013.

[42] S. Singh, H. S. Dhillon, and J. G. Andrews, "Offloading in heterogeneous networks: Modeling, analysis, and design insights", *IEEE Transactions on Wireless Communications*, vol. 12, no. 5, pp. 2484–2497, May 2013.

[43] Dhillon, H.S.; Andrews, J.G., " Downlink Rate Distribution in Heterogeneous Cellular Networks under Generalized Cell Selection", *IEEE Wireless Communications Letters*, vol.3, no.1, pp.42-45, February 2014.

[44] T. Bai and R. W. Heath Jr., "Coverage and rate analysis for millimeter wave cellular networks", *IEEE Transactions on Wireless Communications*, vol. 14, no. 2, pp. 1100–1114, Feb. 2015.

[45] S. Singh, M. N. Kulkarni, A. Ghosh, and J. G. Andrews, "Tractable model for rate in self-backhauled millimeter wave cellular networks", *IEEE Journal on Selected Areas in Communications*, submitted. [Online]. Available: http://arxiv.org/pdf/1407.5537v2.pdf.

[46] M. Di Renzo, "Stochastic geometry modeling and analysis of multi-tier millimeter wave cellular networks", *IEEE Transactions on Wireless Communications*, vol.14, no.9, pp.5038-5057, Sept. 2015

[47] T. D. Novlan, H. S. Dhillon, and J. G. Andrews, "Analytical modeling of uplink cellular networks", *IEEE Transactions on Wireless Communications*, vol. 12, no. 6, pp. 2669–2679, June 2013.

[48] H. ElSawy and E. Hossain, "On stochastic geometry modeling of cellular uplink transmission with truncated channel inversion power control", *IEEE Transactions on Wireless Communications*, vol. 13, no. 8, pp. 4454–4469, Aug. 2014.

[49] H. Y. Lee, Y. J. Sang, and K. S. Kim, "On the uplink SIR distributions in heterogeneous cellular networks", *IEEE Communications Letters*, vol. 18, no. 12, pp. 2145–214, Dec. 2014.

[50] S. Singh, X. Zhang, and J. G. Andrews, "Joint rate and SINR coverage analysis for decoupled uplink–downlink biased cell associations in HetNets", *IEEE Transactions on Wireless Communications*, to appear. [Online]. Available: IEEE Early Access.

[51] Y. Lin, W. Bao, W. Yu, and B. Liang, "Optimizing user association and spectrum allocation in HetNets: A utility perspective", *IEEE Journal on Selected Areas in Communications*, vol. 33, no. 6, pp. 1025–1039, June 2015.

[52] K. Smiljkovikj, P. Popovski, and L. Gavrilovska, "Analysis of the decoupled access for downlink and uplink in wireless heterogeneous networks", *IEEE Wireless Communications Letters*, vol. 4, no. 2, pp. 173–176, Apr. 2015.

[53] K. Smiljkovikj *et al.*, "Capacity analysis of decoupled downlink and uplink access in 5G heterogeneous systems", *IEEE Transactions on Wireless Communications*, submitted. [Online]. Available: http://arxiv.org/abs/1407.0536v2.

[54] J. Gil-Pelaez, "Note on the inversion theorem" *Biometrika*, vol. 38, pp. 481–482, Dec. 1951.

[55] A. Goldsmith, *Wireless Communications*, Cambridge University Press, 2005.

[56] M. Abramowitz and I. A. Stegun, *Handbook of Mathematical Functions with Formulas, Graphs, and Mathematical Tables*, June 1964.

[57] A. Erdelyi, W. Magnus, F. Oberhettinger, and F. G. Tricomi, *Higher Transcendental Functions – Vol I*, McGraw-Hill Book Company, Inc., 1953.

[58] A. P. Prudnikov, Y. A. Brychkov, and O. I. Marichev, *Integrals and Series – Vol. 3: More Special Functions*, ISBN 5-9221-0325-3, 2003.

[59] M. Zorzi and S. Pupolin, "Slotted ALOHA for high-capacity voice cellular communications", *IEEE Transactions on Vehicular Technology*, vol. 43, no. 4, pp. 1011–1021, Nov. 1994.

[60] M. K. Simon and M.-S. Alouini, *Digital Communication over Fading Channels*, John Wiley & Sons, Inc., 2st ed., 2005.

[61] K. Gulati, B. L. Evans, J. G. Andrews, and K. R. Tinsley, "Statistics of co-channel interference in a field of Poisson and Poisson-Poisson clustered interferers", *IEEE Transactions on Signal Processing*, vol. 58, no. 12, pp. 6207–6222, Dec. 2010.

[62] P. Madhusudhanan, J. G. Restrepo, Y. Liu, and T. X. Brown, "Carrier to interference ratio analysis for the shotgun cellular system", *IEEE Global Communications Conference*, pp. 1–6, Dec. 2009.

[63] B. Blaszczyszyn, M. K. Karray, and H. P. Keeler, "Using Poisson processes to model lattice cellular networks", *IEEE International Conference on Computer Communications*, pp. 773–781, Apr. 2013.

[64] F. Yilmaz and M.-S. Alouini, "A novel unified expression for the capacity and bit error probability of wireless communication systems over generalized fading channels", *IEEE Transactions on Communications*, vol. 60, no. 7, pp. 1862–1876, July 2012.

[65] I. S. Gradshteyn and I. M. Ryzhik, *Tables of Integrals, Series, and Products*, San Diego, CA: Academic, 7th ed., 2007.

[66] C. Merola, A. Guidotti, M. Di Renzo, F. Santucci, and G. E. Corazza, "Average symbol error probability in the presence of network interference and noise", *IEEE International Conference on Communications*, pp. 1–6, June 2012.

[67] G. Samorodnitsky and M. Taqqu, *Non-Gaussian Random Processes*, Chapman and Hall, June 1994.

[68] M. Di Renzo, F. Graziosi, and F. Santucci, "On the cumulative distribution function of quadratic-form receivers over generalized fading channels with tone interference", *IEEE Transactions on Communications*, vol. 57, no. 7, pp. 2122–2137, July 2009.

[69] E. Biglieri, G. Caire, G. Taricco, and J. Ventura-Traveset, "Computing error probabilities over fading channels: A unified approach", *European Transactions on Telecommunications*, vol. 9, no. 1, pp. 15–25, Jan./Feb. 1998.

[70] N. C. Beaulieu and J. Cheng, "Precise error-rate analysis of bandwidth-efficient BPSK in Nakagami fading and cochannel interference", *IEEE Transactions on Communications*, vol. 52, no. 1, pp. 149–158, Jan. 2004.

[71] The Wolfram Functions Site. [Online].
Available: http://functions.wolfram.com/HypergeometricFunctions/Hypergeometric1F1/06/02/0006/.

[72] The Wolfram Functions Site. [Online].
Available: http://functions.wolfram.com/HypergeometricFunctions/Hypergeometric2F2/06/02/02/0003/.

[73] A. Winkelbauer, "Moments and absolute moments of the normal distribution". [Online].
Available: http://arxiv.org/pdf/1209.4340.pdf.

[74] A. Hedayat, H. Shah, and A. Nosratinia, "Analysis of space-time coding in correlated fading channels", *IEEE Transactions on Wireless Communications*, vol. 4, no. 6, pp. 2882–2891, Nov. 2005.

[75] Z. Wang and G. B. Giannakis, "A simple and general parameterization quantifying performance in fading channels", *IEEE Transactions on Communications*, vol. 51, no. 8, pp. 1389–1398, Aug. 2003.

[76] The Wolfram Functions Site. [Online]. Available: http://functions.wolfram.com/HypergeometricFunctions/MeijerG/06/01/03/01/0006/.

[77] Járai-Szabó Ferenc, Zoltán Néda, "On the size distribution of Poisson Voronoi cells", *Physica A: Statistical Mechanics and its Applications*, vol.385, no.2, pp.518-526, Nov. 2007.

[78] Louie, Raymond H.Y.; McKay, M.R.; Collings, I.B., "Open-loop spatial multiplexing and diversity communications in ad hoc networks", *IEEE Transactions on Information Theory*, vol.57, no.1, pp.317-344, Jan. 2011.

[79] Hunter, Andrew Marcus, "Capacity of multi-antenna ad hoc networks via stochastic geometry", *Ph.D. Thesis*, The University of Texas at Austin, 2012. [Online]. Available: https://repositories.lib.utexas.edu/handle/2152/ETD-UT-2012-12-6694.

[80] Kang, Ming, and M-S. Alouini, "A comparative study on the performance of MIMO MRC systems with and without cochannel interference", *IEEE Transactions on Communications*, vol.52, no.8, pp.1417-1425, Aug. 2004.

[81] Maaref, Amine, and Sonia Aïssa, "Closed-form expressions for the outage and ergodic Shannon capacity of MIMO MRC systems", *IEEE Transactions on Communications*, vol.53, no.7, pp.1092-1095, July 2005.

[82] Zaidi, S.A.R.; Ghogho, M.; McLernon, D.C.; Swami, A., "Achievable Spatial Throughput in Multi-Antenna Cognitive Underlay Networks with Multi-Hop Relaying", *IEEE Journal on Selected Areas in Communications*, vol.31, no.8, pp.1543-1558, August 2013.

[83] Dighe, Parag A., Ranjan K. Mallik, and Sudhanshu Shekhar Jamuar, "Analysis of transmit-receive diversity in Rayleigh fading", *IEEE Transactions on Communications*, vol.51, no.4, pp.694-703, April 2003.

[84] W. Liu, S. Han, C. Yang, and C. Sun, "Massive MIMO or small cell network: Who is more energy efficient?", *IEEE Wireless Communications and Networking Conference*, pp. 1–6, Apr. 2012.

[85] Wolfram Mathematica 9, Symbolic Integral Computation.

[86] Nokia Networks, "5G radio access system design aspects", *White Paper*, [Online]. Available: http://networks.nokia.com.

[87] A. Simonsson, A. Furuskar, "Uplink power control in LTE – Overview and performance", *IEEE Vehicular Technology Conference Fall*, pp. 1–5, Sep. 2008.

[88] ,3GPP TS 36.21 "LTE – Evolved Universal Terrestrial Radio Access (E-UTRA) Physical layer procedures", *version 10.13.0*, 2015 [Online].
Available:http://www.etsi.org/deliver/etsi_ts/136200_136299/136213/10.13.00_60/ts_136213v101300p.pdf

[89] J. G. Andrews, "Seven ways that HetNets are a cellular paradigm shift", *IEEE Communications Magazine*, vol. 51, no. 3, pp 136–144, Mar. 2013.

[90] Ericsson, "3GPP TSG-RAN WG2 #81bis – Tdoc R2-131381", *Improving offloading potential with UL/DL split*, Apr. 2013. [Online]. Available: http://www.3gpp.org/ftp/tsg_ran/WG2_RL2/TSGR2_81bis/docs/R2-131381.zip.

[91] Ericsson, "3GPP TSG-RAN WG2 #82 – Tdoc R2-1316781", *Further discussions on UL/DL split*, May. 2013. [Online]. Available: http://www.3gpp.org/ftp/tsg_ran/WG2_RL2/TSGR2_82/docs/R2-131678.zip.

[92] V. Chandrasekhar and J. G. Andrews, "Uplink capacity and interference avoidance for two-tier femtocell networks", *IEEE Transactions on Wireless Communications*, vol. 8, no. 7, pp. 3498–3509, July 2009.

[93] T. L. Marzetta, "Noncooperative cellular wireless with unlimited numbers of base station antennas", *IEEE Transactions on Wireless Communications*, vol. 9, no. 11, pp. 3590–3600, Nov. 2010.

[94] K. Guo, Y. Guo, G. Fodor, and G. Ascheid, "Uplink power control with MMSE receiver in multi-cell MU-massive-MIMO systems", *IEEE International Conference on Communications*, pp. 1–7, June 2014.

[95] J. B. Andersen, T. S Rappaport, and S. Yoshida, "Propagation measurements and models for wireless communications channels", *IEEE Communications Magazine*, vol. 33, no. 1, pp. 42–49, Jan. 1995.

[96] G. L. Stuber, *Principles of Mobile Communication*, Springer, 3rd ed., 2012.

[97] The Wolfram Functions Site, [Online].
Available: http://functions.wolfram.com/HypergeometricFunctions/Hypergeometric2F1/03/06/07/02/0005/.

[98] H. Gao, P. J. Smith, and M. V. Clark, "Theoretical reliability of MMSE linear diversity combining in Rayleigh-fading additive interference channels", *IEEE Transactions on Communications*, vol. 46, no. 5, pp. 666–672, May 1998.

[99] 3GPP TSG RAN, WG1 meeting #66bis (R1-113118.doc) and 3GPP TSG RAN WG2 meeting #78 (R2-122726.doc).

[100] T. S. Rappaport, R. W. Heath Jr., R. C. Daniels, and J. N. Murdock, *Millimeter Wave Wireless Communication*, Cambridge University Press, Prentice Hall, 2014.

[101] Rappaport, T.S.; Shu Sun; Mayzus, R.; Hang Zhao; Azar, Y.; Wang, K.; Wong, G.N.; Schulz, J.K.; Samimi, M.; Gutierrez, F., "Millimeter Wave Mobile Communications for 5G Cellular: It Will Work!", *Access, IEEE*, vol.1, no., pp.335-349, 2013

[102] H. Zhang, N. Prasad, S. Rangarajan,S. Mekhail, S.Said, R.Arnott, "Standards-compliant LTE and LTE-A uplink power control", *IEEE International Conference on Communications*, pp.5275-5279, June 2012.

[103] H. Elshaer, F. Boccardi, M. Dohler, R. Irmer, " Load and Backhaul Aware Decoupled Downlink/Uplink Access in 5G Systems", *IEEE International Conference on Communications*, to appear, June 2015.

[104] Behnad, Aydin, and Norman C. Beaulieu, "Best neighbor communication in a Poisson field of nodes", *IEEE Trans. Vehicular Technology*, vol. 64, no. 2, pp. 818-823, 2015.

[105] Behnad, Aydin, and Xianbin Wang, "Distance Statistics of the Communication Best Neighbor in a Poisson Field of Nodes", *IEEE Transactions on Communications*, vol. 63, no. 3, pp. 997-1005, 2015.

[106] Na Deng; Wuyang Zhou; Haenggi, M., "The Ginibre Point Process as a Model for Wireless Networks With Repulsion", *IEEE Transactions on Wireless Communications*, vol.14, no.1, pp.107-121, Jan. 2015

[107] Y. Chun, M. O. Hasna, A. Ghrayeb, M. Di Renzo, "On Modeling Heterogeneous Wireless Networks Using Non-Poisson Point Processes", *IEEE Communications Magazine*, submitted. [Online]. Available: http://arxiv.org/abs/1506.06296v1.pdf.

[108] M. Di Renzo and P. Guan, "A mathematical framework to the computation of the error probability of downlink MIMO cellular networks by using stochastic geometry", *IEEE Transactions on Communications*, vol. 62, no. 8, pp. 2860–2879, Aug. 2014.

[109] M. Di Renzo and P. Guan, "Stochastic geometry modeling of coverage and rate of cellular networks using the Gil-Pelaez inversion theorem", *IEEE Communications Letters*, vol. 18, no. 9, pp. 1575–1578, Sep. 2014.

[110] P. Guan and M. Di Renzo, "Stochastic Geometry Modeling, System-Level Analysis and Optimization of Uplink Heterogeneous Cellular Networks with Multi-Antenna Base Stations", *IEEE Transactions on Communications*, submitted, 2015.

[111] P. Guan and M. Di Renzo, "Stochastic geometry analysis of the average error probability of downlink cellular networks", *IEEE International Conference on Computing, Networking and Communications*, pp. 1–7, Feb. 2014.

[112] P. Guan and M. Di Renzo, "Stochastic Geometry Analysis of the Energy Efficiency of Downlink MIMO Cellular Networks", *IEEE Vehicular Technology Conference spring*, vol., no., pp.1,5, 11-14 May 2015.

[113] P. Guan; M. Di Renzo; C. Verikoukis and T. Q. Duong, "Error Probability of Downlink MIMO Cellular Networks by Using Stochastic Geometry", *2015 European Conference on Networks and Communications (EuCNC)*, to appear, July 2015.

[114] P. Guan and M. Di Renzo, "Stochastic Geometry Modeling and Performance Evaluation of Downlink MIMO Cellular Networks", *IEEE Vehicular Technology Conference fall*, to appear, Sept. 2015.

[115] P. Guan and M. Di Renzo, " Stochastic Geometry Analysis of Uplink Cellular Networks with Multi-Antenna Base Stations and Interference-Aware Fractional Power Control", *IEEE International Conference on Computing, Management and Telecommunications*, to appear, Dec. 2015.

[116] P. Guan and M. Di Renzo, "Stochastic Geometry Analysis and Optimization of Uplink Cellular Networks with Fractional Power Control and Optimum Combining", *2016 IEEE International Conference on Communications (ICC)*, submitted, 2015.

Titre : Analyse de Réseaux Cellulaires LTE-A : Une Approche Fondée sur la Géométrie Stochastique

Mots clés : Géométrie stochastique, réseaux cellulaires, LTE-A, processus de Poisson, Évaluation de performances

Résumé : L'objectif principal de cette thèse est l'analyse des performances des réseaux LTE-A (Long Term Evolution- Advanced) au travers de la géométrie stochastique. L'analyse mathématique des réseaux cellulaires est un problème difficile, pour lesquels ils existent déjà un certain nombre de résultats mais qui demande encore des efforts et des contributions sur le long terme. L'utilisation de la géométrie aléatoire et des processus ponctuels de Poisson (PPP) s'est avérée être une approche permettant une modélisation pertinente des réseaux cellulaires et d'une complexité faible (tractable). Dans cette thèse, nous nous intéressons tout particulièrement à des modèles s'appuyant sur ces processus de Poisson : PPP-based abstraction. Nous développons un cadre mathématique qui permet le calcul de quantités reflétant les performances des réseaux LTE-A, tels que la probabilité d'erreur, la probabilité et le taux de couverture, pour plusieurs scénarios couvrant entre autres le sens montant et descendant. Nous considérons également des transmissions multi-antennes, des déploiements hétérogènes, et des systèmes de commande de puissance de la liaison montante. L'ensemble de ces propositions a été validé par un grand nombre de simulations. Le cadre mathématique développé dans cette thèse se veut général, et doit pouvoir s'appliquer à un nombre d'autres scénarios importants. L'intérêt de l'approche proposée est de permettre une évaluation des performances au travers de l'évaluation des formules, et permettent en conséquences d'éviter des simulations qui peuvent prendre énormément de temps en terme de développement ou d'exécution.

Title : Stochastic Geometry Analysis of LTE-A Cellular Networks

Keywords : Stochastic Geometry, Cellular Networks, LTE-A, Poisson Point Process, Performance Analysis

Abstract : The main focus of this thesis is on performance analysis and system optimization of Long Term Evolution - Advanced (LTE-A) cellular networks by using stochastic geometry. Mathematical analysis of cellular networks is a long-lasting difficult problem. Modeling the network elements as points in a Poisson Point Process (PPP) has been proven to be a tractable yet accurate approach to the performance analysis in cellular networks, by leveraging the powerful mathematical tools such as stochastic geometry. In particular, relying on the PPP-based abstraction model, this thesis develops the mathematical frameworks to the computations of important performance measures such as error probability, coverage probability and average rate in several application scenarios in both uplink and downlink of LTE-A cellular networks, for example, multi-antenna transmissions, heterogeneous deployments, uplink power control schemes, etc. The mathematical frameworks developed in this thesis are general enough and the accuracy has been validated against extensive Monte Carlo simulations. Insights on performance trends and system optimization can be done by directly evaluating the formulas to avoid the time-consuming numerical simulations.